Nonlinear Control for Low and High Alpha Aircraft Maneuvers under Lateral Centre of Gravity Uncertainty

THESIS

Submitted in partial fulfillment of the requirements for the degree of

DOCTOR OF PHILOSOPHY

by

Anukaran Khanna

ID No. 2018PHXF0018P

Under the supervision of

Dr. Bijoy Krishna Mukherjee

BITS Pilani
Pilani | Dubai | Goa | Hyderabad

BIRLA INSTITUTE OF TECHNOLOGY AND SCIENCE

PILANI (RAJASTHAN) INDIA

2024

BIRLA INSTITUTE OF TECHNOLOGY AND SCIENCE

DEPARTMENT OF ELECTRICAL AND ELECTRONICS ENGINEERING

PILANI- CAMPUS PILANI (RAJASTHAN) INDIA

CERTIFICATE

This is to certify that the thesis entitled **"Nonlinear Control for Low and High Alpha Aircraft Maneuvers under Lateral Centre of Gravity Uncertainty"** submitted by **Anukaran Khanna,** ID. No. **2018PHXF0018P** for an award of Ph.D. of the Institute embodies his original work under my supervision.

Signature of the Supervisor

Name **Dr. Bijoy Krishna Mukherjee**

Designation **Assistant Professor**

Department of Electrical & Electronics Engg.
Birla Institute of Technology & Science Pilani
Rajasthan, INDIA

Date

BIRLA INSTITUTE OF TECHNOLOGY AND SCIENCE

DEPARTMENT OF ELECTRICAL AND ELECTRONICS ENGINEERING

PILANI- CAMPUS PILANI (RAJASTHAN) INDIA

DECLARATION

I hereby declare that this submission is solely my original work. To the best of my knowledge and belief, it does not include any content previously published or authored by another individual, nor does it incorporate material that has substantially contributed to the conferral of any other academic degree or diploma from a university or other institution of higher learning.

I further authorize the Birla Institute of Technology and Science (BITS), Pilani to reproduce this thesis, either in whole or in part, through photocopying or any other means. This authorization extends to fulfilling requests from other institutions or individuals exclusively for scholarly research purposes.

Signature

Name **Anukaran Khanna**

Date

Acknowledgement

I would like to express my sincere gratitude to all those who have contributed to completing this thesis. First and foremost, I am grateful to my supervisor, Dr. Bijoy K. Mukherjee, for his unwavering support, guidance, and expertise throughout the entire research process. His insights and encouragement played a crucial role in shaping the direction and quality of this thesis. I am highly thankful to my Doctoral Advisory Committee members, Prof. S. Bhanot (retd.), Prof. H. D. Mathur and Dr. Aditya Gautam for their insightful feedback and constructive criticism. Their expertise greatly enriched the quality of this research.

I am grateful to the EEE department, I owe my sincere gratitude to HoD Prof. N. Gupta and Ex HoD Prof. V. K. Chaubey for providing the necessary resources and facilities to conduct this research. I am thankful to Prof. Praveen A. V. (Convener-Departmental Research Committee), Dr. Puneet Mishra, Dr. Sujan Yenuganti, and other faculty members of the EEE department for their constant motivation and encouragement. Special thanks to Prof. V. R. Rao, Vice-Chancellor of BITS Pilani, and Prof. S. K. Barai, Director, Pilani campus, for allowing me to pursue my research successfully.

I am also grateful to my, friends and colleagues Dr. Dhananjay, Dr. Ravinder, Dr. Akhilesh, Dr. Radha Bhardwaj, Dr. Rishi Parvanda, Ms. Pavitra Sharma, Mr. Krishna, Mr. Somesh, Mr. Jeevan and Ms. Surabhi who kept me inspiring and helped in difficult times. I would always cherish happy moments spent with my friends at BITS Pilani campus for the whole life. During my teaching assistantship, I got support from, Mr. Ravindra Kumar, and Mr. Vijay Yadav, for the successful course delivery. I extend my gratitude to Mr. Yogesh and Mr. Sanjay to deal with all the documentation required for a research scholar. They always made processes trouble-free.

I express my deep sense of gratitude, love and respect to my beloved parents Mrs. Neelima and Mr. D. K. Khanna. I extend my warmest thanks and sincere appreciation to my parents-in-laws, Mrs. Deepa and Mr. Ganesh Sehgal, for their unwavering support and understanding throughout this academic endeavor. My heartfelt thanks to my life partner Dr. Reetika for her unconditional love, support, patience, and cooperation that constantly encouraged me and helped me to deal with my tough days. I would like to express my sincere gratitude and thanks to my brother Dr. Prateek and sister-in-law Mrs. Divya for their immense love, support, motivation and taking care of family in my absence with full responsibility. My daughters Aarna and Aadya deserves a special mention here; it is always an absolute joy when they are around!

Anukaran Khanna

Abstract

Safety and security of the pilot and the vehicle are of paramount importance during typical air combat/defense missions. This essentially translates to requiring the vehicle to be able to perform various complex maneuvers. Controlling the motion of the vehicle during such maneuvers becomes challenging as the flight dynamics becomes significantly nonlinear and the aerodynamics may also become both nonlinear and uncertain. The problem gets compounded when the center of gravity (c.g.) of the aircraft gets deviated from the body centerline due to asymmetric distribution/release of stores, structural wing damage, uneven fuel consumption etc. causing coupling in the dynamics and hence further nonlinearity. Control design to enable the aircraft to perform low alpha (negligible aerodynamic nonlinearity and uncertainty) as well as high alpha (large aerodynamic nonlinearity and uncertainty) autonomous maneuvers under such predominantly lateral c.g. uncertainty is not adequately addressed in the literature and the present thesis is aimed at filling this gap.

First, low alpha maneuvers are considered and a robust linear control such as LQR and a nonlinear control such as backstepping are tried and either of them is found to fail to properly execute some relevant lateral maneuvers in the face of significant lateral c.g. uncertainties. To overcome the problem, first an ad-hoc model-based two-step adaptive backstepping control is proposed to automatically adapt to the unknown c.g. position through an adaptation law. Thereafter, for further performance enhancement, a strict feedback form is derived from the asymmetric equations of motion under lateral c.g. offset and a novel adaptive backstepping control is designed after identifying and retaining useful system nonlinearities. In either case, asymptotic stability of the closed loop system is mathematically established. As an additional novel finding, the adaptation law is shown to accurately estimate the actual c.g. position in either case.

Next, the focus is shifted to high alpha maneuvers. Because of the additional uncertainty issue with the high alpha maneuvers, a fast-sliding mode control is combined with the second step of the ad-hoc model-based two-step adaptive backstepping control. Thereafter, for a less conservative control design, the asymmetric dynamics based adaptive backstepping formulation is considered and in a novel way, two sliding mode controls are combined with each of the two individual steps. Asymptotic stability is mathematically proved in both the cases. Both the proposed hybrid controls are shown to be able to successfully mitigate the c.g. uncertainty issue when validated against some benchmark high alpha maneuvers with the second scheme yielding better performance. Hardware in loop simulations are also performed to establish the real time viability of all the proposed controls.

Table of Contents

List of Figures

List of Tables

Nomenclature

6 – DOF	six degrees-of-freedom
LQR	linear quadratic regulator
BSC	backstepping control
SMC	sliding mode control
c.g. (c.m.)	center of gravity of the aircraft (or center of mass)
x_b, y_b, z_b	body reference frame
$X\ Y\ Z$	inertial reference frame
$[x_{cm}, y_{cm}, z_{cm}]^T$	position of the c.g. of the asymmetric aircraft from nominal position
$[I]$	inertia matrix of the symmetric aircraft about the body reference frame
$[I']$	inertia matrix of the asymmetric aircraft about the body reference frame
m	mass of symmetric aircraft
$[u, v, w]^T$	velocity component in body axes
$[p, q, r]^T$	roll, pitch, and yaw body rates
α	angle-of-attack (AOA)
β	sideslip angle
μ	bank angle
γ	flightpath angle
χ	heading angle

ϕ	body axis roll angle
θ	body axis pitch angle
ψ	body axis yaw angle
V	true velocity
h	altitude
S	wing planform area
b	wing span
$\overline{c}$	mean aerodynamic chord
$\overline{q}$	free stream dynamic pressure
g	acceleration due to gravity
δ_a	aileron deflection
δ_e	elevator deflection
δ_r	rudder deflection
δ_{ptv}	pitch thrust vector deflection
δ_{ytv}	yaw thrust vector deflection
δ_T	throttle setting
C_D, C_Y, C_L	drag, side, and lift force coefficient
C_l, C_m, C_n	rolling, pitching, and yawing aerodynamic moment coefficient
T_X, T_Y, T_Z	thrust components along body axes
M_{TX}, M_{TY}, M_{TZ}	moment due to thrust along three body axes
l_x, l_z	location of the engine nozzle from the origin of the body frame (m)

Chapter 1

Introduction and Literature Review

1.1 Background

Controlling the motion of an air vehicle is a challenging task not only because of the availability of full six degrees of freedom (translating in three linear dimensions and rotating in three angular dimensions) in the motion, but also due to complex aerodynamic interactions [1]. Therefore, stability and control are the linchpin of any such vehicle and many of the mission objectives are naturally dependent on the flight control systems. Advancements in control engineering have led to the development of highly advanced control systems that have greatly enhanced the capabilities of such vehicles.

The history of fighter aircraft dates back to the early 20th century, when military strategists recognized the need for specialized aircraft that could engage in aerial combat and provide air superiority over the battlefield. During World War I, fighter aircraft were used primarily for reconnaissance and aerial observation, but as the war progressed, they became more specialized and were equipped with machine guns and other weapons. The first aircraft to be designed specifically for air-to-air combat was the Fokker Eindecker, which entered services in 1915 [2]. The outbreak of

World War II in 1930s and 1940s and parallel developments in the field of linear control theory saw a further evolution in fighter aircraft technology, with fighter planes such as the Messerschmitt Bf 109, the Spitfire, and the P-51 Mustang becoming legendary for their role in air combat [3]. During the war, fighter aircraft were used not only for combat but also for escort missions. Gain scheduled linear controllers could meet the reasonable mission demands from the fighter aircraft of those times. Linearization of the dynamics led to separation of the complete six degrees of freedom equations of motion into longitudinal and lateral-directional parts thereby simplifying various flight control problems to great extents and allowing for linear control techniques to be applied effectively. Such controls were extensively used in aircraft such as the F-86 Sabre, the MiG-15, and the F-4 Phantom II [4]. Later, after the end of cold war, during 1990s interests in sophisticated aircraft flight control continued with the emergence of various sophisticated robust, nonlinear control design techniques. Enhanced stability and maneuverability derived out of such advanced control lead to the development of the F/A-18 and the Su-30 Flanker which became the dominant aircraft in many air forces around the world. Overall, the advancements in control engineering have greatly improved the capabilities of fighter aircraft and have made them more effective in a wide range of missions and they also helped to make the aircraft safer for the pilots. The early 2000s marked the introduction of armed unmanned aerial vehicles (UAVs). UAVs have become integral to modern military operations, used for everything from surveillance and reconnaissance to targeted strikes and electronic warfare [5]. This trend of making the aircraft safer and more effective in increasingly complex warfare situations continues even today.

Therefore, the capabilities of the present-day fighter aircraft are not only limited to their firepower alone but also to their high speed, extreme maneuverability and the agility to execute large number of rapid and complex maneuvers autonomously. Such complex flight conditions invariably lead to trigonometric nonlinearities and inertial and kinematic coupling [6]. Moreover, the maneuver demands sometimes force the vehicles to operate in the high angle of attack regions i.e. regions

beyond the stall limit. The nonlinear and uncertain aerodynamics in these regions make the control task even more challenging. On top of that, the control surfaces are position, rate, and bandwidth constrained. All these factors combine to make the flight control problem a formidable one.

1.2 Literature Review

In this section, we lay out the background and related literature pertaining to the work done in this thesis is presented. It covers the reported literature that motivated us to carry out this research work. It is a well-established fact that stability and control are the linchpins of any aerospace vehicle, and therefore we start with reviewing the previous work from a control design perspective.

In general, well-established linear control techniques are predominantly used to design a flight control system. Various design methods, such as proportional-integral-derivative (PID) control, pole placement, H-infinity control, Linear quadratic regulator (LQR) design, optimal control, etc. [7-11], have been used for flight control of linear aircraft models in the past. It is beyond doubt that linear controllers are easy to implement and provide adequate performance under normal operating conditions. In this approach, the system is linearized around a finite set of trim points in the flight envelope and a specifically tuned controller for each of them is designed. In other words, the flight envelope is discretized into a desired number of operating points, and a single independent controller is developed for each one [12-14]. As the flight configuration changes, the appropriate control law needs to be loaded. This limits this approach to specific areas of the flight envelope due to a finite number of linearization points and thus limits the domain of stability. In order to circumvent these limitations, nonlinear control techniques become unavoidable. The standard approach for flight control design for nonlinear systems is gain scheduling. In this approach, a linear approximation of dynamic equations at several important operating points within the flight envelope is achieved. Depending on these points, linear controllers are designed and then combined continuously as the vehicle flies from one operating point to another [15,16]. Due to linearization, the actual system

performance and stability can be significantly different from the design results due to the approximated nonlinearities. With the rapid development of high-performance computational computers, sensor technology, and integrated electronic devices, nonlinear flight control design methods are expected to provide a control system with high precision and reliability. Thus, the investigation and development of advanced control methods for nonlinear aircraft flight dynamics have been addressed considerably by the aerospace control community but are by no means complete.

Instead of gain-fitting and interpolating between several operation points, the application of a variable-gain optimal output feedback control design methodology is proposed in [17,18] where the feedback gains are continuously calculated and scheduled as a function of the state variables. In the approach in [18], the feedback gains are calculated and scheduled by minimizing a cost function that is dependent on attack angle and surface deflections. The approach is not fully effective and robust for short-period mode control due to the computational cost and convergence of the associated constrained optimization problem.

Nonlinear dynamic inversion (NDI) in [19-24] for flight control system design has been proposed to eliminate the drawbacks of gain-scheduling-based design. [20] uses assumptions in which aerodynamic force coefficients and moment coefficients are nonlinear functions of the angle of attack, sideslip angle, and thrust coefficient but linear functions of the elevator, aileron, and rudder. The motion equations can be rewritten as a triangular system of general form and then a nonlinear dynamic inverse controller is generated and proven valid over the entire flight envelope. The main limitation of NDI based controller in application to flight control problems is its dependence on a precise knowledge of the aerodynamic coefficients, which is not easy to have in high angle of attack regions as the flow separation is a very complex aerodynamic phenomenon. To compensate this deficiency of NDI, in [25] an adaptive neural network-based NDI control design is proposed. As an alternate to the proposal in [25], some researchers proposed gain scheduled linear H∞ based control

as reported in [26, 27]. Many researchers also combined H∞ or mu-synthesis or probabilistic robust control techniques with NDI controllers to make the overall closed loop system more robust [28-30]. A better approach of NDI design for full nonlinear flight control is presented in [23, 24] which uses the fact that control surface deflections do not directly affect slow dynamics. Therefore, control systems are designed separately for slow-state variable dynamics and fast-state variable dynamics. With the designed fast-state controller, a separate and approximate inversion procedure is carried out to design the slow-state controller for slow-state variable dynamics. The achieved slow-state control system outputs are used as commands for the controller augmenting the fast-state variable dynamics. A justification of the reliability of the proposed algorithm is confirmed analytically using the longitudinal dynamics. A general disadvantage of the NDI approach that prevents the popular adoption of the method for nonlinear flight systems is the poor robustness of NDI-based control design, i.e., system parameters of the aircraft dynamics are included and essentially inverted in the control law. Therefore, the aircraft model used for control design needs to be accurate in order to achieve good performance and stability of the system.

In past, many researchers have addressed backstepping control (BSC) design [31-36]. The concept of backstepping design was introduced for the first time in [31,32] and has been a motivation for exploring new directions in control design for nonlinear dynamic systems. The backstepping control design is seen as a recursive design process that breaks a design problem on the full system down to a sequence of sub-problems on lower-order systems. Considering each lower-order system with a control Lyapunov function (CLF) and paying attention to the interaction between the various subsystems makes the design of a stabilizing controller modular and easier. The advantages of backstepping control are a stability guarantee, avoidance of dynamic nonlinearity cancellation, wide applicability for a class of nonlinear dynamic systems, and elimination of the requirement for the designed system to appear linear, as noted in [31, 36]. Applications of the backstepping design approach for nonlinear flight control have been considered by many researchers in [37-42]. An online

approximation-based backstepping control approach for advanced flight vehicles is presented in [37] in which the control law is designed using three feedback loops with an online approximation of the aerodynamic force and moment coefficient functions. The approach maintains stability (in the sense of Lyapunov) of the online function approximation process in the presence of magnitude, rate, and bandwidth limitations on the intermediate states and the surfaces. [40] shows how the equations of motion for aircraft are restructured in linear strict-feedback form, and then backstepping control design and adaptive gain scheduling are employed to achieve full envelope flight control. The research in [42] assumes aerodynamic forces and moments as a linear function of attack angle, pitch angle, and elevator. Then backstepping control design is applied to the aircraft model in strict-feedback form. The new contribution is that the aerodynamic parameters of the aircraft are approximated by nominal values and error models and then a parameter adaptive scheme using a multilayer neural network is employed to improve the performance and stability of the aircraft. Limitations of these approaches in [40, 42] are the assumptions of linear-like behavior for the design model used for generating the control law. These above works have not yet addressed in a significant way the robustness and adaptive issues in flight control of nonlinear dynamic systems.

One of the most important ingredients needed for achieving reliable flight is flight safety. Flight safety may be violated when an aircraft meets unforeseen circumstances. Therefore, an advanced control method that can guarantee stability in the presence of these unforeseen flight conditions is needed. Adaptive control has been believed to be a strong candidate to achieve this goal with the potential to improve flight safety. In the context of the underlying dynamic model, most of the non-normal flight conditions can be directly mapped into parametric uncertainties, and adaptive control is the theoretical discipline that was developed with the aim of maintaining stability against parametric uncertainties. Therefore, an adaptation-based reconfigurable flight controller is believed to maintain satisfactory performance under unforeseen changes in the system dynamics. Adaptive control theory itself has been extensively studied over the past three decades, with its basic

performance and robustness properties currently well understood [43-46]. With promising features, such as stability against parametric uncertainties, adaptive control theory has been studied extensively in the context of adaptive flight control systems too after the 2000s and its potential has been verified both theoretically and numerically. More recently, there has been significant interest [47-49] and success in applying adaptive methods to flight. In [50,51] the adaptive backstepping control technique is discussed for controlling the longitudinal flight dynamics of UAV with thrust saturation. Most of the work available in the literature is for control of longitudinal dynamics only and very few works in the literature can be traced for control of lateral/directional dynamics. Control design for lateral/directional dynamics is more challenging because of coupling between roll and yaw dynamics. Though [52] consider adaptive backstepping control of UAV for lateral/directional dynamics, they design two separate controllers for sideslip and roll rate under uncertainty in aerodynamic coefficients.

Sliding mode is another popular nonlinear control design technique applied in many flight control problems [53-55]. It is inherently robust, in particular to parametric uncertainties [56]. In [57], Sliding mode based robust flight path control of aircraft using two-time scale design approach was proposed. [58] considered a MIMO adaptive sliding mode controller for the longitudinal dynamics of a generic hypersonic air vehicle. In [59] a sliding mode controller was designed for controlling angle of attack and velocity by using the modal decomposition into short-period and phugoid approximations. In [60] researchers designed sliding mode controllers for three different maneuvers namely minimum radius level turn, velocity vector roll and spin recovery maneuvers. All the works reported so far in the literature are carried out for symmetric aircraft only i.e. aircraft with their center of gravity (c.g.) located in the plane of symmetry coinciding with the origin of the body frame.

The problem becomes even more challenging when unbalanced payload deployment or release, unbalanced fuel consumption or structural damage etc. contribute to lateral mass asymmetry further complicating the problem. As the center of gravity (c.g.) of the aircraft drifts away significantly from

Figure 1.1. Source of c.g. variation: (a) asymmetric mass distribution (b) partial structural damage

the fuselage centerline leading to further coupling between the longitudinal and the lateral/directional channels. This important issue has been taken up recently by some researchers and have reported some works on modeling and control design for asymmetric aircraft. In [61] asymmetric c.g. issue in aircraft dynamics for an asymmetric aircraft is first modeled. Soon after, [62-64] carried out some further work on control of asymmetric aircraft. Works on modeling the aerodynamics of an asymmetric aircraft were carried out in [65-67]. However, their focus was on civil aircraft; hence, the control objectives were limited to securing steady level flight condition only. Recently, a few works were reported in the context of fighter aircraft performing drastic maneuvers under lateral c.g. offset where, it is shown that even robust nonlinear controllers would fail to automatically execute these demanding maneuvers if the lateral c.g. variation was completely ignored. To overcome this challenge, they designed controllers presuming the actual c.g. information of the aircraft to be known to the controller at every time step. However, in reality, it is rather impractical to assume the exact c.g. information to be available at every time step [68,69]. To gain insensitivity to both matched and unmatched uncertainties and disturbances backstepping and sliding mode controls are combined in the literature in various application domains [70-78]. However, herein, SMC is integrated in the final

step of the backstepping control only. To handle the flight control problem with uncertainties and external disturbances, recently some researchers reported disturbance observer based design [79-81]. However, this approach requires an additional controller which further increases the complexity and computational burden. These gaps present opportunities for further investigation and form the foundation for the research objectives outlined in the subsequent section/chapter. The subsequent chapters will elaborate on the research design, methodology, and findings that build upon the insights gained from the literature review.

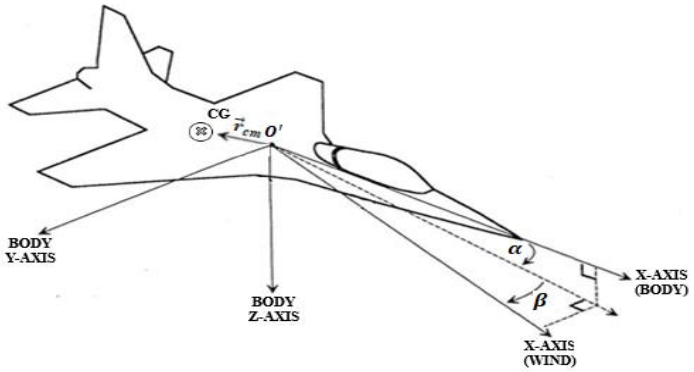

Figure 1.2. Aircraft body reference frame and c.g. position

1.3 Research Gap

Researchers have been applying nonlinear, robust, and adaptive (classical and intelligent) control design techniques to various flight control problems over the last few decades now. Over the last ten-fifteen years, considerable amount of research has been carried out on controls of aircraft having geometric asymmetry due to lateral c.g. movements and partial structural damage. However, most of these efforts were confined to civil aircraft within the framework of steady level flight conditions only. A few works were reported in the literature in the context of fighter aircraft performing complex maneuvers under lateral c.g. variations also; however, therein, it was presumed that the actual c.g. position of the aircraft was known to the controller. In reality, it is rather impractical to assume the exact c.g. information to be available at every time step. To bridge this gap, the present investigation

is aimed at offering some automatic control solutions so that a fighter aircraft undergoing significant and unknown lateral variations of c.g. position can still execute some useful maneuvers and complete its intended mission.

1.4 Research Objectives of the Thesis

In regard to the previous section's discussion, the objectives of the thesis can be succinctly summarized as follows:

- To investigate the effects of lateral mass asymmetry arising from the asymmetrical release of onboard stores on closed-loop performance while executing some standard low alpha maneuvers and offer a practical solution by designing an adaptive backstepping control based on an ad-hoc representation of the flight dynamics of the asymmetric aircraft.
- To explore if further maneuver performance enhancement can be achieved through a more accurate representation of the asymmetric flight dynamics and design of adaptive backstepping control scheme based on this improved model.
- To further investigate the effects of lateral mass asymmetry on closed-loop performance while performing some high alpha maneuvers. Since in the high alpha regime, the aerodynamic data contain significant uncertainty, therefore, to explore the possibility of robustness enhancement of the backstepping control through hybridization with sliding mode control.
- To explore if further maneuver performance enhancement and mitigation of c.g. uncertainty can be achieved through a more accurate representation of the asymmetric flight dynamics and design of the adaptive backstepping sliding mode hybrid control based on this improved representation.

1.5 Contributions of the Thesis

The present thesis encompasses a comprehensive investigation of an asymmetric aircraft performing both low and high angle of attack autonomous maneuvers. Robust nonlinear control design to mitigate the adverse effects of asymmetry on such maneuver performance is addressed in detail. The main contributions and novel elements of the thesis are summarized below.

- Ineffectiveness of robust linear control (LQR) and nonlinear control (Backstepping) to perform low alpha lateral maneuvers in the face of lateral c.g. uncertainty is established.
- An ad-hoc modelling approach is adopted to convert the asymmetric dynamics to strict feedback and c.g. affine form to make backstepping control design possible. Thereafter, a two-step adaptive backstepping control is designed to automatically adapt to the unknown c.g. position through an adaptation law.
- In order to obtain a more accurate model (as opposed to the ad-hoc model), the strict feedback and c.g. affine form is also shown to be obtainable from the asymmetric equations of motion neglecting second order terms of c.g. offset. Useful system nonlinearities are also identified and retained in backstepping control for a less conservative control design.
- It is proved that the adaptation law can accurately estimates the actual c.g. position for the low alpha maneuvers in either of the above two cases.
- For high alpha maneuvers, first a fast sliding mode control is combined with the second step of the ad-hoc model based adaptive backstepping control to mitigate the effects of model simplifications and aerodynamic uncertainties. Asymptotic stability of the proposed hybrid control is proved from first principle through a novel interval matrix analysis.
- The asymmetric model based adaptive backstepping formulation is also extended to high alpha maneuvers. In a novel way, two sliding mode controllers are combined with the two

individual steps of backstepping design and further performance improvement is achieved.

- Along with MATLAB simulations, hardware in loop simulations are also performed to establish the real time viability of the proposed controls in all the above mentioned cases.

1.6 Key Assumptions of the Thesis

In order to make the analysis tractable, the following reasonable assumption are made in the present investigation.

- The aircraft is considered to be a rigid body which means that any two points on or within the airframe remain fixed with respect to each other. This assumption is valid as fighter aircraft are smaller and structurally more compact than civil aircraft, the flexible modes are negligible [82, 83].
- Effects of rotating parts such as the engine fan on the aircraft dynamics is neglected.
- The aircraft is assumed to be equipped with thrust vectoring capabilities in both horizontal and vertical planes.
- All the aerodynamic and thrust control effectors are assumed to be constrained by position and rate saturation limits.
- All the control effectors are assumed to be described by first order stable dynamics.
- All the state variables are assumed to be measured and the measurements are assumed to be perfect or noise free.

1.7 Layout of the Thesis

The thesis is divided into six chapters. Throughout the thesis to cover the entire spectrum of air vehicle low alpha maneuvers are carried on Aerosonde UAV while the high alpha maneuvers are

carried on F-18 HARV fighter aircraft. The main contributions are covered in the second, third, fourth and fifth chapters, the present i.e. first chapter introduces the thesis and the sixth one concludes the same.

In Chapter 2, first the nominal lateral/directional dynamics of a fixed wing Aerosonde UAV is framed into strict feedback form and then the block backstepping approach is used to design the controller to execute low alpha namely horizontal turn and aileron roll maneuvers under no lateral c.g. variation. Thereafter, an adaptive block backstepping controller is designed to adapt to uncertainty in lateral c.g. position considering an ad-hoc model of the asymmetric dynamics.

Chapter 3 starts with an approximation made for the complex 6-degree-of-freedom equations of motion, accounting for the asymmetric center of gravity position. These equations were then transformed into a strict feedback form, enabling the use of a two-step adaptive backstepping control design. Subsequently, an adaptation law was employed to estimate the lateral center of gravity position, allowing the unmanned aerial vehicle (UAV) to execute low alpha namely horizontal turn and aileron roll maneuvers automatically. The proposed adaptive scheme is validated and compared against the same two maneuvers with an approach used in Chapter 2, that utilized an ad-hoc model of the asymmetric equations of motion.

In Chapter 4, first the aircraft flight dynamics under predominantly lateral c.g. movement, is expressed in a block strict feedback form considering an ad-hoc model of dynamics and thereafter an adaptive backstepping controller is proposed to adapt to the c.g. variations. To alleviate the model uncertainty caused by this model approximation and to provide robustness to aerodynamic uncertainties in high-alpha regions, a sliding mode control is further integrated with the adaptive backstepping control law. To validate the proposed control scheme, the high-alpha maneuvers namely cobra and Herbst maneuvers are implemented in simulation for the F18-HARV aircraft.

In Chapter 5, first it is shown that the highly coupled six degrees of freedom dynamics arising because

of c.g. offset can be expressed in block strict feedback form under some reasonable model simplifications. Thereafter, a two-step adaptive backstepping control is designed using an adaptation law to explicitly adapt to the c.g. position. To provide robustness to the model simplifications as well as to aerodynamic uncertainties, a fast sliding mode control is integrated with each of the steps of the backstepping control and the asymptotic stability of the overall closed loop system is proved using the Lyapunov approach. In support of the efficacy of the proposed control strategy, simulation results are presented for two benchmark high-alpha maneuvers cobra and Herbst for the F18-HARV.

Chapter 6 concludes the thesis with concluding remarks and recommendations for further extensions of the present work. Real time implementability of the proposed controls are also verified through hardware in loop simulations and these simulation results along with the complete datasets of the aircraft considered in the present work are provided in the Appendices.

Chapter 2

Adaptive Backstepping Control for Low Alpha Lateral Maneuvers

2.1 Introduction

In modern aerial combat scenarios, the demand for extreme maneuverability in aircraft is paramount for both operational effectiveness and pilot survivability. Moreover, achieving and maintaining control of aircraft executing maneuver is itself a complex task. This complexity is further compounded by various factors such as unbalanced payload distribution, fuel consumption, structural damage, and other unforeseen events, all of which can cause the aircraft's center of gravity to shift significantly away from its nominal position along the fuselage centerline. However, in the present thesis lateral shift in c.g. position arising from asymmetrical release of payload is taken into consideration.

When the center of gravity deviates, the aircraft's stability and controllability are compromised, posing a serious threat to both the vehicle and the pilot. In such scenarios, the ability of the aircraft to execute maneuvers effectively becomes crucial for survival. However, designing a robust controller capable of handling these nonlinear dynamics is a formidable challenge. The design of

such a controller requires a deep understanding of the complex interactions between aerodynamic forces, propulsion systems, and control surfaces. These interactions give rise to complex, nonlinear relationships that must be carefully considered to develop control systems capable of accurately capturing and responding to the aircraft's behavior in real-time. After a comprehensive literature survey, it is now appropriate to address how the sudden unknown lateral center of gravity (c.g.) movement affects maneuver performance to enhance overall aircraft survivability in combat scenarios.

Several control methods have been used over time to study the trajectory tracking control problem for UAVs. Linear control techniques like the Linear Quadratic Regulator (LQR) [84] and the proportional-integral-derivative (PID) approach have been used for UAVs flight problem [85, 86]. These studies, however, did not examine the effects of uncertainties in further detail, making them ineffective for most real-life applications. Nonlinear control approaches have been explored and used in the recent past to strengthen stability and widen the region of operation of the control schemes. The approach of feedback linearization [19, 87, 88], which relies on the cancellation of all nonlinearities to convert a nonlinear system into a system with linear dynamics, is the one that is used frequently among the classical nonlinear control techniques. However, the major limitation of the method comes from the requirement of a complete knowledge of the nonlinearities present in the plant. This makes it susceptible to parametric uncertainty and modeling errors. In the case of flight control systems, in addition to this, the method relies on the two-time scale separation of angular and angular rate dynamics [89, 90]. Another popular nonlinear control algorithm that relies neither on the complete cancellation of the nonlinear dynamics nor on the two-time scale separation principle is the backstepping algorithm [36, 91]. Viewing some of the states as virtual control inputs offers a method for iteratively designing a controller. The backstepping design is often made adaptive to enhance the closed-loop system's robustness [37,41]. Therefore, in the present case, adaptive backstepping control approach is considered.

The outline of the chapter is as follows. The second section gives an introduction of the problem and the same is formulated for low alpha maneuvers. Divided into four subsections, in the third section linear control technique design for a symmetric fixed wing Aerosonde UAV is discussed first and then the control is formulated utilizing the LQR technique. The same control technique is extended for lateral c.g. variations as well. The fourth section discusses the necessity of nonlinear control implementation and the block backstepping control technique is implemented first for symmetric case and the same is extended again for asymmetric situation as well. Fifth section focusses on ad-hoc formulation with unknown shift in c.g. position and estimation of lateral c.g. position using an adaptation law within an adaptive backstepping control design framework. Section six concludes the chapter with a brief prelude to the next chapters.

2.2 Problem formulation and System Dynamics for Low Alpha Lateral Maneuvers

In this section, the 6- degree of freedom (6-DOF) dynamics is formulated aimed at executing standard low-alpha maneuver namely horizontal turn and aileron roll. To achieve these maneuvers, external inputs provide appropriate time profiles of angular variables. Subsequently, the closed-loop controller generates the requisite commands for control surface deflection. The standard symmetric equations of motion in body axes, as described in [92], with conventional notation, are utilized for this purpose.

$$\begin{bmatrix}\dot{u}\\ \dot{v}\\ \dot{w}\end{bmatrix} = \begin{bmatrix}-qw + rv\\ -ru + pw\\ -pv + qu\end{bmatrix} + \frac{1}{m}\begin{bmatrix}-mgsin\theta + \bar{q}SC_X + T_X\\ mgcos\theta sin\phi + \bar{q}SC_Y\\ mgcos\theta cos\phi + \bar{q}SC_Z\end{bmatrix} \tag{2.1}$$

where, $T_X = \frac{1}{2}S_{prop}C_{prop}((K_{motor}\delta_T)^2 - V^2)$ is the thrust model of the UAV [93].

$$\begin{bmatrix} I_{xx} & 0 & -I_{xz}\\ 0 & I_{yy} & 0\\ -I_{xz} & 0 & I_{zz}\end{bmatrix}\begin{bmatrix}\dot{p}\\ \dot{q}\\ \dot{r}\end{bmatrix} = \begin{bmatrix}(I_{yy} - I_{zz})qr + I_{xz}pq\\ (I_{zz} - I_{xx})rp + I_{xz}(r^2 - p^2)\\ (I_{xx} - I_{yy})pq - I_{xz}qr\end{bmatrix} + \begin{bmatrix}\bar{q}SbC_l\\ \bar{q}S\bar{c}C_m\\ \bar{q}SbC_n\end{bmatrix} \tag{2.2}$$

$$\begin{bmatrix}\dot{\phi}\\ \dot{\theta}\\ \dot{\psi}\end{bmatrix}=\begin{bmatrix}1 & sin\phi tan\theta & cos\phi tan\theta\\ 0 & cos\phi & -sin\phi\\ 0 & sin\phi & cos\phi sec\theta\end{bmatrix}\begin{bmatrix}p\\ q\\ r\end{bmatrix} \tag{2.3}$$

Now $(v, \phi, p, r) \in \mathbb{R}^4$ is the state vector associated with the lateral/directional dynamics. The equations of motion of the UAV's lateral/directional dynamics are given by

$$\dot{v} = -ru + pw + \frac{1}{m}(mgcos\theta sin\phi + \bar{q}SC_Y) \tag{2.4}$$

$$\dot{\phi} = p + qsin\phi tan\theta + rcos\phi tan\theta \tag{2.5}$$

$$\dot{p} = (c_1 rq + c_2 pq) + c_3 \bar{q}SbC_l + c_4 \bar{q}SbC_n \tag{2.6}$$

$$\dot{r} = (c_8 pq - c_2 rq) + c_4 \bar{q}SbC_l + c_9 \bar{q}SbC_n \tag{2.7}$$

where, $c_1 = \left(I_y - I_z\right)I_z - I_{xz}^2/\Delta\,, c_2 = \left(I_x - I_y + I_z\right)I_{xz}/\Delta, c_3 = I_z/\Delta, c_4 = I_{xz}/\Delta, c_8 = \left(I_x - I_y\right)I_x + I_{xz}^2/\Delta\,, c_9 = I_x/\Delta$ with $\Delta = I_x I_z - I_{xz}^2$

Under the assumption that α and β remain small throughout the maneuver, total velocity and the longitudinal variables remain nearly constant at their initial steady wing level trim values, in Eq. (2.4) control is ignored since the control surface deflections produce only considerable moments and not force [69]. Eqs. (2.4) – (2.7) can be modified as

$$\dot{\phi} = p + rtan\alpha_t cos\phi \tag{2.8}$$

$$\dot{\beta} = -r + ptan\alpha_t + \frac{g}{V}sin\phi cos\alpha_t + \frac{\bar{q}SC_{Y\beta}\beta}{mV} \tag{2.9}$$

$$\dot{p} = c_3 \bar{q}SbC_l + c_4 \bar{q}SbC_n \tag{2.10}$$

$$\dot{r} = c_4 \bar{q}SbC_l + c_9 \bar{q}SbC_n \tag{2.11}$$

where α_t is the trim angle of attack and V is the trim velocity.

2.3 LQR based Linear Control Design for the Nominal System

In the realm of Unmanned Aerial Vehicles (UAVs) in this chapter, our prime objective is to investigate how variations in lateral center of gravity (c.g.) position affect performance of low alpha lateral maneuvers. Among various low alpha lateral maneuvers, we have considered two significant maneuvers to elucidate this, the horizontal turn (banks the aircraft to one side to initiate a turn while maintaining a steady altitude in a short span) and the aileron roll maneuver (aircraft executing a full 360° revolution about its longitudinal axis.). In low alpha region, the aerodynamics are fairly linear. Therefore, linear control techniques should be applied first and tested.

Since the present problem involves model uncertainty due to c.g. variations, the LQR is considered as the preferred linear control tool because of its excellent robustness property. Its fundamentals, which are briefly outlined in the subsequent subsection, serve as a crucial backbone for ensuring the UAV's stability and performance during these dynamic maneuvers.

2.3.1 A Brief Overview of LQR Theory [84]

The Linear Quadratic Regulator (LQR) is a control technique used in engineering and control theory to design optimal control systems for linear dynamical systems subject to quadratic costs. It's particularly useful for systems where the dynamics can be modeled linearly and the performance criterion is expressed as a quadratic function of the system's state and control inputs.

Here's an overview of LQR control process:

Consider a continuous-time linear time-invariant (LTI) system described by the state-space equations:

$$\dot{x}(t) = Ax(t) + Bu(t) \tag{2.12}$$

$$y(t) = Cx(t) + Du(t) \tag{2.13}$$

where:

- $x(t)$ is the state vector of size $n \times 1$
- $u(t)$ is the control input of size $m \times 1$
- $y(t)$ is the output vector of size $p \times 1$
- A is the $n \times n$ system dynamics matrix.
- B is the $n \times m$ control input matrix.
- C is the $p \times n$ output matrix.
- D is the $p \times m$ feedforward matrix.

The goal is to design a control law of the form:

$$u(t) = -Kx(t) \tag{2.14}$$

where K is the feedback gain matrix, such that it minimizes the following cost function:

$$J = \int_0^\infty (x^T(t)Qx(t) + u^T(t)Ru(t))dt \tag{2.15}$$

where:

- Q is the state weighting matrix, a positive semi-definite matrix of size $n \times n$.
- R is the control input weighting matrix, a positive definite matrix of size $m \times m$.

The solution to the LQR problem involves solving the continuous-time algebraic Riccati equation:

$$A^T P + PA - PBR^{-1}B^T P + Q = 0 \tag{2.16}$$

where P is the solution to the Riccati equation, a positive definite matrix of size $n \times n$.

Once P is found, the optimal feedback gain matrix K can be computed as:

$$K = -R^{-1}B^{T}P \tag{2.17}$$

The optimal control law $u(t) = -Kx(t)$ minimizes the cost function J over an infinite time horizon.

Overall, the Linear Quadratic Regulator is a versatile and widely used technique for designing optimal feedback controllers. It is a robust linear control technique that can handle uncertainties and disturbances. The LQR achieves infinite gain margin and a minimum phase margin of 60^{o}. Since the main concern of the present problem is system uncertainty in a low alpha maneuver, the excellent robustness property of LQR algorithm makes it an automatic choice.

2.3.2 Control Formulation and Design

In this sub-section, the main objective is to reframe the tracking problem into a regulator problem, enabling it to be effectively addressed through LQR-based control design. Aim is to autonomously execute the intended lateral maneuver when aircraft is symmetric along fuselage centerline. The desired time profiles for x_1 i.e. ϕ (roll angle) and β (sideslip angle) are fed externally as reference inputs and the controller generates $\boldsymbol{u}$ i.e. the control surface deflection commands in a closed loop manner as shown in Figure 2.1. The formulation and analysis of the controller is discussed below.

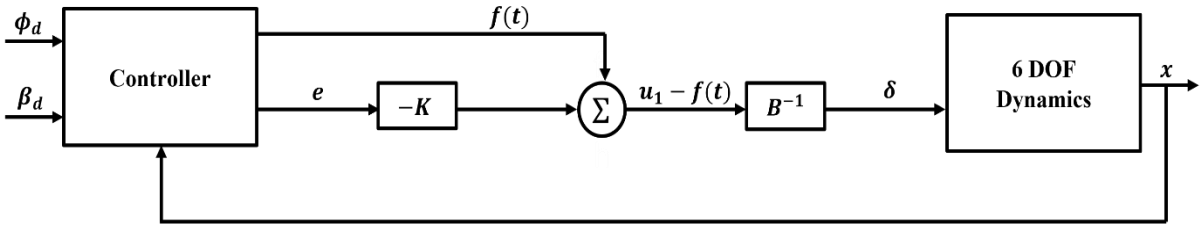

Figure 2.1. Closed loop diagram of LQR control scheme

The Eqs. (2.8) – (2.11) provided in the previous section exhibit nonlinearity, prompting the application of small-disturbance theory to linearize them. According to this theory, all variables can be substituted with a reference value plus a perturbation, as outlined in [92].

$v = v_0 + \Delta v;$ $p = p_0 + \Delta p;$ $r = r_0 + \Delta r;$

$Y = Y_0 + \Delta Y;$ $L = L_0 + \Delta L;$ $N = N_0 + \Delta N;$

$\phi = \phi_0 + \Delta\phi;$ $\psi = \psi_0 + \Delta\psi;$ $\delta_a = \delta_{a0} + \Delta\delta_a;$

$\delta_r = \delta_{r0} + \Delta\delta_r;$ (2.18)

For steady level flight,

$v_0 = 0;$ $p_0 = 0;$ $r_0 = 0$ $Y_0 = 0;$ $L_0 = 0;$

$N = 0;$ $\phi_0 = 0;$ $\psi_0 = 0;$ $\delta_{a0} = 0;$ $\delta_{r0} = 0;$ (2.19)

On substituting Eqs. (2.18) in Eqs. (2.8) – (2.11), we get

$$(\dot{\phi}_0 + \Delta\dot{\phi}) = (p_0 + \Delta p) + (r_0 + \Delta r)tan\alpha_t cos(\phi_0 + \Delta\phi) \quad (2.20)$$

$$(\dot{\beta}_0 + \Delta\dot{\beta}) = -(r_0 + \Delta r) + (p_0 + \Delta p)tan\alpha_t + \frac{g}{V}sin(\phi_0 + \Delta\phi)cos\alpha_t + \frac{\bar{q}S}{mV}[\mathrm{C_{Y\beta}}(\beta_0 + \Delta\beta) + C_{Yp}\frac{(p_0+\Delta p)b}{2V} + C_{Yr}\frac{(r_0+\Delta r)b}{2V}] \quad (2.21)$$

$$(\dot{p}_0 + \Delta\dot{p}) = c_3\bar{q}Sb[\mathrm{C_{l\beta}}(\beta_0 + \Delta\beta) + C_{lp}\frac{(p_0+\Delta p)b}{2V} + C_{lr}\frac{(r_0+\Delta r)b}{2V} + C_{l\delta_a}(\delta_{a0} + \Delta\delta_a) + C_{l\delta_r}(\delta_{r0} + \Delta\delta_r)] + c_4\bar{q}Sb[\mathrm{C_{n\beta}}(\beta_0 + \Delta\beta) + C_{np}\frac{(p_0+\Delta p)b}{2V} + C_{nr}\frac{(r_0+\Delta r)b}{2V} + C_{n\delta_a}(\delta_{a0} + \Delta\delta_a) + C_{n\delta_r}(\delta_{r0} + \Delta\delta_r)] \quad (2.22)$$

$$(\dot{r}_0 + \Delta\dot{r}) = c_4\bar{q}Sb[\mathrm{C_{l\beta}}(\beta_0 + \Delta\beta) + C_{lp}\frac{(p_0+\Delta p)b}{2V} + C_{lr}\frac{(r_0+\Delta r)b}{2V} + C_{l\delta_a}(\delta_{a0} + \Delta\delta_a) + C_{l\delta_r}(\delta_{r0} + \Delta\delta_r)] + c_9\bar{q}Sb[\mathrm{C_{n\beta}}(\beta_0 + \Delta\beta) + C_{np}\frac{(p_0+\Delta p)b}{2V} + C_{nr}\frac{(r_0+\Delta r)b}{2V} + C_{n\delta_a}(\delta_{a0} + \Delta\delta_a) + C_{n\delta_r}(\delta_{r0} + \Delta\delta_r)] \quad (2.23)$$

Now utilizing the condition laid down in Eq. (2.19) in Eqs. (2.20) – (2.23), we get

$$\Delta\dot{\phi} = \Delta p + \Delta r tan\alpha_t \quad (2.24)$$

$$\Delta\dot{\beta} = -\Delta r + \Delta p tan\alpha_t + \frac{g}{V}\Delta\phi cos\alpha_t + \frac{\bar{q}S}{mV}(\mathrm{C_{Y\beta}}\Delta\beta + C_{Yp}\frac{\Delta pb}{2V} + C_{Yr}\frac{\Delta rb}{2V}) \quad (2.25)$$

$$\Delta\dot{p} = c_3\bar{q}Sb(\mathrm{C_{l\beta}}\Delta\beta + C_{lp}\frac{\Delta pb}{2V} + C_{lr}\frac{\Delta rb}{2V} + C_{l\delta_a}\Delta\delta_a + C_{l\delta_r}\Delta\delta_r) +$$

$$c_4\bar{q}Sb(\mathrm{C_{n\beta}}\Delta\beta + C_{np}\frac{\Delta pb}{2V} + C_{nr}\frac{\Delta rb}{2V} + C_{n\delta_a}\Delta\delta_a + C_{n\delta_r}\Delta\delta_r) \tag{2.26}$$

$$\Delta\dot{r} = c_4\bar{q}Sb(\mathrm{C_{l\beta}}\Delta\beta + C_{lp}\frac{\Delta pb}{2V} + C_{lr}\frac{\Delta rb}{2V} + C_{l\delta_a}\Delta\delta_a + C_{l\delta_r}\Delta\delta_r) +$$

$$c_9\bar{q}Sb(\mathrm{C_{n\beta}}\Delta\beta + C_{np}\frac{\Delta pb}{2V} + C_{nr}\frac{\Delta rb}{2V} + C_{n\delta_a}\Delta\delta_a + C_{n\delta_r}\Delta\delta_r) \tag{2.27}$$

The linearized model of aircraft in the state space form of lateral dynamics is given by

$$\begin{bmatrix}\Delta\dot{\phi}\\ \Delta\dot{\beta}\\ \Delta\dot{p}\\ \Delta\dot{r}\end{bmatrix} = \begin{bmatrix} 0 & 0 & 1 & tan\alpha_t \\ \frac{g}{V}cos\alpha_t & \frac{\bar{q}SC_{Y\beta}}{mV} & tan\alpha_t + \frac{C_{Yp}b\bar{q}S}{2mV^2} & -1 + \frac{C_{Yr}b\bar{q}S}{2mV^2} \\ 0 & \bar{q}Sb(c_3C_{l\beta} + c_4C_{n\beta}) & \frac{\bar{q}Sb^2}{2V}(c_3C_{lp} + c_4C_{np}) & \frac{\bar{q}Sb^2}{2V}(c_3C_{lr} + c_4C_{nr}) \\ 0 & \bar{q}Sb(c_4C_{l\beta} + c_9C_{n\beta}) & \frac{\bar{q}Sb^2}{2V}(c_4C_{lp} + c_9C_{np}) & \frac{\bar{q}Sb^2}{2V}(c_4C_{lr} + c_9C_{nr}) \end{bmatrix}\begin{bmatrix}\Delta\phi\\ \Delta\beta\\ \Delta p\\ \Delta r\end{bmatrix}$$

$$+\begin{bmatrix} 0 & 0 \\ 0 & 0 \\ \bar{q}Sb(c_3C_{l\delta_a} + c_4C_{n\delta_a}) & \bar{q}Sb(c_3C_{l\delta_r} + c_4C_{n\delta_r}) \\ \bar{q}Sb(c_4C_{l\delta_a} + c_9C_{n\delta_a}) & \bar{q}Sb(c_4C_{l\delta_r} + c_9C_{n\delta_r}) \end{bmatrix}\begin{bmatrix}\Delta\delta_a\\ \Delta\delta_r\end{bmatrix} \tag{2.28}$$

From the above Eq. (2.28) it is evident that to control four state variables we have only two available control surface deflection elements. Hence, to resolve this issue, the above equation is converted into second order equations in ϕ and β to make it amenable to LQR design as follows:

From Eq. (2.28) we can write,

$$\begin{bmatrix}\Delta\dot{\phi}\\ \Delta\dot{\beta}\end{bmatrix} = \begin{bmatrix} 0 & 0 \\ \frac{g}{V}cos\alpha_t & \frac{\bar{q}SC_{Y\beta}}{mV}\end{bmatrix}\begin{bmatrix}\Delta\phi\\ \Delta\beta\end{bmatrix} + \begin{bmatrix} 1 & tan\alpha_t \\ tan\alpha_t + \frac{C_{Yp}b\bar{q}S}{2VmV} & -1 + \frac{C_{Yr}b\bar{q}S}{2VmV}\end{bmatrix}\begin{bmatrix}\Delta p\\ \Delta r\end{bmatrix} \tag{2.29}$$

$$\begin{bmatrix}\Delta\dot{p}\\ \Delta\dot{r}\end{bmatrix} = \begin{bmatrix} 0 & \bar{q}Sb(c_3C_{l\beta} + c_4C_{n\beta}) \\ 0 & \bar{q}Sb(c_4C_{l\beta} + c_9C_{n\beta})\end{bmatrix}\begin{bmatrix}\Delta\phi\\ \Delta\beta\end{bmatrix} + \begin{bmatrix} \frac{\bar{q}Sb^2}{2V}(c_3C_{lp} + c_4C_{np}) & \frac{\bar{q}Sb^2}{2V}(c_3C_{lr} + c_4C_{nr}) \\ \frac{\bar{q}Sb^2}{2V}(c_4C_{lp} + c_9C_{np}) & \frac{\bar{q}Sb^2}{2V}(c_4C_{lr} + c_9C_{nr})\end{bmatrix}\begin{bmatrix}\Delta p\\ \Delta r\end{bmatrix} +$$

$$\begin{bmatrix} \bar{q}Sb(c_3C_{l\delta_a} + c_4C_{n\delta_a}) & \bar{q}Sb(c_3C_{l\delta_r} + c_4C_{n\delta_r}) \\ \bar{q}Sb(c_4C_{l\delta_a} + c_9C_{n\delta_a}) & \bar{q}Sb(c_4C_{l\delta_r} + c_9C_{n\delta_r})\end{bmatrix}\begin{bmatrix}\Delta\delta_a\\ \Delta\delta_r\end{bmatrix} \tag{2.30}$$

From Eq. (2.29), $\begin{bmatrix}\Delta p\\ \Delta r\end{bmatrix}$ is extracted as

$$\begin{bmatrix}\Delta p\\ \Delta r\end{bmatrix} = \begin{bmatrix}1 & tan\alpha_t\\ tan\alpha_t + \frac{C_{Yp}b\bar{q}S}{2VmV} & -1 + \frac{C_{Yr}b\bar{q}S}{2VmV}\end{bmatrix}^{-1}\begin{bmatrix}\Delta\dot{\phi}\\ \Delta\dot{\beta} - \frac{g}{V}cos\alpha_t\Delta\phi - \frac{\bar{q}SC_{Y\beta}}{mV}\Delta\beta\end{bmatrix} \quad (2.31)$$

$$\begin{bmatrix}\Delta\ddot{\phi}\\ \Delta\ddot{\beta}\end{bmatrix} = \begin{bmatrix}0 & 0\\ \frac{g}{V}cos\alpha_t & \frac{\bar{q}SC_{Y\beta}}{mV}\end{bmatrix}\begin{bmatrix}\Delta\dot{\phi}\\ \Delta\dot{\beta}\end{bmatrix} + \begin{bmatrix}1 & tan\alpha_t\\ tan\alpha_t + \frac{C_{Yp}b\bar{q}S}{2VmV} & -1 + \frac{C_{Yr}b\bar{q}S}{2VmV}\end{bmatrix}\begin{bmatrix}\Delta\dot{p}\\ \Delta\dot{r}\end{bmatrix} \quad (2.32)$$

On substituting Eq. (2.29) and Eq. (2.30) in Eq. (2.32) can be finally expressed in the form

$$\Delta\ddot{\phi} = a_{11}\Delta\phi + a_{12}\Delta\dot{\phi} + a_{13}\Delta\beta + a_{14}\Delta\dot{\beta} + b_{11}\,\Delta\delta_a + b_{12}\,\Delta\delta_r \quad (2.33)$$

$$\Delta\ddot{\beta} = a_{21}\Delta\phi + a_{22}\Delta\dot{\phi} + a_{23}\Delta\beta + a_{23}\Delta\dot{\beta} + b_{21}\,\Delta\delta_a + b_{22}\,\Delta\delta_r \quad (2.34)$$

where a_{ij} and b_{ij} are constants. Since the equilibrium values of ϕ, β and δ_a, δ_r are all zero for steady wing-level flight, $\Delta\phi = \phi$, $\Delta\beta = \beta$, $\Delta\delta_a = \delta_a$, $\Delta\delta_r = \delta_r$. Therefore,

$$\ddot{\phi} = a_{11}\phi + a_{12}\dot{\phi} + a_{13}\beta + a_{14}\dot{\beta} + b_{11}\delta_a + b_{12}\delta_r \quad (2.35)$$

$$\ddot{\beta} = a_{21}\phi + a_{22}\dot{\phi} + a_{23}\beta + a_{23}\dot{\beta} + b_{21}\delta_a + b_{22}\delta_r \quad (2.36)$$

To convert the tracking problem into a regulator problem, let us define the errors as follows:

$$e_\phi = \phi - \phi_d \text{ and } \dot{e}_\phi = \dot{\phi} - \dot{\phi}_d \quad (2.37)$$

$$e_\beta = \beta - \beta_d \text{ and } \dot{e}_\beta = \dot{\beta} - \dot{\beta}_d \quad (2.38)$$

Substituting Eq. (2.37) in Eq. (2.35) we get,

$$\ddot{e}_\phi = a_{11}e_\phi + a_{12}\dot{e}_\phi + a_{13}e_\beta + a_{14}\dot{e}_\beta + b_{11}\delta_a + b_{12}\delta_r + a_{11}\phi_d + a_{12}\dot{\phi}_d + a_{13}\,\beta_d + a_{14}\dot{\beta}_d - \ddot{\phi}_d \quad (2.39)$$

$$\ddot{e}_\phi = a_{11}e_\phi + a_{12}\dot{e}_\phi + a_{13}e_\beta + a_{14}\dot{e}_\beta + b_{11}\delta_a + b_{12}\delta_r + f_1(t) \quad (2.40)$$

where

$$f_1(t) = a_{11}\phi_d + a_{12}\dot{\phi}_d + a_{13}\,\beta_d + a_{14}\dot{\beta}_d - \ddot{\phi}_d \quad (2.41)$$

Similarly,

$$\ddot{e}_\beta = a_{21}e_\phi + a_{22}\dot{e}_\phi + a_{23}e_\beta + a_{14}\dot{e}_\beta + b_{21}\delta_a + b_{22}\delta_r + a_{21}\phi_d + a_{22}\dot{\phi}_d + a_{23}\,\beta_d + a_{24}\dot{\beta}_d + \ddot{\beta}_d \quad (2.42)$$

$$\ddot{e}_\beta = a_{21}e_\phi + a_{22}\dot{e}_\phi + a_{23}e_\beta + a_{14}\dot{e}_\beta + b_{21}\delta_a + b_{22}\delta_r + f_2(t) \quad (2.43)$$

where

$$f_2(t) = a_{21}\phi_d + a_{22}\dot{\phi}_d + a_{23}\,\beta_d + a_{24}\dot{\beta}_d + \ddot{\beta}_d \tag{2.44}$$

Letting $x_1 = e_\phi,\ x_2 = \dot{e}_\phi,\ x_3 = e_\beta,\ x_4 = \dot{e}_\beta$ and $u_1 = b_{11}\delta_a + b_{12}\delta_r + f_1(t),\ u_2 = b_{21}\delta_a + b_{22}\delta_r + f_2(t)$, Eqs (2.40) and (2.43) can be expressed as

$$\begin{bmatrix}\dot{x}_1\\ \dot{x}_2\\ \dot{x}_3\\ \dot{x}_4\end{bmatrix} = \begin{bmatrix}0 & 1 & 0 & 0\\ a_{11} & a_{12} & a_{13} & a_{14}\\ 0 & 0 & 0 & 1\\ a_{21} & a_{22} & a_{23} & a_{24}\end{bmatrix}\begin{bmatrix}x_1\\ x_2\\ x_3\\ x_4\end{bmatrix} + \begin{bmatrix}0 & 0\\ 1 & 0\\ 0 & 0\\ 0 & 1\end{bmatrix}\begin{bmatrix}u_1\\ u_2\end{bmatrix} \tag{2.45}$$

Now, considering the dynamics given by Eq. (2.45), $u_1(t)$ and $u_2(t)$ can be generated from LQR algorithm. Since

$$\begin{bmatrix}u_1\\ u_2\end{bmatrix} = \begin{bmatrix}b_{11} & b_{12}\\ b_{21} & b_{22}\end{bmatrix}\begin{bmatrix}\delta_a\\ \delta_r\end{bmatrix} + \begin{bmatrix}f_1(t)\\ f_2(t)\end{bmatrix} \tag{2.46}$$

the final control surface deflection commands can be obtained as

$$\begin{bmatrix}\delta_a\\ \delta_r\end{bmatrix} = \begin{bmatrix}b_{11} & b_{12}\\ b_{21} & b_{22}\end{bmatrix}^{-1}\begin{bmatrix}u_1 - f_1(t)\\ u_2 - f_2(t)\end{bmatrix} \tag{2.47}$$

LQR is a controller that is alike to pole placement method, but instead of computing the controller gain matrix based on the selected pole locations, it is calculated by minimizing the cost functional $J = \int_0^\infty (x^T Q x + u^T R u)dt$ where Q is the weighing function of states and R is the weighing function of the control variables. Q and R, are normally treated as tuning parameters.

2.3.3 Simulation Results and Performance Analysis

In this sub-section, low alpha maneuvers namely the horizontal turn maneuver and the aileron roll maneuvers are implemented using LQR control technique as formulated in the previous subsection when the c.g. of aircraft is at the reference point in the plane of symmetry. To perform the horizontal turn maneuver using LQR control design approach, a bell-shaped curve for desired roll angle (φ) profile as shown in Figure 2.2 is generated as $\phi_d(t) = \frac{1}{1+\left|\frac{t-c}{a}\right|^{2b}}$ the value of a, b, and c are set with

trial and error and listed in Table 2.1 keeping sideslip angle (β) zero. A maneuver duration of $18s$ starting at $t = 0$ is considered with the initial trim at a velocity of $20m/s$ at an altitude of $1000m$. The trajectory, time evolution of relevant variables and the profiles of the control signals are shown in Figure 2.4. Similarly, for aileron roll maneuver, a sigmoid function for desired roll angle (φ) profile as shown in Figure 2.2 is taken into consideration while keeping sideslip angle (β) zero. The UAV is commanded to execute two full rotation about its body x-axis in $4s$. Initial trim conditions are kept at the same values as considered for horizontal turn maneuver. The time evolution of relevant variables and the profiles of control signals for aileron roll maneuver are shown in Figure 2.5. On substituting the values of various aerodynamics and geometric parameters as given in Appendix-C [93], the error dynamics given by Eq. (2.45) is

$$\begin{bmatrix}\dot{x_1}\\ \dot{x}_2\\ \dot{x}_3\\ \dot{x}_4\end{bmatrix} = \begin{bmatrix}0 & 1 & 0 & 0\\ 2 & -7.315 & -36.6 & -4.168\\ 0 & 0 & 0 & 1\\ 2.72 & 0.20 & -59.21 & -6.125\end{bmatrix}\begin{bmatrix}x_1\\ x_2\\ x_3\\ x_4\end{bmatrix} + \begin{bmatrix}0 & 0\\ 1 & 0\\ 0 & 0\\ 0 & 1\end{bmatrix}\begin{bmatrix}u_1\\ u_2\end{bmatrix} \tag{2.48}$$

LQR for above Eq. (2.48) will give $u_1(t)$ and $u_2(t)$.

$$\text{Now, } \begin{bmatrix}u_1\\ u_2\end{bmatrix} = \begin{bmatrix}39.56 & 43.78\\ -6.915 & 13.256\end{bmatrix}\begin{bmatrix}\delta_a\\ \delta_r\end{bmatrix} + \begin{bmatrix}f_1(t)\\ f_2(t)\end{bmatrix} \tag{2.49}$$

$$\text{hence } \begin{bmatrix}\delta_a\\ \delta_r\end{bmatrix} = \begin{bmatrix}39.56 & 43.78\\ -6.915 & 13.256\end{bmatrix}^{-1}\begin{bmatrix}u_1 - f_1(t)\\ u_2 - f_2(t)\end{bmatrix} \tag{2.50}$$

Various controller parameters such as Q, R and K are listed in Table 2.2.

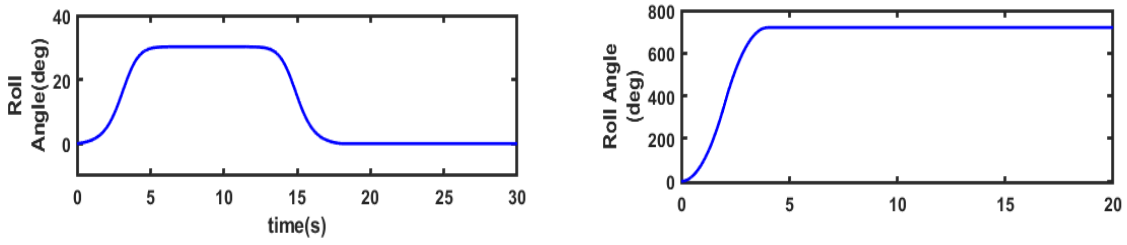

Figure 2.2. Time profiles of reference signals for Horizontal turn and Aileron roll maneuver

Table 2.1: Desired reference signal parameters: Horizontal turn maneuver

Reference signal	***a***	***b***	***c***
Roll Angle (ϕ)	6	5	9

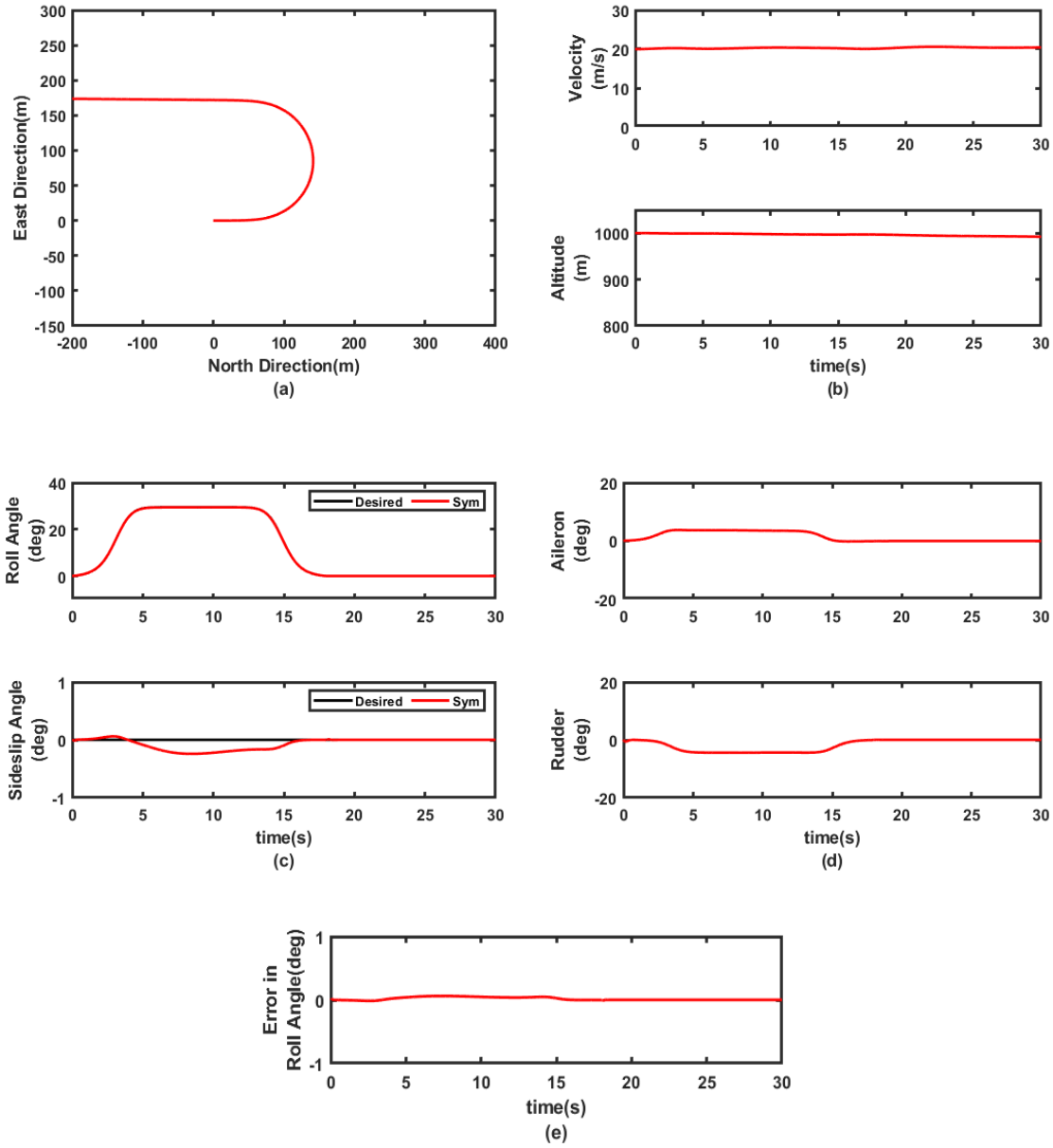

Figure 2.3. Time evolution of states and controls for horizontal turn maneuver when c.g. at nominal position: LQR design approach

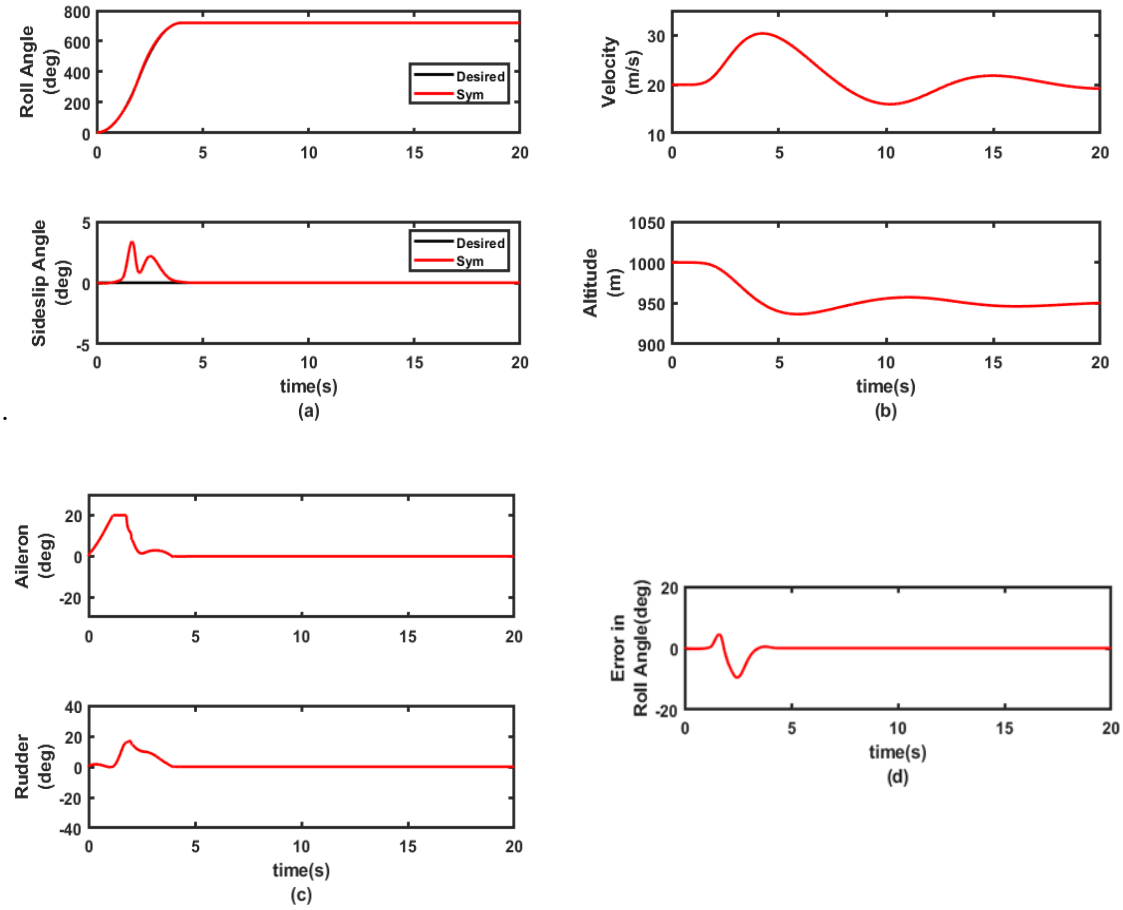

Figure 2.4. Time evolution of states and controls for aileron roll maneuver when c.g. at nominal position: LQR design approach

Table 2.2: LQR controller parameters

Maneuver	***Q***	***R***	**Controller gain matrix *K***
Horizontal turn	$\begin{bmatrix} 1 & 0 & 0 & 0 \\ 0 & 0.1 & 0 & 0 \\ 0 & 0 & 0.1 & 0 \\ 0 & 0 & 0 & 0.1 \end{bmatrix}$	$\begin{bmatrix} 0.2 & 0 \\ 0 & 0.1 \end{bmatrix}$	$\begin{bmatrix} 67.0331 & 7.7252 & -16.5118 & -2.2863 \\ -36.7360 & -4.5726 & 14.8027 & 7.8315 \end{bmatrix}$
Aileron roll	$\begin{bmatrix} 10 & 0 & 0 & 0 \\ 0 & 0.1 & 0 & 0 \\ 0 & 0 & 0.01 & 0 \\ 0 & 0 & 0 & 0.01 \end{bmatrix}$	$\begin{bmatrix} 0.001 & 0 \\ 0 & 0.002 \end{bmatrix}$	$\begin{bmatrix} 99.1795 & 11.2361 & -18.5499 & -3.5505 \\ -14.2350 & -1.7520 & 4.1753 & 1.5797 \end{bmatrix}$

In Figure 2.4, the results clearly showcase outstanding performance during the horizontal turn maneuver, with the commanded and actual profiles nearly overlapping, and aileron and rudder deflections well within their limits. Altitude and velocity variations are minimal, reflecting a good tracking capability. This commendable tracking performance is also observed during the aileron roll maneuver, as illustrated in Figure 2.5.

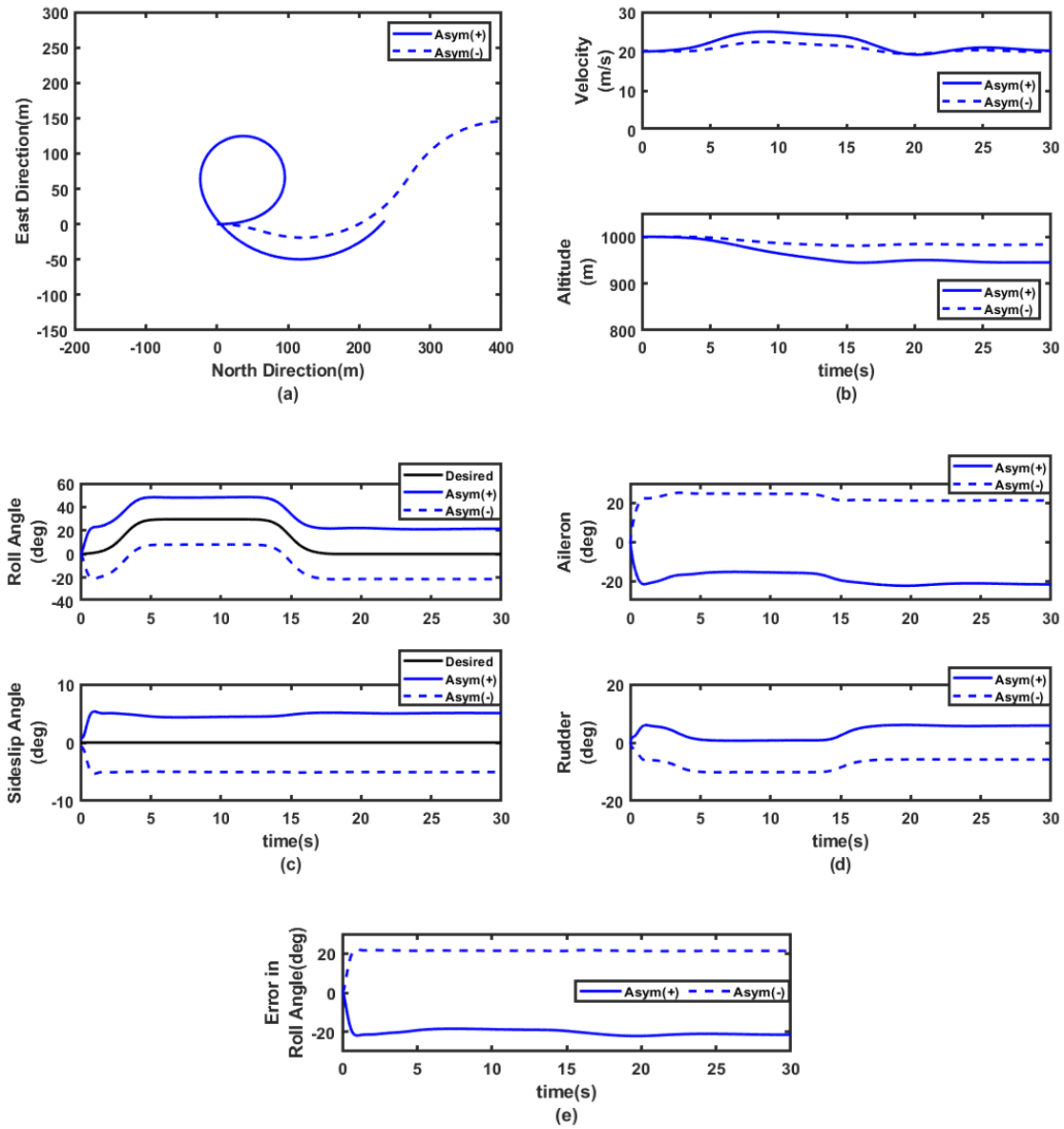

Figure 2.5. Time evolution of states and controls for horizontal turn maneuver under lateral c.g. variation: LQR design approach

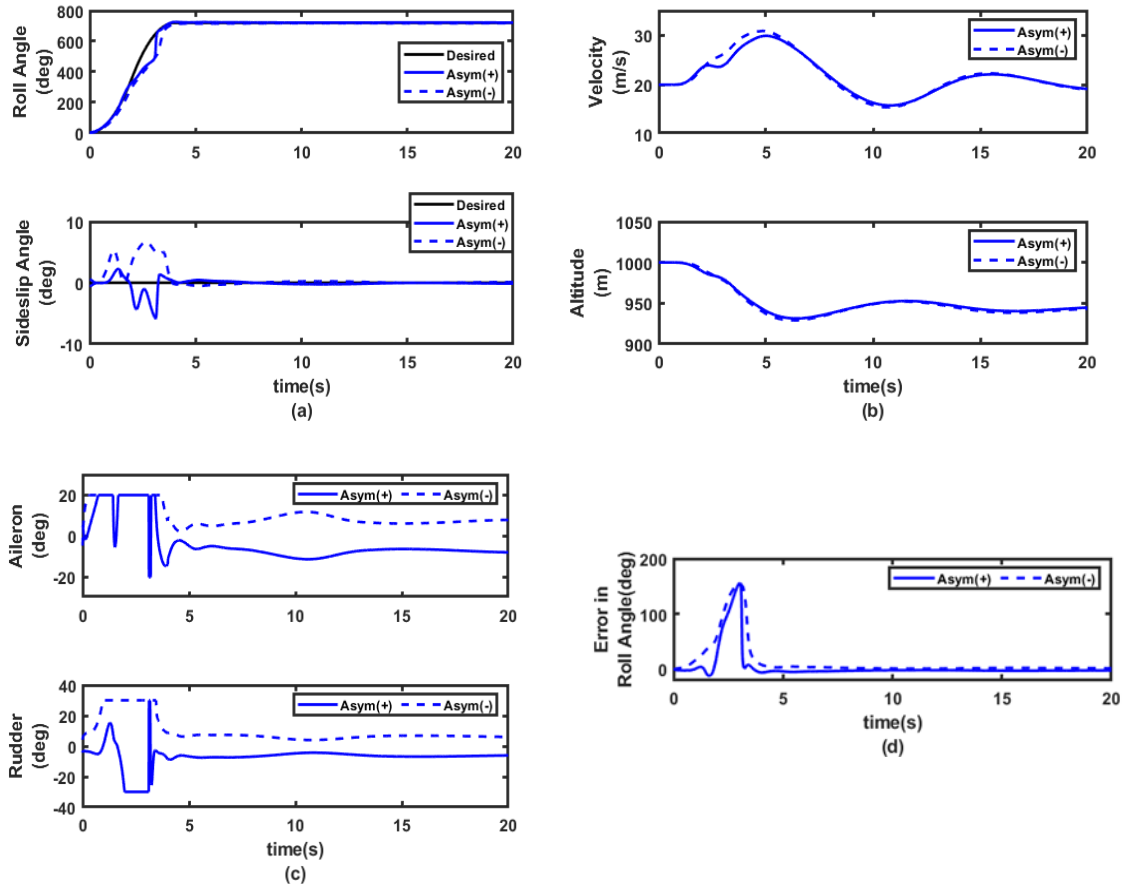

Figure 2.6. Time evolution of states and controls for aileron roll maneuver under lateral c.g. variation: LQR design approach

However, when the same controller is subjected to the asymmetric conditions, the horizontal turn maneuver could not be performed at all, whereas, for the aileron roll maneuver, the closed-loop system experiences a noticeable decline in maneuver performance as evident from Figures 2.5 and 2.6. To simulate the asymmetric dynamics, the c.g. of the UAV is assumed to move laterally on either side of the fuselage centerline. It is assumed that the UAV carries a single store of 1.5 kg (which is 10% of the mass of the UAV and the store combined) mounted either on the starboard side (referred to as Asym+) or on the port side (referred to as Asym-) half of the semispan away from the body centerline. This gives rise to a lateral c.g. movement of $\pm 7.0\ cm$. The UAV is assumed to be initially

trimmed at the same conditions as considered before. The aerodynamic control surfaces are assumed to have saturation limits (values given in Appendix-C). The failure of a robust linear control technique such as the LQR to successfully mitigate the c.g. uncertainty issue prompts us to try a nonlinear control law, which is discussed next.

2.4 Backstepping based Nonlinear Control Design for the Nominal System

The previous section highlights a limitation of linear control techniques in adequately handling maneuvers when the center of gravity deviates from its nominal position due to various reasons such as uneven fuel consumption, asymmetric payload distribution or release, structural damage, etc. This inadequacy necessitates the implementation of nonlinear control techniques to automatically execute such maneuvers. To investigate the effects of lateral c.g. variations on lateral maneuvers, let us first consider the nominal or symmetric case. The same two lateral maneuvers namely horizontal turn and aileron roll maneuvers are analyzed in the same manner as in the previous section.

In this context, a well-established nonlinear control technique capable of effectively handling nonlinear dynamics is employed. Specifically, the backstepping control law is chosen as unlike the nonlinear dynamic inversion technique, it does not have to rely on two time scale separation principle when applied to flight control problems [41,111]. In the subsequent subsection, the basics of backstepping control are briefly reviewed.

2.4.1 A Brief Overview of Backstepping Control [94]

Backstepping, as an energy-based method, emerges as a potent tool in tackling the control challenges posed by nonlinear systems. Rooted in Lyapunov theory, it offers a versatile approach to control design. A key strength lies in its unique ability to decompose the control problem of an nth order system into n numbers of first order interconnected system. The general idea behind backstepping

control is to transform the original nonlinear system into a series of subsystems, and then design controllers for each subsystem. The control law is constructed in a recursive manner, starting from the final state of the system and working backward toward the initial state. This recursive approach of the backstepping often serves as an advantageous feature during the design of control law for complicated nonlinear dynamic systems.

However, the ordinary integral backstepping method relies on the assumption that the system conforms to a strict feedback structure, typically found in single-input single-output (SISO) nonlinear systems. But, when dealing with multivariable control problems, it is common to encounter systems that do not fit into strict feedback or semi-strict feedback (i.e., lower triangular) form. Consequently, applying the integral backstepping approach directly becomes impractical for devising control laws in multiple-input multiple-output (MIMO) systems. This limitation prompts the need for alternative strategies. One such effective approach is the block backstepping technique, which offers a solution for addressing control challenges in diverse nonlinear MIMO systems.

Here is an overview of the block backstepping control algorithm:

Let $\dot{\boldsymbol{x_1}} = \boldsymbol{f_1}(\boldsymbol{x_1}) + G_1(\boldsymbol{x_1})\boldsymbol{x_2}$ (2.51)

be the highest-order dynamics of the system, where $\boldsymbol{x_1}$ represents the states that are being regulated, $\boldsymbol{f_1}(\boldsymbol{x_1})$ represents the nominal dynamics, and $G_1(\boldsymbol{x_1})$ represents the control input influence matrix.

To ensure asymptotic convergence of $\boldsymbol{x_1}$, the desired profile for the virtual control is computed as

$$\boldsymbol{x_{2d}} = (G_1)^{-1}(-\boldsymbol{f_1} - K_1\boldsymbol{x_1}) \quad (2.52)$$

Now, considering the next highest-order dynamics as

$$\dot{\boldsymbol{x_2}} = \boldsymbol{f_2}(\boldsymbol{x}) + G_2(\boldsymbol{x})\,\boldsymbol{u} \quad (2.53)$$

the final control $\boldsymbol{u}$ can be computed as

$$\boldsymbol{u} = (G_2)^{-1}(-\boldsymbol{f_2} - K_2\boldsymbol{e_2} - G_1^T\boldsymbol{x_1} + \dot{\boldsymbol{x}}_{\boldsymbol{2d}}) \tag{2.54}$$

to ensure asymptotic convergence of both of $\boldsymbol{x_1}$ and $\boldsymbol{e_2}$ where $\boldsymbol{e_2} = \boldsymbol{x_2} - \boldsymbol{x_{2d}}$ is the error in the virtual control.

Backstepping control finds extensive use in controlling highly nonlinear systems, such as those encountered in robotics, aerospace, and many other engineering domains. . It is a powerful tool in the control engineer's toolkit for addressing challenging nonlinear control problems. However, its successful application requires accurate knowledge of the system dynamics.

2.4.2 Control Formulation and Design

In this sub-section, the coupled aircraft equations of motion are converted to strict feedback form to make it amenable to backstepping based control design. The formulation is aimed to autonomously execute the intended lateral maneuver when aircraft is symmetric along fuselage centerline. For carrying out such maneuvers, suitable time profiles of appropriate angular variables are fed externally as reference input in same manner as in previous section, and the closed loop controller then generates the necessary control surface deflection commands as shown in Figure 2.7. The detailed analysis of the proposed controller is discussed below.

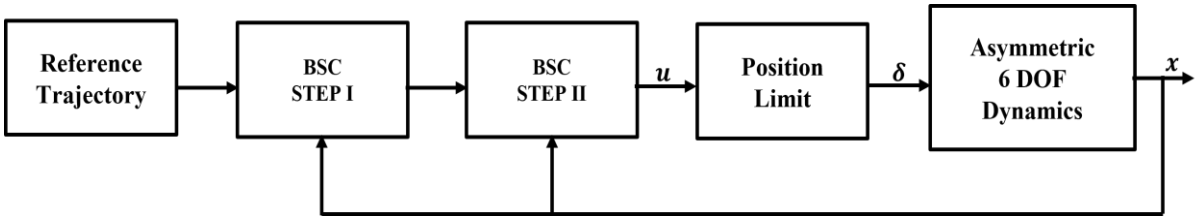

Figure 2.7. Closed loop diagram of backstepping control scheme

From Eqs. (2.8) - (2.11), angular and angular rate dynamics can be separated as

$$\begin{bmatrix}\dot{\phi}\\ \dot{\beta}\end{bmatrix} = \begin{bmatrix}0\\ \frac{g}{V}sin\phi cos\alpha_t + \frac{\bar{q}SC_Y(\beta)}{mV}\end{bmatrix} + \begin{bmatrix}1 & tan\alpha_t cos\phi\\ tan\alpha_t & -1\end{bmatrix}\begin{bmatrix}p\\ r\end{bmatrix} \tag{2.55}$$

$$\begin{bmatrix}\dot{p}\\ \dot{r}\end{bmatrix} = \begin{bmatrix}c_3 & c_4\\ c_4 & c_9\end{bmatrix}\begin{bmatrix}\bar{q}Sb(C_{l\beta}\beta + C_{lp}\frac{pb}{2V} + C_{lr}\frac{rb}{2V})\\ \bar{q}Sb(C_{n\beta}\beta + C_{np}\frac{pb}{2V} + C_{nr}\frac{rb}{2V})\end{bmatrix} + \bar{q}Sb\begin{bmatrix}c_3 & c_4\\ c_4 & c_9\end{bmatrix}\begin{bmatrix}C_{l\delta a} & C_{l\delta r}\\ C_{n\delta a} & C_{n\delta r}\end{bmatrix}\begin{bmatrix}\delta_a\\ \delta_r\end{bmatrix} \tag{2.56}$$

Let $x_1 = \begin{bmatrix}\phi\\ \beta\end{bmatrix}$, and $x_2 = \begin{bmatrix}p\\ r\end{bmatrix}$ be the virtual control, and $u = \begin{bmatrix}\delta_a\\ \delta_r\end{bmatrix}$ be the actual control variables. Therefore, Eqs. (2.55) and (2.56) can be represented in the general block strict feedback form

$$\boldsymbol{\dot{x}_1} = \boldsymbol{f_1}(\boldsymbol{x_1}) + G_1(\boldsymbol{x_1})\boldsymbol{x_2} \tag{2.57}$$

$$\boldsymbol{\dot{x}_2} = \boldsymbol{f_2}(x) + G_2\boldsymbol{u} \tag{2.58}$$

where $\boldsymbol{f_1}, \boldsymbol{f_2}$ are 2×1 vector valued functions and G_1, G_2 are 2×2 matrices and all these are known at every time step from the assumption of availability of full state feedback.

Introducing error variables $\boldsymbol{e_1}$ and $\boldsymbol{e_2}$ as $\boldsymbol{e_1} = \boldsymbol{x_1} - \boldsymbol{x_{1d}}$ and $\boldsymbol{e_2} = \boldsymbol{x_2} - \boldsymbol{x_{2d}}$ where $\boldsymbol{x_{1d}}$ and $\boldsymbol{x_{2d}}$ are the desired trajectories of $\boldsymbol{x_1}$ and $\boldsymbol{x_2}$, the dynamic equation of $\boldsymbol{e_1}$ is given by

$$\boldsymbol{\dot{e}_1} = \boldsymbol{\dot{x}_1} - \boldsymbol{\dot{x}_{1d}} = \boldsymbol{f_1}(\boldsymbol{x_1}) + G_1(\boldsymbol{x_1})\boldsymbol{x_2} - \boldsymbol{\dot{x}_{1d}} \tag{2.59}$$

Let the Lyapunov function for the dynamics given by Eq. (2.59) be

$$V_1 = \frac{1}{2}\boldsymbol{e_1^T e_1} \tag{2.60}$$

On differentiating Eq. (2.60)

$$\dot{V}_1 = \boldsymbol{e_1^T \dot{e}_1} = \boldsymbol{e_1^T}[\boldsymbol{f_1} + G_1\boldsymbol{x_2} - \boldsymbol{\dot{x}_{1d}}] \tag{2.61}$$

Let, $\boldsymbol{f_1} + G_1\boldsymbol{x_2} - \boldsymbol{\dot{x}_{1d}} = -K_1\boldsymbol{e_1}$ (2.62)

where K_1 is a constant positive definite matrix.

$$\dot{V}_1 = -\boldsymbol{e_1^T} K_1 \boldsymbol{e_1} < 0 \tag{2.63}$$

From Eq. (2.62), the desired profile for the virtual control is computed as

$$\boldsymbol{x_{2d}} = (G_1)^{-1}(-K_1\boldsymbol{e_1} + \dot{\boldsymbol{x}}_{\boldsymbol{1d}} - \boldsymbol{f_1}) \tag{2.64}$$

The Lyapunov function for the complete dynamics is chosen as

$$V_2 = \frac{1}{2}\boldsymbol{e_1^T e_1} + \frac{1}{2}\boldsymbol{e_2^T e_2} \tag{2.65}$$

Therefore,

$$\dot{V}_2 = \boldsymbol{e_1^T \dot{e}_1} + \boldsymbol{e_2^T \dot{e}_2} = \boldsymbol{e_1^T}[\boldsymbol{f_1} + G_1\boldsymbol{e_2} + G_1\boldsymbol{x_{2d}} - \dot{\boldsymbol{x}}_{\boldsymbol{1d}}] + \boldsymbol{e_2^T \dot{e}_2} \tag{2.66}$$

Substituting Eq. (2.64) in Eq. (2.66),

$$\dot{V}_2 = -\boldsymbol{e_1^T}K_1\boldsymbol{e_1} + \boldsymbol{e_1^T}G_1\boldsymbol{e_2} + \boldsymbol{e_2^T \dot{e}_2} \tag{2.67}$$

Let, $\dot{\boldsymbol{e}}_{\boldsymbol{2}} = -K_2\boldsymbol{e_2} - G_1^T\boldsymbol{e_1}$ (2.68)

where K_2 is a constant positive definite matrix. This leads to

$$\dot{V}_2 = -\boldsymbol{e_1^T}K_1\boldsymbol{e_1} - \boldsymbol{e_2^T}K_2\boldsymbol{e_2} < 0 \tag{2.69}$$

Substituting Eq. (2.68) in Eq. (2.58), the final control input is computed as

$$u = (G_2)^{-1}(-\boldsymbol{f_2} - K_2\boldsymbol{e_2} - G_1^T\boldsymbol{e_1} + \dot{\boldsymbol{x}}_{\boldsymbol{2d}}) \tag{2.70}$$

where $\dot{\boldsymbol{x}}_{\boldsymbol{2d}}$ is computed from Eq. (2.64).

2.4.3 Simulation Results and Performance Analysis

In this sub-section, low alpha maneuvers namely the horizontal turn maneuver and the aileron roll maneuvers are implemented using backstepping control technique as formulated in the previous subsection when the c.g. of aircraft is at the reference point in the plane of symmetry. Let this control approach be called nominal backstepping scheme. Both the maneuvers are considered under the

same initial trim condition as in previous section. The trajectory, time evolution of relevant variables and the profiles of the control signals of horizontal turn and aileron roll maneuvers are shown in Figure 2.8 and Figure 2.9 respectively. Various controller parameters as tuned through trial and error are listed in Table 2.3. Aerodynamic and geometric data of the UAV are summarized in the Appendix-C for the sake of ready reference.

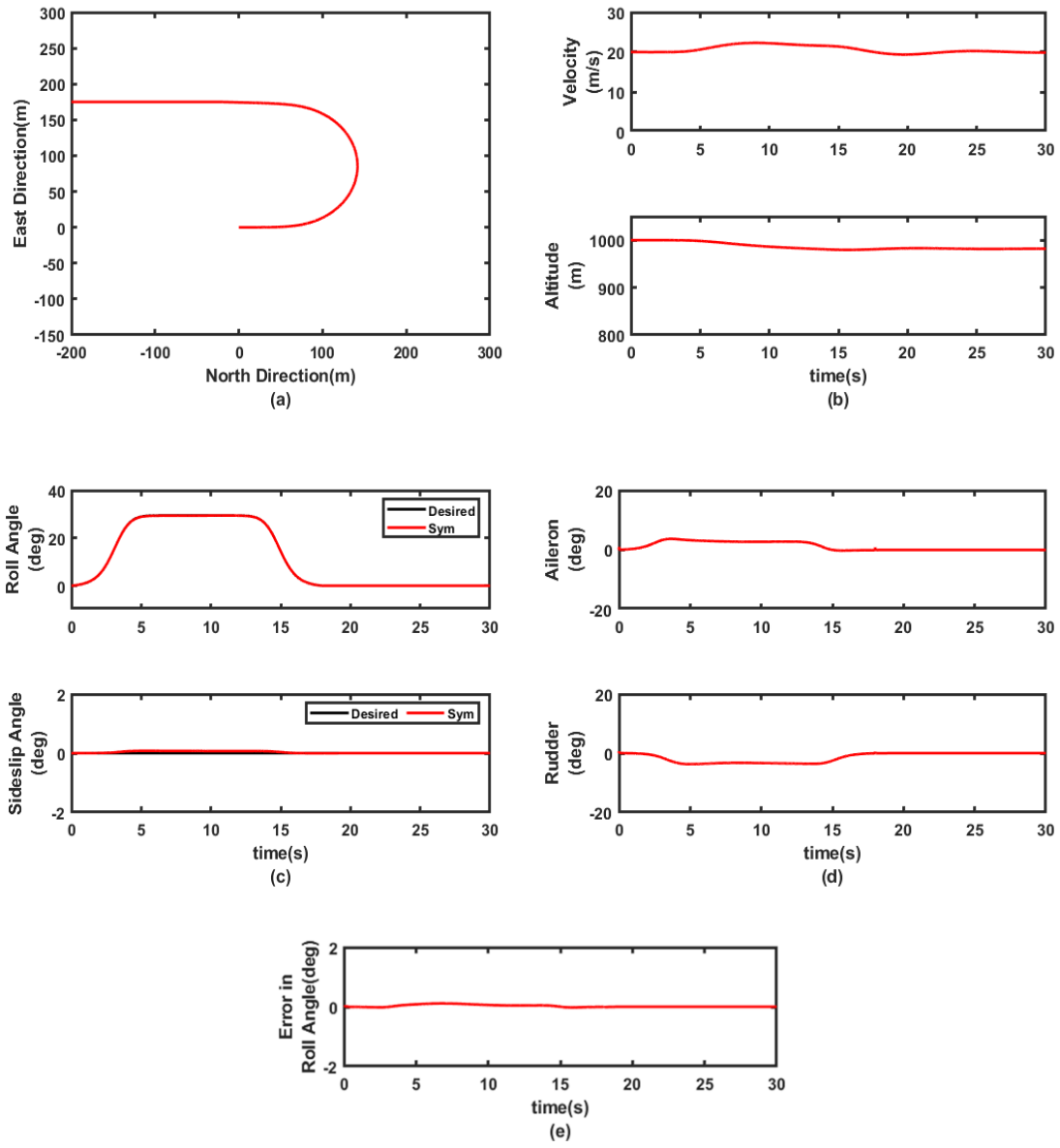

Figure 2.8. Time evolution of states and controls for horizontal turn maneuver when c.g. at nominal position: Backstepping design approach

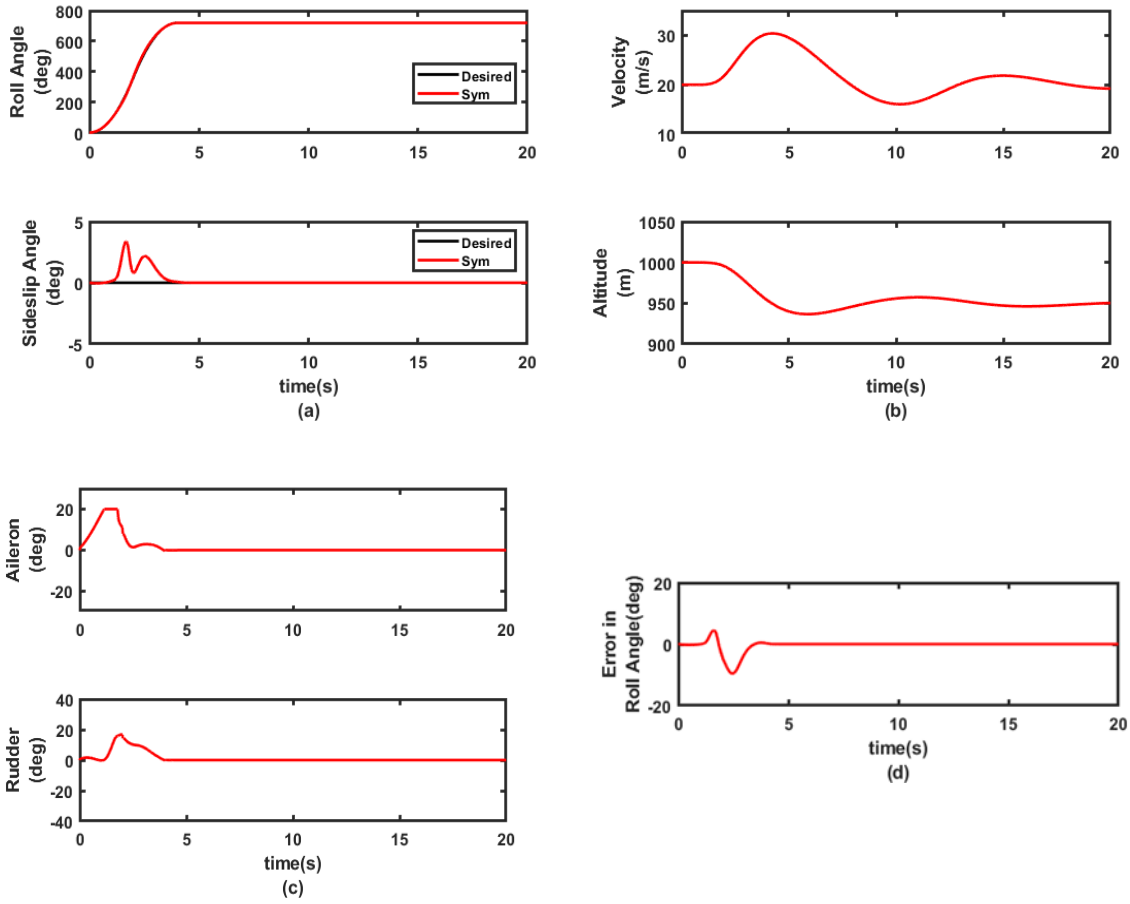

Figure 2.9. Time evolution of states and controls for aileron roll maneuver maneuver when c.g. at nominal position: Backstepping design approach

From Figure 2.8 it is evident that an excellent performance for horizontal turn maneuver is achieved with the flight taking exact turn of 180^0 within 90m turn radius and good tracking result is obtained as commanded and actual profiles are almost overlapping with each other with aileron and rudder deflections well within their saturation limits. Variations in altitude and total velocity are also negligible. Similarly, excellent tracking performance within control surface deflection saturation limit is also obtained for aileron roll maneuver as depicted in Figure 2.9. However, when the same controller is retained in the asymmetric situation, again, the performance of the closed loop system undergoes significant degradation as it is easily noticeable in both the maneuvers as represented in

Figures 2.10 and 2.11. In fact, the controller completely fails to execute the horizontal turn maneuver. To mitigate this performance degradation under lateral c.g. movement, an adaptive backstepping control scheme based on an ad-hoc representation of the asymmetric dynamics is proposed in the next section.

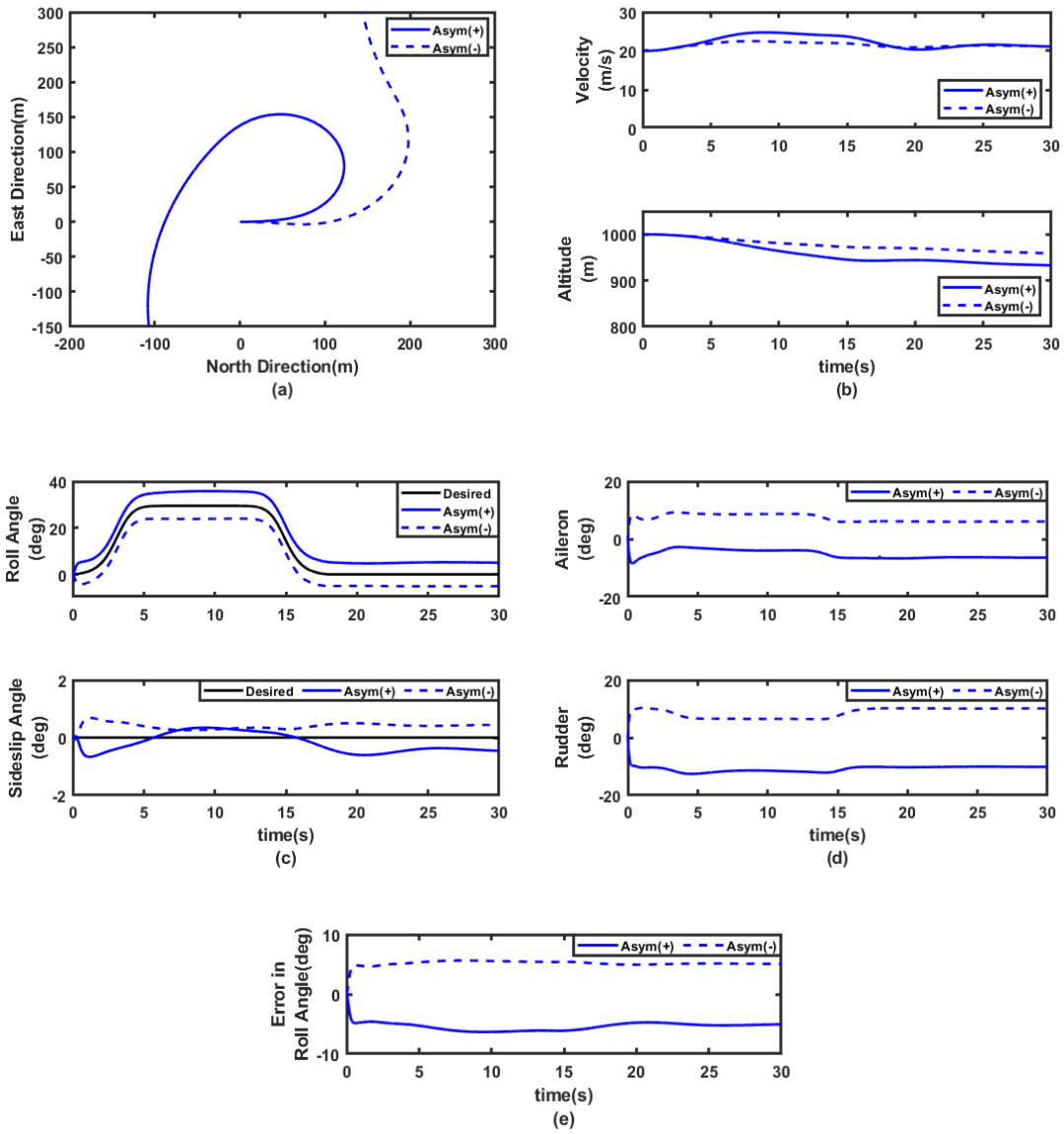

Figure 2.10. Time evolution of states and controls for horizontal turn maneuver under lateral c.g. variation: Backstepping design approach

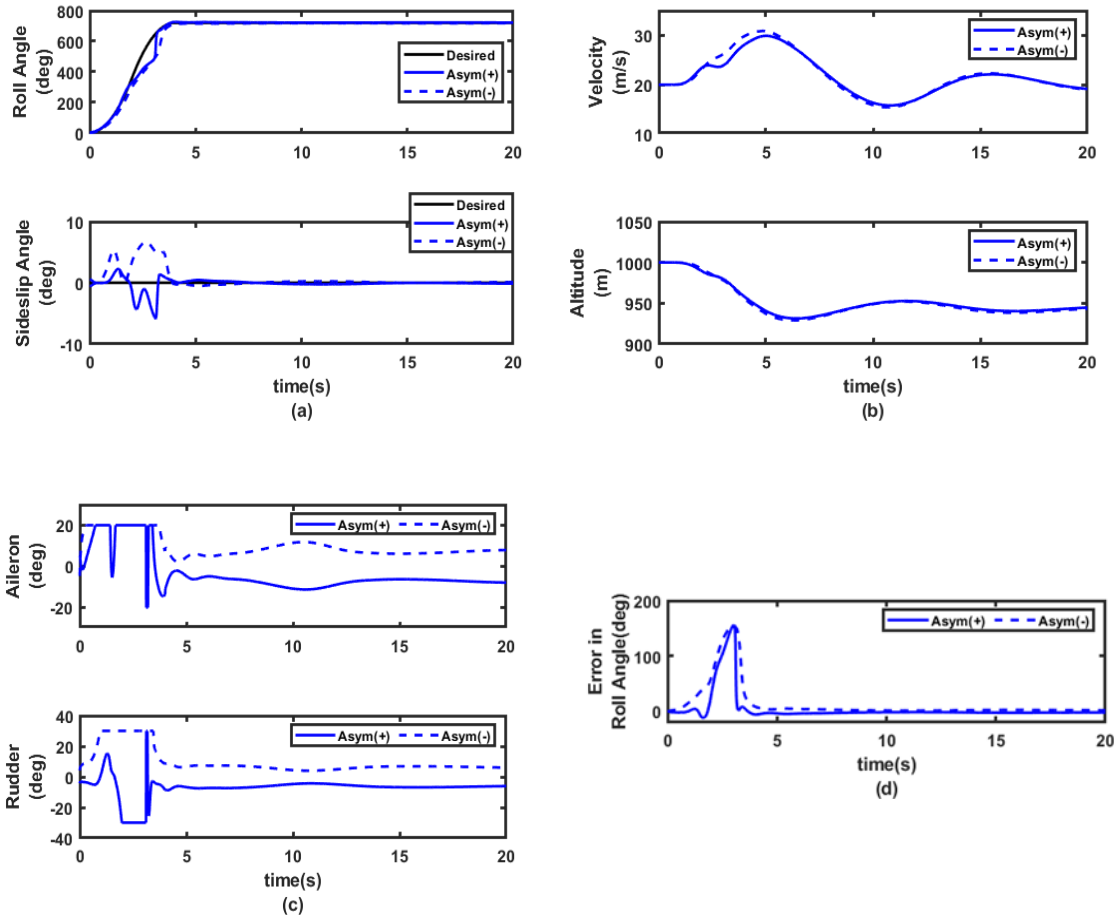

Figure 2.11. Time evolution of states and controls for aileron roll maneuver under lateral c.g. variation: Backstepping design approach

Table 2.3: Backstepping controller parameters

Maneuver	K_1	K_2
Horizontal turn	$\begin{bmatrix} 15 & 0 \\ 0 & 10 \end{bmatrix}$	$\begin{bmatrix} 10 & 0 \\ 0 & 5 \end{bmatrix}$
Aileron roll	$\begin{bmatrix} 15 & 0 \\ 0 & 20 \end{bmatrix}$	$\begin{bmatrix} 18 & 0 \\ 0 & 10 \end{bmatrix}$

2.5 Adaptive Block Backstepping Control Design under Lateral C.G. Uncertainty

It can be observed from the simulation results in the previous section that when the c.g. of the vehicle vary in the lateral direction from the plane of symmetry, the backstepping control itself is not robust enough to handle the c.g. variation caused by various reasons such as uneven fuel consumption, asymmetric payload distribution or release, structural damage, etc. The lateral c.g., shift causes loss of geometric symmetry of the vehicle, leading to complex coupled nonlinear flight dynamics that are extremely challenging from control design perspectives especially when attempting some fast lateral maneuvers.

To address this challenge, our focus shifts in this section towards making the backstepping controller adaptive. This adaptability ensures that the controller can effectively handle maneuvers even in the presence of realistic uncertainty regarding the lateral c.g. location. By making the backstepping controller adaptive, we aim to maintain maneuver performance without experiencing degradation due to unpredictable shifts in c.g. position.

2.5.1 Problem Formulation and System Dynamics

In this sub-section, we turn our focus to make backstepping controller adaptive when the entire mass of the UAV is displaced by specific distances, denoted as x_{cm}, y_{cm}, and z_{cm}, relative to its initial nominal position. The body frame's origin remains fixed in the primary nominal position within the plane of symmetry. As we primarily concentrate on lateral c.g. movements, hence we assume that x_{cm} and z_{cm} are both zero. Since a c.g. offset will predominantly generate a rolling moment, an additional rolling moment due to gravity term is added to the standard rotational dynamics. The rotational kinematics part remains unchanged. This leads to the modified equations of motion as given below by Eqs. (2.71) and (2.72). The second term on the right-hand side of Eq. (2.72) represents the extra rolling moment due to gravity.

$$\begin{bmatrix}\dot{\phi}\\ \dot{\beta}\end{bmatrix} = \begin{bmatrix}0\\ \frac{g}{V}sin\phi cos\alpha_t + \frac{\bar{q}SC_Y(\beta)}{mV}\end{bmatrix} + \begin{bmatrix}1 & tan\alpha_t cos\phi\\ tan\alpha_t & -1\end{bmatrix}\begin{bmatrix}p\\ r\end{bmatrix} \tag{2.71}$$

$$\begin{bmatrix}\dot{p}\\ \dot{r}\end{bmatrix} = \begin{bmatrix}c_3 & c_4\\ c_4 & c_9\end{bmatrix}\begin{bmatrix}\bar{q}Sb(C_{l\beta}\beta + C_{lp}\frac{pb}{2V} + C_{lr}\frac{rb}{2V})\\ \bar{q}Sb(C_{n\beta}\beta + C_{np}\frac{pb}{2V} + C_{nr}\frac{rb}{2V})\end{bmatrix} + \begin{bmatrix}c_3 & c_4\\ c_4 & c_9\end{bmatrix}\begin{bmatrix}mgcos\alpha_t cos\phi\\ mgsin\alpha_t\end{bmatrix} y_{cm} +$$

$$\bar{q}Sb\begin{bmatrix}c_3 & c_4\\ c_4 & c_9\end{bmatrix}\begin{bmatrix}C_{l\delta a} & C_{l\delta r}\\ C_{n\delta a} & C_{n\delta r}\end{bmatrix}\begin{bmatrix}\delta_a\\ \delta_r\end{bmatrix} \tag{2.72}$$

Continuing with the established notations from the preceding section, we can articulate the revised lateral and directional dynamics as

$$\dot{\boldsymbol{x_1}} = \boldsymbol{f_1}(\boldsymbol{x_1}) + G_1(\boldsymbol{x_1})\boldsymbol{x_2} \tag{2.73}$$

$$\dot{\boldsymbol{x_2}} = \boldsymbol{f_2}(x) + \boldsymbol{A}(\boldsymbol{x})\sigma + G_2\boldsymbol{u} \tag{2.74}$$

where σ is the unknown/uncertain parameter (y_{cm} here), $\boldsymbol{f_1}, \boldsymbol{f_2}, \boldsymbol{A}$ are 2×1 vector valued functions and G_1, G_2 are 2×2 matrices and all these are known at every time step from the assumption of availability of full state feedback.

2.5.2 Control Design and Stability Analysis

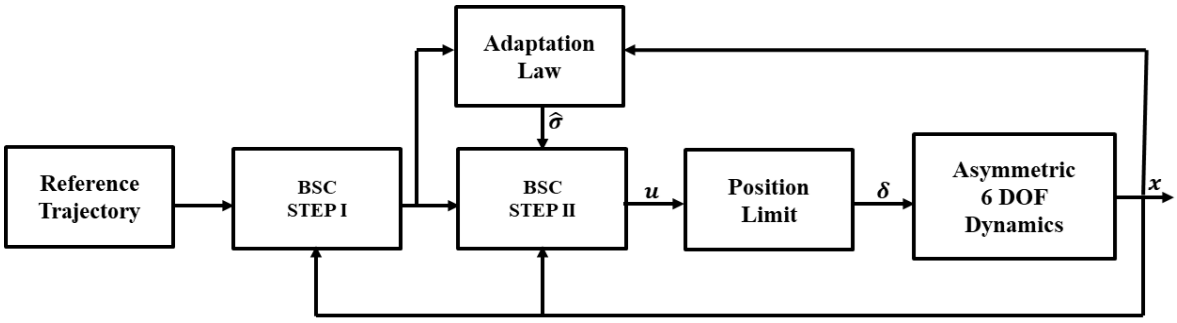

Figure 2.12 Closed loop diagram of adaptive backstepping control scheme

In this sub-section an adaptive backstepping control is formulated to autonomously execute the intended lateral maneuver under unknown lateral c.g. movement on either side of the fuselage

centerline. Referring to Eqs. (2.73) and (2.74), the desired time profiles for $\boldsymbol{x_1}$ i.e. ϕ and β are fed externally as reference inputs and the controller generates $\boldsymbol{u}$ i.e. the control surface deflection commands in a closed loop manner as shown in Figure 2.12. The detailed stability analysis of the proposed controller is discussed below.

Let us introduce the error state variables $\boldsymbol{e_1}$ and $\boldsymbol{e_2}$ as follows:

$$\boldsymbol{e_1} = \boldsymbol{x_1} - \boldsymbol{x_{1d}} \tag{2.75}$$

$$\boldsymbol{e_2} = \boldsymbol{x_2} - \boldsymbol{x_{2d}} \tag{2.76}$$

where $\boldsymbol{x_{1d}}$ and $\boldsymbol{x_{2d}}$ are the desired trajectories of $\boldsymbol{x_1}$ and $\boldsymbol{x_2}$.

The dynamic equations of the error states are given as follows:

$$\dot{\boldsymbol{e_1}} = \dot{\boldsymbol{x_1}} - \dot{\boldsymbol{x}}_{\boldsymbol{1d}} = \boldsymbol{f_1}(\boldsymbol{x_1}) + G_1(\boldsymbol{x_1})\boldsymbol{x_2} - \dot{\boldsymbol{x}}_{\boldsymbol{1d}} \tag{2.77}$$

The Lyapunov function for the $\boldsymbol{x_1}$ dynamics assuming $\boldsymbol{x_2}$ to be the virtual control as

$$V_1 = \frac{1}{2}\boldsymbol{e_1^T e_1} \tag{2.78}$$

$$\dot{V}_1 = \boldsymbol{e_1^T \dot{e}_1} \tag{2.79}$$

$$\dot{V}_1 = \boldsymbol{e_1^T}[\boldsymbol{f_1} + G_1\boldsymbol{x_2} - \dot{\boldsymbol{x}}_{\boldsymbol{1d}}] \tag{2.80}$$

Let us choose

$$\boldsymbol{f_1} + G_1\boldsymbol{x_2} - \dot{\boldsymbol{x}}_{\boldsymbol{1d}} = -K_1\boldsymbol{e_1} \tag{2.81}$$

where K_1 is a constant positive definite matrix. Substituting (2.81) in (2.80), we get

$$\dot{V}_1 = \boldsymbol{e_1^T}(-K_1\boldsymbol{e_1}) \tag{2.82}$$

$$\dot{V}_1 = -\boldsymbol{e_1^T}K_{11}\boldsymbol{e_1} < 0 \tag{2.83}$$

Now, from Eq. (2.81),

$$G_1\boldsymbol{x_2} = -K_1\boldsymbol{e_1} + \dot{\boldsymbol{x}}_{\boldsymbol{1d}} - f_1 \tag{2.84}$$

From here, the desired value of $\boldsymbol{x_2}$ is obtained as

$$\boldsymbol{x_{2d}} = (G_1)^{-1}(-K_1\boldsymbol{e_1} + \dot{\boldsymbol{x}}_{\boldsymbol{1d}} - \boldsymbol{f_1}) \tag{2.85}$$

The Lyapunov function for the complete dynamics is chosen as

$$V_2 = \frac{1}{2}\boldsymbol{e_1^T e_1} + \frac{1}{2}\boldsymbol{e_2^T e_2} + \frac{1}{2}\tilde{\sigma}^T K_3\tilde{\sigma} \tag{2.86}$$

where $\tilde{\sigma} = \sigma - \hat{\sigma}$ is the error in parameter estimation and K_3 is the adaptation gain.

$$\dot{V}_2 = \boldsymbol{e_1^T}\dot{\boldsymbol{e}}_{\boldsymbol{1}} + \boldsymbol{e_2^T}\dot{\boldsymbol{e}}_{\boldsymbol{2}} + \tilde{\sigma}^T K_3\dot{\tilde{\sigma}} \tag{2.87}$$

$$\dot{V}_2 = \boldsymbol{e_1^T}[\boldsymbol{f_1} + G_1\boldsymbol{x_2} - \dot{\boldsymbol{x}}_{\boldsymbol{1d}}] + \boldsymbol{e_2^T}\dot{\boldsymbol{e}}_{\boldsymbol{2}} + \tilde{\sigma}^T K_3\dot{\tilde{\sigma}} \tag{2.88}$$

$$\dot{V}_2 = \boldsymbol{e_1^T}[\boldsymbol{f_1} + G_1\boldsymbol{e_2} + G_1\boldsymbol{x_{2d}} - \dot{\boldsymbol{x}}_{\boldsymbol{1d}}] + \boldsymbol{e_2^T}\dot{\boldsymbol{e}}_{\boldsymbol{2}} + \tilde{\sigma}^T K_3\dot{\tilde{\sigma}} \tag{2.89}$$

Substituting Eq. (2.85) in Eq. (2.89),

$$\dot{V}_2 = \boldsymbol{e_1^T}[\boldsymbol{f_1} + G_1\boldsymbol{e_2} - K_1\boldsymbol{e_1} + \dot{\boldsymbol{x}}_{\boldsymbol{1d}} - \boldsymbol{f_1} - \dot{\boldsymbol{x}}_{\boldsymbol{1d}}] + \boldsymbol{e_2^T}\dot{\boldsymbol{e}}_{\boldsymbol{2}} + \tilde{\sigma}^T K_3\dot{\tilde{\sigma}} \tag{2.90}$$

$$\dot{V}_2 = -\boldsymbol{e_1^T}K_1\boldsymbol{e_1} + \boldsymbol{e_1^T}G_1\boldsymbol{e_2} + \boldsymbol{e_2^T}\dot{\boldsymbol{e}}_{\boldsymbol{2}} + \tilde{\sigma}^T K_3\dot{\tilde{\sigma}} \tag{2.91}$$

Let us choose

$$\dot{\boldsymbol{e}}_{\boldsymbol{2}} = -K_2\boldsymbol{e_2} - G_1^T\boldsymbol{e_1} \tag{2.92}$$

where K_2 is a constant positive definite matrix

Now from Eq. (2.92),

$$\dot{\boldsymbol{x}}_{\boldsymbol{2}} = -K_2\boldsymbol{e_2} - G_1^T\boldsymbol{e_1} + \dot{\boldsymbol{x}}_{\boldsymbol{2d}} \tag{2.93}$$

$$\boldsymbol{f_2} + \boldsymbol{A}\sigma + G_2\boldsymbol{u} = -K_2\boldsymbol{e_2} - G_1^T\boldsymbol{e_1} + \dot{\boldsymbol{x}}_{\boldsymbol{2d}} \tag{2.94}$$

Since σ is not known, using its estimate in Eq. (2.94), the final control input is computed as

$$\boldsymbol{u} = (G_2)^{-1}(-\boldsymbol{f_2} - \boldsymbol{A}\hat{\sigma} - K_2\boldsymbol{e_2} - G_1^T\boldsymbol{e_1} + \dot{\boldsymbol{x}}_{\boldsymbol{2d}}) \tag{2.95}$$

Now, $\dot{V}_2 = \boldsymbol{e_1^T}\dot{\boldsymbol{e}}_{\boldsymbol{1}} + \boldsymbol{e_2^T}\dot{\boldsymbol{e}}_{\boldsymbol{2}} + \tilde{\sigma}^T K_3\dot{\tilde{\sigma}}$ (2.96)

$$\dot{V}_2 = \boldsymbol{e_1^T}(G_1\boldsymbol{e_2} - K_1\boldsymbol{e_1}) + \boldsymbol{e_2^T}(\dot{x}_2 - \dot{\boldsymbol{x}}_{\boldsymbol{2d}}) + \tilde{\sigma}^T K_3\dot{\tilde{\sigma}} \tag{2.97}$$

$$\dot{V}_2 = \boldsymbol{e_1^T}G_1\boldsymbol{e_2} - \boldsymbol{e_1^T}K_1\boldsymbol{e_1} + \boldsymbol{e_2^T}(\dot{\boldsymbol{x}}_{\boldsymbol{2}} - \dot{\boldsymbol{x}}_{\boldsymbol{2d}}) + \tilde{\sigma}^T K_3\dot{\tilde{\sigma}} \tag{2.98}$$

$$\dot{V}_2 = \boldsymbol{e_1^T}G_1\boldsymbol{e_2} - \boldsymbol{e_1^T}K_1\boldsymbol{e_1} + \boldsymbol{e_2^T}(\boldsymbol{f_2} + \boldsymbol{A}\sigma - \boldsymbol{f_2} - \boldsymbol{A}\hat{\sigma} - K_2\boldsymbol{e_2} - G_1^T\boldsymbol{e_1} + \dot{\boldsymbol{x}}_{\boldsymbol{2d}} - \dot{\boldsymbol{x}}_{\boldsymbol{2d}}) + \tilde{\sigma}^T K_3\dot{\tilde{\sigma}} \tag{2.99}$$

$$\dot{V}_2 = -\boldsymbol{e_1^T}K_{11}\boldsymbol{e_1} + \boldsymbol{e_2^T}\boldsymbol{A}\sigma - \boldsymbol{e_2^T}\boldsymbol{A}(\sigma - \tilde{\sigma}) - \boldsymbol{e_2^T}K_2\boldsymbol{e_2} + \tilde{\sigma}^T K_3\dot{\tilde{\sigma}} \tag{2.100}$$

$$\dot{V}_2 = -\boldsymbol{e_1^T}K_{11}\boldsymbol{e_1} + \boldsymbol{e_2^T}\boldsymbol{A}\sigma - \boldsymbol{e_2^T}\boldsymbol{A}\sigma + \boldsymbol{e_2^T}\boldsymbol{A}\tilde{\sigma} - \boldsymbol{e_2^T}K_2\boldsymbol{e_2} + \tilde{\sigma}^T K_3\dot{\tilde{\sigma}} \tag{2.101}$$

$$\dot{V}_2 = -\boldsymbol{e_1^T}K_1\boldsymbol{e_1} - \boldsymbol{e_2^T}K_2\boldsymbol{e_2} + \boldsymbol{e_2^T}\boldsymbol{A}\tilde{\sigma} + \tilde{\sigma}^T K_3\dot{\tilde{\sigma}} \tag{2.102}$$

Now, to ensure

$$\dot{V}_2 = -\boldsymbol{e_1^T}K_1\boldsymbol{e_1} - \boldsymbol{e_2^T}K_2\boldsymbol{e_2} \leq 0 \tag{2.103}$$

the following condition must be satisfied

$$\boldsymbol{e_2^T}\boldsymbol{A}\tilde{\sigma} + \tilde{\sigma}^T K_3\dot{\tilde{\sigma}} = 0 \tag{2.104}$$

Assuming σ to be constant, and since the term $\boldsymbol{e_2^T}\boldsymbol{A}\tilde{\sigma}$ is scalar, replacing it by its transpose, Eq. (2.104) reduces to the final adaptation law

$$\dot{\hat{\sigma}} = K_3^{-1}\boldsymbol{A^T}\boldsymbol{e_2} \tag{2.105}$$

Eq. (2.95) gives the final control input where$\boldsymbol{x}_{\boldsymbol{2d}}$ is given by Eq. (2.85) and $\hat{\sigma}$ is given by Eq. (2.105). Since $\dot{V}_2$ in Eq. (2.103) is positive semi definite, there is no guarantee that the estimation error in the estimate of the uncertain parameter will converge to zero.

Remark 1: The following theorem is used to prove asymptotic stability of the closed loop system.

Theorem 2.1 [95, 96]: *For nonlinear non autonomous system. If there exist a positive definite Lyapunov function* $V(x)$ *and that its derivative* $\dot{V}(x,t)$ *is negative semi definite. For any initial condition* $x(t=0)=x_0$ *define the domain* $\Omega_0=\{x|V(x)\leq V(x_0)\}$*. Since, Lyapunov derivative is negative semi definite, it is clear that trajectories are bounded and contained within the domain* Ω_0*. Now, define the domain* $\Omega_e=\{x|\dot{V}(x,t)=0\}$ *and* $\Omega_i=\{x|\dot{V}(x,t)\equiv 0\}$*. Then if any of the assumptions A or B holds, all limit points of the bounded trajectory* $x(t)$ *belong to the domain* $\Omega_f=\Omega_0\cap\Omega_e$*. In particular; limit points that are also equilibrium points of* $x(t)$ *belong to* $\Omega_f=\Omega_0\cap\Omega_i$*.*

(A) $|f(x(t),t)|$ *is bounded for any bounded* x*. Or*

(B) $|\int_a^b f(x(\tau),\tau)d\tau|$ *is bounded for any finite time interval* $c=b-a$*.*

where $\dot{x}=f(x(t),t)$ *represents the system dynamics.*

Substituting the controls in the system dynamics, the error dynamics can be expressed as

$$\dot{\boldsymbol{e}}_{\boldsymbol{1}}=G_1\boldsymbol{e}_{\boldsymbol{2}}-K_1\boldsymbol{e}_{\boldsymbol{1}} \tag{2.106}$$

$$\dot{\boldsymbol{e}}_{\boldsymbol{2}}=\boldsymbol{A}\tilde{\sigma}-K_2\boldsymbol{e}_{\boldsymbol{2}}-G_1^T\boldsymbol{e}_{\boldsymbol{1}} \tag{2.107}$$

And from Eq. (2.105),

$$\dot{\tilde{\sigma}}=-\frac{1}{K_3}\left(\boldsymbol{A}^{\boldsymbol{T}}\boldsymbol{e}_{\boldsymbol{2}}\right) \tag{2.108}$$

Clearly, in the present problem, Condition (A) of Theorem 2.1 holds (referring to the dynamics given by Eqs. (2.71) and (2.73)). The main contribution of the new invariance principle i.e. Theorem 2.1 is consideration of $\dot{V}\equiv 0$ instead of merely $\dot{V}=0$. Now, from Eq. (2.103), $\dot{V}_2\equiv 0$ implies that $\boldsymbol{e}_{\boldsymbol{1}}\equiv\boldsymbol{0}$ and $\boldsymbol{e}_{\boldsymbol{2}}\equiv\boldsymbol{0}$. This, in turn, implies that $\dot{\boldsymbol{e}}_{\boldsymbol{1}}=\boldsymbol{0}$ and $\dot{\boldsymbol{e}}_{\boldsymbol{2}}=\boldsymbol{0}$ implying asymptotic stability of the tracking errors $\boldsymbol{e}_{\boldsymbol{1}}$ and $\boldsymbol{e}_{\boldsymbol{2}}$. Further, under this condition, Eqs. (2.106) - (2.108) now reduce to

$$\dot{\boldsymbol{e}}_1 = \mathbf{0} \tag{2.109}$$

$$\dot{\boldsymbol{e}}_2 = \boldsymbol{A}\tilde{\sigma} \tag{2.110}$$

$$\dot{\tilde{\sigma}} = 0 \tag{2.111}$$

It can be further concluded from Theorem 2.1 that if the condition $\lim_{t\to\infty} \boldsymbol{A} = \mathbf{0}$ is satisfied, then $\lim_{t\to\infty} \tilde{\sigma} \neq 0$ i.e. $\tilde{\sigma}$ will converge to some nonzero constant value. On the other hand, if $\lim_{t\to\infty} \boldsymbol{A} \neq 0$ is o then $\lim_{t\to\infty} \tilde{\sigma} = 0$.

Since it is already established that the lateral dynamics is asymptotically stable, therefore, $\lim_{t\to\infty} p = 0$ and $\lim_{t\to\infty} r = 0$. However, $\lim_{t\to\infty} \boldsymbol{A} \neq \mathbf{0}$. Since the longitudinal dynamics is assumed to remain unaffected during the maneuver, it can be safely assumed that the aircraft will retain longitudinal trim post maneuver. Therefore, $\lim_{t\to\infty} \boldsymbol{A} = \begin{bmatrix} c_3 & c_4 \\ c_4 & c_9 \end{bmatrix} \begin{bmatrix} mg\ cos\alpha_t\ cos\phi \\ mg\ sin\alpha_t \end{bmatrix} \neq \mathbf{0}$. This proves the asymptotic stability of the parameter estimation error (i.e. $\tilde{\sigma}$) as well along with the errors in states.

2.5.3 Simulation Results and Discussions

To validate the adaptive backstepping control, the same amount of lateral c.g. movement as considered previously ($\pm 7.0\ cm$) is considered again. A large number of Monte Carlo runs are performed considering lateral c.g. position randomly in the range $[-7\ cm, 7\ cm]$ and nearly identical maneuver performance is observed in each run. However, plots for the extreme ends on both sides corresponding to $y_{cm} = \pm 7.0\ cm$ are shown for the sake of brevity. The ad-hoc model is considered for the controller design only; the exact equations of motion under laterally asymmetric c.g. positions are taken into consideration when simulating the 6-DOF dynamics (refer to Figure 2.12).

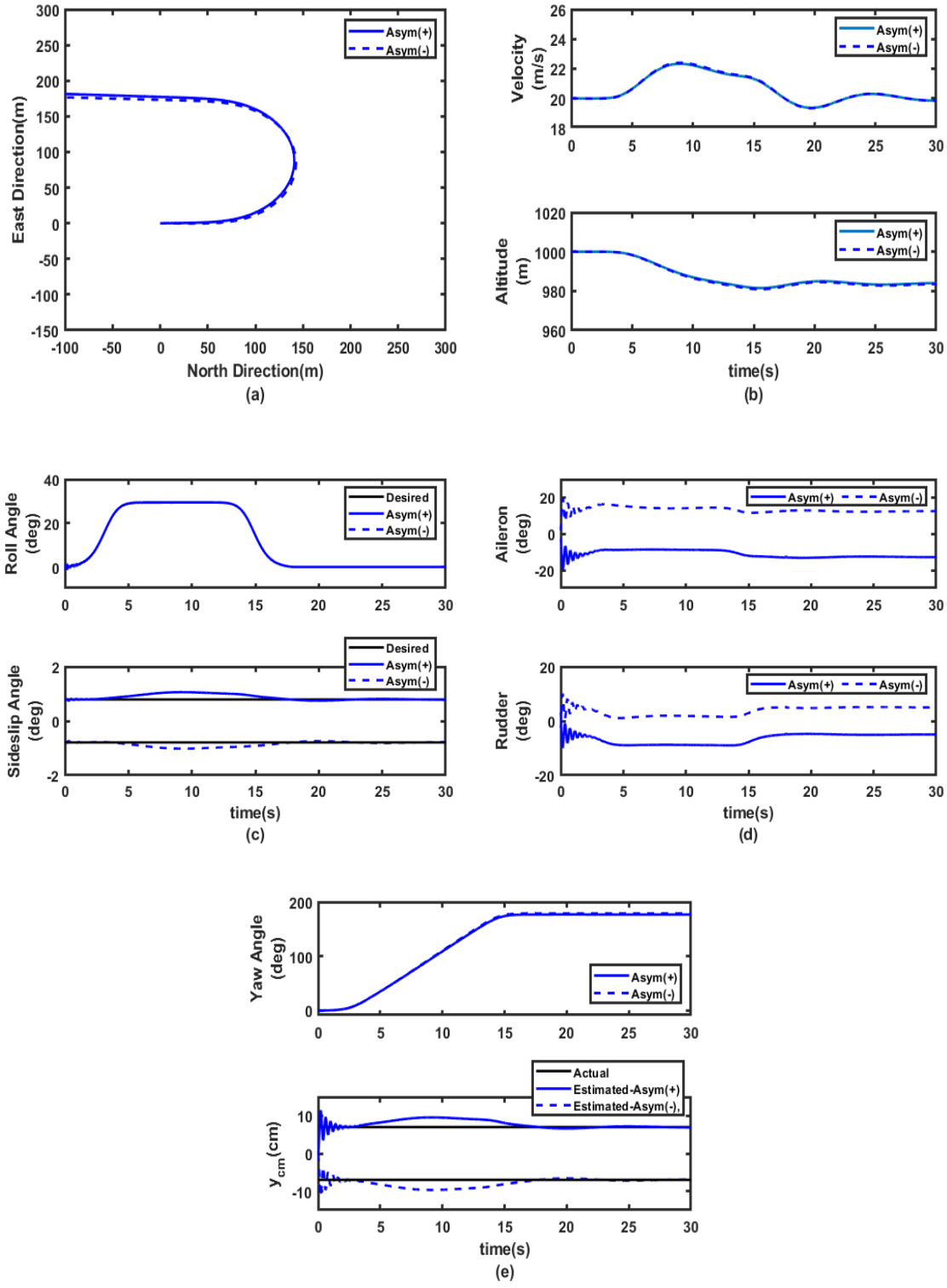

Figure 2.13. Time evolution of states and controls for horizontal turn maneuver under lateral c.g. shift: Adaptive backstepping design approach

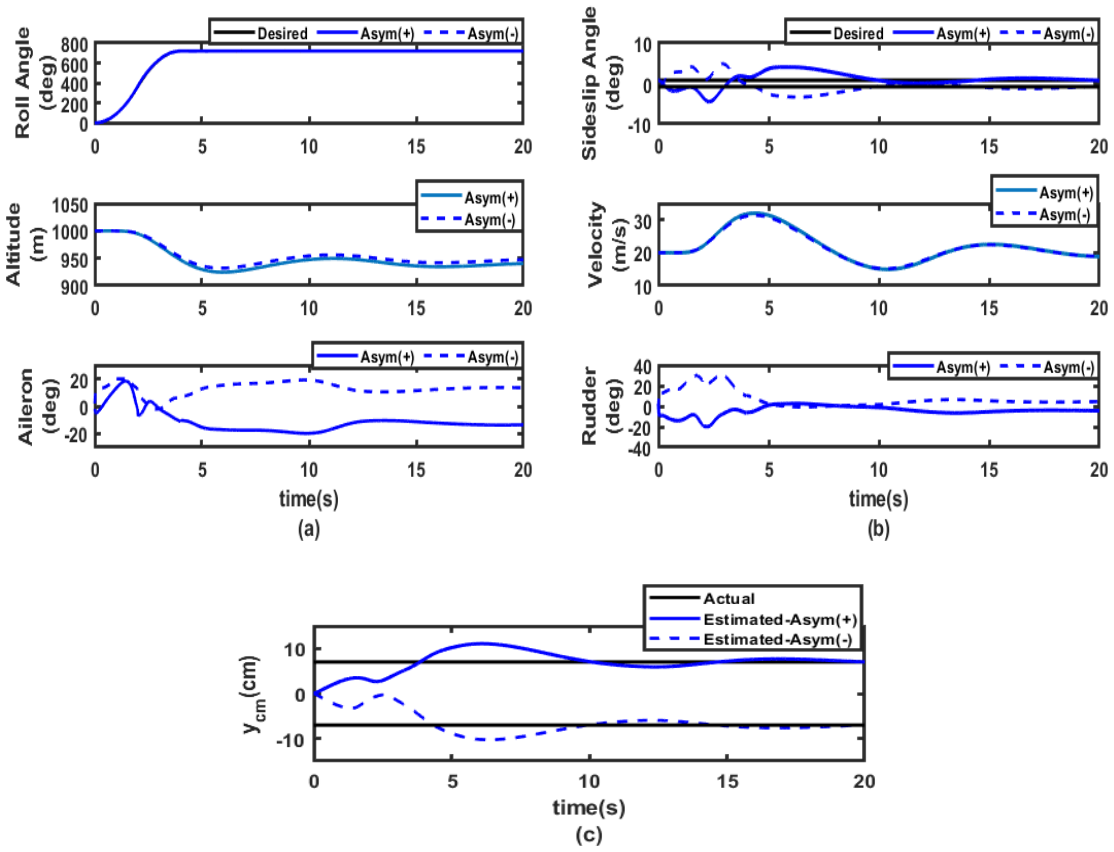

Figure 2.14. Time evolution of states and controls for aileron roll maneuver under lateral c.g. shift: Adaptive backstepping design approach

Horizontal turn and aileron roll maneuvers are considered under the same initial trim condition as in previous cases. However, due to the asymmetry there will arise a small sideslip angle in the initial trim. The maneuver performance corresponding to the above mentioned two cases of c.g. locations are illustrated in Figures 2.13 and 2.14. It is clearly observed from Figures 2.13 and 2.14 that the nominal maneuver performance is almost completely recovered by the adaptive backstepping controller. As theoretically established, $\hat{y}_{cm}$ also asymptotically converged to the actual y_{cm} in either case. Excellent tracking of the φ and β profiles are also achieved and the longitudinal variables also remained near their initial trim values. Various controller parameters which are tuned from trial and error are listed in Table 2.4.

Table 2.4: Adaptive backstepping controller parameters

Maneuver	$\boldsymbol{K_1}$	$\boldsymbol{K_2}$	$\boldsymbol{K_3}$
Horizontal turn	$\begin{bmatrix} 18 & 0 \\ 0 & 35 \end{bmatrix}$	$\begin{bmatrix} 10 & 0 \\ 0 & 5 \end{bmatrix}$	0.01
Aileron roll	$\begin{bmatrix} 30 & 0 \\ 0 & 5 \end{bmatrix}$	$\begin{bmatrix} 35 & 0 \\ 0 & 5 \end{bmatrix}$	0.001

2.6 Conclusion

The practical problem of controlling the lateral/directional flight of a fixed wing UAV under considerable lateral c.g. uncertainty was addressed in this chapter. First the linear control technique namely LQR is implemented. However, under lateral c.g. variation results shows it is inadequate in handling such cases. This inadequacy necessitates the implementation of nonlinear control techniques. For implementing nonlinear control technique the dynamics was formulated in strict feedback form for the nominal c.g. position and a block backstepping controller was designed to execute a horizontal turn and an aileron roll maneuver. It was demonstrated that the control performance deteriorated significantly when the same nonlinear controller was used under lateral c.g. variations. To regain the lost performance, thereafter, an adaptive backstepping controller was formulated considering a simplified dynamical model of the UAV for lateral c.g. offset. The c.g. position of the UAV was estimated online using an adaptation law and stability of the proposed control scheme was established using the Lyapunov stability approach. Furthermore, the analysis presumed that the UAV would operate within the low angle of attack region exclusively. Consequently, uncertainties associated with aerodynamic coefficients were deemed negligible for this specific investigation. This issue is undertaken in next chapter once the UAV or the aircraft is made to operate in the high angle of attack regions along with lateral c.g. movements.

Chapter 3

Robust Adaptive Backstepping Control for High Alpha Maneuvers

3.1 Introduction

In the realm of modern aerial combat, agility is paramount for gaining air superiority. The previous discussion centered on how c.g. shifts affect low angles of attack (AOA) maneuvers. To comprehensively understand the aircraft's capabilities across its operational spectrum, it's imperative to now explore how lateral c.g. movements influence specific high-angle-of-attack maneuvers. Unlike low AOA maneuvers, where lateral c.g. movements were the primary focus and assumed to be restricted to the y direction only, high AOA maneuvers introduce complexities as lateral c.g. shifts affect the aircraft's c.g. position across all three axes. As it is established in the previous chapter that the robust linear control technique was not able to handle lateral c.g. movement which compel us to go for robust nonlinear control scheme. In particular, adaptive backstepping (ABS) control algorithm is applied therein to execute maneuver in presence of lateral c.g. movement with the aim to adapt to the c.g. uncertainty. Unlike low alpha maneuver, aerodynamic uncertainty in high alpha maneuver is profound. This calls for further robustness enhancement of the adaptive backstepping controller.

Among the available robust scheme for nonlinear uncertain systems, sliding mode control (SMC) is widely used due to its attractive property of fast response and robustness to exogenous disturbances and plant parametric uncertainties [55, 97, 98]. Moreover, it has been applied to various nonlinear flight control problems also [53, 54, 60, 99]. Inspired from this, in the present chapter, a hybrid control law is established where the adaptive backstepping technique is further robustified with a fast sliding mode algorithm. Backstepping and sliding mode controls are combined in the literature in various application domains to gain insensitivity to both matched and unmatched uncertainties and disturbances [70-78]. However, the present approach to handle a part of the uncertainty, which can be modeled in terms of an uncertain parameter (the c.g. position in the present work), with the help of an adaptive backstepping algorithm and the remaining lumped uncertainties and disturbances with the help of a sliding mode algorithm is a completely novel approach. Also, in the available literature, mostly the sliding mode control part is made adaptive where the upper bound on the disturbance is estimated; whereas here the backstepping part is made adaptive where the c.g. position is estimated with an adaptation law. Further, most of the available works in the literature has a part of the dynamics in the simple $\dot{\boldsymbol{x}}_{\boldsymbol{1}} = \boldsymbol{x}_{\boldsymbol{2}}$ form, while in the present problem the same part is in the form $\dot{\boldsymbol{x}}_{\boldsymbol{1}} = \boldsymbol{f}_{\boldsymbol{1}}(\boldsymbol{x}_{\boldsymbol{1}}) + G_1(\boldsymbol{x}_{\boldsymbol{1}})\boldsymbol{x}_{\boldsymbol{2}}$ leading to increased complexities in mathematical proof for stability. A comprehensive stability analysis of the proposed controller is carried out using Lyapunov method and sufficient conditions for guaranteed closed loop stability are also derived. Thereafter, asymptotic convergence is proved using Barbalat's lemma. To validate the proposed control, the F18-HARV fighter aircraft is considered as its aerodynamic dataset is available in the open domain [60, 100] and a standard high-alpha cobra and Herbst maneuver which are regarded as benchmarks for maneuverability and agility of modern-day fighter aircraft is implemented in simulation.

The outline of the chapter is as follows. The second section presents the problem formulation, while the third section starts with brief introduction of sliding mode control and thereafter gives the design

and stability analysis of the proposed hybrid adaptive backstepping sliding mode control. Simulation results obtained by applying proposed control technique are presented in the fourth section with a comparison against a standard adaptive sliding mode control. Section five concludes the chapter with a brief prelude to the next chapter.

3.2 System Dynamics for High Alpha Maneuvers under Lateral C.G. Uncertainty

In this section, the aircraft dynamics is expressed in strict feedback form so as to make it amenable to the proposed backstepping based sliding mode control scheme under lateral center of gravity uncertainty. Further, the formulation is aimed at executing some standard high-alpha maneuver. For executing such maneuvers, the angle of attack, angle of sideslip and bank angle profiles are supplied externally and the closed loop controller generates the required moments about the three body axes [68, 101]. The moment commands are then converted to the control surface deflection commands through a control allocation method such as the matrix pseudoinverse [102]. However, when the c.g. of the aircraft undergoes arbitrary movements the standard equations of motion get modified. The complete 6-degree of freedom (DOF) equations of motion of an aircraft when the c.g. of the aircraft assumes an arbitrary position are given in the body frame as [61, 68]

$$\begin{bmatrix} 1 & 0 & 0 & 0 & z_{cm} & -y_{cm} \\ 0 & 1 & 0 & -z_{cm} & 0 & x_{cm} \\ 0 & 0 & 1 & y_{cm} & -x_{cm} & 0 \\ 0 & -mz_{cm} & my_{cm} & I'_{xx} & -I'_{xy} & -I'_{xz} \\ mz_{cm} & 0 & -mx_{cm} & -I'_{xy} & I'_{yy} & -I'_{yz} \\ -my_{cm} & mx_{cm} & 0 & -I'_{xz} & -I'_{yz} & I'_{zz} \end{bmatrix} \begin{bmatrix} \dot{u} \\ \dot{v} \\ \dot{w} \\ \dot{p} \\ \dot{q} \\ \dot{r} \end{bmatrix} = \begin{bmatrix} -qw + rv \\ -ru + pw \\ -pv + qu \\ I'_{xz}pq + (I'_{yy} - I'_{zz})qr - I'_{xy}rp + I'_{yz}(q^2 - r^2) \\ I'_{xy}qr + (I'_{zz} - I'_{xx})rp - I'_{yz}pq + I'_{xz}(r^2 - p^2) \\ I'_{yz}rp + (I'_{xx} - I'_{yy})pq - I'_{xz}qr + I'_{xy}(p^2 - q^2) \end{bmatrix} +$$

$$\begin{bmatrix} (q^2 + r^2)x_{cm} - pqy_{cm} - rpz_{cm} \\ (r^2 + p^2)y_{cm} - pqx_{cm} - qrz_{cm} \\ (p^2 + q^2)z_{cm} - rpx_{cm} - qry_{cm} \\ m(qu - pv)y_{cm} + m(ru - pw)z_{cm} \\ m(pv - qu)x_{cm} + m(rv - qw)z_{cm} \\ m(pw - ru)x_{cm} + m(qw - rv)y_{cm} \end{bmatrix} + \begin{bmatrix} -gsin\theta \\ gcos\theta sin\phi \\ gcos\theta cos\phi \\ -z_{cm}mgcos\theta sin\phi + y_{cm}mgcos\theta cos\phi \\ -z_{cm}mgsin\theta - x_{cm}mgcos\theta cos\phi \\ y_{cm}mgsin\theta + x_{cm}mgcos\theta sin\phi \end{bmatrix} + \begin{bmatrix} \frac{F_x}{m} \\ \frac{F_y}{m} \\ \frac{F_z}{m} \\ M_x \\ M_y \\ M_z \end{bmatrix} \quad (3.1)$$

where (x_{cm}, y_{cm}, z_{cm}) is the actual c.g. position w.r.t. the nominal c.g position or the origin of the

body/wind frame and $I' = \begin{bmatrix} I'_{xx} & -I'_{xy} & -I'_{xz} \\ -I'_{xy} & I'_{yy} & -I'_{yz} \\ -I'_{xz} & -I'_{yz} & I'_{zz} \end{bmatrix}$ is the new inertia matrix. Extracting the translational and rotational dynamics parts from Eq. (3.1) yields,

$$\begin{bmatrix} \dot{u} \\ \dot{v} \\ \dot{w} \end{bmatrix} = -\frac{A}{m}\left(\frac{1}{m}A^2 + I'\right)^{-1} \left\{ A \begin{bmatrix} -qw + rv + (q^2 + r^2)x_{cm} - pqy_{cm} - rpz_{cm} \\ -ru + pw - pqx_{cm} + (r^2 + p^2)y_{cm} - qrz_{cm} \\ -pv + qu - rpx_{cm} - qry_{cm} + (p^2 + q^2)z_{cm} \end{bmatrix} + \begin{bmatrix} -gsin\theta + \frac{1}{m}(\bar{q}SC_X + T_x) \\ gcos\theta sin\phi + \frac{1}{m}(\bar{q}SC_Y + T_y) \\ gcos\theta cos\phi + \frac{1}{m}(\bar{q}SC_Z + T_z) \end{bmatrix} \right\} +$$

$$\begin{bmatrix} I'_{xz}pq + (I'_{yy} - I'_{zz})qr - I'_{xy}rp + I'_{yz}(q^2 - r^2) + m(qu - pv)y_{cm} + m(ru - pw)z_{cm} \\ I'_{xy}qr + (I'_{zz} - I'_{xx})rp - I'_{yz}pq + I'_{xz}(r^2 - p^2) + m(pv - qu)x_{cm} + m(rv - qw)z_{cm} \\ I'_{yz}rp + (I'_{xx} - I'_{yy})pq - I'_{xz}qr + I'_{xy}(p^2 - q^2) + m(pw - ru)x_{cm} + m(qw - rv)y_{cm} \end{bmatrix} +$$

$$\begin{bmatrix} -z_{cm}mgcos\theta sin\phi + y_{cm}mgcos\theta cos\phi + \bar{q}SbC_l + M_{TX} \\ -z_{cm}mgsin\theta - x_{cm}mgcos\theta cos\phi + \bar{q}S\bar{c}C_m + M_{TY} \\ y_{cm}mgsin\theta + x_{cm}mgcos\theta sin\phi + \bar{q}SbC_n + M_{TZ} \end{bmatrix}$$

$$\begin{bmatrix} -qw + rv + (q^2 + r^2)x_{cm} - pqy_{cm} - rpz_{cm} \\ -ru + pw - pqx_{cm} + (r^2 + p^2)y_{cm} - qrz_{cm} \\ -pv + qu - rpx_{cm} - qry_{cm} + (p^2 + q^2)z_{cm} \end{bmatrix} + \begin{bmatrix} -gsin\theta + \frac{1}{m}(\bar{q}SC_X + T_x) \\ gcos\theta sin\phi + \frac{1}{m}(\bar{q}SC_Y + T_y) \\ gcos\theta cos\phi + \frac{1}{m}(\bar{q}SC_Z + T_z) \end{bmatrix} \tag{3.2}$$

$$\left(\frac{1}{m}\,A^2 + I'\right)\begin{bmatrix}\dot{p}\\ \dot{q}\\ \dot{r}\end{bmatrix} = A\begin{bmatrix}-qw + rv + (q^2 + r^2)x_{cm} - pqy_{cm} - rpz_{cm}\\ -ru + pw - pqx_{cm} + (r^2 + p^2)y_{cm} - qrz_{cm}\\ -pv + qu - rpx_{cm} - qry_{cm} + (p^2 + q^2)z_{cm}\end{bmatrix} + A\begin{bmatrix}-gsin\theta + \frac{1}{m}(\bar{q}SC_X + T_x)\\ gcos\theta sin\phi + \frac{1}{m}(\bar{q}SC_Y + T_y)\\ gcos\theta cos\phi + \frac{1}{m}(\bar{q}SC_Z + T_z)\end{bmatrix} +$$

$$\begin{bmatrix}I'_{xz}pq + \left(I'_{yy} - I'_{zz}\right)qr - I'_{xy}rp + I'_{yz}(q^2 - r^2) + m(qu - pv)y_{cm} + m(ru - pw)z_{cm}\\ I'_{xy}qr + (I'_{zz} - I'_{xx})rp - I'_{yz}pq + I'_{xz}(r^2 - p^2) + m(pv - qu)x_{cm} + m(rv - qw)z_{cm}\\ I'_{yz}rp + \left(I'_{xx} - I'_{yy}\right)pq - I'_{xz}qr + I'_{xy}(p^2 - q^2) + m(pw - ru)x_{cm} + m(qw - rv)y_{cm}\end{bmatrix} +$$

$$\begin{bmatrix}-z_{cm}mgcos\theta sin\phi + y_{cm}mgcos\theta cos\phi + \bar{q}SbC_l + M_{TX}\\ -z_{cm}mgsin\theta - x_{cm}mgcos\theta cos\phi + \bar{q}S\bar{c}C_m + M_{TY}\\ y_{cm}mgsin\theta + x_{cm}mgcos\theta sin\phi + \bar{q}SbC_n + M_{TZ}\end{bmatrix} \tag{3.3}$$

where $A \triangleq \begin{bmatrix} 0 & mz_{cm} & -my_{cm} \\ -mz_{cm} & 0 & mx_{cm} \\ my_{cm} & -mx_{cm} & 0 \end{bmatrix}$.

Clearly, Eq. (3.2) and Eq. (3.3) are not in strict feedback form, a prerequisite condition to apply backstepping control. Hence, backstepping control cannot be directly applied to system dynamics represented by Eq. (3.2) and Eq. (3.3).

In order to design backstepping control, system dynamics are now modeled in strict feedback form by applying the concept of ad-hoc modelling.

As, $\dot{\alpha} - \dot{\beta} - \dot{\mu}$ equations are largely kinematic in nature. Therefore, these equations may safely be considered to remain nearly unchanged under c.g. movements. They are given by Eq. (3.5) in wind frame under further assumptions that the trigonometric nonlinearities involving the thrust vectors (i.e. $\delta_{\text{ptv}}, \delta_{\text{ytv}}$) are small and control surface deflections produce only moments and no force [92]. It is proposed in the literature that an additional moment due to gravity term can be added to the angular rate dynamics to represent the asymmetric dynamics reasonably accurately [68]. Following this approach, the rotational dynamics under c.g. variations can be modeled in ad-hoc manner and expressed by Eq. (3.6).

$[I] = \begin{bmatrix} I_{xx} & 0 & -I_{xz} \\ 0 & I_{yy} & 0 \\ -I_{xz} & 0 & I_{zz} \end{bmatrix}$ is the inertia matrix and the control surface deflection dependent terms are collected in $\begin{bmatrix} M_{xc} & M_{yc} & M_{zc} \end{bmatrix}^T$ as

$$\begin{bmatrix} M_{xc} \\ M_{yc} \\ M_{zc} \end{bmatrix} = \begin{bmatrix} \bar{q}SbC_{l\delta_a} & \bar{q}SbC_{l\delta_e} & \bar{q}SbC_{l\delta_r} & 0 & -l_z\delta_T T \\ 0 & \bar{q}S\bar{c}C_{m\delta_e} & 0 & -l_x\delta_T T & 0 \\ \bar{q}SbC_{n\delta_a} & \bar{q}SbC_{n\delta_e} & \bar{q}SbC_{n\delta_r} & 0 & -l_x\delta_T T \end{bmatrix} \begin{bmatrix} \delta_a \\ \delta_e \\ \delta_r \\ \delta_{ptv} \\ \delta_{ytv} \end{bmatrix} \tag{3.4}$$

where l_x, l_z denote the location of the engine nozzle from the origin of the body frame, δ_T denotes throttle setting and T is the gross engines thrust.

$$\begin{bmatrix}\dot{\alpha}\\ \dot{\beta}\\ \dot{\mu}\end{bmatrix} = \begin{bmatrix} \frac{g}{V} sec\beta cos\mu\, cos\gamma + \frac{1}{mV}(-sec\beta\, \bar{q}SC_{L_\alpha} - sec\beta\, \delta_T T\, sin\alpha) \\ \frac{g}{V} sin\mu\, cos\gamma + \frac{1}{mV}(\bar{q}SC_{Y_\beta}\beta - \delta_T T cos\alpha\, sin\beta) \\ -\frac{g}{V} tan\beta\, cos\mu\, cos\gamma + \frac{1}{mV}(tan\gamma\, cos\mu\, \bar{q}SC_{Y_\beta}\beta - tan\gamma\, cos\mu\, \delta_T T cos\alpha\, sin\beta + (tan\beta + sin\mu\, tan\gamma)\bar{q}SC_{L_\alpha} + (tan\beta + sin\mu\, tan\gamma)\delta_T T\, sin\alpha) \end{bmatrix} +$$

$$\begin{bmatrix} -cos\alpha\, tan\beta & 1 - \frac{1}{mV} sec\beta\, \bar{q}SC_{L_q}\frac{\bar{c}}{2V} & -sin\alpha\, tan\beta \\ sin\alpha + \frac{1}{mV}\bar{q}SC_{Y_p}\frac{b}{2V} & 0 & -cos\alpha + \frac{1}{mV}\bar{q}SC_{Y_r}\frac{b}{2V} \\ \frac{cos\alpha}{cos\beta} + \frac{1}{mV} tan\gamma\, cos\mu\, \bar{q}SC_{Y_p}\frac{b}{2V} & \frac{1}{mV}(tan\beta + sin\mu\, tan\gamma)\bar{q}SC_{L_q}\frac{\bar{c}}{2V} & \frac{sin\alpha}{cos\beta} + \frac{1}{mV} tan\gamma\, cos\mu\, \bar{q}SC_{Y_r}\frac{b}{2V} \end{bmatrix} \begin{bmatrix} p \\ q \\ r \end{bmatrix} \tag{3.5}$$

$$\begin{bmatrix}\dot{p}\\ \dot{q}\\ \dot{r}\end{bmatrix} = [I]^{-1} \begin{bmatrix} qr(I_{yy} - I_{zz}) + pqI_{xz} + \bar{q}Sb(C_{l\beta}\beta + C_{lp}\frac{pb}{2V} + C_{lr}\frac{rb}{2V}) \\ pr(I_{zz} - I_{xx}) + I_{xz}(r^2 - p^2) - l_z\delta_T T + \bar{q}S\bar{c}(C_m + C_{mq}\frac{q\bar{c}}{2V}) \\ pq(I_{xx} - I_{yy}) - qrI_{xz} + \bar{q}Sb(C_{n\beta}\beta + C_{np}\frac{pb}{2V} + C_{nr}\frac{rb}{2V}) \end{bmatrix} +$$

$$[I]^{-1} \begin{bmatrix} 0 & mgcos\theta cos\phi & -mgcos\theta sin\phi \\ -mgcos\theta\, cos\,\phi & 0 & -mgsin\theta \\ mgcos\theta sin\phi & mgsin\theta & 0 \end{bmatrix} \begin{bmatrix} x_{cm} \\ y_{cm} \\ z_{cm} \end{bmatrix} + [I]^{-1} \begin{bmatrix} M_{xc} \\ M_{yc} \\ M_{zc} \end{bmatrix} + [I]^{-1} \begin{bmatrix} d_1 \\ d_2 \\ d_3 \end{bmatrix} \tag{3.6}$$

where (x_{cm}, y_{cm}, z_{cm}) is the actual c.g. position w.r.t. the origin of the body/wind frame and $[d_1 \quad d_2 \quad d_3]^T$ denotes a vector representing the error incurred due to the approximate representation of the c.g. shifted dynamics along with the matched external disturbances. Therefore, the final system dynamics i.e. Eqs. (3.5) and (3.6) can be expressed respectively as

$$\dot{\boldsymbol{x}}_1 = \boldsymbol{f}_1(\boldsymbol{x}_1) + G_1(\boldsymbol{x}_1)\boldsymbol{x}_2 \tag{3.7}$$

$$\dot{\boldsymbol{x}}_2 = \boldsymbol{f}_2(\boldsymbol{x}) + A(\boldsymbol{x})\boldsymbol{\sigma} + G_2\boldsymbol{u} + \boldsymbol{d} \tag{3.8}$$

where $\boldsymbol{\sigma}$ is the uncertain/unknown c.g. position $[x_{cm} \;\; y_{cm} \;\; z_{cm}]^T$ which can be estimated online in an adaptive backstepping setting. It can be noted that Eqs. (3.7) and (3.8) are now in strict feedback form. To nullify the effects of the disturbance $\boldsymbol{d}$, a sliding mode control is combined with the adaptive backstepping control in the present work. The complete closed loop scheme is depicted in Fig. 3.1.

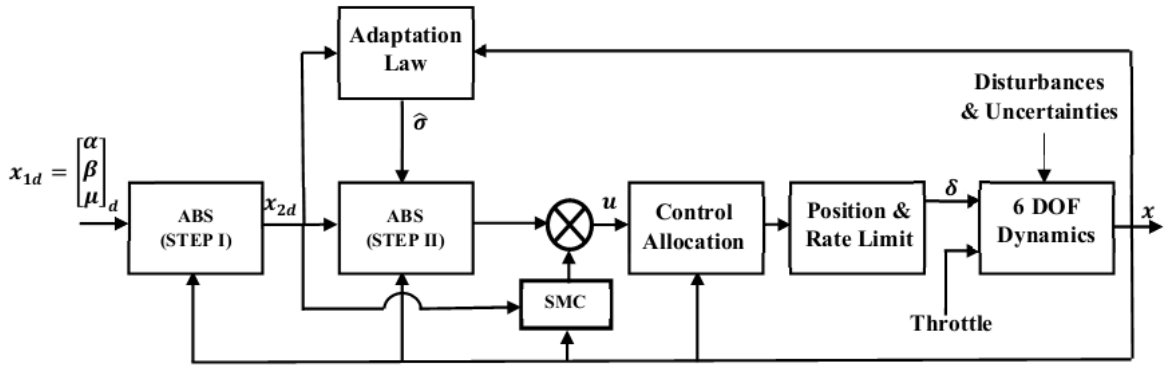

Figure 3.1. Block diagram of the overall closed loop system

3.3 Adaptive Backstepping Sliding Mode Control Design

To investigate the effects of lateral c.g. variation on a fighter aircraft performing high alpha maneuvers, this section addresses the control design issues for an asymmetric aircraft. For this purpose, two well-known high alpha maneuvers, Cobra, and Herbst, are considered. In the Herbst maneuver, the aircraft is made to quickly reverse direction or change heading during aerial combat.

The maneuver involves a combination of yaw, pitch, and roll to rapidly change the aircraft's orientation while maintaining energy and speed. The Herbst maneuver in aviation is a high-performance maneuver used to outmaneuver opponents and gain tactical advantage in aerial engagements. It is considered a standard maneuver for evaluating the agility and maneuverability of an aerial vehicle. In the cobra maneuver, the aircraft pitches up rapidly to a near-vertical angle of attack while maintaining its forward velocity. This causes the aircraft to briefly stand on its tail in a vertical position before quickly returning to level flight. The nose of the aircraft points upward, while the aircraft's velocity vector remains mostly forward. As both are high AOA maneuvers, aerodynamic as well as thrust vectoring control is available. This calls for nonlinear control implementation for carrying out such maneuvers automatically. In the subsequent subsection, the basics of sliding mode control are briefly reviewed to provide context and understanding for its application in addressing the nonlinear dynamics of the aircraft during high alpha maneuvers.

3.3.1 A Brief Overview of Sliding Mode Control [56, 107]

Sliding mode control (SMC) is a nonlinear control method used to regulate the behavior of dynamical systems which is derived from the variable structure systems (VSS) theory recognized as one of the popular and powerful control tools. Its popularity comes from the robustness feature, which eliminates the burden of the necessity of system parameters required for accurate modeling. The main idea behind SMC is to force the system states to make a motion on a predefined sliding surface using discontinuous control, which switches between two different system structures. When a system is in the sliding mode, its state trajectory coincides with the sliding line, which depends neither on the system parameters nor on the disturbance; rather, it depends only on the sliding coefficient. In such a case, the order of the controlled system is reduced by one leading to simplification in the design and decoupling of the state variable dynamics [78]. Despite these attractive advantages, the

SMC method suffers from chattering. Since chattering is the major obstacle in the practical implementation of SMC, its effects should be reduced to acceptable level. Here's an overview

Consider the following nonlinear system:

$$\dot{x}(t) = f(x,t) + g(x,t)u(t) \tag{3.9}$$

where $\dot{x}(t)$ represents the derivative of the state variable vector $x(t)$, $f(x,t)$ and $g(x,t)$ are continuous function depending on $x(t)$ and time t and $u(t)$ represents control input vector

The discontinuous control switching between two different system structures is designed as

$$u(t) = \begin{cases} u^{+}(t)\ if\ S(x) > 0 \\ u^{-}(t)\ if\ S(x) < 0 \end{cases} \tag{3.10}$$

where $u^{+}(t)$ and $u^{-}(t)$ are two distinct control inputs and $S(x)$ is the sliding surface

The control input in Eq. (3.10) should be designed such that the state variables reach to the sliding surface, move along this surface, and keep the movement on the surface. When the surface is reached, the sliding surface function should satisfy $S(x) = 0$ and, in such a case, the sliding mode exists. The necessary and sufficient condition that ensures the existence condition for the system in Eq. (3.9) is given by

$$S(x)\,\dot{S}(x) < 0 \tag{3.11}$$

The main objective of SMC is to force the state variables onto the sliding surface. Hence, the control input should be designed carefully to ensure the above objective. One well-known method is the equivalent control, which is derived by imposing $S(x) = \dot{S}(x) = 0$ and solving for control input Hence, the derivative of the sliding surface function on the surface can be written as

$$\dot{S}(t) = \frac{\partial S}{\partial x} f(x,t) + \frac{\partial S}{\partial x} g(x,t) u_{eq}(t) = 0 \tag{3.12}$$

Assuming that $\frac{\partial S}{\partial x} g(x,t) \neq 0$ and solving $u_{eq}(t)$ from Eq. (3.12) yields

$$u_{eq}(t) = -\left[\frac{\partial S}{\partial x} g(x,t)\right]^{-1} \frac{\partial S}{\partial x} f(x,t) \tag{3.13}$$

Clearly, the equivalent control requires knowledge of $f(x,t)$ and $g(x,t)$. On the other hand, the constant rate reaching law method, which is widely used as an alternative to the equivalent control, can be derived from

$$\dot{S}(t) = -Ksign(S(x)) \tag{3.14}$$

where K is the parameter that determines the rate of convergence. However, the use of the sign function leads to chattering, which is not desired in practical applications. To reduce chattering, a boundary layer can be introduced around the sliding surface. Overall, sliding mode control is a powerful technique for achieving robust and stable control in nonlinear systems, particularly those subject to uncertainties and disturbances.

3.3.2 Control Design and Stability Analysis

Backstepping-based sliding mode control is a sophisticated control strategy used in nonlinear control systems to achieve robust performance in the presence of uncertainties and disturbances. It combines the principles of backstepping control and sliding mode control to design a controller that drives the system states onto a predefined sliding surface.

In this sub-section a backstepping based sliding mode control is formulated to execute explicit high-alpha maneuvers, the desired smooth time profiles for α, β and μ (i.e. $\boldsymbol{x_{1d}}$) are normally fed externally as reference inputs [68, 69] as shown in Fig. 3.1. The aircraft flight dynamics is assumed to be in the form as given by Eqs. (3.7) and (3.8) in the previous sub-section. The proposed backstepping based sliding mode controller design methodology and its stability proof is discussed below

The tracking error variables $\boldsymbol{e_1}$ and $\boldsymbol{e_2}$ are defined as $\boldsymbol{e_1 = x_1 - x_{1d}}$ and $\boldsymbol{e_2 = x_2 - x_{2d}}$ where, $\boldsymbol{x_{1d}}$ and $\boldsymbol{x_{2d}}$ are the desired profiles of $\boldsymbol{x_1}$ and $\boldsymbol{x_2}$ respectively. Therefore,

$$\dot{\boldsymbol{e}}_{\boldsymbol{1}} = \boldsymbol{f_1} + G_1\boldsymbol{x_2} - \dot{\boldsymbol{x}}_{\boldsymbol{1d}} \tag{3.15}$$

Choosing the Lyapunov function for the $\boldsymbol{e_1}$ dynamics as

$$V_1 = \tfrac{1}{2}\boldsymbol{e_1^T e_1} \tag{3.16}$$

and on differentiation

$$\dot{V}_1 = \boldsymbol{e_1^T}(\boldsymbol{f_1} + G_1\boldsymbol{x_2} - \dot{\boldsymbol{x}}_{\boldsymbol{1d}}) \tag{3.17}$$

Let

$$\boldsymbol{f_1} + G_1\boldsymbol{x_2} - \dot{\boldsymbol{x}}_{\boldsymbol{1d}} = -K_1\boldsymbol{e_1} \tag{3.18}$$

where $K_1 = diag\ (k_{11}, k_{22}, k_{33})$ is chosen as a constant positive definite matrix to render $\dot{V}_1$ negative definite.

Therefore, from Eq. (3.18), the desired profile for the virtual control $\boldsymbol{x_2}$ is obtained as

$$\boldsymbol{x_{2d}} = G_1^{-1}(-K_1\boldsymbol{e_1} - \boldsymbol{f_1} + \dot{\boldsymbol{x}}_{\boldsymbol{1d}}) \tag{3.19}$$

The Lyapunov function for the complete dynamics is now chosen as

$$V_2 = \tfrac{1}{2}\boldsymbol{e_1^T e_1} + \tfrac{1}{2}\boldsymbol{S_1^T S_1} + \tfrac{1}{2}\tilde{\boldsymbol{\sigma}}^T K_2\tilde{\boldsymbol{\sigma}} \tag{3.20}$$

where $\boldsymbol{S_1 = 0}$ is the sliding surface (chosen as a function of the tracking error $\boldsymbol{e_2}$) and $\tilde{\boldsymbol{\sigma}} = \boldsymbol{\sigma} - \hat{\boldsymbol{\sigma}}$ is the parameter estimation error. $K_2 = diag\ (k_{211}, k_{222}, k_{233})$ is the adaptation gain chosen as a constant positive definite diagonal matrix. To achieve fast convergence, a nonlinear sliding surface $\boldsymbol{S_1} = [S_p, S_q, S_r]^T = \boldsymbol{0}$ is chosen element wise as

$$S_p = n_{11}e_p + m_{11}|e_p|^{a_1}sgn(e_p);\ S_q = n_{22}e_q + m_{22}|e_q|^{a_1}sgn(e_q);\ S_r = n_{33}e_r + m_{33}|e_r|^{a_1}sgn(e_r) \tag{3.21}$$

The above three Eqs. in (3.21) can be expressed in a compact form as

$$\boldsymbol{S_1} = N_1\boldsymbol{e_2} + M_1 sig(\boldsymbol{e_2})^{a_1} \tag{3.22}$$

where, $N_1 = diag\ (n_{11}, n_{22}, n_{33})$ and $M_1 = diag\ (m_{11}, m_{22}, m_{33})$ are constant positive definite matrices and a_1 is positive constant (>1).

$$sig(\boldsymbol{e_2})^{a_1} \triangleq \left[|e_p|^{a_1}sgn(e_p) \quad |e_q|^{a_1}sgn(e_q) \quad |e_r|^{a_1}sgn(e_r)\right]^T \tag{3.23}$$

Now from Eq. (3.20),

$$\dot{V}_2 = \boldsymbol{e_1^T\dot{e}_1} + \boldsymbol{S_1^T\dot{S}_1} + \tilde{\boldsymbol{\sigma}}^T K_2\dot{\tilde{\boldsymbol{\sigma}}} \tag{3.24}$$

Substituting $\boldsymbol{\dot{e}_1}$ from (3.15), computing $\boldsymbol{\dot{S}_1}$ from (3.22) and letting $\dot{\tilde{\boldsymbol{\sigma}}} = -\dot{\hat{\boldsymbol{\sigma}}}$,

$$\dot{V}_2 = \boldsymbol{e_1^T}(\boldsymbol{f_1} + G_1\boldsymbol{x_2} - \boldsymbol{\dot{x}_{1d}}) + \boldsymbol{S_1^T}(N_1\boldsymbol{\dot{e}_2} + M_1a_1|\boldsymbol{e_2}|^{a_1-1}\,\boldsymbol{\dot{e}_2}) - \tilde{\boldsymbol{\sigma}}^T K_2\dot{\hat{\boldsymbol{\sigma}}} \tag{3.25}$$

Now defining

$$F_3(\boldsymbol{e_2}) \triangleq N_1 + M_1a_1 diag(|\boldsymbol{e_2}|^{a_1-1}) \tag{3.26}$$

and substituting in Eq. (3.25),

$$\dot{V}_2 = \boldsymbol{e_1^T}[\boldsymbol{f_1} + G_1(\boldsymbol{e_2} + \boldsymbol{x_{2d}}) - \boldsymbol{\dot{x}_{1d}}] + \boldsymbol{S_1^T}[F_3(\boldsymbol{e_2})\,\boldsymbol{\dot{e}_2}] - \tilde{\boldsymbol{\sigma}}^T K_2\dot{\hat{\boldsymbol{\sigma}}} \tag{3.27}$$

Since $\boldsymbol{e_2} = \boldsymbol{x_2} - \boldsymbol{x_{2d}}$,

$$\boldsymbol{\dot{e}_2} = \boldsymbol{f_2} + A\boldsymbol{\sigma} + G_2\boldsymbol{u} + \boldsymbol{d} - \boldsymbol{\dot{x}_{2d}} \tag{3.28}$$

Substituting Eqs. (3.19) and (3.28) in Eq. (3.27), $\dot{V}_2$ reduces to

$$\dot{V}_2 = \boldsymbol{e_1^T}(G_1\boldsymbol{e_2} - K_1\boldsymbol{e_1}) + \boldsymbol{S_1^T}[F_3(\boldsymbol{e_2})(\boldsymbol{f_2} + A\boldsymbol{\sigma} + G_2\boldsymbol{u} + \boldsymbol{d} - \boldsymbol{\dot{x}_{2d}})] - \tilde{\boldsymbol{\sigma}}^T K_2\dot{\hat{\boldsymbol{\sigma}}} \tag{3.29}$$

Further substituting $\boldsymbol{\sigma} = \tilde{\boldsymbol{\sigma}} + \hat{\boldsymbol{\sigma}}$

$$\dot{V}_2 = -\boldsymbol{e_1}^T K_1 \boldsymbol{e_1} + \boldsymbol{e_1}^T G_1 \boldsymbol{e_2} + \boldsymbol{S_1}^T [F_3(\boldsymbol{e_2})(\boldsymbol{f_2} + A\hat{\boldsymbol{\sigma}} + G_2 \boldsymbol{u} + \boldsymbol{d} - \dot{\boldsymbol{x}}_{\boldsymbol{2d}})] - \tilde{\boldsymbol{\sigma}}^T (K_2 \dot{\hat{\boldsymbol{\sigma}}} - A^T F_3^T(\boldsymbol{e_2}) \boldsymbol{S_1})$$

(3.30)

Choosing the adaptation law as

$$\dot{\hat{\boldsymbol{\sigma}}} = K_2^{-1} A^T F_3^T(\boldsymbol{e_2})\, \boldsymbol{S_1} \tag{3.31}$$

equation (3.30) reduces to

$$\dot{V}_2 = -\boldsymbol{e_1}^T K_1 \boldsymbol{e_1} + \boldsymbol{e_1}^T G_1 \boldsymbol{e_2} + \boldsymbol{S_1}^T [F_3(\boldsymbol{e_2})(\boldsymbol{f_2} + A\hat{\boldsymbol{\sigma}} + G_2 \boldsymbol{u} + \boldsymbol{d} - \dot{\boldsymbol{x}}_{\boldsymbol{2d}})] \tag{3.32}$$

Considering a fast reaching law for the sliding mode control for a faster convergence rate,

$$\dot{\boldsymbol{S}}_{\boldsymbol{1}} = -H_1 \boldsymbol{S_1} - H_1 sgn(\boldsymbol{S_1}) \tag{3.33}$$

where $H_1 = diag\ (\eta_{11}, \eta_{22}, \eta_{33})$ is a constant positive definite matrix. Now, designing the control law as

$$\boldsymbol{u} = (F_3(\boldsymbol{e_2})\, G_2)^{-1}\, [F_3(\boldsymbol{e_2})(-\boldsymbol{f_2} - A\hat{\boldsymbol{\sigma}} + \dot{\boldsymbol{x}}_{\boldsymbol{2d}}) - H_1 \boldsymbol{S_1} - F_3(\boldsymbol{e_2}) H_1 sgn(\boldsymbol{S_1})] \tag{3.34}$$

Eq. (3.32) reduces to

$$\dot{V}_2 = -\boldsymbol{e_1}^T K_1 \boldsymbol{e_1} + \boldsymbol{e_1}^T G_1 \boldsymbol{e_2} - \boldsymbol{S_1}^T H_1 \boldsymbol{S_1} - \boldsymbol{S_1}^T F_3(\boldsymbol{e_2})[\, H_1\, sgn(\boldsymbol{S_1}) - \boldsymbol{d}] \tag{3.35}$$

Setting the constant matrix H_1 higher than the upper bound of $\boldsymbol{d}$, and observing that $F_3(\boldsymbol{e_2})$ is a positive quantity,

$$\dot{V}_2 \leq -\boldsymbol{e_1}^T K_1 \boldsymbol{e_1} + \boldsymbol{e_1}^T G_1 \boldsymbol{e_2} - \boldsymbol{S_1}^T H_1 \boldsymbol{S_1} \tag{3.36}$$

Introducing a variable $\boldsymbol{c} = M_1 |\boldsymbol{e_2}|^{a_1}\, sgn(\boldsymbol{e_2})$, $\boldsymbol{S_1}$ can be expressed as $\boldsymbol{S_1} = N_1 \boldsymbol{e_2} + \boldsymbol{c}$. Therefore,

$$\dot{V}_2 \leq -\boldsymbol{e_1}^T K_1 \boldsymbol{e_1} + \boldsymbol{e_1}^T G_1 \boldsymbol{e_2} - (N_1 \boldsymbol{e_2} + \boldsymbol{c})^T H_1 (N_1 \boldsymbol{e_2} + \boldsymbol{c}) \tag{3.37}$$

Now, except the second term all other terms on the right hand side of Eq. (3.37) are negative definite. Adding and subtracting the term $\boldsymbol{e_2}^T N_1 \boldsymbol{c}$ in Eq. (3.37),

$$\dot{V}_2 \leq -\boldsymbol{e_1^T} K_1 \boldsymbol{e_1} + \boldsymbol{e_1^T} G_1 \boldsymbol{e_2} - (N_1 \boldsymbol{e_2} + \boldsymbol{c})^T H_1 (N_1 \boldsymbol{e_2} + \boldsymbol{c}) + \boldsymbol{e_2^T} N_1 \boldsymbol{c} - \boldsymbol{e_2^T} N_1 \boldsymbol{c} \tag{3.38}$$

Expanding the last term $-\boldsymbol{e_2^T} N_1 \boldsymbol{c}$ into its elements,

$$\dot{V}_2 \leq -\boldsymbol{e_1^T} K_1 \boldsymbol{e_1} + \boldsymbol{e_1^T} G_1 \boldsymbol{e_2} - (N_1 \boldsymbol{e_2} + \boldsymbol{c})^T H_1 (N_1 \boldsymbol{e_2} + \boldsymbol{c}) + \boldsymbol{e_2^T} N_1 \boldsymbol{c} - n_{11} m_{11} \left|e_p\right|^{a_1+1} - n_{22} m_{22} \left|e_q\right|^{a_1+1} - n_{33} m_{33} |e_r|^{a_1+1} \tag{3.39}$$

The first four terms of the right-hand side of Eq. (3.39) can be expressed in the form $-\boldsymbol{z}^T Q \boldsymbol{z}$ where

$$\boldsymbol{z}^T Q \boldsymbol{z} = \begin{bmatrix} \boldsymbol{e_1^T} & \boldsymbol{e_2^T} & \boldsymbol{c^T} \end{bmatrix} \begin{bmatrix} K_1 & -\frac{1}{2} G_1 & 0 \\ -\frac{1}{2} G_1^T & N_1^2 H_1 & N_1 H_1 - \frac{N_1}{2} \\ 0 & N_1 H_1 - \frac{N_1}{2} & H_1 \end{bmatrix} \begin{bmatrix} \boldsymbol{e_1} \\ \boldsymbol{e_2} \\ \boldsymbol{c} \end{bmatrix} \tag{3.40}$$

Therefore, Eq. (3.39) can be simplified to

$$\dot{V}_2 \leq -\boldsymbol{z}^T Q \boldsymbol{z} - n_{11} m_{11} \left|e_p\right|^{a_1+1} - n_{22} m_{22} \left|e_q\right|^{a_1+1} - n_{33} m_{33} |e_r|^{a_1+1} \tag{3.41}$$

Clearly, $\dot{V}_2 \leq 0$ and therefore, $\boldsymbol{z}$ (i.e. $\boldsymbol{e_1}$, $\boldsymbol{e_2}$ and $\boldsymbol{S_1}$) is bounded if and only if the Q matrix in Eq. (3.41) is positive definite. Therefore, conditions for positive definiteness of Q are derived next.

Remark 1: Referring to Eqs. (3.5) and (3.7), the matrix G_1 can be expressed as

$$G_1 = \begin{bmatrix} -cos\alpha\ tan\beta & \left(1 - \frac{\rho S \bar{c} C_{Lq}}{4m\ cos\beta}\right) & -sin\alpha\ tan\beta \\ \left(sin\alpha + \frac{\rho S b C_{Yp}}{4m}\right) & 0 & \left(-cos\alpha + \frac{\rho s b C_{Yr}}{4m}\right) \\ \left(cos\alpha\ sec\beta + \frac{tan\gamma\ cos\mu\ \rho S b C_{Yp}}{4m}\right) & \left(\frac{(tan\beta + sin\mu\ tan\gamma)\rho S \bar{c} C_{Lq}}{4m}\right) & \left(sin\alpha\ sec\beta + \frac{tan\gamma\ cos\mu\ \rho S b C_{Yr}}{4m}\right) \end{bmatrix} \tag{3.42}$$

Now the terms containing $\frac{1}{4\,m}$ in Eq. (3.42) can be safely neglected as the mass of the aircraft m is very high (~10^4 kg) compared to the other terms. Also, the term $tan\,\gamma$ does not go beyond the range 3 to 4 as the flight path angle γ usually does not go beyond 70-75° even for very drastic high-alpha maneuvers such as the Herbst [103]. Further, β is also kept small and therefore $tan\,\beta$ is also very

small. Therefore, the matrix Q in Eq. (3.40) can be simplified to the following form after substituting K_1, N_1, H_1.

$$Q = \left[\begin{array}{cccc|cccc|cccc}
k_{11} & 0 & 0 & 0 & \frac{cosatan\beta}{2} & -\frac{1}{2} & \frac{sinatan\beta}{2} & 0 & 0 & 0 & 0 & 0 \\
0 & k_{22} & 0 & 0 & -\frac{sin\alpha}{2} & 0 & \frac{cos\alpha}{2} & 0 & 0 & 0 & 0 & 0 \\
0 & 0 & k_{33} & 0 & -\frac{cosasec\beta}{2} & 0 & -\frac{sinasec\beta}{2} & 0 & 0 & 0 & 0 & 0 \\
\hline
\frac{cosatan\beta}{2} & -\frac{sin\alpha}{2} & -\frac{(cosasec\beta)}{2} & 0 & n_{11}^2\eta_{11} & 0 & 0 & n_{11}\eta_{11} - \frac{n_{11}}{2} & 0 & 0 & 0 & 0 \\
-\frac{1}{2} & 0 & 0 & 0 & 0 & n_{22}^2\eta_{22} & 0 & 0 & n_{22}\eta_{22} - \frac{n_{22}}{2} & 0 & 0 & 0 \\
\frac{sinatan\beta}{2} & \frac{cos\alpha}{2} & -\frac{sinasec\beta}{2} & 0 & 0 & 0 & n_{33}^2\eta_{33} & 0 & 0 & 0 & n_{33}\eta_{33} - \frac{n_{33}}{2} & \\
0 & 0 & 0 & 0 & n_{11}\eta_{11} - \frac{n_{11}}{2} & 0 & 0 & \eta_{11} & 0 & 0 & 0 & \\
0 & 0 & 0 & 0 & 0 & n_{22}\eta_{22} - \frac{n_{22}}{2} & 0 & 0 & \eta_{22} & 0 & & \\
0 & 0 & 0 & 0 & 0 & 0 & n_{33}\eta_{33} - \frac{n_{33}}{2} & 0 & 0 & \eta_{33} & &
\end{array}\right] \tag{3.43}$$

Theorem 3.1: The 9×9 Q matrix given by Eq. (3.43) is positive definite if and only if

$$\eta_{11}, \eta_{22}, \eta_{33} > \frac{1}{4} \tag{3.44}$$

and the following 3×3 matrix is positive definite

$$\begin{bmatrix} 4k_{11} - a_{1a}(cos\alpha\ tan\beta)^2 - a_{2a} - a_{3a}(sin\alpha\ tan\beta)^2 & (a_{1a} - a_{3a})cos\alpha\ tan\beta\ sin\alpha & a_{1a}\cos^2\alpha\ tan\beta\ sec\beta + a_{3a}sin^2\alpha\ tan\beta\ sec\beta \\ (a_{1a} - a_{3a})cos\alpha\ tan\beta\ sin\alpha & 4k_{22} - (a_{1a}\sin^2\alpha + a_{3a}\cos^2\alpha) & -(a_{1a} - a_{3a})sin\alpha\ cos\alpha\ sec\beta \\ a_{1a}\cos^2\alpha\ tan\beta\ sec\beta + a_{3a}sin^2\alpha\ tan\beta\ sec\beta & -(a_{1a} - a_{3a})sin\alpha\ cos\alpha\ sec\beta & 4k_{33} - a_{1a}(cos\alpha\ sec\beta)^2 - a_{3a}(sin\alpha\ sec\beta)^2 \end{bmatrix} \tag{3.45}$$

where $a_{1a} \triangleq \frac{4\eta_{11}}{4n_{11}^2\eta_{11} - n_{11}^2}$, $a_{2a} \triangleq \frac{4\eta_{22}}{4n_{22}^2\eta_{22} - n_{22}^2}$, $a_{3a} \triangleq \frac{4\eta_{33}}{4n_{33}^2\eta_{33} - n_{33}^2}$.

Proof: The following lemma is needed to prove Theorem 3.1.

Lemma 1: According to Schur Complement method [104] for any block symmetric matrix of the form $Q = \begin{bmatrix} A & B \\ B^T & C \end{bmatrix}$, if C is invertible, then $Q \geq 0$ if and only if $C \geq 0$ and $A - BC^{-1}B^T \geq 0$.

Partitioning the Q matrix as shown in Eq. (3.43), A, B, C are given by

$$A = K_1 = \begin{bmatrix} k_{11} & 0 & 0 \\ 0 & k_{22} & 0 \\ 0 & 0 & k_{33} \end{bmatrix} \tag{3.46}$$

$$B = \frac{1}{2}\begin{bmatrix} cos\alpha\ tan\beta & -1 & sin\alpha\ tan\beta & 0 & 0 & 0 \\ -sin\alpha & 0 & cos\alpha & 0 & 0 & 0 \\ -cos\alpha\ sec\beta & 0 & -sin\alpha\ sec\beta & 0 & 0 & 0 \end{bmatrix} \tag{3.47}$$

$$C = \begin{bmatrix} n_{11}^2\eta_{11} & 0 & 0 & n_{11}\eta_{11} - \frac{n_{11}}{2} & 0 & 0 \\ 0 & n_{22}^2\eta_{22} & 0 & 0 & n_{22}\eta_{22} - \frac{n_{22}}{2} & 0 \\ 0 & 0 & n_{33}^2\eta_{33} & 0 & 0 & n_{33}\eta_{33} - \frac{n_{33}}{2} \\ n_{11}\eta_{11} - \frac{n_{11}}{2} & 0 & 0 & \eta_{11} & 0 & 0 \\ 0 & n_{22}\eta_{22} - \frac{n_{22}}{2} & 0 & 0 & \eta_{22} & 0 \\ 0 & 0 & n_{33}\eta_{33} - \frac{n_{33}}{2} & 0 & 0 & \eta_{33} \end{bmatrix} \tag{3.48}$$

Clearly, C is also a block symmetric matrix of the form $\begin{bmatrix} X & Y \\ Y^T & Z \end{bmatrix}$ with X, Y, Z all being 3×3 diagonal matrices. Therefore, applying Lemma 1 once more, $C \geq 0$ if and only if $Z = diag\,(\eta_{11}\,,\ \eta_{22}\,,\ \eta_{33}) > 0$ and $X - YZ^{-1}Y^T \geq 0$. The condition $Z > 0$ is already satisfied since $\eta_{11}, \eta_{22}, \eta_{33}$ are positive constants. For the condition $X - YZ^{-1}Y^T \geq 0$ to be satisfied, substituting the corresponding expressions of X, Y, Z yields,

$$diag\ \left[n_{11}^2\eta_{11} - \frac{1}{\eta_{11}}\left(n_{11}\eta_{11} - \frac{n_{11}}{2}\right)^2,\quad n_{22}^2\eta_{22} - \frac{1}{\eta_{22}}\left(n_{22}\eta_{22} - \frac{n_{22}}{2}\right)^2,\quad n_{33}^2\eta_{33} - \frac{1}{\eta_{33}}\left(n_{33}\eta_{33} - \frac{n_{33}}{2}\right)^2\right] > 0 \tag{3.49}$$

which, on further simplification, reduces to

$$\eta_{11}, \eta_{22}, \eta_{33} > \frac{1}{4} \tag{3.50}$$

Condition (3.50) ensures that $C \geq 0$. Now for the condition $A - BC^{-1}B^T \geq 0$, C^{-1} can be computed using the Matrix Inversion Lemma [105] as

$$C^{-1} = \begin{bmatrix} diag\left(\frac{4\eta_{11}}{4n_{11}^2\eta_{11} - n_{11}^2},\ \frac{4\eta_{22}}{4n_{22}^2\eta_{22} - n_{22}^2},\ \frac{4\eta_{33}}{4n_{33}^2\eta_{33} - n_{33}^2}\right) & diag\left(\frac{2(1-2\eta_{11})}{4n_{11}\eta_{11} - n_{11}},\ \frac{2(1-2\eta_{22})}{4n_{22}\eta_{22} - n_{22}},\ \frac{2(1-2\eta_{33})}{4n_{33}\eta_{33} - n_{33}}\right) \\ diag\left(\frac{2(1-2\eta_{11})}{4n_{11}\eta_{11} - n_{11}},\ \frac{2(1-2\eta_{22})}{4n_{22}\eta_{22} - n_{22}},\ \frac{2(1-2\eta_{33})}{4n_{33}\eta_{33} - n_{33}}\right) & diag\left(\frac{4\eta_{11}}{4\eta_{11} - 1},\ \frac{4\eta_{22}}{4\eta_{22} - 1},\ \frac{4\eta_{33}}{4\eta_{33} - 1}\right) \end{bmatrix}$$

Denoting

$$C^{-1} \triangleq \begin{bmatrix} diag\,(a_{1a},\ \ a_{2a},\ \ a_{3a}) & diag\,(b_{1a},\ \ b_{2a},\ \ b_{3a}) \\ diag\,(b_{1a},\ \ b_{2a},\ \ b_{3a}) & diag\,(c_{1a}\ \ c_{2a}\ \ c_{3a}) \end{bmatrix} \tag{3.51}$$

and substituting A, B, C^{-1} from (3.46), (3.47) and (3.51) respectively results in the following inequality for the condition $A - BC^{-1}B^T \geq 0$

$$\begin{bmatrix} 4k_{11} - a_{1a}(cos\alpha\ tan\beta)^2 - a_{2a} - a_{3a}(sin\alpha\ tan\beta)^2 & (a_{1a} - a_{3a})cos\alpha\ tan\beta\ sin\alpha & a_{1a}\cos^2\alpha\ tan\beta\ sec\beta + a_{3a}sin^2\alpha\ tan\beta\ sec\beta \\ (a_{1a} - a_{3a})cos\alpha\ tan\beta\ sin\alpha & 4k_{22} - (a_{1a}\sin^2\alpha + a_{3a}\cos^2\alpha) & -(a_{1a} - a_{3a})\ sin\alpha\ cos\alpha\ sec\beta \\ a_{1a}\cos^2\alpha\ tan\beta\ sec\beta + a_{3a}sin^2\alpha\ tan\beta\ sec\beta & -(a_{1a} - a_{3a})sin\alpha\ cos\alpha\ sec\beta & 4k_{33} - a_{1a}(cos\alpha\ sec\beta)^2 - a_{3a}(sin\alpha\ sec\beta)^2 \end{bmatrix} > 0 \tag{3.52}$$

Remark 2: It is evident that the condition in Eq. (3.52) is state (i.e. angle of attack and the angle of sideslip) dependent. Therefore, the condition is further simplified in the following proposition considering realistic ranges for these two state variables.

As inequality (3.52) involves α and β dependent terms, maximum possible range of variations in their values are considered to establish stability. For F18-HARV, the aircraft considered in the present study, aerodynamic data are available over the α range of -14^o to +90^o. Moreover, for the standard high alpha maneuvers, usually β is commanded to remain zero. It is observed from the literature [66, 99] that even under feasible system uncertainties and external disturbances β remains well within ±15^o. Therefore, considering $\beta \in [-15^o, +15^o]$ and $\alpha \in [-14^o, +90^o]$, and considering the worst case variations in the elements of the matrix in (3.58) the following condition involving an interval matrix can be arrived at

$$\begin{bmatrix} 4k_{11} - (a_{1a} + a_{3a})\,[0,\ 0.07] - a_{2a} & (a_{1a} - a_{3a})\,[-0.13,\ 0.13] & (a_{1a} + a_{3a})\,[-0.27,\ 0.27] \\ (a_{1a} - a_{3a})\,[-0.13, 0.13] & 4k_{22} - (a_{1a} + a_{3a})[0, 1] & -(a_{1a} - a_{3a})\,[-0.26, 0.52] \\ (a_{1a} + a_{3a})\,[-0.27, 0.27] & -(a_{1a} - a_{3a})\,[-0.26\,, 0.52] & 4k_{33} - (a_{1a} + a_{3a})\,[0, 1.07] \end{bmatrix} > 0 \tag{3.53}$$

Clearly, for the above condition to hold

$$4k_{11} - (a_{1a} + a_{3a})\,[0,\ 0.07] - a_{2a} > 0 \tag{3.54}$$

$$\begin{vmatrix} 4k_{11} - (a_{1a} + a_{3a})\,[0,\ 0.07] - a_{2a} & (a_{1a} - a_{3a})\,[-0.13,0.13] \\ (a_{1a} - a_{3a})\,[-0.13,0.13] & 4k_{22} - (a_{1a} + a_{3a})[0, 1] \end{vmatrix} > 0 \tag{3.55}$$

$$\begin{vmatrix} 4k_{11} - (a_{1a} + a_{3a})\,[0,\ 0.07] - a_{2a} & (a_{1a} - a_{3a})\,[-0.13, 0.13] & (a_{1a} + a_{3a})\,[-0.27, 0.27] \\ (a_{1a} - a_{3a})\,[-0.13, 0.13] & 4k_{22} - (a_{1a} + a_{3a})[0, 1] & -(a_{1a} - a_{3a})\,[-0.26, 0.52] \\ (a_{1a} + a_{3a})\,[-0.27, 0.27] & -(a_{1a} - a_{3a})\,[-0.26, 0.52] & 4k_{33} - (a_{1a} + a_{3a})\,[0, 1.07] \end{vmatrix} > 0 \tag{3.56}$$

Now applying the interval arithmetic formulas [106] such as:

If $[x_1, y_1]$ and $[x_2, y_2]$ are bounded, nonempty, real intervals, then

$[x_1, x_2] + [y_1, y_2] = [x_1 + y_1, x_2 + y_2]$

$[x_1, x_2] - [y_1, y_2] = [x_1 - y_2, x_2 - y_1]$

$[x_1, x_2]\,[y_1, y_2] = [\min(Z), \max(Z)]$ where $Z = \{x_1y_1, x_1y_2, x_2y_1, x_2y_2\}$

and considering the worst case scenarios i.e. upper limit for negative terms and lower limits for positive terms, the above three inequalities are simplified one by one as

First Condition

$$k_{11} > \tfrac{1}{4}\{0.07(a_{1a} + a_{3a}) + a_{2a}\} \tag{3.57}$$

Second Condition

$$\{4k_{11} - (a_{1a} + a_{3a})\,[0, 0.07] - a_{2a}\}\{4k_{22} - (a_{1a} + a_{3a})[0, 1]\} - \{(a_{1a} - a_{3a})\,[-0.13, 0.13]\}^2 > 0 \tag{3.58}$$

On expanding Eq. (3.58), we get

$$16k_{11}k_{22} - 4k_{11}(a_{1a} + a_{3a})[0,1] - 4k_{22}(a_{1a} + a_{3a})[0,0.07] + (a_{1a} + a_{3a})[0,0.07](a_{1a} + a_{3a})[0,1] -$$

$$4k_{22}a_{2a} + a_{2a}(a_{1a} + a_{3a})[0,1] - \{(a_{1a} - a_{3a})\,[-0.13, 0.13]\}^2 > 0 \tag{3.59}$$

Now, applying interval arithmetic and considering the worst case scenarios i.e. upper limit for negative terms and lower limits for positive terms, the Eq. (3.59) reduces to

$$16k_{11}k_{22} - 4k_{11}(a_{1a} + a_{3a}) - 4k_{22}(a_{1a} + a_{3a})(0.07) - 4k_{22}a_2 - (a_{1a} - a_{3a})^2(0.169) > 0 \tag{3.60}$$

Further rearranging Eq. (3.60) leads to

$$k_{22}\{4k_{11} - (a_{1a} + a_{3a})0.07 - a_{2a}\} > k_{11}(a_{1a} + a_{3a}) + (a_{1a} - a_{3a})^2 0.0423 \tag{3.61}$$

Third Condition

$$\{4k_{11} - (a_{1a} + a_{3a})\,[0, 0.07] - a_{2a}\}\{(4k_{22} - (a_{1a} + a_{3a})[0, 1])(4k_{33} - (a_{1a} + a_{3a})[0, 1.07]) - (a_{1a} -$$

$$a_{3a})^2\,[-0.26, 0.52]\} - \{(a_{1a} - a_{3a})\,[-0.13, 0.13]\}\{((a_{1a} - a_{3a})\,[-0.13, 0.13])(4k_{33} - (a_{1a} +$$

$a_{3a})\,[0,1.07]) - ((a_{1a} + a_{3a})\,[-0.27,0.27])(-(a_{1a} - a_{3a})\,[-0.26,0.52])\} + \{((a_{1a} +$

$a_{3a})\,[-0.27,0.27])\}\{((a_{1a} - a_{3a})\,[-0.13,0.13])(-(a_{1a} - a_{3a})\,[-0.26,0.52]) - ((4k_{22} - (a_{1a} +$

$a_{3a})[0,1])(a_{1a} + a_{3a})\,[-0.27,0.27])\} > 0$ (3.62)

On expanding Eq. (3.62), we get

$64k_{11}k_{22}k_{33} - 16k_{11}k_{22}(a_{1a} + a_{3a})[0,1.07] - 16k_{11}k_{33}(a_{1a} + a_{3a})[0,1] + 4k_{11}(a_{1a} + a_{3a})[0,1](a_{1a} +$

$a_{3a})[0,1.07] - 4k_{11}(a_{1a} - a_{3a})^2[-0.26,0.52]^2 - 16k_{22}k_{33}(a_{1a} + a_{3a})[0,0.07] + 4k_{22}(a_{1a} +$

$a_{3a})[0,1.07](a_{1a} + a_{3a})[0,1.07] + 4k_{33}(a_{1a} + a_{3a})[0,1](a_{1a} + a_{3a})[0,0.07] - (a_{1a} +$

$a_{3a})[0.0.07](a_{1a} + a_{3a})[0,1.07](a_{1a} + a_{3a})[0,0.07] + (a_{1a} + a_{3a})[0,0.07](a_{1a} - a_{3a})^2[-0.26,0.52]^2 -$

$16k_{22}k_{33}a_{2a} + 4k_{22}a_{2a}(a_{1a} + a_{3a})[0,1.07] + 4k_{33}a_{2a}(a_{1a} + a_{3a})[0,1] - a_{2a}(a_{1a} + a_{3a})[0,1] +$

$a_{2a}(a_{1a} - a_{3a})^2[-0.26,0.52]^2 - 4k_{33}(a_{1a} - a_{3a})[-0.13,0.13](a_{1a} - a_{3a})[-0.13,0.13] + (a_{1a} -$

$a_{3a})[-0.13,0.13](a_{1a} - a_{3a})[-0.13,0.13](a_{1a} + a_{3a})[0,1.07] - (a_{1a} - a_{3a})[-0.13,0.13](a_{1a} +$

$a_{3a})[-0.27,0.27](a_{1a} - a_{3a})[-0.26,0.52] - (a_{1a} + a_{3a})[-0.27,0.27](a_{1a} - a_{3a})[-0.13,0.13](a_{1a} -$

$a_{3a})[-0.26,0.52] - 4k_{22}(a_{1a} + a_{3a})[-0.27,0.27](a_{1a} - a_{3a})[-0.27,0.27] + (a_{1a} +$

$a_{3a})[-0.27,0.27](a_{1a} + a_{3a})[0,1](a_{1a} + a_{3a})[-0.27,0.27] > 0$ (3.63)

Now, applying interval arithmetic and considering the worst case scenarios i.e. upper limit for negative terms and lower limits for positive terms, the Eq. (3.63) reduces to

$64k_{11}k_{22}k_{33} - 16k_{11}k_{22}(a_{1a} + a_{3a})(1.07) - 16k_{11}k_{33}(a_{1a} + a_{3a}) - 4k_{11}(a_{1a} - a_{3a})^2(0.27) -$

$16k_{22}k_{33}(a_{1a} + a_{3a})(0.07) - (a_{1a} + a_{3a})^3(0.07)^2(1.07) - 16k_{22}k_{33}a_{2a} - a_{2a}(a_{1a} + a_{3a})^2(1.07) +$

$a_{2a}(a_{1a} - a_{3a})^2(0.06) - 4k_{33}(a_{1a} - a_{3a})^2(0.169) - (a_{1a} - a_{3a})^2(0.13)(0.52)(a_{1a} + a_{3a})(0.27) -$

$(a_{1a} + a_{3a})(0.27)(a_{1a} - a_{3a})^2(0.13)(0.52) - 4k_{22}a_{2a}(a_{1a} + a_{3a})^2(0.27)^2 > 0$ (3.64)

Further rearrangement of Eq. (3.64) leads to

$k_{33}\{16k_{11}k_{22} - 4k_{11}(a_{1a} + a_{3a}) - 4k_{22}(a_{1a} + a_{3a})0.07 - 4k_{22}a_{2a} - (a_{1a} - a_{3a})^2 0.169\} >$

$4k_{11}k_{22}(a_{1a} + a_{3a})1.07 + (a_{1a} - a_{3a})^2\{k_{11}0.27 - a_{2a}0.0150 - 0.0423 + 2(a_{1a} +$

$a_{3a})0.0046\} + \quad (a_{1a} + a_{3a})^2\{k_{22}0.0729 + (a_{1a} + a_{3a})0.0013 + a_{2a}0.2675\}$ (3.65)

Remark 3: The design parameters a_{1a}, a_{2a}, a_{3a} are dependent on the elements of the matrices H_1 and N_1; therefore, they should be chosen first (H_1 further satisfying the conditions in Eq. (3.44)) and thereafter the elements of the matrix K_1 should be designed so that the inequalities given by Eq. (3.57), Eq. (3.61), and Eq. (3.65) are satisfied.

Remark 4: Equation (3.41) establishes negative semi-definiteness of $\dot{V}_2$. Therefore, Barbalat's lemma can now be invoked to investigate asymptotic stability of the origin. Integrating Eq. (3.41),

$$\int_0^\infty \left(\boldsymbol{z}^T(\tau)Q\boldsymbol{z}(\tau)+n_{11}m_{11}\left|e_p(\tau)\right|^{a_1+1}+n_{22}m_{22}\left|e_q(\tau)\right|^{a_1+1}+n_{33}m_{33}|e_r(\tau)|^{a_1+1}\right)d\tau \leq -\int_0^\infty \dot{V}_2(\tau)d\tau$$

$$= V_2(0) - V_2(\infty) < \infty \tag{3.66}$$

Because $\lim_{t\to\infty}\int_0^t \left(\boldsymbol{z}^T(\tau)Q\boldsymbol{z}(\tau)+n_{11}m_{11}\left|e_p(\tau)\right|^{a_1+1}+n_{22}m_{22}\left|e_q(\tau)\right|^{a_1+1}+n_{33}m_{33}|e_r(\tau)|^{a_1+1}\right)d\tau$ is bounded, according to Barbalat's lemma [56, 107] it can be concluded that

$$\lim_{t\to\infty}\left(\boldsymbol{z}^T(\tau)Q\boldsymbol{z}(\tau)+n_{11}m_{11}\left|e_p(\tau)\right|^{a_1+1}+n_{22}m_{22}\left|e_q(\tau)\right|^{a_1+1}+n_{33}m_{33}|e_r(\tau)|^{a_1+1}\right)=0 \tag{3.67}$$

In other words, $\boldsymbol{z}$ (i.e. $\boldsymbol{e_1}$, $\boldsymbol{e_2}$ and $\boldsymbol{S_1}$) converges to zero asymptotically. Therefore, the proposed controller guarantees asymptotic stability of $\boldsymbol{z}$.

3.4 Simulation Validation and Performance Analysis

To validate the proposed control scheme, high-alpha cobra and Herbst maneuver is considered for the F18-HARV aircraft. The geometric and mass properties of the aircraft along with the control surface characteristics and the aerodynamic coefficients can be found in [60, 100] and for the sake of ready reference is also given in Appendix-C. Three cases of c.g. positions are considered for the simulation studies. First the c.g. is assumed to be at the nominal position and thereafter at laterally shifted positions on both port (denoted as Asym(-)) and starboard sides (denoted as Asym(+)) and the controller performances in each of the three situations are compared. It is assumed that the aircraft

is initially trimmed at an altitude of $2000\,m$ and at a velocity of $150\,m/s$ before initiating the maneuver. To simulate a significant c.g. variation, the aircraft is assumed to carry a single store weighing $800\,kg$ housed first on the starboard side and thereafter on the port side under the wing at a lateral distance of one third of the semispan from the fuselage centerline. Along the x- and z- body axes, the store is assumed to be at $0.45\,m$ downward from the local horizontal plane and $0.5\,m$ along the nose from the nominal c.g. position or the origin of the body reference frame respectively. These would cause the aircraft c.g. to shift to the location $[2.3\ \pm 8.8\ \ 2.1]^T\,cm$ with respect to the origin of the body frame. The 6-DOF aircraft dynamics is simulated considering the exact asymmetric equations of motion under c.g. offset as shown in Eq. (3.1). Further, along with the c.g. variations, the aerodynamic coefficients are also assumed to be uncertain with a $\pm 30\%$ uncertainty band about their nominal values. Large number of Monte Carlo runs are performed taking aerodynamic coefficients randomly within this band and almost identical maneuver performance is observed in each run. However, the results corresponding to only three sample runs (one each for maximum c.g variations denoted as Asym(+) and Asym(-) and one without any c.g variation denoted as Sym) are presented in the figures below for the sake of brevity. Also, a tanh function is used instead of signum function to reduce chattering. Numerical simulations are performed using the standard fourth order Runge-Kutta method.

To perform cobra maneuver, the aircraft is pitched up to a high value and then quickly brought back to the initial pitch to achieve a sudden and drastic drop in forward velocity [68, 69]. Therefore, a smooth bell-shaped curve for desired angle of attack (α) profile as shown in Fig. 3.2 are generated as $\alpha_d = \frac{1}{1+\left|\frac{t-c}{a}\right|^{2b}}$ the value of a, b, and c are set with trial and error and listed in Table 3.1 and is fed to the controller (where peak value of desired α is taken to about 60°). Bank angle (μ), and sideslip angle (β) are commanded at their initial trim values i.e. zero throughout the maneuver. The total maneuver duration is considered to be $6s$ initiated at $t = 0$. To enhance the thrust vector control

power, throttle is increased to 50% in an open loop manner over the maneuver duration. Figures 3.3 and 3.4 depict the time evolutions of various states, c.g. estimates, sliding surfaces corresponding to the aforementioned three cases of c.g. locations and the control surface deflections respectively Figure 3.3 shows that the desired α, β, μ profiles are very closely tracked. As expected in cobra maneuver, the aircraft pitches up to a maximum of 90^o and its velocity nearly halves in about $4s$. Control surface deflections are also found to remain largely within their respective saturation limits. It is also observed in Figures 3.3 and 3.4 that the responses corresponding to all the three cases of c.g. positions are almost completely overlapping. This clearly demonstrates excellent robustness of the proposed controller to the c.g. and aerodynamic uncertainties.

To perform the Herbst maneuver, the aircraft is first taken to a high angle of attack value and then a velocity vector roll is initiated [68, 103]. Therefore, bell-shaped curves for α and μ commands as shown in Fig.3.5. are generated same as in cobra maneuver the value of a, b, and c are set with trial and error and listed in Table 3.2 keeping β at the initial trim value. The total maneuver duration of $18s$ is considered initiating the maneuver at $t = 0$. Bank angle command is increased from the initial trim value after $3s$. Figures 3.6 and 3.7 shows the time evolutions of the states and the controls. Figure 3.6 clearly manifests excellent tracking performance as well as robustness of the proposed closed loop scheme since responses for all the situations are nearly overlapping. The ground track of the trajectories do not show any significant variations either. From Fig. 3.7 it is readily observed that the controls remained largely within their saturation limits. For pitch and yaw thrust vectors position and rate limit values are considered to be $\pm 20\, deg$ and $\pm 80\, deg/s$ respectively. Other control surface properties are given in Appendix-C. Throttle is increased in an open loop manner during the maneuver. A stable first order throttle dynamics is considered. Various controller parameters designed satisfying the set of conditions as given in Eqs. (3.57), (3.61), and (3.65) are listed in Table 3.3.

For c.g. estimates and actual c.g. positions (i.e. $\hat{\boldsymbol{\sigma}}$ and $\boldsymbol{\sigma}$), however, the results corresponding to only three sample runs (one each for maximum c.g variations denoted as Asym(+) and Asym(-) along positive and negative y- directions respectively and one without any c.g variation denoted as Sym) are presented for the sake of brevity for both the maneuver. It is clearly observed that the error in c.g estimate i.e. $\tilde{\boldsymbol{\sigma}}$ does not converge to zero. The asymptotic stability proof as presented through Barbalat's lemma in Remark 4 in Section 3.3.2, guarantees asymptotic convergence of the tracking error vector $\boldsymbol{e_1}$ and the sliding surface vector $\boldsymbol{S_1}$, but does not guarantee asymptotic convergence of $\tilde{\boldsymbol{\sigma}}$; $\tilde{\boldsymbol{\sigma}}$ is guaranteed to remain only bounded as established from negative semi-definiteness of the Lyapunov function V_2. The inexact estimate $\hat{\boldsymbol{\sigma}}$ will impact the controller output $\boldsymbol{u}$ as evident from Eq. (3.34), and therefore, will have some effect on the transient response of the tracking error $\boldsymbol{e_1}$. However, the steady state value of $\boldsymbol{e_1}$ will remain zero as mathematically guaranteed from Barbalat's lemma. Figure 3.3(d) and 3.6(h) also shows the asymptotically convergent nature of the sliding surface vector $\boldsymbol{S_1}$.

Table 3.1: Desired reference signal parameters: Cobra maneuver

Reference signal	$\boldsymbol{a}$	$\boldsymbol{b}$	$\boldsymbol{c}$
Angle of attack (α)	1.5	1	3

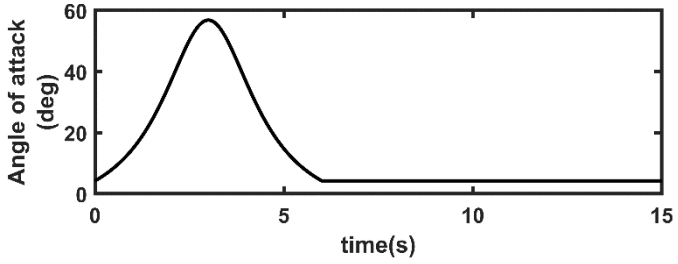

Figure 3.2. Time evolution of desired reference signal: Cobra maneuver

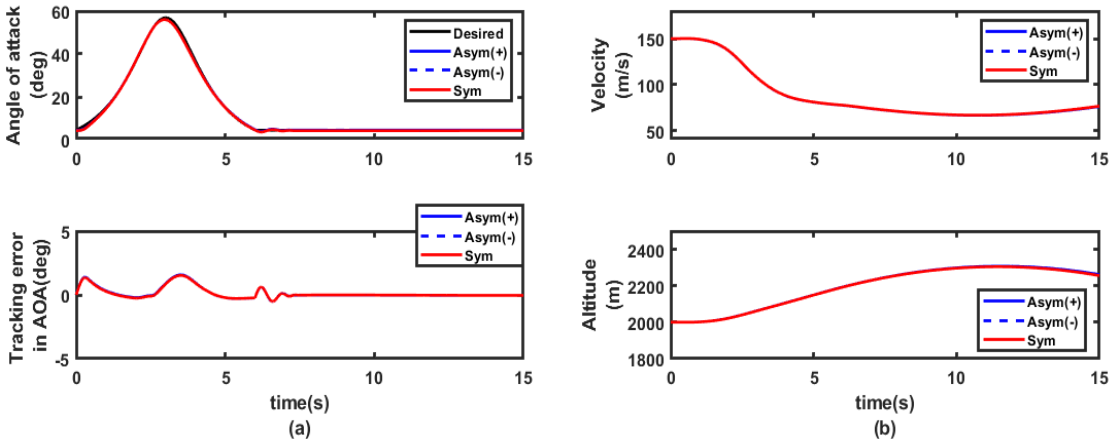
Angle of attack (deg)
Desired
Asym(+)
Asym(-)
Sym
Velocity (m/s)
Asym(+)
Asym(-)
Sym
Tracking error in AOA(deg)
Asym(+)
Asym(-)
Sym
Altitude (m)
Asym(+)
Asym(-)
Sym
time(s)
(a)
time(s)
(b)

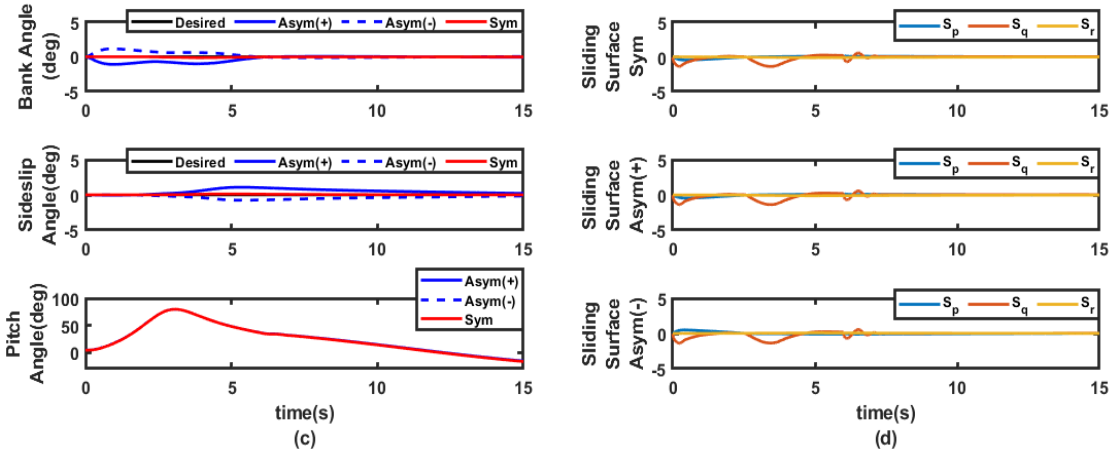
Bank Angle (deg)
Desired
Asym(+)
Asym(-)
Sym
Sliding Surface Sym
S_p
S_q
S_r
Sideslip Angle(deg)
Desired
Asym(+)
Asym(-)
Sym
Sliding Surface Asym(+)
S_p
S_q
S_r
Pitch Angle(deg)
Asym(+)
Asym(-)
Sym
Sliding Surface Asym(-)
S_p
S_q
S_r
time(s)
(c)
time(s)
(d)

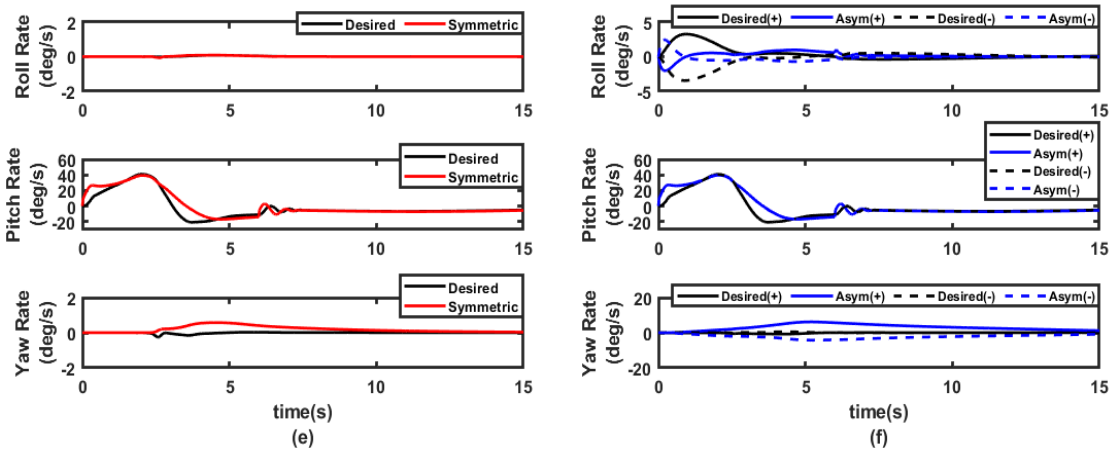
Roll Rate (deg/s)
Desired
Symmetric
Roll Rate (deg/s)
Desired(+)
Asym(+)
Desired(-)
Asym(-)
Pitch Rate (deg/s)
Desired
Symmetric
Pitch Rate (deg/s)
Desired(+)
Asym(+)
Desired(-)
Asym(-)
Yaw Rate (deg/s)
Desired
Symmetric
Yaw Rate (deg/s)
Desired(+)
Asym(+)
Desired(-)
Asym(-)
time(s)
(e)
time(s)
(f)

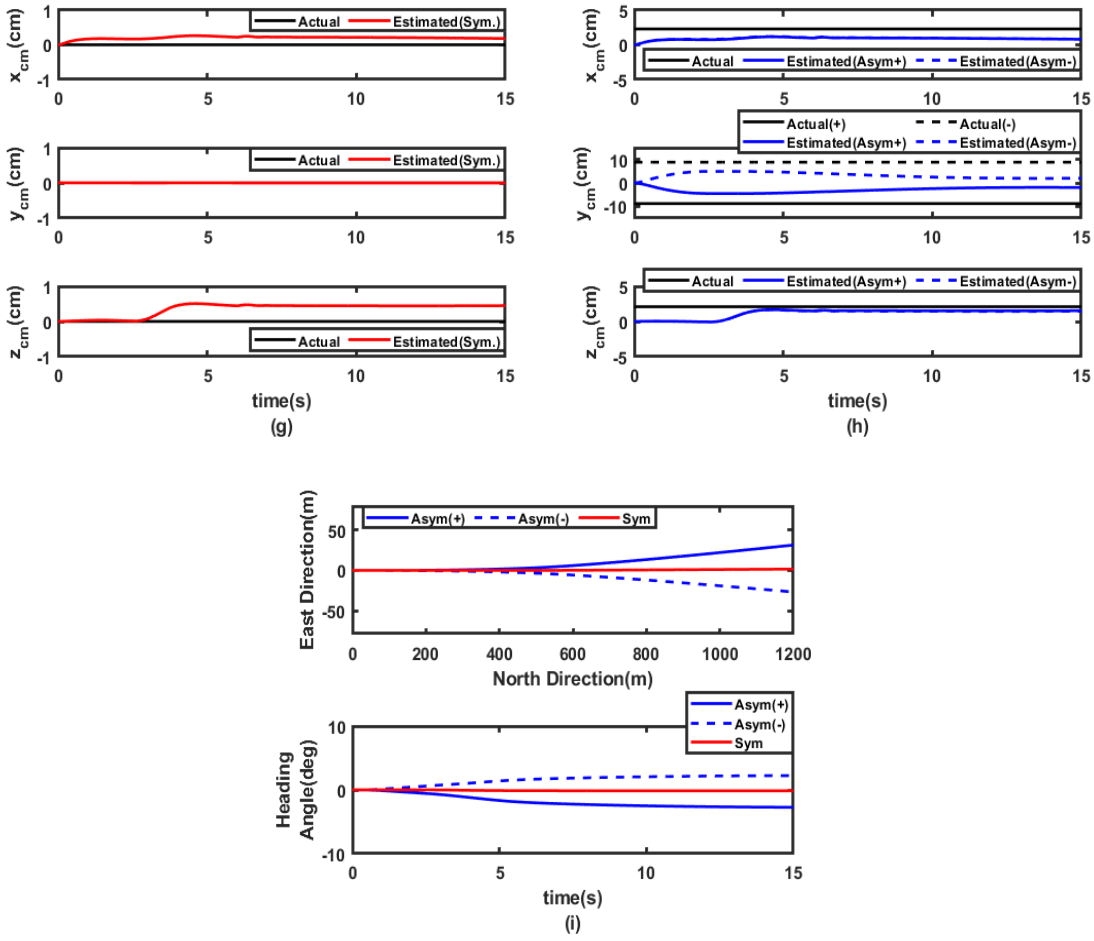

Figure 3.3. Ground track, time evolution of states, sliding surfaces and c.g. position: Cobra maneuver (c.g. at nominal as well as shifted position)

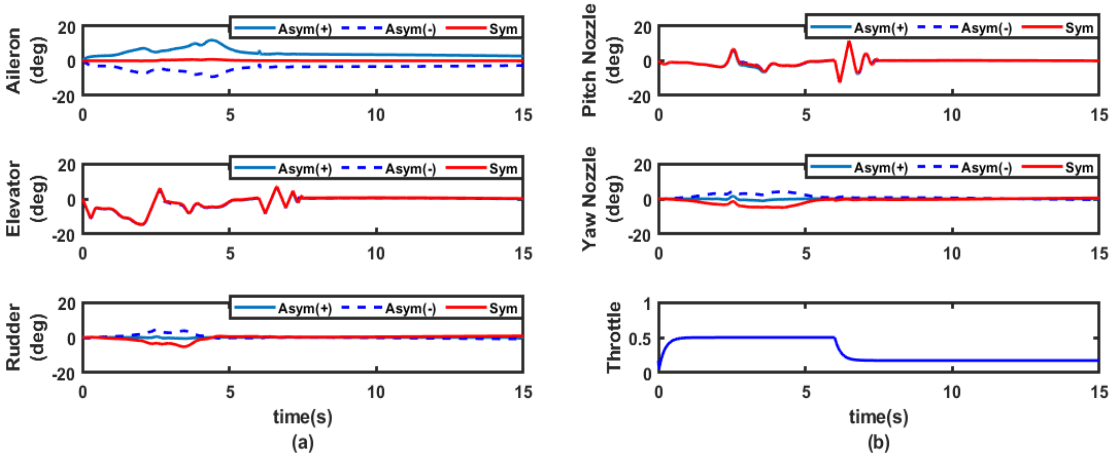

Figure 3.4. Time evolution of control deflections: Cobra maneuver (c.g. at nominal as well as shifted position)

Table 3.2: Desired reference signal parameters: Herbst maneuver

Reference signal	a	b	c
Angle of attack (α)	7	4	9
Bank angle (μ)	5	3	10.5

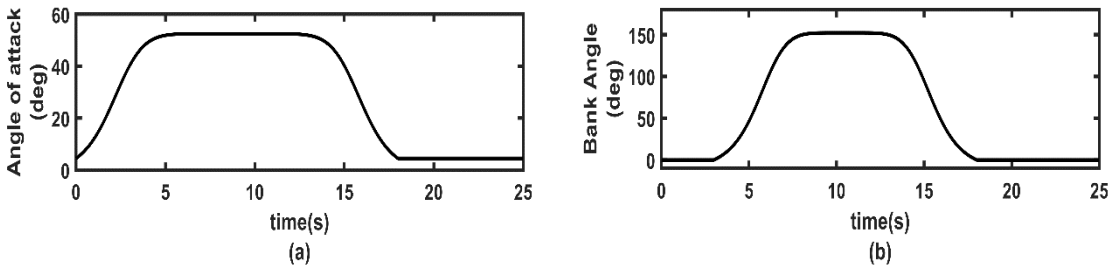

Figure 3.5. Time evolution of desired reference signal: Herbst maneuver

Table 3.3: Controller parameters

Maneuver	K_1	N_1	M_1	a_1	H_1	K_2
Cobra	$\begin{bmatrix}12 & 0 & 0\\ 0 & 4 & 0\\ 0 & 0 & 3\end{bmatrix}$	$\begin{bmatrix}7 & 0 & 0\\ 0 & 4 & 0\\ 0 & 0 & 1\end{bmatrix}$	$\begin{bmatrix}1 & 0 & 0\\ 0 & 0.2 & 0\\ 0 & 0 & 4\end{bmatrix}$	2	$\begin{bmatrix}3 & 0 & 0\\ 0 & 1 & 0\\ 0 & 0 & 0.8\end{bmatrix}$	$\begin{bmatrix}30 & 0 & 0\\ 0 & 50 & 0\\ 0 & 0 & 25\end{bmatrix}$
Herbst	$\begin{bmatrix}8 & 0 & 0\\ 0 & 10 & 0\\ 0 & 0 & 3\end{bmatrix}$	$\begin{bmatrix}7 & 0 & 0\\ 0 & 4 & 0\\ 0 & 0 & 1\end{bmatrix}$	$\begin{bmatrix}1 & 0 & 0\\ 0 & 0.2 & 0\\ 0 & 0 & 4\end{bmatrix}$	2	$\begin{bmatrix}2 & 0 & 0\\ 0 & 1 & 0\\ 0 & 0 & 0.8\end{bmatrix}$	$\begin{bmatrix}25 & 0 & 0\\ 0 & 140 & 0\\ 0 & 0 & 60\end{bmatrix}$

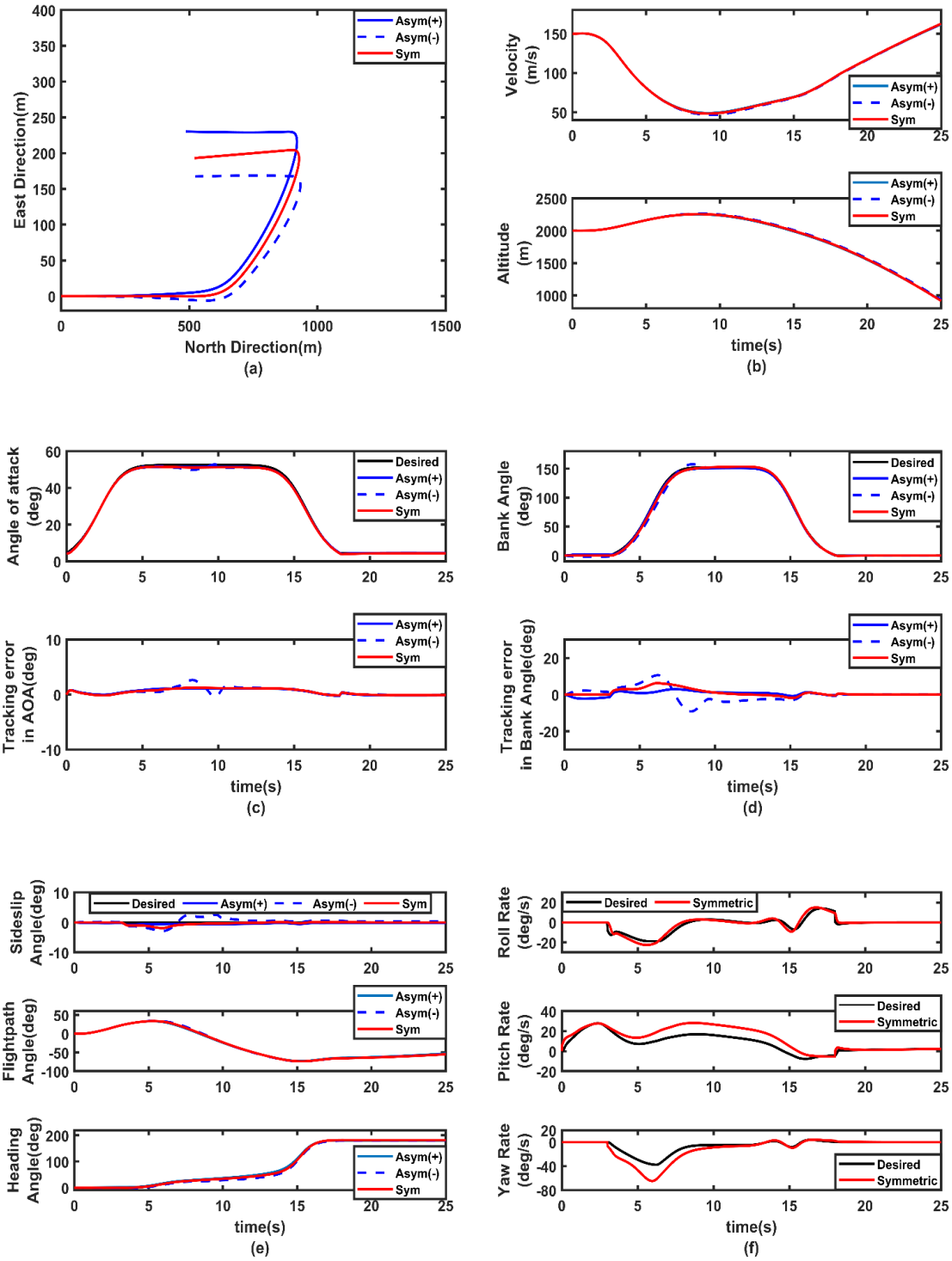
East Direction(m)
North Direction(m)
(a)
Asym(+)
Asym(-)
Sym
Velocity (m/s)
Altitude (m)
time(s)
(b)
Angle of attack (deg)
Desired
Tracking error in AOA(deg)
time(s)
(c)
Bank Angle (deg)
Tracking error in Bank Angle(deg)
(d)
Sideslip Angle(deg)
Flightpath Angle(deg)
Heading Angle(deg)
(e)
Roll Rate (deg/s)
Symmetric
Pitch Rate (deg/s)
Yaw Rate (deg/s)
(f)

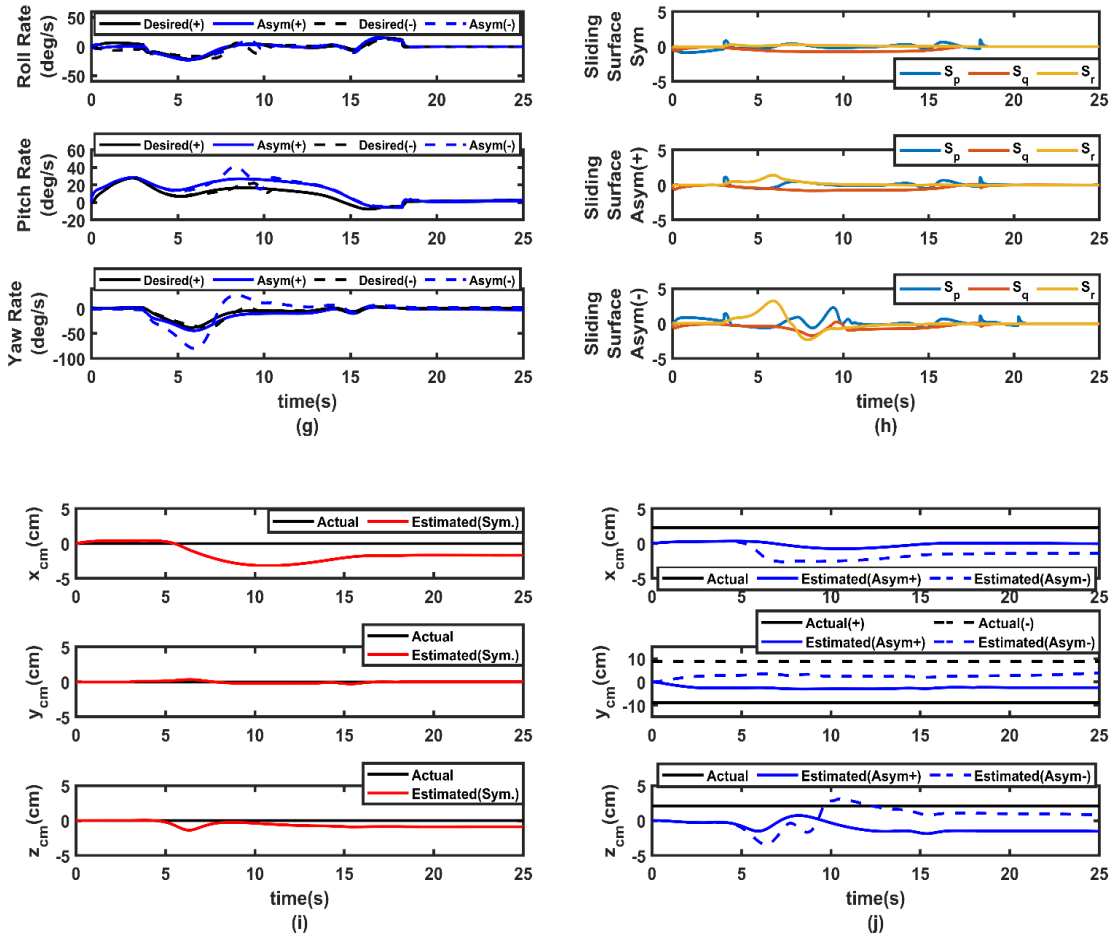

Figure 3.6. Ground track, time evolution of states, sliding surfaces and c.g. position: Herbst maneuver (c.g. at nominal as well as shifted position)

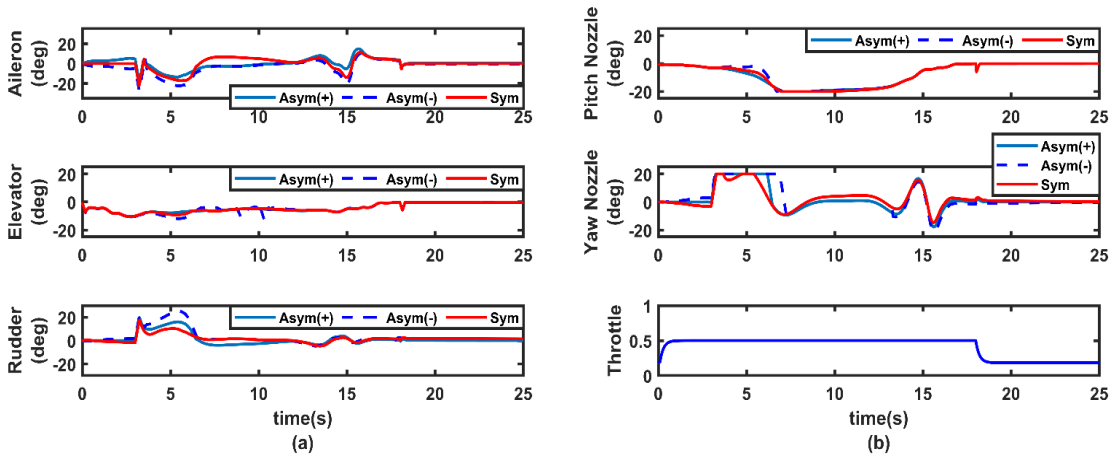

Figure 3.7. Time evolution of control deflections: Herbst maneuver (c.g. at nominal as well as shifted position)

3.5 Comparison with a Standard Adaptive Sliding Mode Control

To further demonstrate the efficacy of the proposed ABSMC control, the results are now compared against a standard Adaptive Sliding Mode Control (ASMC). A standard ASMC control is not directly applicable to the system dynamics described by Eqs. (3.7) and (3.8) as control input $\boldsymbol{u}$ is not directly appearing in Eq. (3.7). To make it amenable to SMC design Eq. (3.7) can be approximated, if the angle of attack and the sideslip angle remain small, as

$$\begin{bmatrix} \dot{\mu} \\ \dot{\alpha} \\ -\dot{\beta} \end{bmatrix} = \begin{bmatrix} p \\ q \\ r \end{bmatrix} + \begin{bmatrix} d_\mu \\ d_\alpha \\ d_\beta \end{bmatrix} \tag{3.68}$$

where $[d_\mu \quad d_\alpha \quad d_\beta]^T$ represents a lumped uncertainty which will evidently be particularly significant when the aircraft moves into high angle of attack regions. Under this simplification, defining $\boldsymbol{x_{11}} = [\mu \quad \alpha \quad -\beta]^T$, Eqs. (3.7) and (3.8) can now be combined in the form of a second order nonlinear dynamics given by the generic form

$$\ddot{\boldsymbol{x}}_{\boldsymbol{11}} = \boldsymbol{f_2}(\boldsymbol{x}) + G_2\boldsymbol{u} + \boldsymbol{d}_1 \tag{3.69}$$

It is needless to emphasize that the lumped uncertainty $\boldsymbol{d_1}$ is now much higher than the $\boldsymbol{d}$ as considered thus far. Eq. (3.69) is amenable to an adaptive sliding mode control design where the unknown upper bound of $\boldsymbol{d_1}$ (denoted as say, $\boldsymbol{D_1}$) can be estimated through an adaptation law in the line of [108]. Defining the tracking error $\boldsymbol{e_{11}} = \boldsymbol{x_{11}} - \boldsymbol{x_{11d}}$, the sliding surface and reaching law can be chosen in similar lines as considered in Section 3.3 as

$$\boldsymbol{S_1} = \dot{\boldsymbol{e}}_{\boldsymbol{11}} + N_1\boldsymbol{e_{11}} + M_1 sig(\boldsymbol{e_{11}})^{a_1} \tag{3.70}$$

$$\dot{\boldsymbol{S}}_{\boldsymbol{1}} = -H_1\boldsymbol{S_1} - \widehat{\boldsymbol{D}}_{\boldsymbol{1}} sgn(\boldsymbol{S_1}) \tag{3.71}$$

ASMC control design can be carried out in the same line as described in Section 3.3.2 with a Lyapunov function

$$V = \frac{1}{2}\boldsymbol{S_1^T S_1} + \frac{1}{2}\widetilde{\boldsymbol{D}}_1{}^T K_2 \widetilde{\boldsymbol{D}}_1 \tag{3.72}$$

It can be shown in the same line as previously that

$$\dot{V} \leq -\boldsymbol{S_1^T} H_1 \boldsymbol{S_1} \leq 0 \tag{3.73}$$

Thus, the stability is proved. Asymptotic stability can be proved applying Barbalat's lemma in the same way as done in Section 3.3.2. The control and adaptation laws are given by

$$\boldsymbol{u} = G_2^{-1}\left[-\boldsymbol{f_2} + \ddot{\boldsymbol{x}}_{\boldsymbol{11d}} - F_3(\boldsymbol{e_{11}})\dot{\boldsymbol{e}}_{\boldsymbol{11}} - H_1\boldsymbol{S_1} - \widehat{\boldsymbol{D}}_{\boldsymbol{1}} sgn\,(\boldsymbol{S_1})\right. \tag{3.74}$$

$$\dot{\widehat{\boldsymbol{D}}}_{\boldsymbol{1}} = K_2^{-1}|\boldsymbol{S_1}| \tag{3.75}$$

Since the representation of the system dynamics got changed, the various controller parameters are tuned afresh and are listed in Table 3.4. The maneuver performance under the standard ASMC control is shown in Fig. 3.8 and Fig. 3.9 for the three c.g. positions namely Sym, Asym(+) and Asym(-) for both cobra and Herbst maneuver respectively. Figure 3.8 and 3.9 clearly shows that the cobra and Herbst maneuver could not be performed properly under the degree of lateral c.g. variations considered in the present work. Comparison of Fig.3.8 with Fig. 3.6 and Fig. 3.9 with Fig. 3.7 reveals clear and significant performance and robustness improvement in the proposed ABSMC control scheme as compared to the ASMC scheme.

Table 3.4: ASMC Controller parameters

Maneuver	$\boldsymbol{N_1}$	$\boldsymbol{M_1}$	$\boldsymbol{a_1}$	$\boldsymbol{H_1}$	$\boldsymbol{K_2}$
Cobra	$\begin{bmatrix}3 & 0 & 0\\ 0 & 4 & 0\\ 0 & 0 & 1\end{bmatrix}$	$\begin{bmatrix}1 & 0 & 0\\ 0 & 0.2 & 0\\ 0 & 0 & 4\end{bmatrix}$	2	$\begin{bmatrix}0.5 & 0 & 0\\ 0 & 2.5 & 0\\ 0 & 0 & 3.8\end{bmatrix}$	$\begin{bmatrix}25 & 0 & 0\\ 0 & 140 & 0\\ 0 & 0 & 60\end{bmatrix}$
Herbst	$\begin{bmatrix}4 & 0 & 0\\ 0 & 2 & 0\\ 0 & 0 & 1\end{bmatrix}$	$\begin{bmatrix}1 & 0 & 0\\ 0 & 0.2 & 0\\ 0 & 0 & 4\end{bmatrix}$	2	$\begin{bmatrix}2.5 & 0 & 0\\ 0 & 1 & 0\\ 0 & 0 & 3\end{bmatrix}$	$\begin{bmatrix}25 & 0 & 0\\ 0 & 140 & 0\\ 0 & 0 & 60\end{bmatrix}$

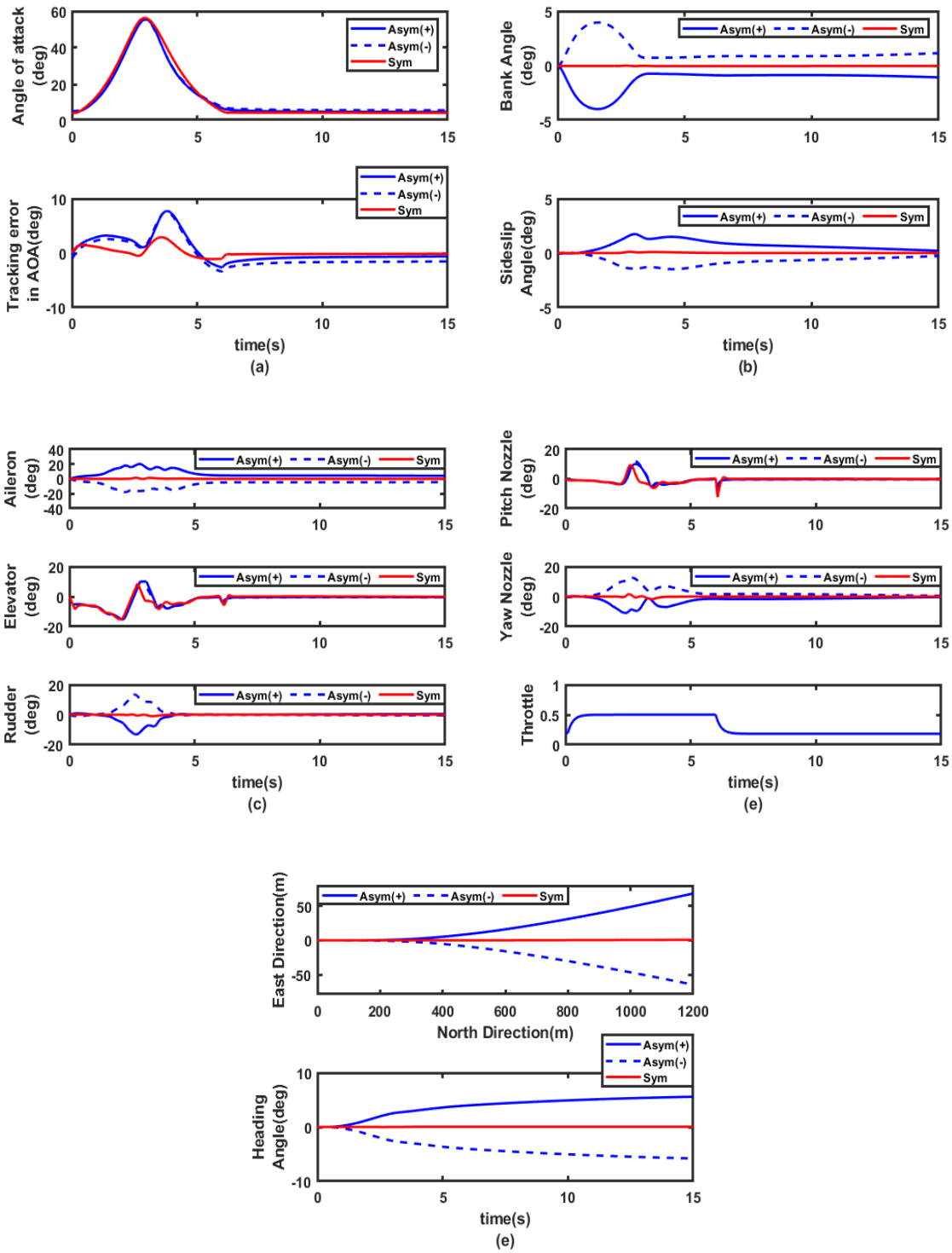

Figure 3.8. Time evolution of tracking errors, relevant states and controls under ASMC control: Cobra maneuver

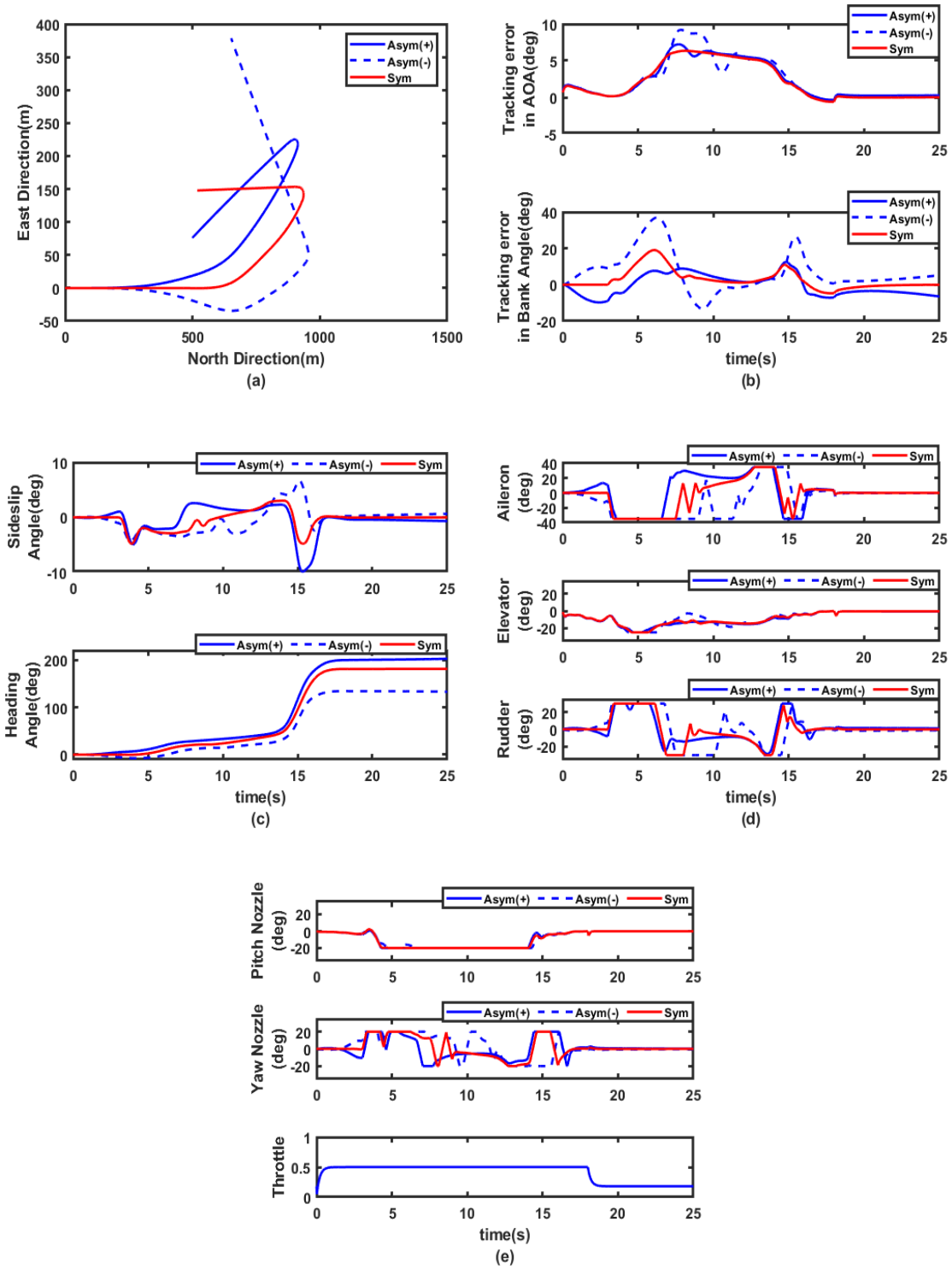

Figure 3.9. Ground track and time evolution of tracking errors, relevant states and controls under ASMC control: Herbst maneuver

3.6 Conclusion

The novel and challenging problem of controlling an aircraft performing autonomous high-α rmaneuver under significant lateral center of gravity uncertainties was addressed in this chapter. For controller design purpose under asymmetric c.g. position, the aircraft flight dynamics was first simplified and expressed in block strict feedback form. A multivariable adaptive backstepping control law was then proposed so that the aircraft flight could be controlled even under arbitrary and unknown c.g. variations. To mitigate the model uncertainty arising from the approximate representation of the off-nominal c.g. dynamics, a fast-sliding mode control was combined with the adaptive backstepping control law. The sliding mode controller was also meant to handle the parametric uncertainties in the aerodynamic coefficients of the aircraft occurring in the high angle of attack regions. A detailed stability analysis of the proposed control scheme was presented and conditions on the controller parameters were derived using the Lyapunov approach. Thereafter, the proposed controller was validated against a popular high-alpha cobra and Herbst maneuver considering the F18-HARV aircraft under significant c.g. movements on either side of the fuselage centerline as well as moderate uncertainties in the aerodynamic dataset. Results demonstrated the effectiveness of the proposed controller in retaining nearly the same level of maneuver performance under the c.g. and aerodynamic uncertainties. Moreover, the results were compared with a standard adaptive sliding mode control-based scheme and it was observed that the proposed adaptive backstepping and sliding mode hybrid control was able to produce considerably superior maneuver performance. The work is further extended in the next chapter by modifying the asymmetric dynamics and making control design less conservative.

Chapter 4

Asymmetric Dynamics based Adaptive Backstepping Control for Low Alpha Lateral Maneuvers

4.1 Introduction

In the previous two chapters, for executing low as well as high alpha maneuver under c.g. shift scenario, the asymmetric equations of motion were described in an ad-hoc manner by simply adding an extra rolling moment due to gravity term to the standard symmetric equations of motion to mathematically represent the lateral c.g. offset scenario. The present chapter analyzes that the highly coupled 6-DOF equations of motion resulting from lateral c.g. offset can be rearranged, simplified and cast in the required strict feedback form while attempting some specific low alpha lateral maneuvers without resorting to any heuristic ad-hoc method as already discussed in detail in previous chapter(s). The c.g. position can be cast as an adaptable parameter which can be estimated through an adaptation law in an adaptive backstepping setting. However, in the formulation, it is observed that the adaptable parameter appears in both steps of the two-step backstepping design. The works

reported in the literature normally have the adaptable parameter appearing only in the final step of the backstepping design [109, 110]. Therefore, in the present chapter, in a novel way, both the steps are made adaptive. Further, it is detected that the dynamics in both the steps contain some nonlinear terms which are favorable from the point of view of stability. Therefore, these terms are retained in designing the backstepping control law. This is another novel contribution of the present chapter as the available literature where backstepping control is applied to flight control problems, these favorable terms are also cancelled by the controller [41, 111]. Retention of useful nonlinearities has the obvious advantage of resulting in a less conservative control. Asymptotic stability of the overall closed loop system is established using Lyapunov's direct method and the new developments in LaSalle's invariance principle [95, 96]. Both tracking errors and the estimation error in the adaptable parameter are proved to remain asymptotically stable. Establishing asymptotic convergence of the parameter estimate, which is the lateral c.g. position in the present problem, is of particular significance since it also allows for accurate online estimation of the actual c.g. position of the vehicle through the proposed adaptation law.

Overall, this chapter contributes novel insights and methodologies in adaptive control, particularly in handling coupled nonlinear dynamics with adaptive parameters appearing in multiple steps of the backstepping process, and demonstrates the benefits of retaining useful nonlinearities in the control design.

The outline of the chapter is as follows. The second section gives an introduction of the problem and the same is formulated for low alpha maneuvers. Third section discusses the design and stability analysis of the proposed adaptive backstepping control. Simulation results obtained by applying proposed control technique is presented in fourth section. The effectiveness of the proposed control scheme is validated by comparing it with ad-hoc model-based control technique. Section five concludes the chapter with a brief prelude to the next chapters.

4.2 Asymmetric Dynamics based Modelling for Low Alpha Lateral Maneuvers

In this section, the highly coupled 6-DOF dynamics under lateral c.g. offset is cast in block strict feedback form which is essential for a multivariable adaptive backstepping control design. The present work focuses particularly on lateral maneuvers. For carrying out such maneuvers, suitable time profiles of appropriate angular variables are supplied externally and the closed loop controller then generates the necessary control surface deflection commands [68]. When an aircraft's c.g. moves to an arbitrary position (x_{cm}, y_{cm}, z_{cm}) w.r.t. the nominal c.g position or the origin of the body/wind frame, the complete 6-DOF equations of motion are given in the body frame by [61, 68]

$$\begin{bmatrix} 1 & 0 & 0 & 0 & z_{cm} & -y_{cm} \\ 0 & 1 & 0 & -z_{cm} & 0 & x_{cm} \\ 0 & 0 & 1 & y_{cm} & -x_{cm} & 0 \\ 0 & -mz_{cm} & my_{cm} & I'_{xx} & -I'_{xy} & -I'_{xz} \\ mz_{cm} & 0 & -mx_{cm} & -I'_{xy} & I'_{yy} & -I'_{yz} \\ -my_{cm} & mx_{cm} & 0 & -I'_{xz} & -I'_{yz} & I'_{zz} \end{bmatrix} \begin{bmatrix} \dot{u} \\ \dot{v} \\ \dot{w} \\ \dot{p} \\ \dot{q} \\ \dot{r} \end{bmatrix} = \begin{bmatrix} -qw + rv \\ -ru + pw \\ -pv + qu \\ I'_{xz}pq + (I'_{yy} - I'_{zz})qr - I'_{xy}rp + I'_{yz}(q^2 - r^2) \\ I'_{xy}qr + (I'_{zz} - I'_{xx})rp - I'_{yz}pq + I'_{xz}(r^2 - p^2) \\ I'_{yz}rp + (I'_{xx} - I'_{yy})pq - I'_{xz}qr + I'_{xy}(p^2 - q^2) \end{bmatrix} +$$

$$\begin{bmatrix} (q^2 + r^2)x_{cm} - pqy_{cm} - rpz_{cm} \\ (r^2 + p^2)y_{cm} - pqx_{cm} - qrz_{cm} \\ (p^2 + q^2)z_{cm} - rpx_{cm} - qry_{cm} \\ m(qu - pv)y_{cm} + m(ru - pw)z_{cm} \\ m(pv - qu)x_{cm} + m(rv - qw)z_{cm} \\ m(pw - ru)x_{cm} + m(qw - rv)y_{cm} \end{bmatrix} + \begin{bmatrix} -gsin\theta \\ gcos\theta sin\phi \\ gcos\theta cos\phi \\ -z_{cm}mgcos\theta sin\phi + y_{cm}mgcos\theta cos\phi \\ -z_{cm}mgsin\theta - x_{cm}mgcos\theta cos\phi \\ y_{cm}mgsin\theta + x_{cm}mgcos\theta sin\phi \end{bmatrix} + \begin{bmatrix} \frac{F_x}{m} \\ \frac{F_y}{m} \\ \frac{F_z}{m} \\ M_x \\ M_y \\ M_z \end{bmatrix} \quad (4.1)$$

where $I = \begin{bmatrix} I_{xx} & 0 & -I_{xz} \\ 0 & I_{yy} & 0 \\ -I_{xz} & 0 & I_{zz} \end{bmatrix}$ is the nominal inertia matrix and $I' = \begin{bmatrix} I'_{xx} & -I'_{xy} & -I'_{xz} \\ -I'_{xy} & I'_{yy} & -I'_{yz} \\ -I'_{xz} & -I'_{yz} & I'_{zz} \end{bmatrix}$ is the new inertia matrix under c.g. offset. In the present investigation since the focus is on lateral c.g. movement, therefore, x_{cm} and z_{cm} are assumed to be zero. As a result, the asymmetric equations of motion given by Eq. (4.1) simplifies to

$$\begin{bmatrix} 1 & 0 & 0 & 0 & 0 & -y_{cm} \\ 0 & 1 & 0 & 0 & 0 & 0 \\ 0 & 0 & 1 & y_{cm} & 0 & 0 \\ 0 & 0 & my_{cm} & I'_{xx} & 0 & -I_{xz} \\ 0 & 0 & 0 & 0 & I_{yy} & 0 \\ -my_{cm} & 0 & 0 & -I_{xz} & 0 & I'_{zz} \end{bmatrix} \begin{bmatrix} \dot{u} \\ \dot{v} \\ \dot{w} \\ \dot{p} \\ \dot{q} \\ \dot{r} \end{bmatrix} = \begin{bmatrix} -qw + rv \\ -ru + pw \\ -pv + qu \\ I_{xz}pq + (I_{yy} - I'_{zz})qr \\ (I_{zz} - I_{xx})rp + I_{xz}(r^2 - p^2) \\ (I'_{xx} - I_{yy})pq - I_{xz}qr \end{bmatrix} + \begin{bmatrix} -pqy_{cm} \\ (r^2 + p^2)y_{cm} \\ -qry_{cm} \\ m(qu - pv)y_{cm} \\ 0 \\ m(qw - rv)y_{cm} \end{bmatrix} +$$

$$+\begin{bmatrix} -gsin\theta \\ gcos\theta sin\phi \\ gcos\theta cos\phi \\ y_{cm}mgcos\theta cos\phi \\ 0 \\ y_{cm}mgsin\theta \end{bmatrix}+\begin{bmatrix} \frac{F_x}{m} \\ \frac{F_y}{m} \\ \frac{F_z}{m} \\ M_x \\ M_y \\ M_z \end{bmatrix} \tag{4.2}$$

From equation (4.2),

$$\dot{u} - y_{cm}\dot{r} = -qw + rv - pqy_{cm} - gsin\theta + \frac{F_x}{m} \tag{4.3}$$

$$\dot{w} + y_{cm}\dot{p} = -pv + qu - qry_{cm} + gcos\theta cos\phi + \frac{F_z}{m} \tag{4.4}$$

$$my_{cm}\dot{w} + I'_{xx}\dot{p} - I_{xz}\dot{r} = I_{xz}pq + \left(I_{yy} - I'_{zz}\right)qr + m(qu - pv)y_{cm} + y_{cm}mgcos\theta cos\phi + M_x \tag{4.5}$$

$$-my_{cm}\dot{u} - I_{xz}\dot{p} + I'_{zz}\dot{r} = \left(I'_{xx} - I_{yy}\right)pq - I_{xz}qr + m(qw - rv)y_{cm} + y_{cm}mgsin\theta + M_z \tag{4.6}$$

Now, multiplying Eq. (4.3) with $-my_{cm}$ and Eq. (4.4) with my_{cm}

$$-my_{cm}\dot{u} + my_{cm}^2\dot{r} = -m(-qw + rv)y_{cm} + my_{cm}^2pq + y_{cm}mgsin\theta + y_{cm}F_x \tag{4.7}$$

$$my_{cm}\dot{w} + my_{cm}^2\dot{p} = m(-pv + qu)y_{cm} - my_{cm}^2qr + y_{cm}mgcos\theta cos\phi + y_{cm}F_z \tag{4.8}$$

From Eqs. (4.5) and (4.6) and Eqs. (4.7) and (4.8) eliminating $\dot{u}$ and $\dot{w}$, the lateral-directional angular dynamics can be expressed as

$$(I'_{xx} - my_{cm}^2)\,\dot{p} - I_{xz}\,\dot{r} = \left(I_{yy} - I'_{zz}\right)qr + I_{xz}pq + my_{cm}^2qr + M_x - y_{cm}F_z \tag{4.9}$$

$$-I_{xz}\,\dot{p} + (I'_{zz} - my_{cm}^2)\,\dot{r} = \left(I'_{xx} - I_{yy}\right)pq - I_{xz}qr - my_{cm}^2pq + M_z + y_{cm}F_x \tag{4.10}$$

For carrying out a lateral maneuver, a desired roll angle (ϕ) profile is supplied externally keeping the desired sideslip angle (β) at zero [101]. Therefore, the system dynamics is required to be expressed in terms of the state variables ϕ, β and the lateral-directional body rates p, r. The roll angle dynamics is given by [92]

$$\dot{\phi} = p + qsin\phi tan\theta + rcos\phi tan\theta \tag{4.11}$$

and side velocity component can be extracted from Eq. (4.2) as

$$\dot{v} = -ru + pw + (r^2 + p^2)y_{cm} + gcos\theta sin\phi + \frac{F_y}{m} \tag{4.12}$$

Assuming α and β to remain small throughout the maneuver and the total velocity and the longitudinal variables to remain nearly constant at their initial steady wings level trim values, Eqs. (4.11) and (4.12) modifies to

$$\dot{\phi} = p + rtan\alpha_t cos\phi \tag{4.13}$$

$$\dot{\beta} = -r + ptan\alpha_t + (r^2 + p^2)\frac{y_{cm}}{V} + \frac{g}{V}sin\phi cos\alpha_t + \frac{\bar{q}SC_Y(\beta)}{mV} \tag{4.14}$$

where α_t is the trim angle of attack and V is the trim velocity. Eqs. (4.13) and (4.14) can be expressed in compact form as

$$\begin{bmatrix}\dot{\phi}\\ \dot{\beta}\end{bmatrix} = \begin{bmatrix}0\\ \frac{g}{V}\ sin\phi\ cos\alpha_t + \frac{\bar{q}SC_Y(\beta)}{mV}\end{bmatrix} + \begin{bmatrix}0\\ \frac{r^2+p^2}{V}\end{bmatrix} y_{cm} + \begin{bmatrix}1 & tan\alpha_t\ cos\phi\\ tan\alpha_t & -1\end{bmatrix}\begin{bmatrix}p\\ r\end{bmatrix} \tag{4.15}$$

Further, assuming pitch rate q to be zero, angular rate dynamics from Eqs. (4.9) and (4.10) can be expressed as

$$\begin{bmatrix}(I'_{xx} - my_{cm}^2) & -I_{xz}\\ -I_{xz} & (I'_{zz} - my_{cm}^2)\end{bmatrix}\begin{bmatrix}\dot{p}\\ \dot{r}\end{bmatrix} = \begin{bmatrix}M_x\\ M_z\end{bmatrix} + \begin{bmatrix}-y_{cm}F_z\\ y_{cm}F_x\end{bmatrix} \tag{4.16}$$

Since y_{cm} is small, the changes in inertia due to c.g. shift can be safely ignored in Eq. (4.16). Therefore (after substituting M_x and M_z),

$$\begin{bmatrix}I_{xx} & -I_{xz}\\ -I_{xz} & I_{zz}\end{bmatrix}\begin{bmatrix}\dot{p}\\ \dot{r}\end{bmatrix} = \begin{bmatrix}\bar{q}Sb\left(C_{l\beta}\beta + C_{lp}\frac{pb}{2V} + C_{lr}\frac{rb}{2V}\right)\\ \bar{q}Sb\left(C_{n\beta}\beta + C_{np}\frac{pb}{2V} + C_{nr}\frac{rb}{2V}\right)\end{bmatrix} + \begin{bmatrix}-F_z\\ F_x\end{bmatrix} y_{cm} + \begin{bmatrix}\bar{q}SbC_{l\delta a} & \bar{q}SbC_{l\delta r}\\ \bar{q}SbC_{n\delta a} & \bar{q}SbC_{n\delta r}\end{bmatrix}\begin{bmatrix}\delta_a\\ \delta_r\end{bmatrix} \tag{4.17}$$

$$\begin{bmatrix}\dot{p}\\ \dot{r}\end{bmatrix}=\begin{bmatrix}I_{xx} & -I_{xz}\\ -I_{xz} & I_{zz}\end{bmatrix}^{-1}\begin{bmatrix}\bar{q}Sb(C_{l\beta}\beta+C_{lp}\frac{pb}{2V}+C_{lr}\frac{rb}{2V})\\ \bar{q}Sb(C_{n\beta}\beta+C_{np}\frac{pb}{2V}+C_{nr}\frac{rb}{2V})\end{bmatrix}+\begin{bmatrix}I_{xx} & -I_{xz}\\ -I_{xz} & I_{zz}\end{bmatrix}^{-1}\begin{bmatrix}-F_z\\ F_x\end{bmatrix}y_{cm}+$$

$$\begin{bmatrix}I_{xx} & -I_{xz}\\ -I_{xz} & I_{zz}\end{bmatrix}^{-1}\begin{bmatrix}\bar{q}SbC_{l\delta a} & \bar{q}SbC_{l\delta r}\\ \bar{q}SbC_{n\delta a} & \bar{q}SbC_{n\delta r}\end{bmatrix}\begin{bmatrix}\delta_a\\ \delta_r\end{bmatrix} \tag{4.18}$$

Since control surface deflections do not contribute significantly to force, they can be ignored in force components F_x and F_z in the above equation. Therefore, F_x and F_z are state dependent terms given by

$$F_x\approx\bar{q}S\left[\left(C_{L0}+C_{L\alpha}\alpha+C_{Lq}\frac{q\bar{c}}{2V}\right)sin\alpha-\left(C_{D0}+C_{D0}\alpha+C_{Dq}\frac{q\bar{c}}{2V}+C_{Dp}\frac{bp}{2V}\right)cos\alpha\ cos\beta-\left(C_{Y0}+\right.\right.$$

$$\left.\left.C_Y\beta+C_{Yp}\frac{bp}{2V}+C_{Yr}\frac{br}{2V}\right)cos\alpha\ sin\beta\right]+T_x \tag{4.19}$$

$$F_z\approx\bar{q}S\left[-\left(C_{D0}+C_{D0}\alpha+C_{Dq}\frac{q\bar{c}}{2V}+C_{Dp}\frac{bp}{2V}\right)sin\alpha\ cos\beta-\left(C_{Y0}+C_Y\beta+C_{Yp}\frac{bp}{2V}+\right.\right.$$

$$\left.\left.C_{Yr}\frac{br}{2V}\right)sin\alpha\ sin\beta-\left(C_{L0}+C_{L\alpha}\alpha+C_{Lq}\frac{q\bar{c}}{2V}\right)cos\alpha\right] \tag{4.20}$$

Usually the aerodynamic coefficients $C_{Y\beta}$, C_{lp} and C_{nr} are negative and the same is true with the aerodynamic dataset of present UAV as given in the Appendix-C. Therefore, referring to Eq. (4.15) the term $\frac{\bar{q}SC_Y(\beta)}{mV}$ and in Eq. (4.20) the term $\bar{q}SbC_{lp}\frac{pb}{2V}$ and $\bar{q}SbC_{nr}\frac{rb}{2V}$ are favorable terms as far as stability is concerned and, therefore, should be retained. It is further noted that $[I]^{-1}$ is positive definite. Therefore, we can separate the unfavorable and favorable terms in Eqs. (4.15) and (4.20) as

$$\begin{bmatrix}\dot{\phi}\\ \dot{\beta}\end{bmatrix}=\begin{bmatrix}0\\ \frac{g}{V}\ sin\phi\ cos\alpha_t\end{bmatrix}+\begin{bmatrix}0 & 0\\ 0 & \frac{\bar{q}SC_{Y\beta}}{mV}\end{bmatrix}\begin{bmatrix}\phi\\ \beta\end{bmatrix}+\begin{bmatrix}0\\ \frac{r^2+p^2}{V}\end{bmatrix}y_{cm}+\begin{bmatrix}1 & tan\alpha_t\ cos\phi\\ tan\alpha_t & -1\end{bmatrix}\begin{bmatrix}p\\ r\end{bmatrix} \tag{4.21}$$

$$\begin{bmatrix}\dot{p}\\ \dot{r}\end{bmatrix}=\begin{bmatrix}I_{xx} & -I_{xz}\\ -I_{xz} & I_{zz}\end{bmatrix}^{-1}\begin{bmatrix}\bar{q}Sb(C_{l\beta}\beta+C_{lr}\frac{rb}{2V})\\ \bar{q}Sb(C_{n\beta}\beta+C_{np}\frac{pb}{2V})\end{bmatrix}+\begin{bmatrix}I_{xx} & -I_{xz}\\ -I_{xz} & I_{zz}\end{bmatrix}^{-1}\begin{bmatrix}\bar{q}SbC_{lp}\frac{b}{2V} & 0\\ 0 & \bar{q}SbC_{nr}\frac{b}{2V}\end{bmatrix}\begin{bmatrix}p\\ r\end{bmatrix}+$$

$$\begin{bmatrix}I_{xx} & -I_{xz}\\ -I_{xz} & I_{zz}\end{bmatrix}^{-1}\begin{bmatrix}-F_z\\ F_x\end{bmatrix}y_{cm}+\begin{bmatrix}I_{xx} & -I_{xz}\\ -I_{xz} & I_{zz}\end{bmatrix}^{-1}\begin{bmatrix}\bar{q}SbC_{l\delta a} & \bar{q}SbC_{l\delta r}\\ \bar{q}SbC_{n\delta a} & \bar{q}SbC_{n\delta r}\end{bmatrix}\begin{bmatrix}\delta_a\\ \delta_r\end{bmatrix} \tag{4.22}$$

Now defining $\boldsymbol{x_1} = [\phi \quad \beta]^T$, the virtual control $\boldsymbol{x_2} = [p \quad r]^T$ and the control signal $\boldsymbol{u} = [\delta_a \quad \delta_r]^T$, the asymmetric flight dynamics described by Eqs. (4.21) and (4.22) can be expressed in strict feedback form

$$\dot{\boldsymbol{x}}_{\boldsymbol{1}} = \boldsymbol{f_{11}} + F_{12}\boldsymbol{x_1} + \boldsymbol{f_{13}}\,\sigma + G_1\boldsymbol{x_2} \tag{4.23}$$

$$\dot{\boldsymbol{x}}_{\boldsymbol{2}} = \boldsymbol{f_{21}} + F_{22}\boldsymbol{x_2} + \boldsymbol{f_{23}}\,\sigma + G_2\boldsymbol{u} \tag{4.24}$$

where σ is the uncertain/unknown c.g. position y_{cm} from the origin of the body frame which can be estimated through a suitable adaptation law. Further, $\boldsymbol{f_{11}}, \boldsymbol{f_{13}}, \boldsymbol{f_{21}}, \boldsymbol{f_{23}}$ are 2×1 vector valued functions and F_{12}, F_{22}, G_1, G_2 are 2×2 matrices and all these are known at every time step from the assumption of availability of full state feedback. Moreover, F_{12}, F_{22} are negative semidefinite matrices representing the favorable nonlinearities.

4.3 An Efficient Adaptive Backstepping Control

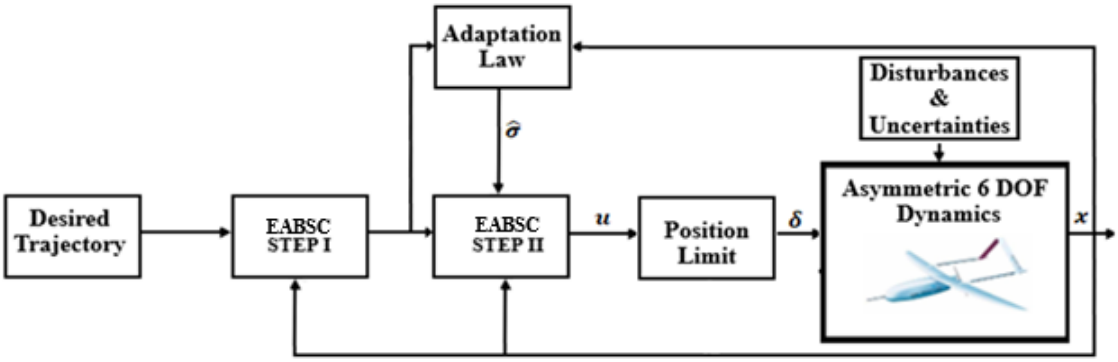

Figure 4.1. Block diagram of the proposed closed loop system

In this section, an efficient adaptive backstepping control (EABSC) is proposed to autonomously execute the intended lateral maneuver under significant lateral c.g. variations considering the system dynamics as formulated in the previous section. Referring to Eq. (4.23) and Eq.(4.24), the desired time profiles for $\boldsymbol{x_1}$ are fed externally as reference inputs and the controller generates $\boldsymbol{u}$ i.e. the

control surface deflection commands in a closed loop manner under the assumption of availability of state feedback. The shift in c.g. position, σ is assumed to be unknown and made adaptive through a suitable adaptation law. Since the control explicitly retains useful nonlinearities, resulting in a less conservative control, the name EABSC is coined. The complete closed loop scheme is illustrated in Figure 4.1. The detailed stability analysis of the proposed controller is discussed below.

Let the errors in the states $\boldsymbol{x_1}$ and $\boldsymbol{x_2}$ be defined as $\boldsymbol{e_1} = \boldsymbol{x_1} - \boldsymbol{x_{1d}}$ and $\boldsymbol{e_2} = \boldsymbol{x_2} - \boldsymbol{x_{2d}}$ where, $\boldsymbol{x_{1d}}$ and $\boldsymbol{x_{2d}}$ are the desired trajectories of $\boldsymbol{x_1}$ and $\boldsymbol{x_2}$ respectively. Therefore,

$$\dot{\boldsymbol{e}}_{\boldsymbol{1}} = \dot{\boldsymbol{x}}_{\boldsymbol{1}} - \dot{\boldsymbol{x}}_{\boldsymbol{1d}} = \boldsymbol{f_{11}} + F_{12}\boldsymbol{x_1} + \boldsymbol{f_{13}}\,\sigma + G_1\boldsymbol{x_2} - \dot{\boldsymbol{x}}_{\boldsymbol{1d}} \tag{4.25}$$

$$\dot{\boldsymbol{e}}_{\boldsymbol{2}} = \dot{\boldsymbol{x}}_{\boldsymbol{2}} - \dot{\boldsymbol{x}}_{\boldsymbol{2d}} = \boldsymbol{f_{21}} + F_{22}\boldsymbol{x_2} + \boldsymbol{f_{23}}\,\sigma + G_2\boldsymbol{u} - \dot{\boldsymbol{x}}_{\boldsymbol{2d}} \tag{4.26}$$

Let the Lyapunov function for the dynamics given by Eq. (4.25) be

$$V_1 = \tfrac{1}{2}\boldsymbol{e_1^T e_1} \tag{4.27}$$

Therefore, on differentiation and on substitution of Eq. (4.25),

$$\dot{V}_1 = \boldsymbol{e_1^T}[\boldsymbol{f_{11}} + F_{12}\boldsymbol{x_1} + \boldsymbol{f_{13}}\,\sigma + G_1\boldsymbol{x_2} - \dot{\boldsymbol{x}}_{\boldsymbol{1d}}] \tag{4.28}$$

Let us choose,

$$\boldsymbol{f_{11}} + \boldsymbol{f_{13}}\,\hat{\sigma} + G_1\boldsymbol{x_2} - \dot{\boldsymbol{x}}_{\boldsymbol{1d}} + F_{12}\boldsymbol{x_{1d}} = -K_1\boldsymbol{e_1} \tag{4.29}$$

where $K_1 = diag\ (k_{11}, k_{12})$ is chosen as constant positive definite matrix and $\hat{\sigma}$ is the estimate of the unknown parameter σ. This will ensure stability of the $\boldsymbol{e_1}$ dynamics when $\hat{\sigma}$ tends to σ as we get

$$\dot{V}_1 = \boldsymbol{e_1^T}[F_{12}\boldsymbol{e_1} - K_1\boldsymbol{e_1}] < 0 \tag{4.30}$$

From Eq. (4.29), the desired profile for the virtual control $\boldsymbol{x_2}$ can be obtained as

$$\boldsymbol{x_{2d}} = G_1^{-1}(-K_1\boldsymbol{e_1} - \boldsymbol{f_{11}} - \boldsymbol{f_{13}}\,\hat{\sigma} + \dot{\boldsymbol{x}}_{\boldsymbol{1d}} - F_{12}\boldsymbol{x_{1d}}) \tag{4.31}$$

The Lyapunov function for the complete dynamics is now chosen as

$$V_2 = \frac{1}{2}\boldsymbol{e_1^T e_1} + \frac{1}{2}\boldsymbol{e_2^T e_2} + \frac{1}{2}K_3\tilde{\sigma}^2 \tag{4.32}$$

where $\tilde{\sigma}$ is the parameter estimation error and K_3 is a constant positive adaptation gain.

Now from Eq. (4.32),

$$\dot{V}_2 = \boldsymbol{e_1^T \dot{e}_1} + \boldsymbol{e_2^T \dot{e}_2} + K_3\,\tilde{\sigma}\dot{\tilde{\sigma}} \tag{4.33}$$

Substituting corresponding expressions of $\boldsymbol{\dot{e}_1, \dot{e}_2}$ into Eq. (4.33),

$$\dot{V}_2 = \boldsymbol{e_1^T}[\boldsymbol{f_{11}} + F_{12}\boldsymbol{e_1} + F_{12}\boldsymbol{x_{1d}} + \boldsymbol{f_{13}}\,\sigma + G_1\boldsymbol{x_{2d}} + G_1\boldsymbol{e_2} - \boldsymbol{\dot{x}_{1d}}] + \boldsymbol{e_2^T}[\boldsymbol{f_{21}} + F_{22}\boldsymbol{e_2} + F_{22}\boldsymbol{x_{2d}} + \boldsymbol{f_{23}}\,\sigma + G_2\boldsymbol{u} - \boldsymbol{\dot{x}_{2d}}] - K_3\tilde{\sigma}\,\dot{\hat{\sigma}} \tag{4.34}$$

Substituting $\boldsymbol{x_{2d}}$ from Eq. (4.31) into Eq. (4.34)

$$\dot{V}_2 = -\boldsymbol{e_1^T}K_1\boldsymbol{e_1} + \boldsymbol{e_1^T}G_1\boldsymbol{e_2} + \boldsymbol{e_1^T}F_{12}\boldsymbol{e_1} + \boldsymbol{e_2^T}[\boldsymbol{f_{21}} + F_{22}\boldsymbol{e_2} + F_{22}G_1^{-1}(-K_1\boldsymbol{e_1} - \boldsymbol{f_{11}} - \boldsymbol{f_{13}}\,\hat{\sigma} + \boldsymbol{\dot{x}_{1d}} - F_{12}\boldsymbol{x_{1d}}) + \boldsymbol{f_{23}}\,\hat{\sigma} + G_2\boldsymbol{u} - \boldsymbol{\dot{x}_{2d}}] - \tilde{\sigma}(K_3\dot{\hat{\sigma}} - \boldsymbol{f_{13}^T}\,\boldsymbol{e_1} - \boldsymbol{f_{23}^T}\,\boldsymbol{e_2}) \tag{4.35}$$

Now, designing the control law as

$$\boldsymbol{u} = G_2^{-1}[-G_1^T\boldsymbol{e_1} - \boldsymbol{f_{21}} - \boldsymbol{f_{23}}\,\hat{\sigma} + \boldsymbol{\dot{x}_{2d}} - K_2\boldsymbol{e_2} - F_{22}G_1^{-1}(-K_1\boldsymbol{e_1} - \boldsymbol{f_{11}} - \boldsymbol{f_{13}}\,\hat{\sigma} + \boldsymbol{\dot{x}_{1d}} - F_{12}\boldsymbol{x_{1d}})] \tag{4.36}$$

where $K_2 = diag\,(k_{21}, k_{22})$ is a constant positive definite matrix and the adaptation law as,

$$\dot{\hat{\sigma}} = \frac{1}{K_3}\,(\boldsymbol{f_{13}^T}\,\boldsymbol{e_1} + \boldsymbol{f_{23}^T}\,\boldsymbol{e_2}) \tag{4.37}$$

Eq. (4.35) reduces to

$$\dot{V}_2 \leq -\boldsymbol{e_1^T}K_1\boldsymbol{e_1} - \boldsymbol{e_2^T}K_2\boldsymbol{e_2} + \boldsymbol{e_1^T}F_{12}\boldsymbol{e_1} + \boldsymbol{e_2^T}F_{22}\boldsymbol{e_2} \tag{4.38}$$

Since F_{12} and F_{22} are negative semidefinite matrices, Eq. (4.38) can be further simplified to

$$\dot{V}_2 \leq -\boldsymbol{e_1^T} K_1 \boldsymbol{e_1} - \boldsymbol{e_2^T} K_2 \boldsymbol{e_2} \tag{4.39}$$

Clearly, $\dot{V}_2$ is negative semidefinite guaranteeing boundedness of the tracking error vectors $\boldsymbol{e_1}$ and $\boldsymbol{e_2}$. The control signal from Eq. (4.36) can also be expressed as

$$\boldsymbol{u} = G_2^{-1}(-G_1^T \boldsymbol{e_1} - \boldsymbol{f_{21}} - \boldsymbol{f_{23}}\, \hat{\sigma} + \dot{\boldsymbol{x}}_{\boldsymbol{2d}} - K_2 \boldsymbol{e_2} - F_{22}\, \boldsymbol{x_{2d}}) \tag{4.40}$$

Remark 1: In the similar line of Theorem 2.1 as stated in chapter 2 is now used to prove asymptotic stability of the closed loop system.

Substituting Eqs. (4.31) and (4.36) in Eqs. (4.25) and (4.26), the error dynamics can be expressed as

$$\dot{\boldsymbol{e}}_{\boldsymbol{1}} = G_1 \boldsymbol{e_2} - K_1 \boldsymbol{e_1} + \boldsymbol{f_{13}} \tilde{\sigma} + F_{12} \boldsymbol{e_1} \tag{4.41}$$

$$\dot{\boldsymbol{e}}_{\boldsymbol{2}} = \boldsymbol{f_{23}} \tilde{\sigma} - K_2 \boldsymbol{e_2} - G_1^T \boldsymbol{e_1} + F_{22} \boldsymbol{e_2} \tag{4.42}$$

And from Eq. (4.37),

$$\dot{\tilde{\sigma}} = -\frac{1}{K_3} (\boldsymbol{f_{13}^T e_1} + \boldsymbol{f_{23}^T e_2}) \tag{4.43}$$

Clearly, in the present problem, condition A of Theorem 4.1 holds (referring to the dynamics given by Eqs. (4.15) and (4.23)). The main contribution of the new invariance principle i.e. Theorem 4.1 is consideration of $\dot{V} \equiv 0$ instead of merely $\dot{V} = 0$. Now, from equation (4.39), $\dot{V}_2 \equiv 0$ implies that $\boldsymbol{e_1} \equiv \boldsymbol{0}$ and $\boldsymbol{e_2} \equiv \boldsymbol{0}$. This, in turn, implies that $\dot{\boldsymbol{e}}_{\boldsymbol{1}} = \boldsymbol{0}$ and $\dot{\boldsymbol{e}}_{\boldsymbol{2}} = \boldsymbol{0}$ implying asymptotic stability of the tracking errors $\boldsymbol{e_1}$ and $\boldsymbol{e_2}$. Further, under this condition, Eqs. (4.41) - (4.43) now reduce to

$$\boldsymbol{f_{13}} \tilde{\sigma} = \boldsymbol{0} \tag{4.44}$$

$$\boldsymbol{f_{23}} \tilde{\sigma} = \boldsymbol{0} \tag{4.45}$$

$$\dot{\tilde{\sigma}} = 0 \tag{4.46}$$

It can be further concluded from Theorem 4.1 that if both of the conditions $\lim_{t\to\infty} \boldsymbol{f_{13}} = \mathbf{0}$ and $\lim_{t\to\infty} \boldsymbol{f_{23}} = \mathbf{0}$ are satisfied, then $\lim_{t\to\infty} \tilde{\sigma} \neq 0$ i.e. $\tilde{\sigma}$ will converge to some nonzero constant value. On the other hand, if either of $\lim_{t\to\infty} \boldsymbol{f_{13}}$ or $\lim_{t\to\infty} \boldsymbol{f_{23}}$ is nonzero then $\lim_{t\to\infty} \tilde{\sigma} = 0$.

From Eqs. (4.15) and (4.23), $\boldsymbol{f_{13}} = \begin{bmatrix} 0 \\ \frac{r^2+p^2}{V} \end{bmatrix}$. Since it is already established that the lateral dynamics is asymptotically stable, therefore, $\lim_{t\to\infty} p = 0$ and $\lim_{t\to\infty} r = 0$. As a result, $\lim_{t\to\infty} \boldsymbol{f_{13}} = \mathbf{0}$. However, $\lim_{t\to\infty} \boldsymbol{f_{23}} \neq \mathbf{0}$ as evident from the following.

From Eqs. (4.18) and (4.24), $\boldsymbol{f_{23}} = \begin{bmatrix} I_{xx} & 0 \\ 0 & I_{zz} \end{bmatrix}^{-1} \begin{bmatrix} -F_z \\ F_x \end{bmatrix}$ where F_z and F_x contain aerodynamic and propulsive components of forces as per Eqs. (4.19) and (4.20). Since the longitudinal dynamics is assumed to remain unaffected during the maneuver, it can be safely assumed that the aircraft will retain longitudinal trim post maneuver. Now, under the longitudinal trim condition, $\boldsymbol{F}_{gravity} + \boldsymbol{F}_{aerodynamic} + \boldsymbol{F}_{propulsion} = \mathbf{0}$. Therefore, $\lim_{t\to\infty} (\boldsymbol{F}_{aerodynamic} + \boldsymbol{F}_{propulsion}) \neq \mathbf{0}$ implying $\lim_{t\to\infty} \boldsymbol{f_{23}} \neq \mathbf{0}$. This proves the asymptotic stability of the estimation error (i.e. $\tilde{\sigma}$) as well.

4.4 Simulation Results and Discussions

In this section, the coordinated horizontal turn and aileron maneuver is simulated in MATLAB environment for the Aerosonde UAV to validate the effectiveness of the proposed control scheme. To perform the maneuver, c.g. is assumed to move laterally on either side of the fuselage centerline. To simulate the c.g. offset conditions, it is assumed that the UAV carries a single store of 1.5 kg (which is 10% of the mass of the UAV and the store combined) mounted either on the starboard side (referred to as Asym+) or on the port side (referred to as Asym-) half of the semispan away from the body centerline. This gives rise to a c.g. movement of $\pm 7.0\ cm$. Further, the vehicle is assumed to have an initial trimmed flight at an altitude of 1000 m, with a velocity of 20 m/s. A large number

of Monte Carlo runs are performed considering lateral c.g. position randomly in the range $[-7\ cm, 7\ cm]$ and nearly identical maneuver performance is observed in each run. However, plots for the extreme ends on both sides corresponding to $y_{cm} = \pm 7.0\ cm$ are shown for the sake of brevity. The exact equations of motion under laterally asymmetric c.g. positions, which are enumerated in Eq. (4.2), are taken into consideration when simulating the 6-DOF dynamics (refer to Fig. 4.1). The aerodynamic control surfaces are assumed to have saturation limits and availability of state feedback is also assumed.

To perform a coordinated horizontal turn maneuver, a smooth bell-shaped curve for desired roll angle profile (ϕ_d) is considered keeping desired sideslip angle (β_d) at the initial trim value throughout the maneuver. The total maneuver duration is taken to be $18s$ starting at $t = 0$. Figure 4.2 depicts the ground track, time evolutions of various states, c.g. estimates and the control surface deflection profiles corresponding to the above mentioned two cases of c.g. locations. Clearly, these results reveal high robustness to lateral c.g. variations and excellent tracking performance as the desired profiles and actual variables are nearly identical for all different c.g. positions. The estimate of c.g. is also found to converge to the actual c.g. position as predicted mathematically. Moreover, it was observed from Figure 4.2 that control surface deflections remained well within their respective saturation limits. Various controller parameters tuned through trial and error are listed in Table 4.1.

Table 4.1: Adaptive backstepping controller parameters

Maneuver	$\boldsymbol{K_1}$	$\boldsymbol{K_2}$	$\boldsymbol{K_3}$
Horizontal turn	$\begin{bmatrix} 18 & 0 \\ 0 & 35 \end{bmatrix}$	$\begin{bmatrix} 10 & 0 \\ 0 & 5 \end{bmatrix}$	0.01
Aileron roll	$\begin{bmatrix} 30 & 0 \\ 0 & 5 \end{bmatrix}$	$\begin{bmatrix} 35 & 0 \\ 0 & 5 \end{bmatrix}$	0.001

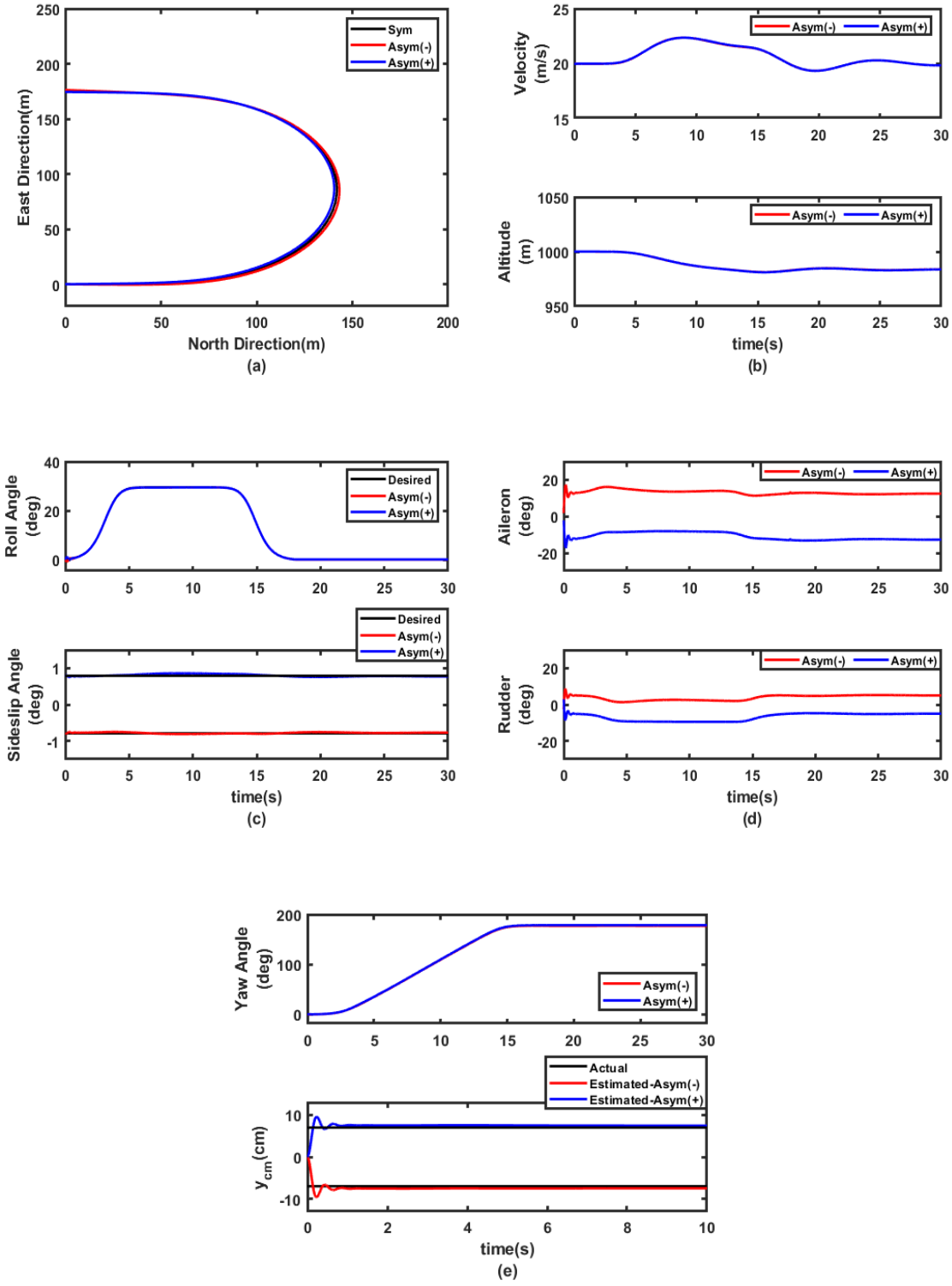

Figure 4.2. Ground track, time profile of states, c.g. position and control deflections

In a similar way, for aileron roll maneuver, a sigmoid function for desired roll angle (ϕ_d) profile is taken into consideration ensuring sideslip angle (β_d) remains at initial trim value. The UAV is directed to execute two full rotations about its body x-axis in 4s starting at $t = 0$. Initial trim conditions are kept the same as considered for horizontal turn maneuver. Figure 4.3 shows the time evolutions of various states, c.g. estimates and the control surface deflections. The results obtained demonstrate the system's robustness against lateral c.g. variations, showcasing excellent tracking performance as the actual variables almost overlap with the desired profiles. The c.g. position estimate converges to the actual c.g. position as well.

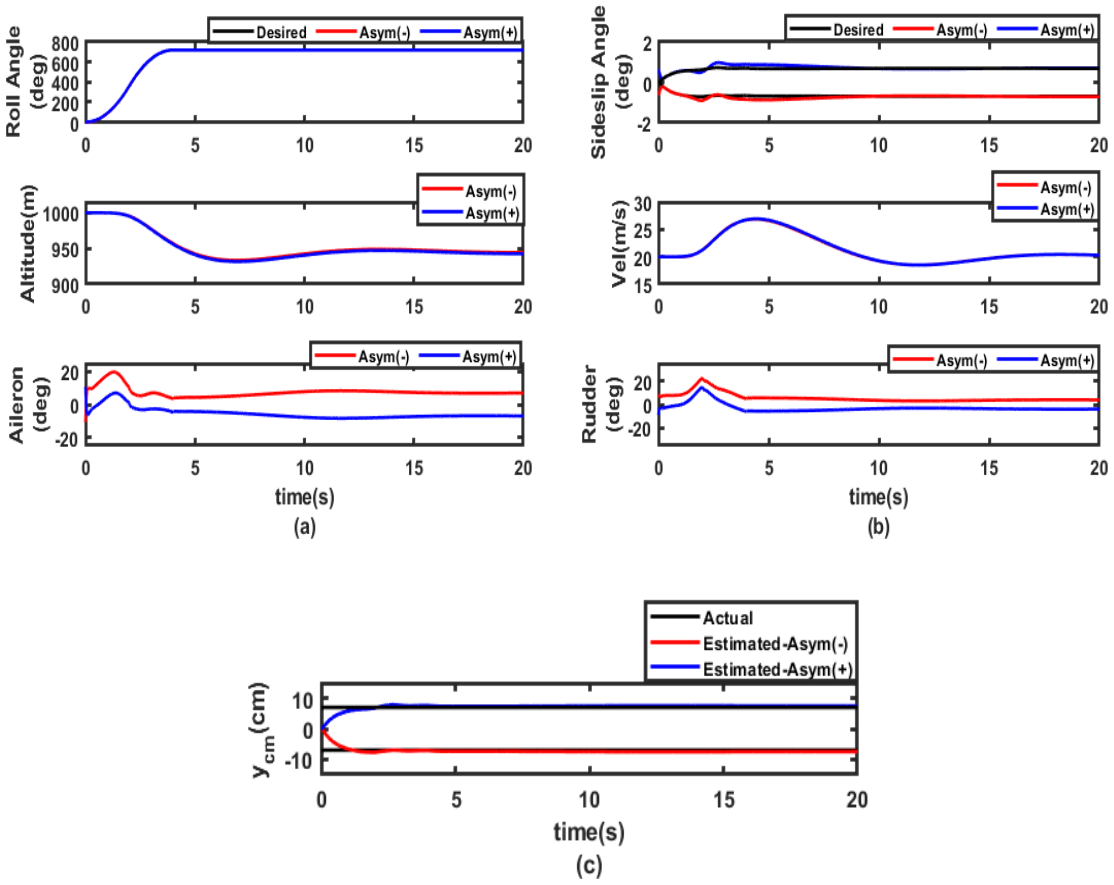

Figure 4.3. Time profile of states, c.g. position and control deflections: Aileron roll maneuver

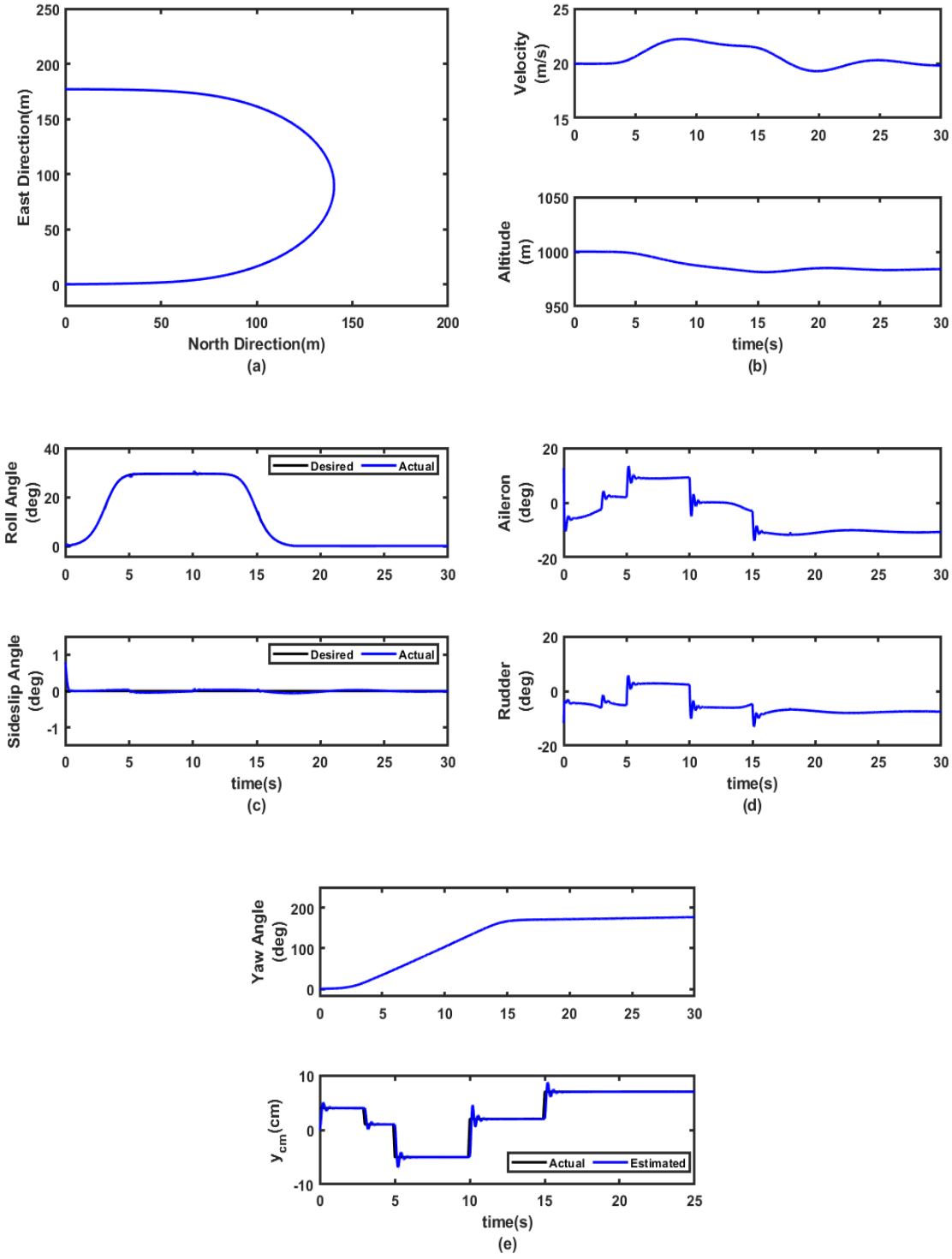

Figure 4.4. Ground track, time profile of states, arbitrary c.g. position and control deflections: Horizontal turn maneuver

To provide a more comprehensive validation of the proposed control scheme, a scenario is also examined where the lateral center of gravity position undergoes arbitrary multiple step changes during the maneuver and the results are presented in Figures 4.4 and 4.5. It is evident from these two sets of figures that the same level of tracking and maneuver performance is achieved under this situation too.

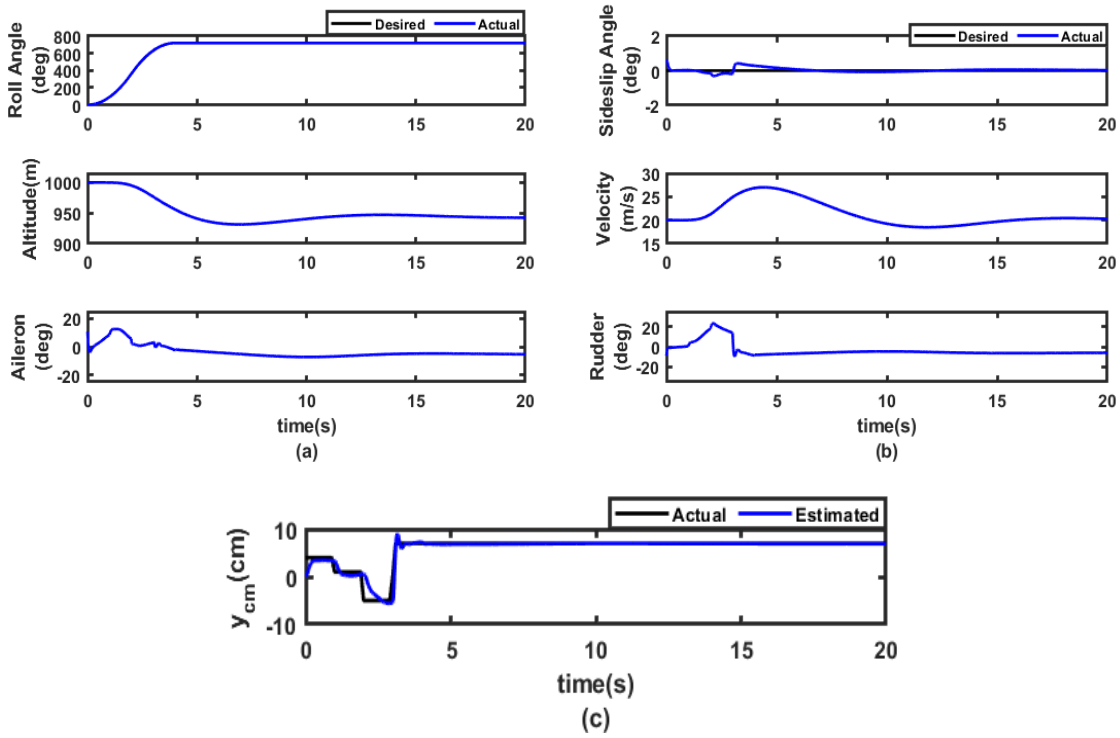

Figure 4.5. Time profile of states, arbitrary c.g. position and control deflections: Aileron roll maneuver

4.5 Comparison with the Control Proposed in Chapter 2

As discussed earlier in detail in Chapter 2, that a lateral c.g. offset issue can also be tackled by considering an ad-hoc dynamics where simply a moment due to gravity term is added to the symmetric 6-DOF dynamics. Therefore, tracking performance under the proposed controller is compared against the same under the ad-hoc model-based control and the proposed controller is

found to give significantly improved control performance. The standard ITAE, IAE, ITSE and ISE performance index values are compared and tabulated in Table 4.2. These indices are calculated for each of the three errors components e_ϕ, e_β and $\tilde{\sigma}$ (i.e. tracking errors in roll angle, sideslip angle and error in c.g. estimate) separately and then added up; E.g., $ITAE = \int_0^\infty t\left(|e_\phi| + |e_\beta| + |\tilde{\sigma}|\right) dt$ (other indices are also calculated in a similar manner). Units of e_ϕ, e_β are considered to be $radian$ and that of $\tilde{\sigma}$ is considered to be $meter$ in computing the entries of Tables 4.2 and 4.3. These three error profiles are also compared in Figures 4.6 and 4.7. Clearly, Table 4.2 and Tables 4.3 and Figures 4.6 and 4.7 show performance improvement substantiating the superiority and the significantly less conservative nature of the present control.

System dynamics considered for the ad-hoc model-based control design (obtained from Chapter 2) are summarized below in Eqs. (4.47) - (4.50) for ready reference. These equations are parallel to the Eqs. (4.21) - (4.24), which represent the approximate model of the asymmetric dynamics.

$$\begin{bmatrix}\dot{\phi}\\ \dot{\beta}\end{bmatrix} = \begin{bmatrix}0\\ \frac{g}{V}\, sin\phi\, cos\alpha_t + \frac{\bar{q}SC_Y(\beta)}{mV}\end{bmatrix} + \begin{bmatrix}1 & tan\alpha_t\, cos\phi\\ tan\alpha_t & -1\end{bmatrix}\begin{bmatrix}p\\ r\end{bmatrix} \tag{4.47}$$

$$\begin{bmatrix}\dot{p}\\ \dot{r}\end{bmatrix} = \begin{bmatrix}I_{xx} & -I_{xz}\\ -I_{xz} & I_{zz}\end{bmatrix}^{-1}\begin{bmatrix}\bar{q}Sb(C_{l\beta}\beta + C_{lp}\frac{pb}{2V} + C_{lr}\frac{rb}{2V})\\ \bar{q}Sb(C_{n\beta}\beta + C_{np}\frac{pb}{2V} + C_{nr}\frac{rb}{2V})\end{bmatrix} +$$
$$\begin{bmatrix}I_{xx} & -I_{xz}\\ -I_{xz} & I_{zz}\end{bmatrix}^{-1}\begin{bmatrix}mg\, cos\alpha_t\, cos\phi\\ mg\, sin\alpha_t\end{bmatrix} y_{cm} + \begin{bmatrix}I_{xx} & -I_{xz}\\ -I_{xz} & I_{zz}\end{bmatrix}^{-1}\begin{bmatrix}\bar{q}Sb\, C_{l\delta a} & \bar{q}Sb\, C_{l\delta r}\\ \bar{q}Sb\, C_{n\delta a} & \bar{q}Sb\, C_{n\delta r}\end{bmatrix}\begin{bmatrix}\delta_a\\ \delta_r\end{bmatrix} \tag{4.48}$$

Equations (4.47) and (4.48) can be expressed in generic vector-matrix forms as

$$\dot{\boldsymbol{x}}_{\boldsymbol{1}} = \boldsymbol{f}_{\boldsymbol{1}} + G_1\boldsymbol{x}_{\boldsymbol{2}} \tag{4.49}$$

$$\dot{\boldsymbol{x}}_{\boldsymbol{2}} = \boldsymbol{f}_{\boldsymbol{2}} + \boldsymbol{f}_{\boldsymbol{3}}\,\sigma + G_2\boldsymbol{u} \tag{4.50}$$

The control and adaptation laws as formulated for this ad-hoc model-based control are given by

$$\boldsymbol{u} = G_2^{-1}[-G_1^T\boldsymbol{e}_{\boldsymbol{1}} - \boldsymbol{f}_{\boldsymbol{1}} - \boldsymbol{f}_{\boldsymbol{3}}\,\hat{\sigma} + \dot{\boldsymbol{x}}_{\boldsymbol{2d}} - K_2\boldsymbol{e}_{\boldsymbol{2}}] \tag{4.51}$$

$$\boldsymbol{x_{2d}} = G_1^{-1}(-K_1\boldsymbol{e_1} - \boldsymbol{f_1} + \dot{\boldsymbol{x}}_{\boldsymbol{1d}}) \tag{4.52}$$

$$\dot{\hat{\sigma}} = \frac{1}{K_3}\,\boldsymbol{f_3^T}\,\boldsymbol{e_2} \tag{4.53}$$

Eqs. (4.51), (4.52) and (4.53) are comparable to equations (4.40), (4.31) and (4.37) respectively as the latter set describe the control and adaptation laws proposed in the present work. It is needless to mention that, for comparison purpose, the same control parameters, as listed in Table 4.1, are used for both the ad-hoc model-based control and the proposed control.

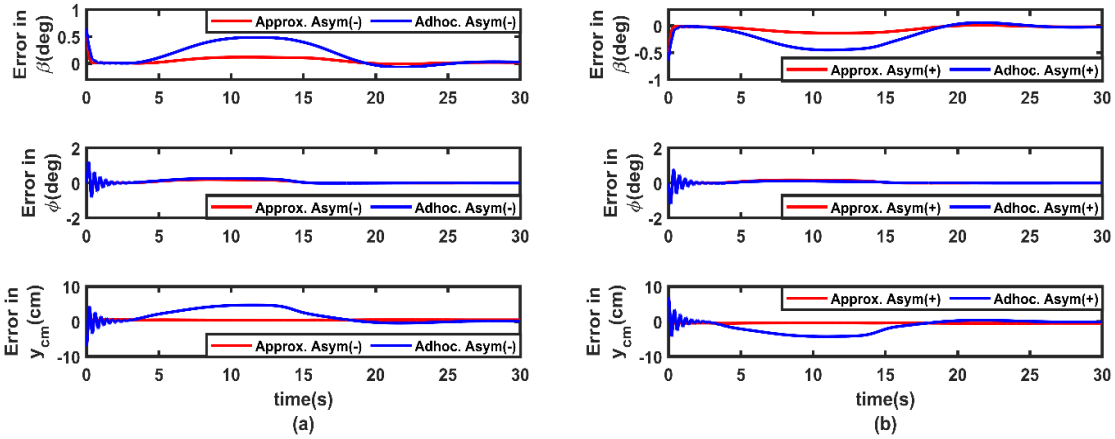

Figure 4.6. Tracking errors in Ad-hoc and Approximate (Proposed) model-based controls: Horizontal turn maneuver

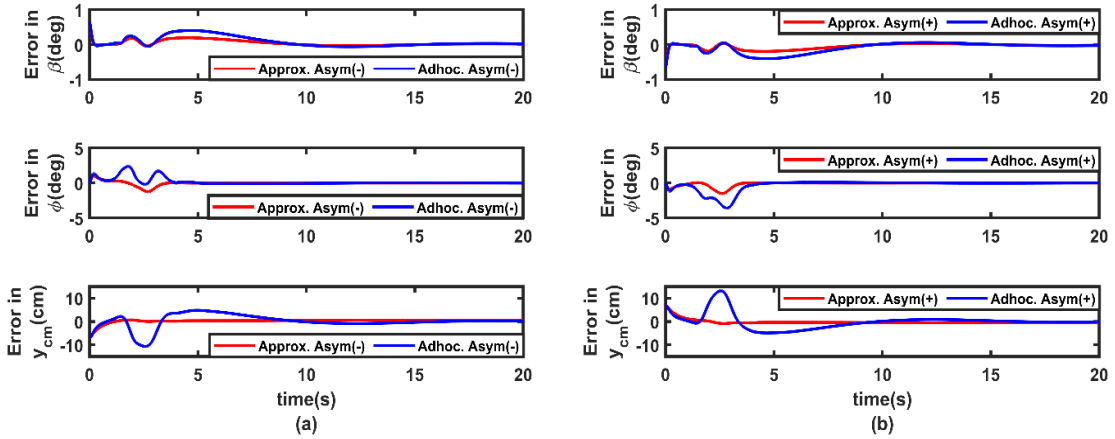

Figure 4.7. Tracking errors in Ad-hoc and Approximate (Proposed) model-based controls: Aileron roll maneuver

Table 4.2: Comparison of different performance indices: Horizontal turn maneuver

Model	Case	ITAE	IAE	ITSE	ISE
Ad-hoc [Chapter 2]	Asym(-)	7.2981	0.6354	0.1569	1.51×10^{-2}
	Asym(+)	6.4789	0.5690	0.1277	1.26×10^{-2}
Approximate (Proposed)	Asym(-)	0.8026	0.0860	0.0014	5.95×10^{-4}
	Asym(+)	0.7580	0.0808	0.0014	5.81×10^{-4}

Table 4.3: Comparison of different performance indices: Aileron roll maneuver

Model	Case	IAE	ITAE	ISE	ITSE
Ad-hoc [Chapter 2]	Asym(-)	0.4945	2.6839	1.597×10^{-2}	0.0678
	Asym(+)	0.5651	2.8995	2.72×10^{-2}	0.0882
Approximate (Proposed)	Asym(-)	0.1045	0.3039	2.05×10^{-3}	0.0015
	Asym(+)	0.1186	0.3249	2.57×10^{-3}	0.0022

4.6 Conclusion

This chapter addressed the challenging problem of designing robust nonlinear controller for executing lateral/directional maneuvers with a fixed wing UAV having significant unknown lateral c.g. movements. First, the highly coupled 6-DOF equations of motion under asymmetric c.g. position was approximated and cast in strict feedback form making it appropriate for a two-step adaptive backstepping control design where the lateral c.g. position could be estimated from an adaptation law. An adaptive backstepping control law retaining the useful nonlinearities in the dynamics was then proposed so that the UAV could perform the maneuvers automatically. The asymptotic stability of the proposed control was established using Lyapunov's method and new invariance principle. The proposed controller was found to yield very good maneuver performance and high insensitivity to lateral c.g. perturbation while performing two maneuvers - horizontal turn maneuver and aileron roll

considering the Aerosonde UAV. The proposed control scheme was also found to outperform an ad-hoc model based adaptive backstepping control scheme which is discussed in detail in chapter 2. It can be emphasized that the work can be easily extended to fighter aircraft or other airborne vehicles and to longitudinal maneuvers also. This issue is undertaken in next chapter once the UAV or the aircraft is made to operate in the high angle of attack regions along with lateral c.g. movements.

Chapter 5

Asymmetric Dynamics based Robust Adaptive Backstepping Control for High Alpha Maneuvers

5.1 Introduction

The previous chapter demonstrated that the complex 6-DOF equations of motion, under asymmetric center of gravity (c.g.) positions, can be approximated and reformulated into a strict feedback structure. This makes it suitable for a two-step adaptive backstepping control design, where the lateral c.g. position can be estimated through an adaptation law. Additionally, it was shown that an adaptive backstepping control law, which preserves useful nonlinearities in the dynamics, can autonomously execute maneuvers. However, in previous chapter the focus is on how c.g. shifts affect low-angle-of-attack (AOA) maneuvers. The present chapter investigates how c.g. movements impact specific high-angle-of-attack maneuvers.

In the present chapter, the first objective is to cast the off-c.g. equations of motion in the strict feedback form. It was proved that the coupled longitudinal and lateral/directional dynamics under

c.g. offset can also be cast in block strict feedback form under some reasonable assumptions such as neglecting the second order terms involving c.g. shifts (retaining the first order terms) and assuming the lateral c.g. movements to affect largely the rotational dynamics and not the translational dynamics. The final mathematical model turned out to be expressible in the form $\dot{\boldsymbol{x}}_{\boldsymbol{1}} = \boldsymbol{x}_{\boldsymbol{2}} + \boldsymbol{d}_{\boldsymbol{1}}$ and $\dot{\boldsymbol{x}}_{\boldsymbol{2}} = \boldsymbol{f}(\boldsymbol{x}) + A(\boldsymbol{x})\boldsymbol{\sigma} + G\boldsymbol{u} + \boldsymbol{d}_{\boldsymbol{2}}$ where the vector $\boldsymbol{\sigma}$ is the c.g. shift from the nominal c.g. location. Since the equation is in affine form of $\boldsymbol{\sigma}$, it becomes amenable to a two-step adaptive backstepping framework where $\boldsymbol{\sigma}$ can be estimated through an adaptation law. It was further observed that the model simplifications led to two additive exogenous disturbance inputs of $\boldsymbol{d}_1$ and $\boldsymbol{d}_{\boldsymbol{2}}$ in the individual steps of the backstepping design calling for further robustification of the proposed adaptive backstepping control. It is needless to emphasize that the uncertainties in the aerodynamic coefficients at high angles of attack will further increase the magnitudes of these exogenous disturbances. Further, it is also observed that the nonlinear term $\boldsymbol{f}(\boldsymbol{x})$ in the dynamics contains both favorable and unfavorable nonlinearities. Therefore, in the present chapter, the backstepping controller is designed in such a way that the favorable nonlinearities are explicitly retained (instead of cancelling them) in the same manner as in chapter 4, so that a less conservative control is achieved. As already emphasized, this is a novel addition since the works available on backstepping method applied to aircraft flight control problems such as [41, 111] do not retain the useful nonlinearities.

It has already been discussed in detail in chapter 3, for nonlinear uncertain system, sliding mode control (SMC) is widely used due to its various attractive properties. Using sliding mode in both the steps of the backstepping control is a novel situation as faced in the present problem. A comprehensive asymptotic stability analysis of the proposed hybrid controller is carried out using Lyapunov direct method and Barbalat's lemma. Two high-alpha maneuvers namely cobra and Herbst, are simulated in MATLAB and it is shown that almost identical maneuver performance is obtained over a wide range of lateral c.g. uncertainties on either side of the body centerline as well as under considerable aerodynamic uncertainties.

The outline of the chapter is as follows. The detailed mathematical modeling to represent the off c.g dynamics in strict feedback form is presented in second section. Third section describes the proposed adaptive backstepping adaptive sliding mode hybrid control law and its asymptotic stability proof. Simulation results are given in fourth section to validate the proposed control scheme against two benchmark post stall maneuvers and finally conclusions are drawn in section five.

5.2 Asymmetric Dynamics based Modelling for High Alpha Maneuvers

In this section, the coupled aircraft equations of motion under c.g. offset are converted to strict feedback form to make it amenable to backstepping based control design. The formulation is aimed at autonomously performing high alpha maneuvers such as cobra and Herbst, for which, usually the desired angle of attack (α), angle of sideslip (β) and bank angle (μ) time-profiles are supplied externally and the closed loop controller generates the required moments about the three body axes [68]. This requires the dynamics in terms of the state variables α, β, μ and the body rates p, q, r to be extracted from the complete set of equations. The complete 6-degree of freedom (DOF) equations of motion when the c.g. of the aircraft assumes an arbitrary position (x_{cm}, y_{cm}, z_{cm}) from the nominal c.g position or the origin of the body/wind frame are given by [63, 69]

$$\begin{bmatrix} 1 & 0 & 0 & 0 & z_{cm} & -y_{cm} \\ 0 & 1 & 0 & -z_{cm} & 0 & x_{cm} \\ 0 & 0 & 1 & y_{cm} & -x_{cm} & 0 \\ 0 & -mz_{cm} & my_{cm} & I'_{xx} & -I'_{xy} & -I'_{xz} \\ mz_{cm} & 0 & -mx_{cm} & -I'_{xy} & I'_{yy} & -I'_{yz} \\ -my_{cm} & mx_{cm} & 0 & -I'_{xz} & -I'_{yz} & I'_{zz} \end{bmatrix} \begin{bmatrix} \dot{u} \\ \dot{v} \\ \dot{w} \\ \dot{p} \\ \dot{q} \\ \dot{r} \end{bmatrix} = \begin{bmatrix} -qw + rv \\ -ru + pw \\ -pv + qu \\ I'_{xz}pq + (I'_{yy} - I'_{zz})qr - I'_{xy}rp + I'_{yz}(q^2 - r^2) \\ I'_{xy}qr + (I'_{zz} - I'_{xx})rp - I'_{yz}pq + I'_{xz}(r^2 - p^2) \\ I'_{yz}rp + (I'_{xx} - I'_{yy})pq - I'_{xz}qr + I'_{xy}(p^2 - q^2) \end{bmatrix} +$$

$$\begin{bmatrix} (q^2 + r^2)x_{cm} - pqy_{cm} - rpz_{cm} \\ (r^2 + p^2)y_{cm} - pqx_{cm} - qrz_{cm} \\ (p^2 + q^2)z_{cm} - rpx_{cm} - qry_{cm} \\ m(qu - pv)y_{cm} + m(ru - pw)z_{cm} \\ m(pv - qu)x_{cm} + m(rv - qw)z_{cm} \\ m(pw - ru)x_{cm} + m(qw - rv)y_{cm} \end{bmatrix} + \begin{bmatrix} -gsin\theta \\ gcos\theta sin\phi \\ gcos\theta cos\phi \\ -z_{cm}mgcos\theta sin\phi + y_{cm}mgcos\theta cos\phi \\ -z_{cm}mgsin\theta - x_{cm}mgcos\theta cos\phi \\ y_{cm}mgsin\theta + x_{cm}mgcos\theta sin\phi \end{bmatrix} + \begin{bmatrix} \frac{F_x}{m} \\ \frac{F_y}{m} \\ \frac{F_z}{m} \\ M_x \\ M_y \\ M_z \end{bmatrix} \quad (5.1)$$

where $I' = \begin{bmatrix} I'_{xx} & -I'_{xy} & -I'_{xz} \\ -I'_{xy} & I'_{yy} & -I'_{yz} \\ -I'_{xz} & -I'_{yz} & I'_{zz} \end{bmatrix}$ is the modified inertia matrix (modified because of c.g. shift).

Eliminating the translational dynamics part (i.e. $\dot{u}, \dot{v}, \dot{w}$ equations) from Eq. (5.1), the rotational dynamics can be extracted as

$$\left(\frac{1}{m}A^2 + I'\right)\begin{bmatrix}\dot{p}\\ \dot{q}\\ \dot{r}\end{bmatrix} = -A\begin{bmatrix}-qw + rv + (q^2 + r^2)x_{cm} - pqy_{cm} - rpz_{cm}\\ -ru + pw - pqx_{cm} + (r^2 + p^2)y_{cm} - qrz_{cm}\\ -pv + qu - rpx_{cm} - qry_{cm} + (p^2 + q^2)z_{cm}\end{bmatrix} - A\begin{bmatrix}-gsin\theta + \frac{1}{m}(\bar{q}SC_X + T_x)\\ gcos\theta sin\phi + \frac{1}{m}(\bar{q}SC_Y + T_y)\\ gcos\theta cos\phi + \frac{1}{m}(\bar{q}SC_Z + T_z)\end{bmatrix} +$$

$$\begin{bmatrix}I'_{xz}pq + (I'_{yy} - I'_{zz})qr - I'_{xy}rp + I'_{yz}(q^2 - r^2) + m(qu - pv)y_{cm} + m(ru - pw)z_{cm}\\ I'_{xy}qr + (I'_{zz} - I'_{xx})rp - I'_{yz}pq + I'_{xz}(r^2 - p^2) + m(pv - qu)x_{cm} + m(rv - qw)z_{cm}\\ I'_{yz}rp + (I'_{xx} - I'_{yy})pq - I'_{xz}qr + I'_{xy}(p^2 - q^2) + m(pw - ru)x_{cm} + m(qw - rv)y_{cm}\end{bmatrix} +$$

$$\begin{bmatrix}-z_{cm}mgcos\theta sin\phi + y_{cm}mgcos\theta cos\phi + \bar{q}SbC_l + M_{TX}\\ -z_{cm}mgsin\theta - x_{cm}mgcos\theta cos\phi + \bar{q}S\bar{c}C_m + M_{TY}\\ y_{cm}mgsin\theta + x_{cm}mgcos\theta sin\phi + \bar{q}SbC_n + M_{TZ}\end{bmatrix} \quad (5.2)$$

where as in Chapter 3, $A \triangleq \begin{bmatrix} 0 & -mz_{cm} & my_{cm} \\ mz_{cm} & 0 & -mx_{cm} \\ -my_{cm} & mx_{cm} & 0 \end{bmatrix}$.

In Eq.(5.2), thrust components are given by $T_x = \delta_T\, T\, cos\delta_{ptv}\, \cos\delta_{ytv}$, $T_y = \delta_T\, T\, sin\delta_{ytv}$, $T_z = -\delta_T\, T\, sin\delta_{ptv}\, \cos\delta_{ytv}$ and moments due to thrust are given by $M_{TX} = -l_z\delta_T T sin\delta_{ytv}$, $M_{TY} = -l_z\delta_T T cos\delta_{ptv} cos\delta_{ytv} - l_x\delta_T T sin\delta_{ptv} cos\delta_{ytv}$, $M_{TZ} = -l_x\delta_T T sin\delta_{ytv}$, with $\delta_{ptv}, \delta_{ytv}$ being the thrust vectoring angles in the pitch and yaw planes respectively, δ_T the throttle setting, T the gross engine thrust and l_x, l_z denoting the distances of the engine nozzle from the origin of the body frame along the x- and z- body axes respectively. Now, a predominantly lateral c.g. variation will not have significant impact on the translational dynamics. Further, the $\dot{\alpha} - \dot{\beta} - \dot{\mu}$ equations are largely kinematic in nature. Therefore, these equations may be considered to remain nearly unchanged under c.g. movements. The standard equations (i.e. for no c.g. offset) for $\dot{\alpha} - \dot{\beta} - \dot{\mu}$ are given in Eq. (5.3) below in wind frame under further assumption that the trigonometric nonlinearities involving thrust vector angles (i.e. $\delta_{ptv}, \delta_{ytv}$) are negligible and control surface deflections produce only moments and no force [92].

$$\begin{bmatrix}\dot{\alpha}\\ \dot{\beta}\\ \dot{\mu}\end{bmatrix} = \begin{bmatrix} \frac{g}{V} sec\beta cos\mu\, cos\gamma + \frac{1}{mV}(-sec\beta\, \bar{q}SC_{L_\alpha} - sec\beta\, \delta_T T\, sin\alpha) \\ \frac{g}{V} sin\mu\, cos\gamma + \frac{1}{mV}(\bar{q}SC_{Y_\beta}\beta - \delta_T T cos\alpha\, sin\beta) \\ -\frac{g}{V} tan\beta\, cos\mu\, cos\gamma + \frac{1}{mV}(tan\gamma\, cos\mu\, \bar{q}SC_{Y_\beta}\beta - tan\gamma\, cos\mu\, \delta_T T cos\alpha\, sin\beta + (tan\beta + sin\mu\, tan\gamma)\bar{q}SC_{L_\alpha} + (tan\beta + sin\mu\, tan\gamma)\delta_T T\, sin\alpha) \end{bmatrix}$$

$$+\begin{bmatrix} -cos\alpha\, tan\beta & 1 - \frac{1}{mV} sec\beta\, \bar{q}SC_{L_q}\frac{\bar{c}}{2V} & -sin\alpha\, tan\beta \\ sin\alpha + \frac{1}{mV}\bar{q}SC_{Y_p}\frac{b}{2V} & 0 & -cos\alpha + \frac{1}{mV}\bar{q}SC_{Y_r}\frac{b}{2V} \\ \frac{cos\alpha}{cos\beta} + \frac{1}{mV} tan\gamma\, cos\mu\, \bar{q}SC_{Y_p}\frac{b}{2V} & \frac{1}{mV}(tan\beta + sin\mu\, tan\gamma)\bar{q}SC_{L_q}\frac{\bar{c}}{2V} & \frac{sin\alpha}{cos\beta} + \frac{1}{mV} tan\gamma\, cos\mu\, \bar{q}SC_{Y_r}\frac{b}{2V} \end{bmatrix}\begin{bmatrix} p \\ q \\ r \end{bmatrix} \quad (5.3)$$

If the angle of attack and the sideslip angle are assumed to remain small, Eq. (5.3) can be drastically simplified to

$$\begin{bmatrix} \dot{\mu} \\ \dot{\alpha} \\ -\dot{\beta} \end{bmatrix} = \begin{bmatrix} p \\ q \\ r \end{bmatrix} + \begin{bmatrix} d_\mu \\ d_\alpha \\ d_\beta \end{bmatrix} \tag{5.4}$$

where the vector $[d_\mu \quad d_\alpha \quad d_\beta]^T$ represents a lumped disturbance which captures the effects of modelling approximations. Clearly, the disturbance term will be particularly significant when the aircraft moves into high angle of attack regions. Now, substituting the matrix A on the right-hand side of Eq. (5.2) and also denoting $I'' \triangleq \frac{1}{m} A^2 + I'$

$$[I''] \begin{bmatrix} \dot{p} \\ \dot{q} \\ \dot{r} \end{bmatrix} =$$

$$\begin{bmatrix} 0 & mz_{cm} & -my_{cm} \\ -mz_{cm} & 0 & mx_{cm} \\ my_{cm} & -mx_{cm} & 0 \end{bmatrix} \begin{bmatrix} -qw + rv + (q^2 + r^2)x_{cm} - pqy_{cm} - rpz_{cm} \\ -ru + pw - pqx_{cm} + (r^2 + p^2)y_{cm} - qrz_{cm} \\ -pv + qu - rpx_{cm} - qry_{cm} + (p^2 + q^2)z_{cm} \end{bmatrix} +$$

$$\begin{bmatrix} 0 & mz_{cm} & -my_{cm} \\ -mz_{cm} & 0 & mx_{cm} \\ my_{cm} & -mx_{cm} & 0 \end{bmatrix} \begin{bmatrix} -gsin\theta + \frac{1}{m}(\bar{q}SC_X + T_x) \\ gcos\theta sin\phi + \frac{1}{m}(\bar{q}SC_Y + T_y) \\ gcos\theta cos\phi + \frac{1}{m}(\bar{q}SC_Z + T_z) \end{bmatrix} +$$

$$\begin{bmatrix} I'_{xz}pq + (I'_{yy} - I'_{zz})qr - I'_{xy}rp + I'_{yz}(q^2 - r^2) + m(qu - pv)y_{cm} + m(ru - pw)z_{cm} \\ I'_{xy}qr + (I'_{zz} - I'_{xx})rp - I'_{yz}pq + I'_{xz}(r^2 - p^2) + m(pv - qu)x_{cm} + m(rv - qw)z_{cm} \\ I'_{yz}rp + (I'_{xx} - I'_{yy})pq - I'_{xz}qr + I'_{xy}(p^2 - q^2) + m(pw - ru)x_{cm} + m(qw - rv)y_{cm} \end{bmatrix} +$$

$$\begin{bmatrix} -z_{cm}mgcos\theta sin\phi + y_{cm}mgcos\theta cos\phi + \bar{q}SbC_l + M_{TX} \\ -z_{cm}mgsin\theta - x_{cm}mgcos\theta cos\phi + \bar{q}S\bar{c}C_m + M_{TY} \\ y_{cm}mgsin\theta + x_{cm}mgcos\theta sin\phi + \bar{q}SbC_n + M_{TZ} \end{bmatrix} \tag{5.5}$$

Carrying out the multiplications on the right-hand side, Eq. (5.5) takes the form

$$[I'']\begin{bmatrix}\dot{p}\\ \dot{q}\\ \dot{r}\end{bmatrix}=\begin{bmatrix}-rumz_{cm}+pwmz_{cm}-pqmz_{cm}x_{cm}+(r^2+p^2)mz_{cm}y_{cm}-qrmz_{cm}^2+pvmy_{cm}-qumy_{cm}+rpmy_{cm}x_{cm}+qrmy_{cm}^2-(p^2+q^2)my_{cm}z_{cm}\\ qwmz_{cm}-rvmz_{cm}-(q^2+r^2)mz_{cm}x_{cm}+pqmz_{cm}y_{cm}+rpmz_{cm}^2-pvmx_{cm}+qumx_{cm}-rpmx_{cm}^2-qrmx_{cm}y_{cm}+(p^2+q^2)mx_{cm}z_{cm}\\ -qwmy_{cm}+rvmy_{cm}+(q^2+r^2)my_{cm}x_{cm}-pqmy_{cm}^2-rpmy_{cm}z_{cm}+rumx_{cm}-pwmx_{cm}+pqmx_{cm}^2-(r^2+p^2)mx_{cm}y_{cm}+qrmx_{cm}z_{cm}\end{bmatrix}+$$

$$\begin{bmatrix}z_{cm}mgcos\theta sin\phi+z_{cm}(\bar{q}SC_Y+T_y)-y_{cm}mg\,cos\theta cos\phi-y_{cm}(\bar{q}SC_Z+T_z)\\ z_{cm}mgsin\theta-z_{cm}(\bar{q}SC_X+T_x)+x_{cm}mgcos\theta cos\phi+x_{cm}(\bar{q}SC_Z+T_z)\\ y_{cm}mgsin\theta+y_{cm}(\bar{q}SC_X+T_x)-x_{cm}mgcos\theta sin\phi-x_{cm}(\bar{q}SC_Y+T_y)\end{bmatrix}\quad\begin{bmatrix}-z_{cm}mgcos\theta sin\phi+y_{cm}mgcos\theta cos\phi+\bar{q}SbC_l+M_{TX}\\ -z_{cm}mgsin\theta-x_{cm}mgcos\theta cos\phi+\bar{q}S\bar{c}C_m+M_{TY}\\ y_{cm}mgsin\theta+x_{cm}mgcos\theta sin\phi+\bar{q}SbC_n+M_{TZ}\end{bmatrix}+$$

$$\begin{bmatrix}I'_{xz}pq+(I'_{yy}-I'_{zz})qr-I'_{xy}rp+I'_{yz}(q^2-r^2)+m(qu-pv)y_{cm}+m(ru-pw)z_{cm}\\ I'_{xy}qr+(I'_{zz}-I'_{xx})rp-I'_{yz}pq+I'_{xz}(r^2-p^2)+m(pv-qu)x_{cm}+m(rv-qw)z_{cm}\\ I'_{yz}rp+(I'_{xx}-I'_{yy})pq-I'_{xz}qr+I'_{xy}(p^2-q^2)+m(pw-ru)x_{cm}+m(qw-rv)y_{cm}\end{bmatrix}\tag{5.6}$$

Since the c.g. shift would be typically a small fraction of one $metre$; therefore, their second order terms in the first term on the right-hand side of Eq. (5.6) can be neglected. Further, adding the second and third terms on the right-hand side of Eq. (5.6)

$$[I'']\begin{bmatrix}\dot{p}\\ \dot{q}\\ \dot{r}\end{bmatrix} = \begin{bmatrix}-rumz_{cm} + pwmz_{cm} + pvmy_{cm} - qumy_{cm}\\ qwmz_{cm} - rvmz_{cm} - pvmx_{cm} + qumx_{cm}\\ -qwmy_{cm} + rvmy_{cm} + rumx_{cm} - pwmx_{cm}\end{bmatrix} +$$

$$\begin{bmatrix} z_{cm}(\bar{q}SC_Y + T_y) - y_{cm}(\bar{q}SC_Z + T_z) + \bar{q}SbC_l + M_{TX}\\ -z_{cm}(\bar{q}SC_X + T_x) + x_{cm}(\bar{q}SC_Z + T_z) + \bar{q}S\bar{c}C_m + M_{TY}\\ y_{cm}(\bar{q}SC_X + T_x) - x_{cm}(\bar{q}SC_Y + T_y) + \bar{q}SbC_n + M_{TZ}\end{bmatrix} +$$

$$\begin{bmatrix} I'_{xz}pq + (I'_{yy} - I'_{zz})qr - I'_{xy}rp + I'_{yz}(q^2 - r^2) + m(qu - pv)y_{cm} + m(ru - pw)z_{cm}\\ I'_{xy}qr + (I'_{zz} - I'_{xx})rp - I'_{yz}pq + I'_{xz}(r^2 - p^2) + m(pv - qu)x_{cm} + m(rv - qw)z_{cm}\\ I'_{yz}rp + (I'_{xx} - I'_{yy})pq - I'_{xz}qr + I'_{xy}(p^2 - q^2) + m(pw - ru)x_{cm} + m(qw - rv)y_{cm}\end{bmatrix} \quad (5.7)$$

On further rearrangement of the right-hand side of Eq. (5.7),

$$[I'']\begin{bmatrix}\dot{p}\\ \dot{q}\\ \dot{r}\end{bmatrix} = \begin{bmatrix} I'_{xz}pq + (I'_{yy} - I'_{zz})qr - I'_{xy}rp + I'_{yz}(q^2 - r^2)\\ I'_{xy}qr + (I'_{zz} - I'_{xx})rp - I'_{yz}pq + I'_{xz}(r^2 - p^2)\\ I'_{yz}rp + (I'_{xx} - I'_{yy})pq - I'_{xz}qr + I'_{xy}(p^2 - q^2)\end{bmatrix} +$$

$$\begin{bmatrix} 0 & -(\bar{q}SC_Z + T_Z) & (\bar{q}SC_Y + T_y)\\ (\bar{q}SC_Z + T_Z) & 0 & -(\bar{q}SC_X + T_x)\\ -(\bar{q}SC_Y + T_y) & (\bar{q}SC_X + T_x) & 0\end{bmatrix}\begin{bmatrix}x_{cm}\\ y_{cm}\\ z_{cm}\end{bmatrix} + \begin{bmatrix}\bar{q}SbC_l + M_{TX}\\ \bar{q}S\bar{c}C_m + M_{TY}\\ \bar{q}SbC_n + M_{TZ}\end{bmatrix} \quad (5.8)$$

Since $[I'']^{-1}$ can be expressed as $[I'']^{-1} = [I]^{-1} + \Delta$ where $I = \begin{bmatrix} I_{xx} & 0 & -I_{xz}\\ 0 & I_{yy} & 0\\ -I_{xz} & 0 & I_{zz}\end{bmatrix}$ is the nominal inertia matrix (before c.g. movement), the term Δ will give rise to an additive uncertainty in Eq. (5.8). Further, in the first term on the right-hand side of Eq. (5.8), the change in the inertia terms due to c.g. movements may also be ignored. These ignored inertia terms will add to the additive uncertainty term appearing in Eq. (5.8). Therefore, Eq. (5.8) can be simplified as

$$\begin{bmatrix}\dot{p}\\ \dot{q}\\ \dot{r}\end{bmatrix} = [I]^{-1}\begin{bmatrix} I_{xz}pq + (I_{yy} - I_{zz})qr \\ (I_{zz} - I_{xx})rp + I_{xz}(r^2 - p^2) \\ (I_{xx} - I_{yy})pq - I_{xz}qr \end{bmatrix} +$$

$$[I]^{-1}\begin{bmatrix} 0 & -(\bar{q}SC_Z + T_Z) & (\bar{q}SC_Y + T_y) \\ (\bar{q}SC_Z + T_Z) & 0 & -(\bar{q}SC_X + T_x) \\ -(\bar{q}SC_Y + T_y) & (\bar{q}SC_X + T_x) & 0 \end{bmatrix}\begin{bmatrix}x_{cm}\\ y_{cm}\\ z_{cm}\end{bmatrix} + [I]^{-1}\begin{bmatrix}\bar{q}SbC_l + M_{TX}\\ \bar{q}S\bar{c}C_m + M_{TY}\\ \bar{q}SbC_n + M_{TZ}\end{bmatrix} + \begin{bmatrix}d_p\\ d_q\\ d_r\end{bmatrix} \quad (5.9)$$

where $[d_p \quad d_q \quad d_r]^T$ denotes the lumped disturbance vector capturing the matched model uncertainties and external disturbances. Since control surface deflections do not contribute significantly to force, they are customarily ignored for control design purposes in force components in the equations of motion. Therefore, in Eq. (5.9), the terms $(\bar{q}SC_X + T_x)$, $(\bar{q}SC_y + T_y)$ and $(\bar{q}SC_z + T_z)$ are state dependent and control independent. On the other hand, the external moment term $[\bar{q}SbC_l + M_{TX} \quad \bar{q}S\bar{c}C_m + M_{TY} \quad \bar{q}SbC_n + M_{TZ}]^T$ in Eq. (5.9) has both state and control surface deflection dependent components given respectively by

$$\begin{bmatrix}M_{xs}\\ M_{ys}\\ M_{zs}\end{bmatrix} = \begin{bmatrix}\bar{q}Sb(C_{l\beta}\beta + C_{lp}\frac{pb}{2V} + C_{lr}\frac{rb}{2V}) \\ \bar{q}S\bar{c}(C_m + C_{mq}\frac{q\bar{c}}{2V}) - l_z\delta_T T \\ \bar{q}Sb(C_{n\beta}\beta + C_{np}\frac{pb}{2V} + C_{nr}\frac{rb}{2V})\end{bmatrix} \quad (5.10)$$

$$\begin{bmatrix}M_{xc}\\ M_{yc}\\ M_{zc}\end{bmatrix} = \begin{bmatrix}\bar{q}SbC_{l\delta_a} & \bar{q}SbC_{l\delta_e} & \bar{q}SbC_{l\delta_r} & 0 & -l_z\delta_T T \\ 0 & \bar{q}S\bar{c}C_{m\delta_e} & 0 & -l_x\delta_T T & 0 \\ \bar{q}SbC_{n\delta_a} & \bar{q}SbC_{n\delta_e} & \bar{q}SbC_{n\delta_r} & 0 & -l_x\delta_T T\end{bmatrix}\begin{bmatrix}\delta_a\\ \delta_e\\ \delta_r\\ \delta_{ptv}\\ \delta_{ytv}\end{bmatrix} \quad (5.11)$$

Therefore, combining the state dependent terms together, Eq. (5.9) finally reduces to

$$\begin{bmatrix}\dot{p}\\ \dot{q}\\ \dot{r}\end{bmatrix} = [I]^{-1}\begin{bmatrix} I_{xz}pq + (I_{yy} - I_{zz})qr + M_{xs} \\ (I_{zz} - I_{xx})rp + I_{xz}(r^2 - p^2) + M_{ys} \\ (I_{xx} - I_{yy})pq - I_{xz}qr + M_{zs} \end{bmatrix} +$$

$$[I]^{-1}\begin{bmatrix} 0 & -(\bar{q}SC_Z + T_Z) & (\bar{q}SC_Y + T_y) \\ (\bar{q}SC_Z + T_Z) & 0 & -(\bar{q}SC_X + T_x) \\ -(\bar{q}SC_Y + T_y) & (\bar{q}SC_X + T_x) & 0 \end{bmatrix}\begin{bmatrix}x_{cm}\\ y_{cm}\\ z_{cm}\end{bmatrix} + [I]^{-1}\begin{bmatrix}M_{xc}\\ M_{yc}\\ M_{zc}\end{bmatrix} + \begin{bmatrix}d_p\\ d_q\\ d_r\end{bmatrix} \quad (5.12)$$

Now, it is observed from the aerodynamic dataset of F-18 HARV [19] that C_{lp} and C_{nr} are negative over the entire α range. Therefore, referring to Eq. (5.10), the term $C_{lp}\frac{pb}{2V}$ in M_{xs} and the term $C_{nr}\frac{rb}{2V}$ in M_{zs} are useful as far as stability is concerned and hence should be retained. It is further noted that $[I]^{-1}$ is positive definite. Therefore, we can separate the unfavorable and favorable terms in Eq. (5.12) as

$$\begin{bmatrix}\dot{p}\\ \dot{q}\\ \dot{r}\end{bmatrix} = [I]^{-1}\begin{bmatrix} I_{xz}pq + (I_{yy}-I_{zz})qr + \bar{q}Sb\left(C_{l\beta}\beta + C_{lr}\frac{rb}{2V}\right)\\ (I_{zz}-I_{xx})rp + I_{xz}(r^2-p^2) + \bar{q}S\bar{c}\left(C_m + C_{mq}\frac{q\bar{c}}{2V}\right) - l_z\delta_T T\\ (I_{xx}-I_{yy})pq - I_{xz}qr + \bar{q}Sb\left(C_{n\beta}\beta + C_{np}\frac{pb}{2V}\right)\end{bmatrix} +$$

$$[I]^{-1}\begin{bmatrix}\bar{q}SbC_{lp}\frac{b}{2V} & 0 & 0\\ 0 & 0 & 0\\ 0 & 0 & \bar{q}SbC_{nr}\frac{b}{2V}\end{bmatrix}\begin{bmatrix}p\\ q\\ r\end{bmatrix} + [I]^{-1}\begin{bmatrix}0 & -(\bar{q}SC_Z+T_Z) & (\bar{q}SC_Y+T_y)\\ (\bar{q}SC_Z+T_Z) & 0 & -(\bar{q}SC_X+T_x)\\ -(\bar{q}SC_Y+T_y) & (\bar{q}SC_X+T_x) & 0\end{bmatrix}\begin{bmatrix}x_{cm}\\ y_{cm}\\ z_{cm}\end{bmatrix} +$$

$$[I]^{-1}\begin{bmatrix}M_{xc}\\ M_{yc}\\ M_{zc}\end{bmatrix} + \begin{bmatrix}d_p\\ d_q\\ d_r\end{bmatrix} \tag{5.13}$$

Now, defining $\boldsymbol{x_1} = [\mu \quad \alpha \quad -\beta]^T$, the virtual control $\boldsymbol{x_2} = [p \quad q \quad r]^T$ and the control signal $\boldsymbol{u} = [M_{xc} \quad M_{yc} \quad M_{zc}]^T$, Eqs. (5.4) and (5.13) can be expressed in the generic vector-matrix form as

$$\dot{\boldsymbol{x}}_1 = \boldsymbol{x_2} + \boldsymbol{d_1} \tag{5.14}$$

$$\dot{\boldsymbol{x}}_2 = \boldsymbol{f_1}(\boldsymbol{x}) + \boldsymbol{F_2}\boldsymbol{x_2} + \boldsymbol{A}(\boldsymbol{x})\boldsymbol{\sigma} + \boldsymbol{G}\boldsymbol{u} + \boldsymbol{d_1} + \boldsymbol{d_2} \tag{5.15}$$

where the 3×3 matrix F_2 represents the favorable nonlinearity (clearly, F_2 is a negative semidefinite matrix) and $\boldsymbol{\sigma}$ is the uncertain/unknown c.g. position $[x_{cm} \;\; y_{cm} \;\; z_{cm}]^T$ from the origin of the body frame. It is readily observed that Eqs. (14) and (15) are in strict feedback form making the system dynamics suitable for a two-step backstepping control design with the term $\boldsymbol{\sigma}$ being estimated in an adaptive backstepping setting. However, since both Eqs. (14) and (15) contain exogenous disturbance terms, we propose to integrate sliding mode control with both the steps of the backstepping design for robustness enhancement. Further, the sliding mode controls are made adaptive assuming the

upper bounds of the disturbances $\boldsymbol{d_1}$ and $\boldsymbol{d_2}$ (denoted as $\boldsymbol{D_1}$ and $\boldsymbol{D_2}$ respectively) to be unknown. It is needless to emphasize that $\boldsymbol{d_2}$ will be particularly higher in high alpha regions due to aerodynamic uncertainties. It may be noted that throttle is controlled manually in an open loop manner during the maneuver period to further strengthen the thrust vector controls. The complete closed loop system is depicted in Figure 5.1.

5.3 Adaptive Backstepping Adaptive Sliding Mode Hybrid Control

In this section, an adaptive backstepping based adaptive fast sliding mode control (ABAFSMC) is proposed to autonomously execute high alpha maneuvers under unknown c.g. variations considering the aircraft flight dynamics given by Eqs. (5.14) and (5.15) as derived in the previous section. As shown in Figure 5.1, the desired time profiles for $\boldsymbol{x_1}$ (i.e. μ, α and $-\beta$) are fed externally as reference inputs and the controller generates the commanded moment vector $\boldsymbol{u}$ in a closed loop manner under the assumption of state feedback. The moment command as generated by the controller can be converted to the control surface deflection commands through the matrix pseudoinverse method applied to Eq. (5.11).

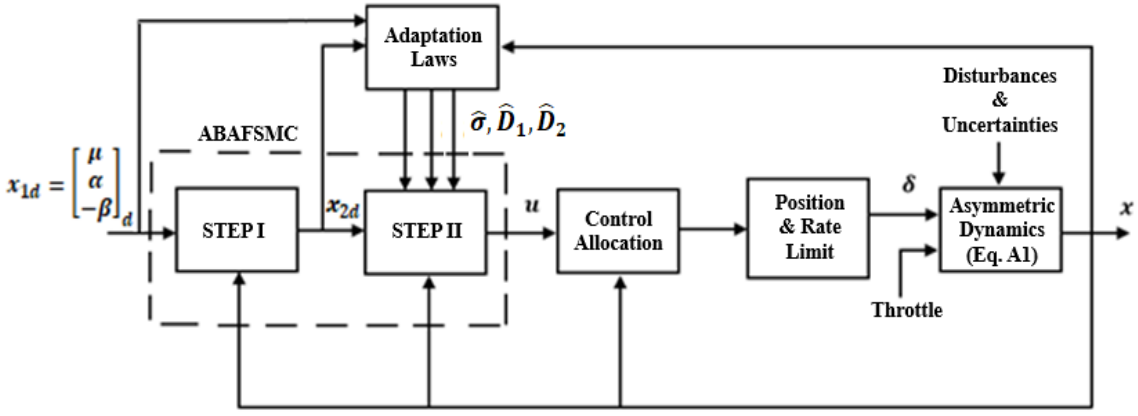

Figure 5.1. Block diagram of the overall closed loop system

Let the errors in the states $\boldsymbol{x_1}$ and $\boldsymbol{x_2}$ be defined as $\boldsymbol{e_1 = x_1 - x_{1d}}$ and $\boldsymbol{e_2 = x_2 - x_{2d}}$ with $\boldsymbol{x_{1d}}$ and $\boldsymbol{x_{2d}}$ being the desired trajectories of $\boldsymbol{x_1}$ and $\boldsymbol{x_2}$ respectively,

$$\boldsymbol{\dot{e}_1 = \dot{x}_1 - \dot{x}_{1d} = x_2 + d_1 - \dot{x}_{1d}} \tag{5.16}$$

Choosing the Lyapunov function for the error dynamics given by Eq. (5.16) as

$$V_1 = \frac{1}{2}\boldsymbol{S_1^T S_1} \tag{5.17}$$

where the sliding surface $\boldsymbol{S_1}$ is given as

$$\boldsymbol{S_1} = K_1 \int \boldsymbol{e_1} dt + \boldsymbol{e_1} \tag{5.18}$$

with $K_1 = diag\ (k_{11},\ k_{12},\ k_{13})$ being constant positive definite matrix

Differentiating V_1 w.r.t. time

$$\dot{V}_1 = \boldsymbol{S_1^T \dot{S}_1} \tag{5.19}$$

$$\dot{V}_1 = \boldsymbol{S_1^T}(K_1\boldsymbol{e_1} + \boldsymbol{\dot{e}_1}) = \boldsymbol{S_1^T}(K_1\boldsymbol{e_1} + \boldsymbol{x_2} + \boldsymbol{d_1} - \boldsymbol{\dot{x}_{1d}}) \tag{5.20}$$

For faster convergence, a fast reaching law is chosen having both linear and power rate terms as

$$\boldsymbol{\dot{S}_1} = -H_1\boldsymbol{S_1} - \boldsymbol{\widehat{D}_1} sgn\ (\boldsymbol{S_1}) - L_1 sig(\boldsymbol{S_1})^{b_1} = K_1\boldsymbol{e_1} + \boldsymbol{x_2} + \boldsymbol{d_1} - \boldsymbol{\dot{x}_{1d}} \tag{5.21}$$

with $H_1 = diag\ (h_{11},\ h_{12},\ h_{13})$, and $L_1 = diag\ (l_{11},\ l_{12},\ l_{13})$, being constant positive definite matrices and $sig(\boldsymbol{S_1})^{b_1} \triangleq \left[|S_\mu|^{b_1} sgn(S_\mu) \quad |S_\alpha|^{b_1} sgn(S_\alpha) \quad |S_\beta|^{b_1} sgn(S_\beta)\right]^T$ where b_1 is positive constants. Further, $\boldsymbol{D_1}$ is 3×1 vectors representing constant but unknown upper bounds of the disturbances $\boldsymbol{d_1}$. The desired profile of $\boldsymbol{x_2}$ is computed from

Now from Eq. (5.21), if the desired profile for the virtual control is designed as

$$\boldsymbol{x_{2d}} = -H_1\boldsymbol{S_1} - \boldsymbol{\widehat{D}_1} sgn\ (\boldsymbol{S_1}) - L_1 sig(\boldsymbol{S_1})^{b_1} - K_1\boldsymbol{e_1} + \boldsymbol{\dot{x}_{1d}} \tag{5.22}$$

then under the condition that $\boldsymbol{x_2 = x_{2d}}$ or $\boldsymbol{e_2 = 0}$, $\dot{V}_1$ reduces to

$$\dot{V}_1 = -\boldsymbol{S_1^T} H_1 \boldsymbol{S_1} - \boldsymbol{S_1^T} L_1 sig(\boldsymbol{S_1})^{b_1} - \boldsymbol{S_1^T}\left(\widehat{\boldsymbol{D}}_\mathbf{1} sgn(\boldsymbol{S_1}) - \boldsymbol{d_1}\right) \tag{5.23}$$

Now defining $\widetilde{\boldsymbol{D}}_\mathbf{1} = \boldsymbol{D_1} - \widehat{\boldsymbol{D}}_\mathbf{1}$, Eq. (5.23) reduces to

$$\dot{V}_1 = -\boldsymbol{S_1^T} H_1 \boldsymbol{S_1} - \boldsymbol{S_1^T} L_1 sig(\boldsymbol{S_1})^{b_1} - \boldsymbol{S_1^T}(\boldsymbol{D_1} sgn(\boldsymbol{S_1}) - \boldsymbol{d_1}) + |\boldsymbol{S_1}|^T \widetilde{\boldsymbol{D}}_\mathbf{1} \tag{5.24}$$

Clearly, $\dot{V}_1 < 0$ under the condition $|\boldsymbol{S_1}| = \mathbf{0}$.

For the second step in the backstepping design, considering a composite Lyapunov function for the complete dynamics as

$$V_2 = \tfrac{1}{2}\boldsymbol{S_1^T S_1} + \tfrac{1}{2}\boldsymbol{S_2^T S_2} + \tfrac{1}{2}\widetilde{\boldsymbol{\sigma}}^T K_2 \widetilde{\boldsymbol{\sigma}} + \tfrac{\mathbf{1}}{\mathbf{2}}\widetilde{\boldsymbol{D}}_\mathbf{1}^\mathbf{T} K_3 \widetilde{\boldsymbol{D}}_\mathbf{1} + \tfrac{\mathbf{1}}{\mathbf{2}}\widetilde{\boldsymbol{D}}_\mathbf{2}^\mathbf{T} K_4 \widetilde{\boldsymbol{D}}_\mathbf{2} \tag{5.25}$$

where $\widetilde{\boldsymbol{\sigma}} = \boldsymbol{\sigma} - \widehat{\boldsymbol{\sigma}}$ and $\widetilde{\boldsymbol{D}}_\mathbf{2} = \boldsymbol{D_2} - \widehat{\boldsymbol{D}}_\mathbf{2}$ are the estimation error vectors and K_2, K_3, K_4 are adaptation gains and the sliding surface $\boldsymbol{S_2} = \mathbf{0}$ is chosen as

$$\boldsymbol{S_2} = \boldsymbol{S_1} + N\boldsymbol{e_2}. \tag{5.26}$$

On differentiation of Eq. (5.25) w.r.t. time,

$$\dot{V}_2 = \dot{V}_1 + \dot{V}_{21} - \widetilde{\boldsymbol{\sigma}}^\mathbf{T} K_2 \dot{\widehat{\boldsymbol{\sigma}}} - \widetilde{\boldsymbol{D}}_\mathbf{1}^\mathbf{T} K_3 \dot{\widehat{\boldsymbol{D}}}_\mathbf{1} - \widetilde{\boldsymbol{D}}_\mathbf{2}^\mathbf{T} K_4 \dot{\widehat{\boldsymbol{D}}}_\mathbf{2} \tag{5.27}$$

where, $\dot{V}_1 = \boldsymbol{S_1^T \dot{S}_1}$ and $\dot{V}_{21} = \boldsymbol{S_2^T \dot{S}_2}$.

For the sake of brevity, the terms $\dot{V}_1$ and $\dot{V}_{21}$on the right-hand side in Eq. (5.27) are analyzed individually.

Substituting $\boldsymbol{x_{2d}}$ from Eq. (5.22) into Eq. (5.20) and also noting that $\boldsymbol{x_2} = \boldsymbol{e_2} + \boldsymbol{x_{2d}}$, and $\widehat{\boldsymbol{D}}_\mathbf{1} = \boldsymbol{D_1} - \widetilde{\boldsymbol{D}}_\mathbf{1}$, Eq. (5.20) reduces to

$$\dot{V}_1 = \boldsymbol{S_1^T}(K_1\boldsymbol{e_1} + e_2 + \boldsymbol{x_{2d}} + \boldsymbol{d_1} - \dot{\boldsymbol{x}}_{\boldsymbol{1d}}) \tag{5.28}$$

$$\dot{V}_1 = -\boldsymbol{S_1^T} H_1 \boldsymbol{S_1} + \boldsymbol{S_1^T e_2} - \boldsymbol{S_1^T} L_1 sig(\boldsymbol{S_1})^{b_1} - \boldsymbol{S_1^T}(\boldsymbol{D_1} sgn(S_1) - \boldsymbol{d_1}) + |\boldsymbol{S_1}|^T \widetilde{\boldsymbol{D}}_\mathbf{1} \tag{5.29}$$

which implies

$$\dot{V}_1 \leq -\boldsymbol{S_1^T} H_1 \boldsymbol{S_1} + \boldsymbol{S_1^T e_2} - \boldsymbol{S_1^T} L_1 sig(\boldsymbol{S_1})^{b_1} + |\boldsymbol{S_1}|^T \widetilde{\boldsymbol{D}}_{\boldsymbol{1}} \tag{5.30}$$

Now differentiating $\boldsymbol{e_2}$ w.r.t. time,

$$\dot{\boldsymbol{e}}_{\boldsymbol{2}} = \dot{\boldsymbol{x}}_{\boldsymbol{2}} - \dot{\boldsymbol{x}}_{\boldsymbol{2d}} = \boldsymbol{f_1} + F_2 \boldsymbol{x_2} + A\boldsymbol{\sigma} + G\boldsymbol{u} + \boldsymbol{d_1} + \boldsymbol{d_2} - \dot{\boldsymbol{x}}_{\boldsymbol{2d}} \tag{5.31}$$

Using the equations of $\dot{\boldsymbol{S}}_{\boldsymbol{1}}$ and $\dot{\boldsymbol{e}}_{\boldsymbol{2}}$,

$$\dot{V}_{21} = \boldsymbol{S_2^T} \dot{\boldsymbol{S}}_{\boldsymbol{2}} = \boldsymbol{S_2^T} \left(\dot{\boldsymbol{S}}_{\boldsymbol{1}} + N \dot{\boldsymbol{e}}_{\boldsymbol{2}} \right) \tag{5.32}$$

$$= \boldsymbol{S_2^T} (K_1 \boldsymbol{e_1} + \boldsymbol{x_2} + \boldsymbol{d_1} - \dot{\boldsymbol{x}}_{\boldsymbol{1d}} + N(\boldsymbol{f_1} + F_2 \boldsymbol{x_2} + A\boldsymbol{\sigma} + G\boldsymbol{u} + \boldsymbol{d_1} + \boldsymbol{d_2} - \dot{\boldsymbol{x}}_{\boldsymbol{2d}})) \tag{5.33}$$

Further substituting $\boldsymbol{x_2} = \boldsymbol{e_2} + \boldsymbol{x_{2d}}$ and $\boldsymbol{\sigma} = \widetilde{\boldsymbol{\sigma}} + \widehat{\boldsymbol{\sigma}}$,

$$\dot{V}_{21} = \boldsymbol{S_2^T} (K_1 \boldsymbol{e_1} + \boldsymbol{e_2} + \boldsymbol{x_{2d}} + \boldsymbol{d_1} - \dot{\boldsymbol{x}}_{\boldsymbol{1d}} + N(\boldsymbol{f_1} + F_2(\boldsymbol{e_2} + \boldsymbol{x_{2d}}) + A\widehat{\boldsymbol{\sigma}} + G\boldsymbol{u} + \boldsymbol{d_1} + \boldsymbol{d_2} - \dot{\boldsymbol{x}}_{\boldsymbol{2d}})) + \boldsymbol{S_2^T} NA\widetilde{\boldsymbol{\sigma}} \tag{5.34}$$

Substituting $\boldsymbol{x_{2d}}$ from Eq. (5.22) and noting that $\boldsymbol{e_2} = N^{-1}(\boldsymbol{S_2} - \boldsymbol{S_1})$ from Eq. (5.26), Eq. (5.34) reduces to

$$\dot{V}_{21} = \boldsymbol{S_2^T} \left(\boldsymbol{e_2} - H_1 \boldsymbol{S_1} - \widehat{\boldsymbol{D}}_{\boldsymbol{1}} sgn(\boldsymbol{S_1}) - \boldsymbol{S_1^T} L_1 sig(\boldsymbol{S_1})^{b_1} + \boldsymbol{d_1} + N(\boldsymbol{f_1} + F_2 \boldsymbol{x_{2d}} + A\widehat{\boldsymbol{\sigma}} + G\boldsymbol{u} + \boldsymbol{d_1} + \boldsymbol{d_2} - \dot{\boldsymbol{x}}_{\boldsymbol{2d}}) + F_2 \boldsymbol{S_2} - F_2 \boldsymbol{S_1} \right) + \boldsymbol{S_2^T} NA\widetilde{\boldsymbol{\sigma}} \tag{5.35}$$

Let us consider another fast-reaching law combining linear and power rate terms [116] for $\boldsymbol{S_2}$ as

$$\dot{\boldsymbol{S}}_{\boldsymbol{2}} = -\widehat{\boldsymbol{D}}_{\boldsymbol{1}} sgn(\boldsymbol{S_2}) - H_2 \boldsymbol{S_2} - N(\widehat{\boldsymbol{D}}_{\boldsymbol{1}} + \widehat{\boldsymbol{D}}_{\boldsymbol{2}}) sgn(\boldsymbol{S_2}) - L_2 sig(\boldsymbol{S_2})^{b_2} \tag{5.36}$$

with $H_2 = diag\ (h_{21},\ h_{22},\ h_{23})$ and $L_2 = diag\ (l_{21},\ l_{22},\ l_{23})$ are constant positive definite matrices and $sig(\boldsymbol{S_2})^{b_2} \triangleq \left[|S_p|^{b_2} sgn(S_p) \quad |S_q|^{b_2} sgn(S_q) \quad |S_r|^{b_2} sgn(S_r) \right]^T$ where b_2 is positive constants. $\boldsymbol{D_1}$ and $\boldsymbol{D_2}$ are 3×1 vectors representing constant but unknown upper bounds of the disturbances $\boldsymbol{d_1}$ and $\boldsymbol{d_2}$ respectively.

Now, designing the control law as

$$\boldsymbol{u} = (NG)^{-1}\big[N(-\boldsymbol{f_1} - A\,\hat{\boldsymbol{\sigma}} + \dot{\boldsymbol{x}}_{\boldsymbol{2d}} - F_2\boldsymbol{x}_{\boldsymbol{2d}}) - \boldsymbol{e_2} + H_1\boldsymbol{S_1} + \hat{\boldsymbol{D}}_{\boldsymbol{1}}sgn(\boldsymbol{S_1}) + L_1 sig\,(\boldsymbol{S_1})^{b_1} + F_2\boldsymbol{S_1} - \hat{\boldsymbol{D}}_{\boldsymbol{1}}sgn(\boldsymbol{S_2}) - H_2\boldsymbol{S_2} - N(\hat{\boldsymbol{D}}_{\boldsymbol{1}} + \hat{\boldsymbol{D}}_{\boldsymbol{2}})sgn(\boldsymbol{S_2}) - L_2 sig(\boldsymbol{S_2})^{b_2}\big] \quad (5.37)$$

and further substituting $\hat{\boldsymbol{D}}_{\boldsymbol{1}} = \boldsymbol{D_1} - \tilde{\boldsymbol{D}}_{\boldsymbol{1}}$ and $\hat{\boldsymbol{D}}_{\boldsymbol{2}} = \boldsymbol{D_2} - \tilde{\boldsymbol{D}}_{\boldsymbol{2}}$ in Eq. (5.35)

$$\dot{V}_{21} \leq -\boldsymbol{S_2^T}H_2\boldsymbol{S_2} - \boldsymbol{S_2^T}L_2 sig(\boldsymbol{S_2})^{b_2} - \boldsymbol{S_2^T}(\boldsymbol{D_1}sgn(\boldsymbol{S_2}) - \boldsymbol{d_1}) + \boldsymbol{S_2^T}\tilde{\boldsymbol{D}}_{\boldsymbol{1}}sgn(\boldsymbol{S_2}) - \boldsymbol{S_2^T}N(\boldsymbol{D_1}sgn(\boldsymbol{S_2}) - \boldsymbol{d_1}) + \boldsymbol{S_2^T}N\tilde{\boldsymbol{D}}_{\boldsymbol{1}}sgn(\boldsymbol{S_2}) - \boldsymbol{S_2^T}N(\boldsymbol{D_2}sgn(\boldsymbol{S_2}) - \boldsymbol{d_2}) + \boldsymbol{S_2^T}N\tilde{\boldsymbol{D}}_{\boldsymbol{2}}sgn(\boldsymbol{S_2}) + \boldsymbol{S_2^T}F_2\boldsymbol{S_2} + \boldsymbol{S_2^T}NA\tilde{\boldsymbol{\sigma}} \quad (5.38)$$

Finally, Eq. (5.38) reduces to

$$\dot{V}_{21} \leq -\boldsymbol{S_2^T}H_2\boldsymbol{S_2} - \boldsymbol{S_2^T}L_2 sig(\boldsymbol{S_2})^{b_2} + \boldsymbol{S_2^T}F_2\boldsymbol{S_2} + |\boldsymbol{S_2}|^{\boldsymbol{T}}\tilde{\boldsymbol{D}}_{\boldsymbol{1}} + |\boldsymbol{S_2}|^{\boldsymbol{T}}N\tilde{\boldsymbol{D}}_{\boldsymbol{1}} + |\boldsymbol{S_2}|^{\boldsymbol{T}}N\tilde{\boldsymbol{D}}_{\boldsymbol{2}} + \boldsymbol{S_2^T}NA\tilde{\boldsymbol{\sigma}} \quad (5.39)$$

Substituting Eqs. (5.30) and (5.39) into Eq. (5.27),

$$\dot{V}_2 \leq -\boldsymbol{S_1^T}H_1\boldsymbol{S_1} + \boldsymbol{S_1^T}\boldsymbol{e_2} - \boldsymbol{S_1^T}L_1 sig(\boldsymbol{S_1})^{b_1} - \boldsymbol{S_2^T}H_2\boldsymbol{S_2} - \boldsymbol{S_2^T}L_2 sig(\boldsymbol{S_2})^{b_2} + \boldsymbol{S_2^T}F_2\boldsymbol{S_2} - \tilde{\boldsymbol{\sigma}}^{\boldsymbol{T}}\big(K_2\dot{\hat{\boldsymbol{\sigma}}} - A^T N^T\boldsymbol{S_2}\big) - \tilde{\boldsymbol{D}}_{\boldsymbol{2}}^{\boldsymbol{T}}(K_4\dot{\hat{\boldsymbol{D}}}_{\boldsymbol{2}} - N^T|\boldsymbol{S_2}|) - \tilde{\boldsymbol{D}}_{\boldsymbol{1}}^{\boldsymbol{T}}\left(K_3\dot{\hat{\boldsymbol{D}}}_{\boldsymbol{1}} - |\boldsymbol{S_1}| - |\boldsymbol{S_2}| - N^T|\boldsymbol{S_1}|\right) \quad (5.40)$$

Now, choosing the adaptation laws for $\hat{\boldsymbol{\sigma}}$, $\hat{\boldsymbol{D}}_{\boldsymbol{1}}$ and $\hat{\boldsymbol{D}}_{\boldsymbol{2}}$ as

$$\dot{\hat{\boldsymbol{\sigma}}} = K_2^{-1}A^T N^T\boldsymbol{S_2} \quad (5.41)$$

$$\dot{\hat{\boldsymbol{D}}}_{\boldsymbol{1}} = K_3^{-1}(|\boldsymbol{S_1}| + |\boldsymbol{S_2}| + N^T|\boldsymbol{S_2}|) \quad (5.42)$$

$$\dot{\hat{\boldsymbol{D}}}_{\boldsymbol{2}} = K_4^{-1}N^T|\boldsymbol{S_2}| \quad (5.43)$$

Eq. (5.40) reduces to

$$\dot{V}_2 \leq -\boldsymbol{S_1^T}H_1\boldsymbol{S_1} + \boldsymbol{S_1^T}\boldsymbol{e_2} - \boldsymbol{S_2^T}H_2\boldsymbol{S_2} - \boldsymbol{S_1^T}L_1 sig(\boldsymbol{S_1})^{b_1} - \boldsymbol{S_2^T}L_2 sig(\boldsymbol{S_2})^{b_2} + \boldsymbol{S_2^T}F_2\boldsymbol{S_2} \quad (5.44)$$

Since F_2 is negative semidefinite, so is the term $\boldsymbol{S_2^T}F_2\boldsymbol{S_2}$. Hence, Eq. (5.44) can be simplified to

$$\dot{V}_2 \leq -\boldsymbol{S_1^T}H_1\boldsymbol{S_1} + \boldsymbol{S_1^T}\boldsymbol{e_2} - \boldsymbol{S_2^T}H_2\boldsymbol{S_2} - \boldsymbol{S_1^T}L_1 sig(\boldsymbol{S_1})^{b_1} - \boldsymbol{S_2^T}L_2 sig(\boldsymbol{S_2})^{b_2} \quad (5.45)$$

On substitution of $\boldsymbol{S_2} = \boldsymbol{S_1} + N\boldsymbol{e_2}$,

$$\dot{V}_2 \leq -\boldsymbol{S_1^T} H_1 \boldsymbol{S_1} + \boldsymbol{S_1^T e_2} - (\boldsymbol{S_1} + N\boldsymbol{e_2})^{\boldsymbol{T}} H_2 (\boldsymbol{S_1} + N\boldsymbol{e_2}) - \boldsymbol{S_1^T} L_1 sig(\boldsymbol{S_1})^{b_1} - \boldsymbol{S_2^T} L_2 sig(\boldsymbol{S_2})^{b_2} \quad (5.46)$$

Clearly, all the terms on the right-hand side of inequality (5.46) are negative definite except for the second term. However, the first three terms of the right-hand side can be expressed in the form $-\boldsymbol{z}^T Q \boldsymbol{z}$ where

$$\boldsymbol{z}^T Q \boldsymbol{z} = [\boldsymbol{S_1^T} \quad \boldsymbol{e_2^T}] \begin{bmatrix} H_1 + H_2 & NH_2 - \frac{1}{2} \\ NH_2 - \frac{1}{2} & N^2 H_2 \end{bmatrix} \begin{bmatrix} \boldsymbol{S_1} \\ \boldsymbol{e_2} \end{bmatrix} \quad (5.47)$$

Therefore, the inequality in (5.46) can be finally expressed as

$$\dot{V}_2 \leq -\boldsymbol{z}^T Q \boldsymbol{z} - l_{11} \left|S_\mu\right|^{b_1+1} - l_{12} |S_\alpha|^{b_1+1} - l_{13} \left|S_\beta\right|^{b_1+1} - l_{21} \left|S_p\right|^{b_2+1} - l_{22} \left|S_q\right|^{b_2+1} - l_{23} |S_r|^{b_2+1} \quad (5.48)$$

Clearly, $\dot{V}_2 \leq 0$ if the Q matrix in Eq. (5.48) is positive semidefinite. Substituting the corresponding expressions of H_1, H_2, N, the Q matrix is given by

$$Q = \left[\begin{array}{ccc|ccc} h_{11} + h_{21} & 0 & 0 & n_{11}h_{21} - \frac{1}{2} & 0 & 0 \\ 0 & h_{12} + h_{22} & 0 & 0 & n_{12}h_{22} - \frac{1}{2} & 0 \\ 0 & 0 & h_{13} + h_{23} & 0 & 0 & n_{13}h_{23} - \frac{1}{2} \\ \hline n_{11}h_{21} - \frac{1}{2} & 0 & 0 & n_{11}^2 h_{21} & 0 & 0 \\ 0 & n_{12}h_{22} - \frac{1}{2} & 0 & 0 & n_{12}^2 h_{22} & 0 \\ 0 & 0 & n_{13}h_{23} - \frac{1}{2} & 0 & 0 & n_{13}^2 h_{23} \end{array}\right] \quad (5.49)$$

Lemma 1 The 6×6 Q matrix given by Eq. (5.49) is positive semidefinite if and only if

$$4n_{11}^2 h_{11}h_{21} + 4n_{11}h_{21} \geq 1; \; 4n_{12}^2 h_{12}h_{22} + 4n_{12}h_{22} \geq 1; \; 4n_{13}^2 h_{13}h_{23} + 4n_{13}h_{23} \geq 1 \quad (5.50)$$

Proof As per the Schur complement method [104], for any block symmetric matrix Q of the form $Q = \begin{bmatrix} A & B \\ B^T & C \end{bmatrix}$, if C is invertible, then $Q \geq 0$ if and only if $C \geq 0$ and $A - BC^{-1}B^T \geq 0$. Partitioning

the Q matrix as shown in Eq. (5.49), the condition $C \geq 0$ is already satisfied since $n_{11}, n_{12}, n_{13}, h_{21}, h_{22}, h_{23}$ are chosen to be positive constants. For the second condition,

$$\begin{bmatrix} h_{11}+h_{21} & 0 & 0 \\ 0 & h_{12}+h_{22} & 0 \\ 0 & 0 & h_{13}+h_{23} \end{bmatrix} - \begin{bmatrix} n_{11}h_{21}-\frac{1}{2} & 0 & 0 \\ 0 & n_{12}h_{22}-\frac{1}{2} & 0 \\ 0 & 0 & n_{13}h_{23}-\frac{1}{2} \end{bmatrix} \begin{bmatrix} \frac{1}{n_{11}^2 h_{21}} & 0 & 0 \\ 0 & \frac{1}{n_{12}^2 h_{22}} & 0 \\ 0 & 0 & \frac{1}{n_{13}^2 h_{23}} \end{bmatrix} \begin{bmatrix} n_{11}h_{21}-\frac{1}{2} & 0 & 0 \\ 0 & n_{12}h_{22}-\frac{1}{2} & 0 \\ 0 & 0 & n_{13}h_{23}-\frac{1}{2} \end{bmatrix} \geq 0 \tag{5.51}$$

which on expansion and simplification yields $4n_{11}^2 h_{11}h_{21} + 4n_{11}h_{21} \geq 1$, $4n_{12}^2 h_{12}h_{22} + 4n_{12}h_{22} \geq 1$, $4n_{13}^2 h_{13}h_{23} + 4n_{13}h_{23} \geq 1$.

Remark 1 Since negative semi-definiteness of the composite Lyapunov function $\dot{V}_2$ is established through the preceding proposition and lemma, the $\boldsymbol{S_1}$ and $\boldsymbol{S_2}$ dynamics are stable, which in turn, implies stability of $\boldsymbol{e_1}$ and $\boldsymbol{e_2}$ dynamics. Now, Barbalat's lemma can be applied in the line of [56, 75, 107] to investigate asymptotic stability of the errors. Integrating both sides of inequality (5.48),

$$\int_0^\infty \left(\boldsymbol{z}^{\boldsymbol{T}}(\tau) Q \boldsymbol{z}(\tau) + l_{11}\left|S_\mu(\tau)\right|^{b_1+1} + l_{12}|S_\alpha(\tau)|^{b_1+1} + l_{13}\left|S_\beta(\tau)\right|^{b_1+1} + l_{21}\left|S_p(\tau)\right|^{b_2+1} + l_{22}\left|S_q(\tau)\right|^{b_2+1} + l_{23}|S_r(\tau)|^{b_2+1} \right) d\tau \leq -\int_0^\infty \dot{V}_2(\tau) d\tau = V_2(0) - V_2(\infty) < \infty \tag{5.52}$$

As $\lim_{t\to\infty} \int_0^t \left(\boldsymbol{z}^{\boldsymbol{T}}(\tau) Q \boldsymbol{z}(\tau) + l_{11}\left|S_\mu(\tau)\right|^{b_1+1} + l_{12}|S_\alpha(\tau)|^{b_1+1} + l_{13}\left|S_\beta(\tau)\right|^{b_1+1} + l_{21}\left|S_p(\tau)\right|^{b_2+1} + l_{22}\left|S_q(\tau)\right|^{b_2+1} + l_{23}|S_r(\tau)|^{b_2+1} \right) d\tau$ is bounded, according to Barbalat's lemma, it can be concluded that

$$\lim_{t\to\infty} \int_0^t \left(\boldsymbol{z}^{\boldsymbol{T}}(\tau) Q \boldsymbol{z}(\tau) + l_{11}\left|S_\mu(\tau)\right|^{b_1+1} + l_{12}|S_\alpha(\tau)|^{b_1+1} + l_{13}\left|S_\beta(\tau)\right|^{b_1+1} + l_{21}\left|S_p(\tau)\right|^{b_2+1} + l_{22}\left|S_q(\tau)\right|^{b_2+1} + l_{23}|S_r(\tau)|^{b_2+1} \right) d\tau = 0 \tag{5.53}$$

In other words, the variables $\boldsymbol{z, S_1, S_2}$ all converge to zero asymptotically. Clearly, asymptotic stability of the sliding surfaces, in turn, implies asymptotic stability of the tracking error variables $\boldsymbol{e_1}$ and $\boldsymbol{e_2}$.

5.4 Simulation Results and Discussions

To validate the proposed control, the same two high-alpha maneuvers as considered in Chapter-3 namely cobra and Herbst are simulated for the F18-HARV aircraft. The same initial steady wings-level trim conditions (at $2000\ m$ altitude and $150\ m/s$ true air velocity) and the same extent of c.g. movements (i.e. $[2.3 \quad \pm 8.8 \quad 2.1]^T\ cm$ along the three axes from the nominal location) are retained. Maneuver durations are also kept unchanged ($6s$ for cobra and $18\ s$ for Herbst). A $tanh$ function is used in place of sgn functions in the simulations to reduce chattering and to enhance the thrust vector control power, throttle is increased to 50% in an open loop manner over the maneuver duration.Along with the c.g. variation, the aerodynamic coefficients are also assumed to be uncertain within a uniform $\pm 30\%$ uncertainty band about their nominal values. As earlier, again several tens of Monte Carlo runs are performed considering random values of the aerodynamic coefficients from within the given uncertainty band and y_{cm} in the range $\pm 8.8\ cm$ to test maneuver performance. Nearly identical performance is observed in each sample run; however, the results corresponding to only three cases one for no c.g. variation and one each for the two extreme lateral variations on either side of the body centerline are shown below. Various controller parameters which are tuned satisfying the set of conditions given in Eq. (5.51) are listed in Table 5.1 and Table 5.2..

Figures 5.2 and 5.3 depict the time evolutions of various states, sliding surfaces corresponding to the aforementioned three cases of c.g. locations, c.g. estimates and the control deflections respectively. Figure 5.2 shows that the desired α, β, μ profiles are very closely tracked. As expected in cobra maneuver, the aircraft pitches up to a maximum of 90° and its velocity nearly halves in about $4s$.

Control surface deflections are also found to remain largely within their respective saturation limits. It is also observed in Figs. 5.2 and 5.3 that the responses corresponding to all the three cases of c.g. positions are almost completely overlapping. This clearly demonstrates the excellent robustness property of the proposed controller to the c.g. and aerodynamic uncertainties.

Herbst maneuver results are shown in Figs. 5.4 and 5.5. In Fig. 5.4, the ground track of the trajectory reveals that the aircraft successfully performed a proper vertical plane turn. Good tracking performance and high insensitivity to c.g. perturbations are again observed from Figure 5.4 justifying the effectiveness of the proposed controller. Control deflections are again found to remain mostly within saturation limits as evident from Figure 5.5.

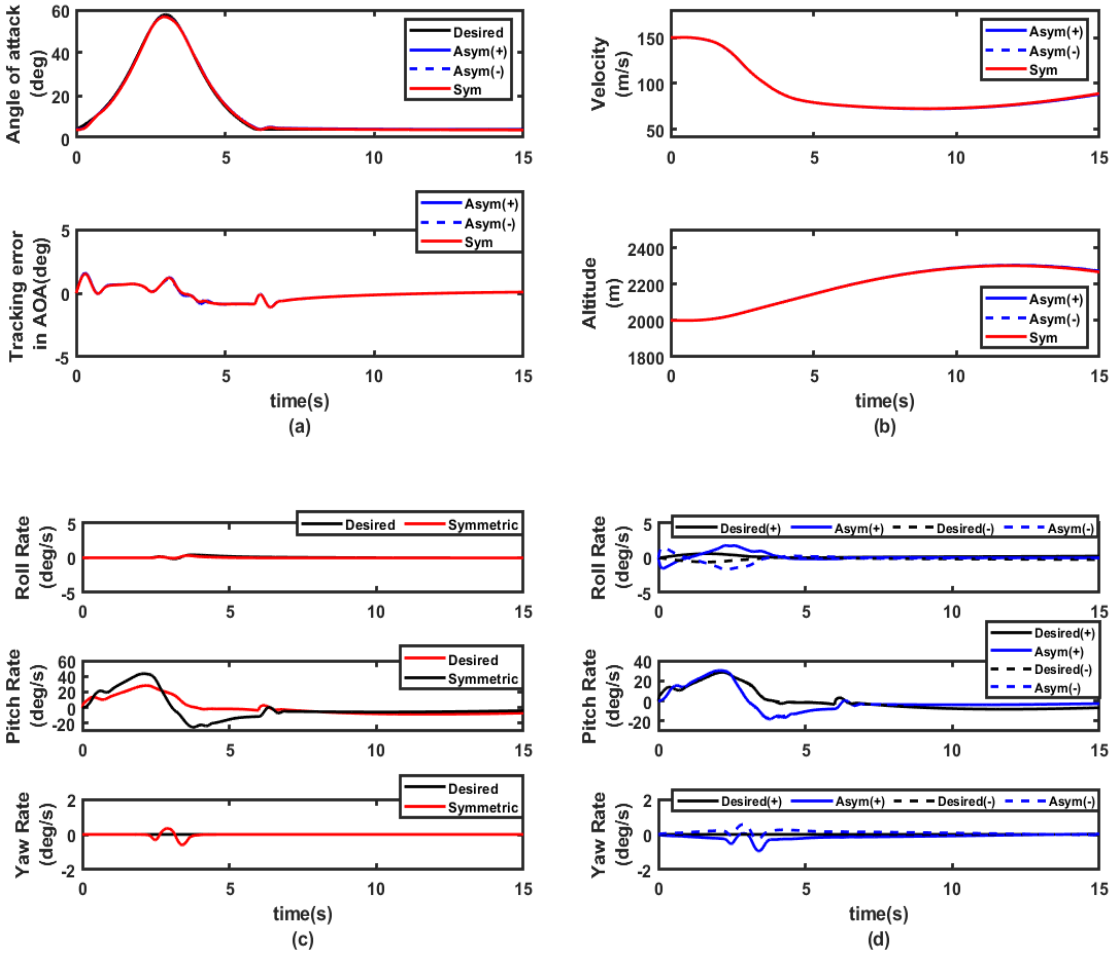

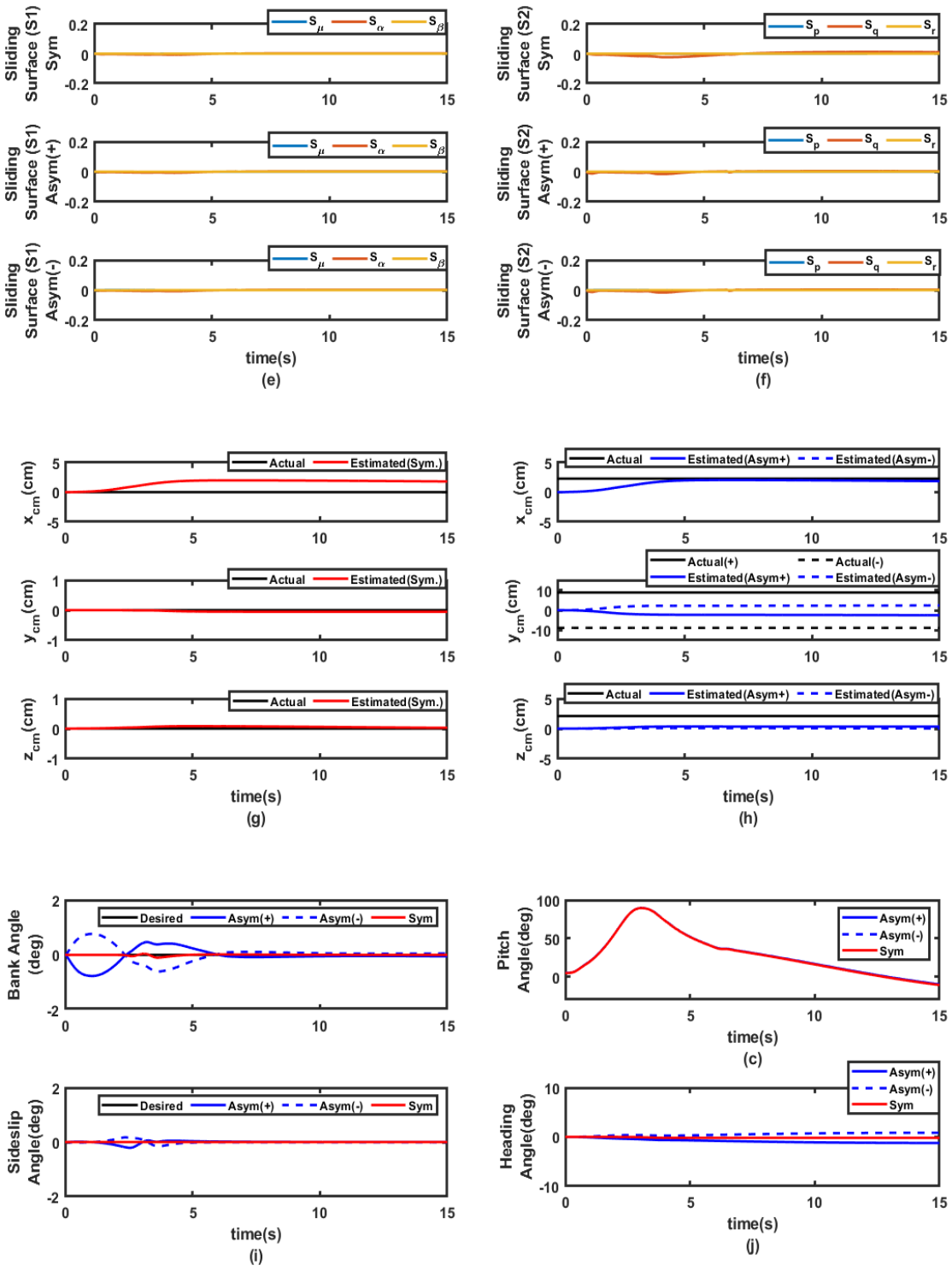

Figure 5.2. Time profile of states, sliding surface and c.g. position: Cobra maneuver

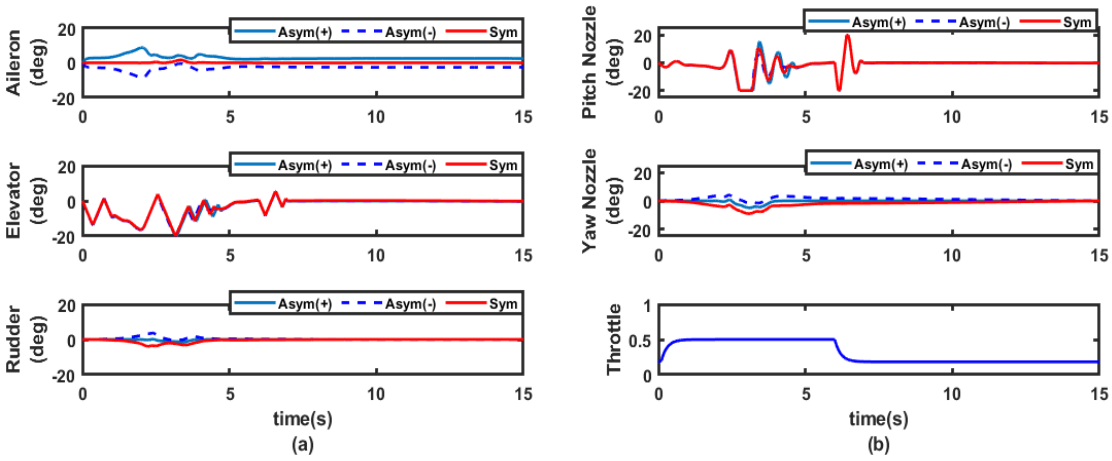

Figure 5.3. Time evolution of control deflections: Cobra maneuver

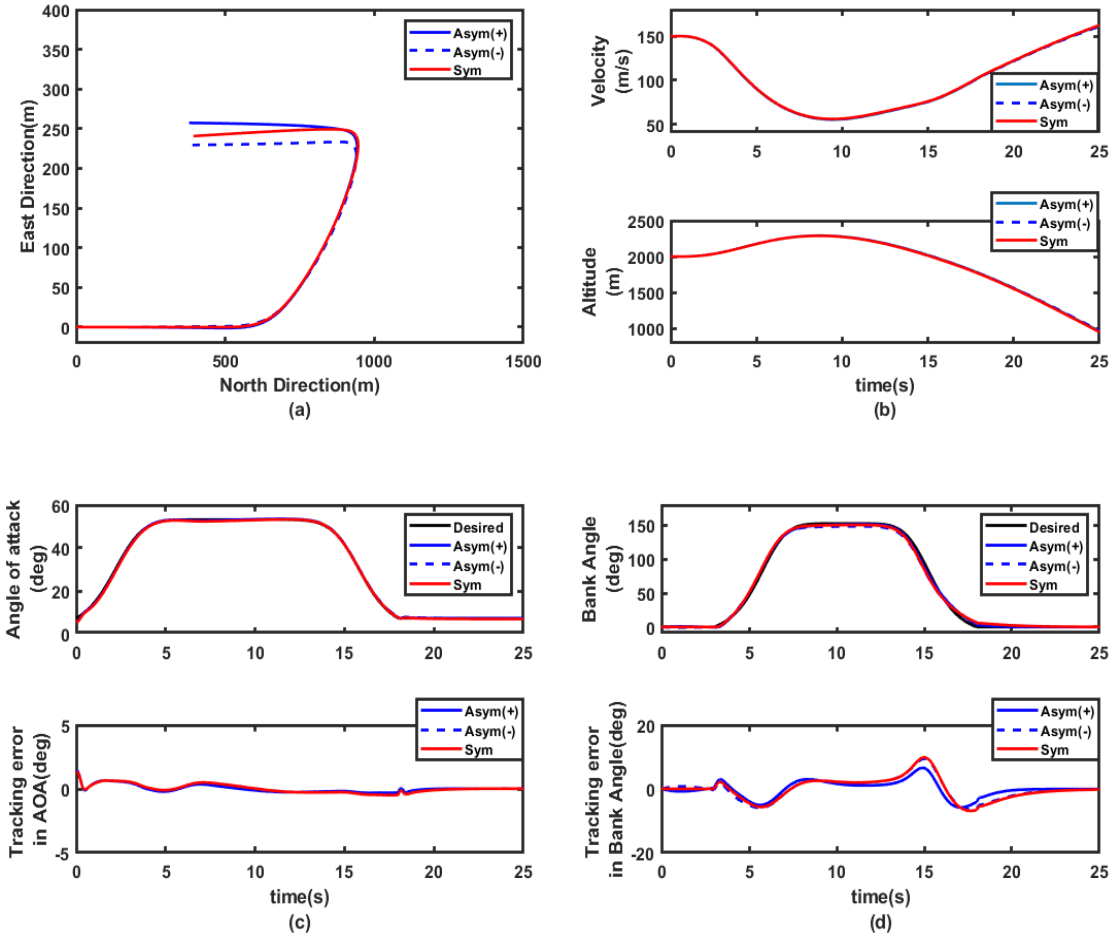

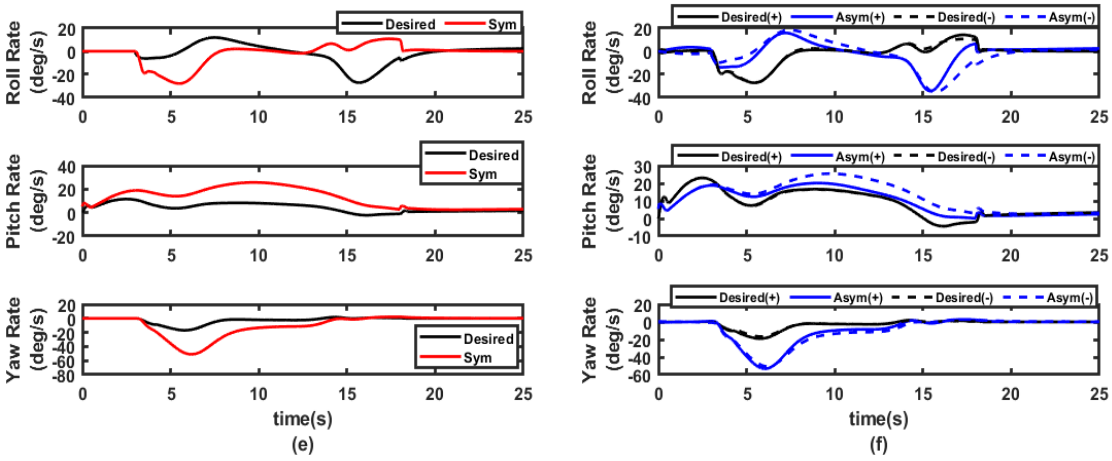
Roll Rate (deg/s)
Pitch Rate (deg/s)
Yaw Rate (deg/s)
Desired
Sym
time(s)
(e)

Roll Rate (deg/s)
Pitch Rate (deg/s)
Yaw Rate (deg/s)
Desired(+)
Asym(+)
Desired(-)
Asym(-)
time(s)
(f)

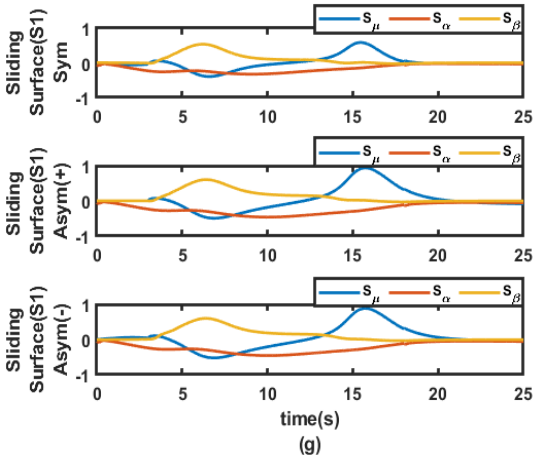
Sliding Surface(S1) Sym
Sliding Surface(S1) Asym(+)
Sliding Surface(S1) Asym(-)
time(s)
(g)

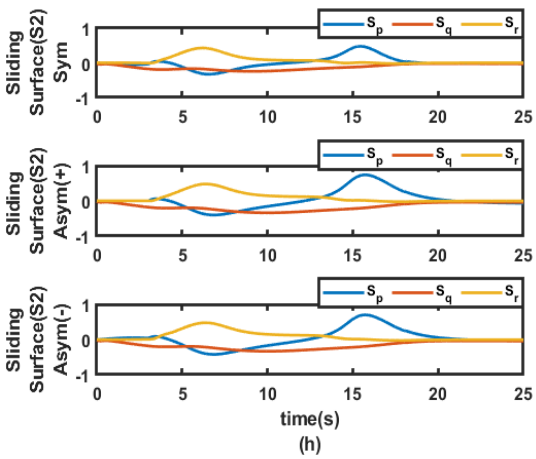
Sliding Surface(S2) Sym
Sliding Surface(S2) Asym(+)
Sliding Surface(S2) Asym(-)
time(s)
(h)

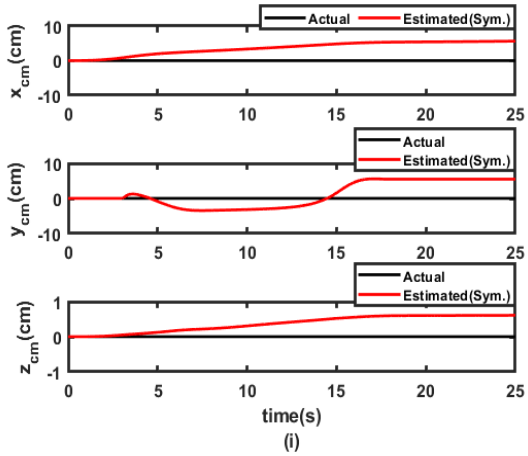
Actual
Estimated(Sym.)
time(s)
(i)

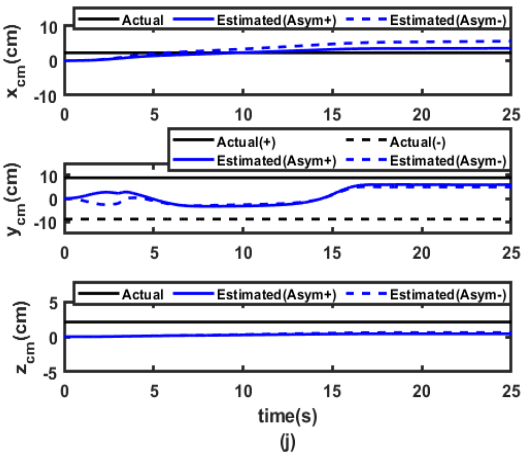
Actual
Estimated(Asym+)
Estimated(Asym-)
Actual(+)
Actual(-)
time(s)
(j)

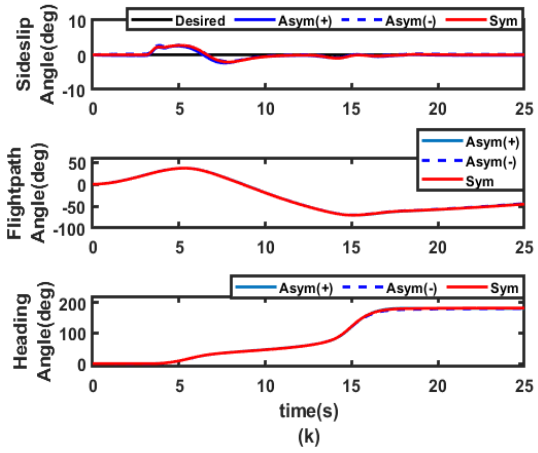

Figure 5.4. Ground track, time evolution of states, sliding surfaces and c.g. position: Herbst maneuver

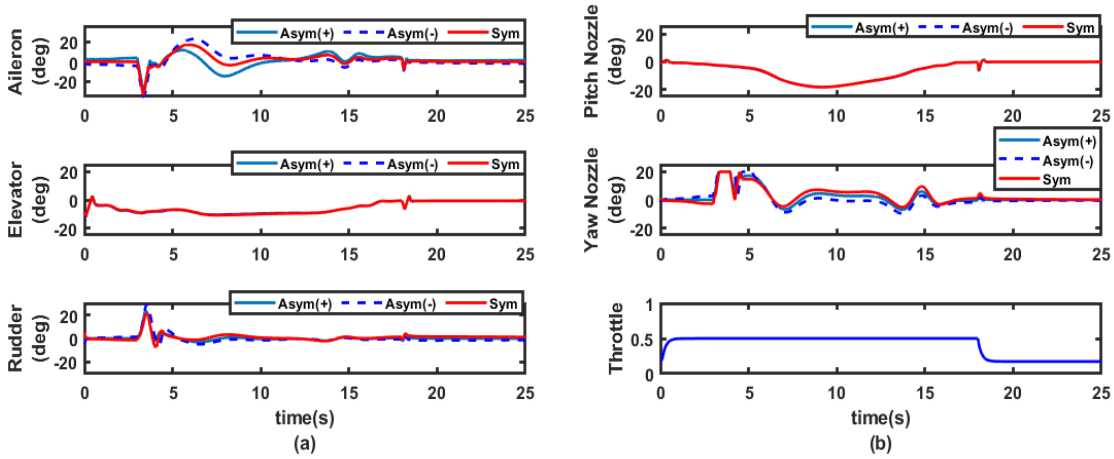

Figure 5.5. Time evolution of control deflections: Herbst maneuver

It can be observed from both Figures. 5.2 (g, h) and 5.4 (i, j) that the error in c.g estimate i.e. $\tilde{\boldsymbol{\sigma}}$ does not converge to zero in either maneuver. This is because asymptotic stability as established from Barbalat's lemma in Remark 1 in Section 5.3, guarantees asymptotic convergence of the sliding surface vectors $\boldsymbol{S_1}$ and $\boldsymbol{S_2}$ and the tracking error vectors $\boldsymbol{e_1}$ and $\boldsymbol{e_2}$; however, it does not guarantee asymptotic convergence of $\tilde{\boldsymbol{\sigma}}$; $\tilde{\boldsymbol{\sigma}}$ is guaranteed to remain only bounded as established from negative semi-definiteness of the time derivative of the composite Lyapunov function V_2.

Table 5.1: Controller parameters

K_1	H_1	L_1	b_1	N	K_2
$\begin{bmatrix} 2 & 0 & 0 \\ 0 & 6 & 0 \\ 0 & 0 & 4 \end{bmatrix}$	$\begin{bmatrix} 1.4 & 0 & 0 \\ 0 & 2 & 0 \\ 0 & 0 & 3 \end{bmatrix}$	$\begin{bmatrix} 2.5 & 0 & 0 \\ 0 & 1 & 0 \\ 0 & 0 & 0.8 \end{bmatrix}$	0.5	$\begin{bmatrix} 0.6 & 0 & 0 \\ 0 & 0.4 & 0 \\ 0 & 0 & 0.5 \end{bmatrix}$	$\begin{bmatrix} 20 & 0 & 0 \\ 0 & 12 & 0 \\ 0 & 0 & 15 \end{bmatrix}$

Table 5.2: Controller parameters (contd…)

K_3	K_4	H_2	b_2	L_2
$\begin{bmatrix} 30 & 0 & 0 \\ 0 & 60 & 0 \\ 0 & 0 & 40 \end{bmatrix}$	$\begin{bmatrix} 15 & 0 & 0 \\ 0 & 30 & 0 \\ 0 & 0 & 20 \end{bmatrix}$	$\begin{bmatrix} 0.3 & 0 & 0 \\ 0 & 0.5 & 0 \\ 0 & 0 & 0.4 \end{bmatrix}$	0.9	$\begin{bmatrix} 0.1 & 0 & 0 \\ 0 & 0.2 & 0 \\ 0 & 0 & 0.6 \end{bmatrix}$

To further demonstrate the effectiveness of the proposed control, a more generic situation is considered when lateral c.g. position is assumed to change in multiple steps during each of the maneuvers. Arbitrary y_{cm} time profiles are considered as shown in Figs. 5.6 and 5.7 (x_{cm} and z_{cm} are kept constant at the values considered in the previous cases). Tracking errors and some other relevant plots are shown and it is observed that the same maneuver performance is achieved in both of the maneuvers.

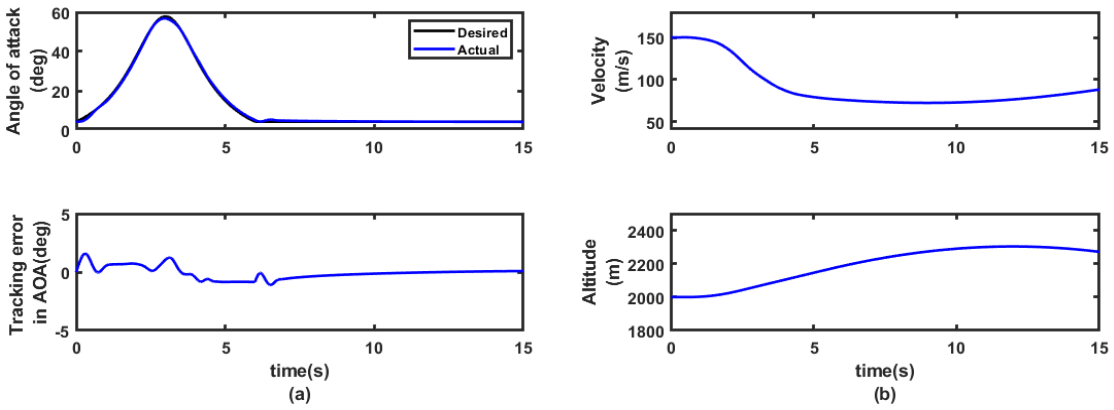

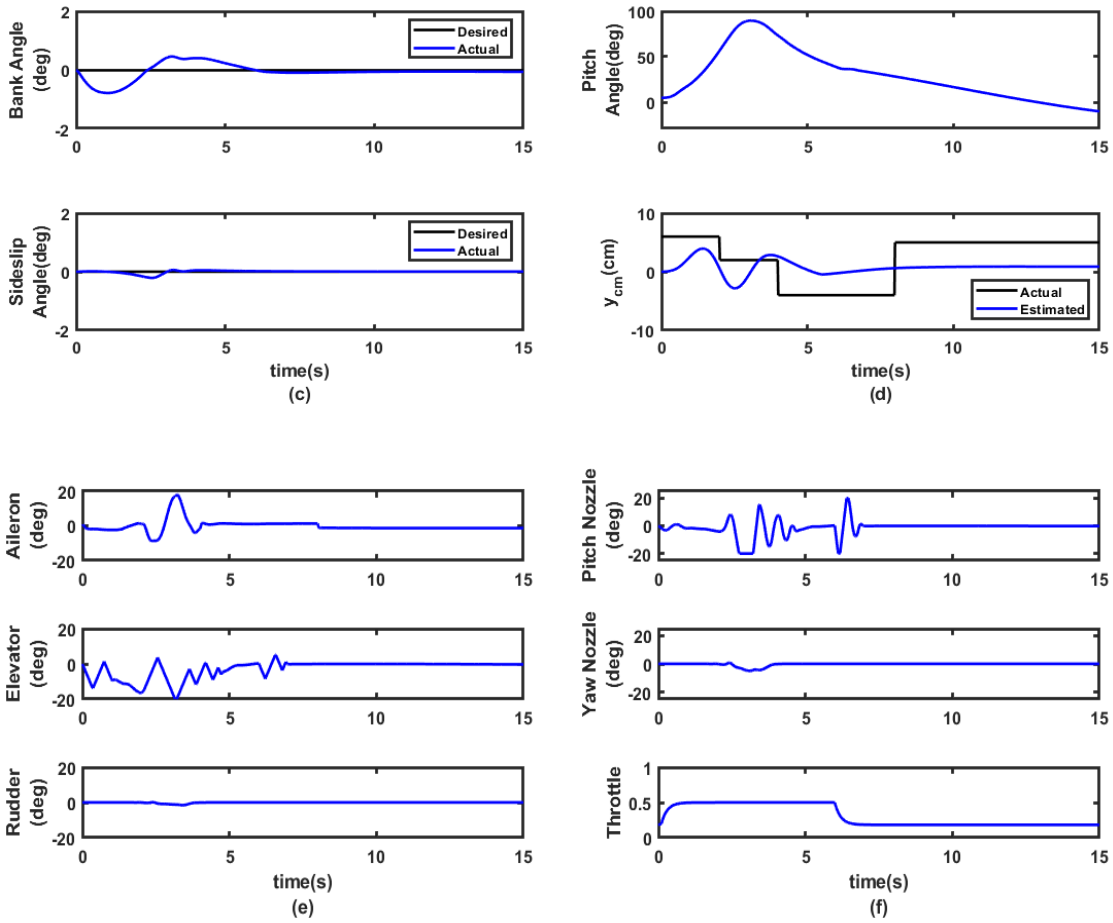

Figure 5.6. Time profile of states, arbitrary c.g. position and control deflections: Cobra maneuver

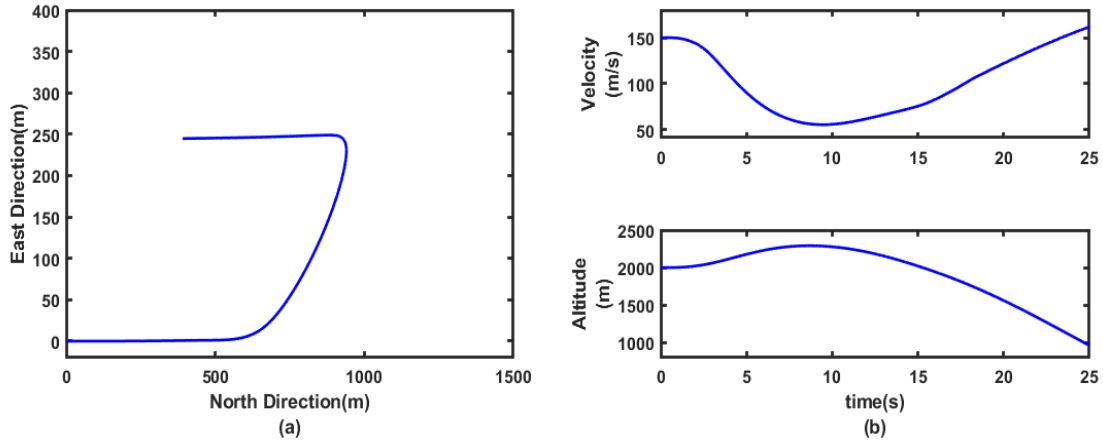

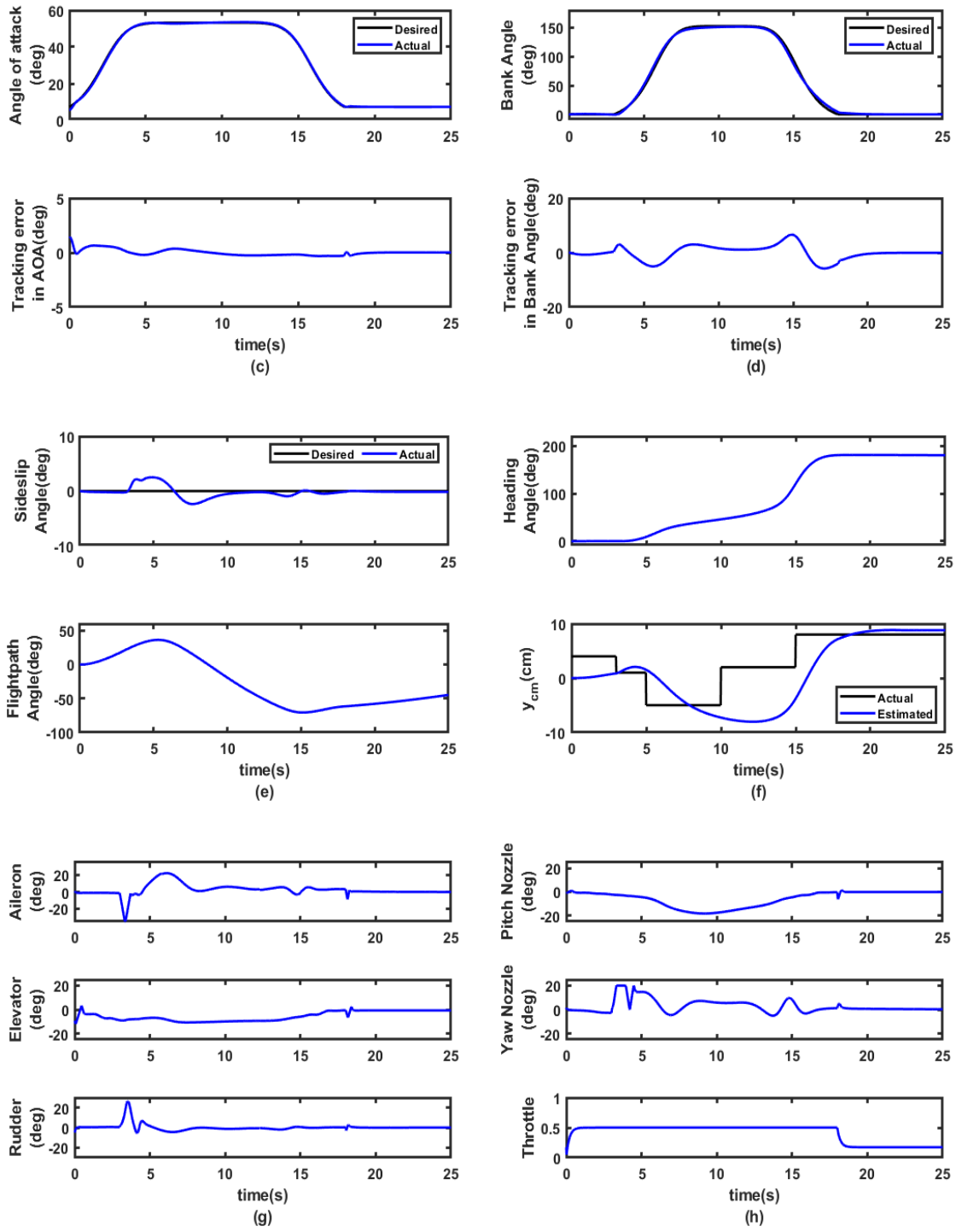

Figure 5.7. Ground track, time profile of states, arbitrary c.g. position and control deflections: Herbst maneuver

5.5 Comparison with the Control Proposed in Chapter 3

As discussed earlier in detail in Chapter 3, that a lateral c.g. offset issue can also be tackled by considering an ad-hoc dynamics where simply a moment due to gravity term is added to the symmetric 6-DOF dynamics. Therefore, tracking performance under the proposed controller is compared against the same under the ad-hoc model-based control and the proposed controller is found to give significantly improved control performance. The standard ITAE, IAE, ITSE and ISE performance index values are compared and tabulated in Table 5.3 and 5.4. These indices are calculated for each of the three errors components e_α, e_β and e_μ (i.e. tracking errors in angle of attack, sideslip angle and bank angle) separately and then added up; E.g., $ITAE = \int_0^\infty t\left(|e_\alpha| + |e_\beta| + |e_\mu|\right) dt$ (other indices are also calculated in a similar manner). Units of e_α, e_β and e_μ are considered to be $radian$ in computing the entries of Table 5.3. These three error profiles are also compared in Figures 5.4 and 5.5. Clearly, Table 5.3, Table 5.4 and Figures 5.6, 5.7 shows performance improvement substantiating the superiority and the significantly less conservative nature of the present control. It is needless to mention that, for comparison purpose, the same control parameters, as listed in Table 5.1 and Table 5.2, are used for both the ad-hoc model-based control and the proposed control.

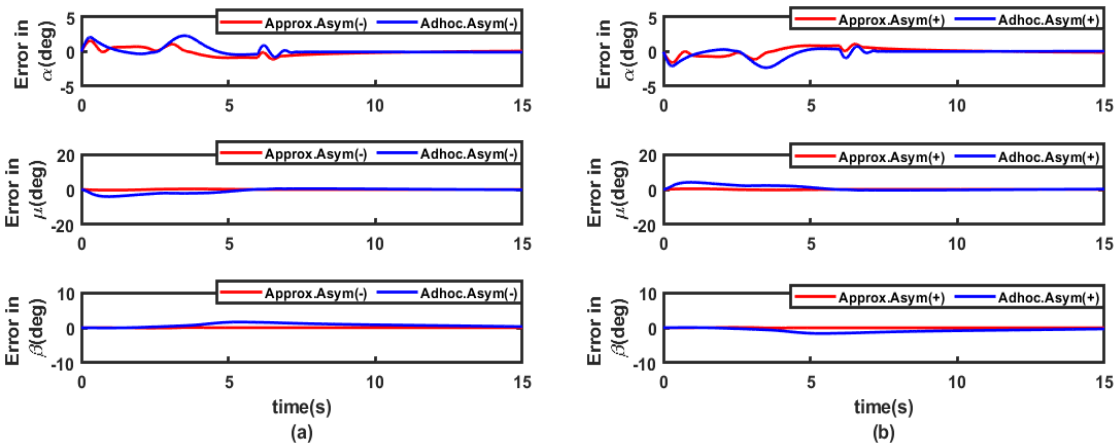

Figure 5.8. Tracking errors in Ad-hoc and Approximate (Proposed) model-based controls: cobra maneuver

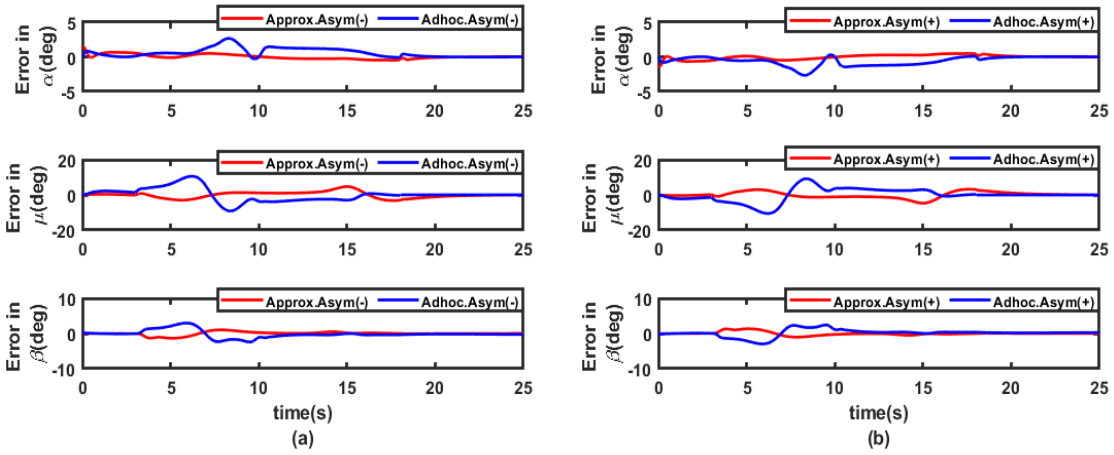

Figure 5.9. Tracking errors in Ad-hoc and Approximate (Proposed) model-based controls: Herbst maneuver

Table 5.3: Comparison of different performance indices: cobra maneuver

Model	Case	IAE	ITAE	ISE	ITSE
Ad-hoc [Chapter 3]	Asym(-)	0.2645	3.7819	0.0014	0.0218
	Asym(+)	0.2498	3.5785	0.0013	0.0201
Approximate (Proposed)	Asym(-)	0.0840	1.1842	0.0002	0.0032
	Asym(+)	0.0792	1.0024	0.0002	0.0020

Table 5.4: Comparison of different performance indices: Herbst maneuver

Model	Case	IAE	ITAE	ISE	ITSE
Ad-hoc [Chapter 3]	Asym(-)	0.8354	7.5125	0.0187	0.1754
	Asym(+)	0.7845	7.2748	0.0175	0.1712
Approximate (Proposed)	Asym(-)	0.5214	4.0684	0.0068	0.0514
	Asym(+)	0.5061	3.9214	0.0061	0.0491

5.6 Conclusion

The novel and challenging problem of designing robust nonlinear controls for executing high angle of attack autonomous maneuvers with a fighter aircraft undergoing significant lateral c.g. uncertainties was addressed. Ignoring the second order terms of the c.g. shift from the nominal position, the highly coupled 6-DOF dynamics under asymmetric c.g. position was successfully cast in strict feedback form affine in c.g. position. This made it possible to design a two-step adaptive backstepping control which could automatically adapt to the unknown c.g. variations. Backstepping control, in turn, allowed for retention of useful nonlinearities in the dynamics thereby resulting in a less conservative control. The effects of neglecting the second order terms of the c.g. position in the equations of motion were shown to give rise to two lumped additive disturbances (along with other exogenous disturbances) in the two individual steps in the backstepping setting. To circumvent these disturbances, an adaptive fast sliding mode control was combined with each step of the baseline adaptive backstepping control. The upper bounds of the disturbances/uncertainties were assumed to be unknown and suitable adaptation laws were designed to estimate the c.g. position and these two upper bounds. Conditions on various controller parameters were derived from Lyapunov's direct method ensuring asymptotic stability of the closed loop system. Performance of the proposed controller was validated against two demanding maneuvers cobra and Herbst considering the F18-HARV aircraft. Simulation results showed nearly identical maneuver performance under significant lateral c.g. variations on either side of the fuselage centreline as well as under considerable aerodynamic uncertainties. The work can be easily extended to various other useful maneuvers.

Chapter 6

Closing Comments

6.1 Conclusion

The impact of laterally asymmetric center of gravity (c.g.) movements in a fixed wing aircraft especially during demanding maneuvers was thoroughly investigated in the present thesis. While recent studies over the last decade or so examined asymmetric aircraft dynamics, they primarily focused on civil aircraft in trim flight states. Works on fighter aircraft executing specific maneuvers under such unfavorable conditions are very few. The present thesis was aimed at addressing this gap. Managing c.g. asymmetry in a fighter aircraft is crucial, as it enables deployment of non-identical pairs of stores, non-paired firing of stores, and eliminates the need for dummy stores thus avoiding a mass penalty. The automatic flight control system must be able to handle such scenarios, ensuring the aircraft can perform the necessary maneuvers to complete the mission successfully and prevent a potential aircraft loss and pilot ejection. In this regard, the present thesis offers some robust and adaptive nonlinear control solutions to successfully mitigate the significant system level uncertainty arising from predominantly lateral c.g. movements. Findings of the thesis are presented four main chapters namely Chapters 2-5.

First, the effects of lateral c.g. uncertainty on low angle of attack lateral maneuvers were investigated. Two standard lateral maneuvers such as horizontal turn maneuver and aileron roll maneuver were considered for benchmarking and the fixed wing Aerosonde UAV dataset was considered for carrying out the numerical validations. Findings of this work were reported in Chapters 2 and 4. Initially, a robust linear control technique such as Linear Quadratic Regulator (LQR) was implemented. However, results showed that, despite its robustness, the LQR failed to mitigate the effects of lateral c.g. variations and the maneuvers could not be properly performed. Since the asymmetric c.g movements led to coupling between the lateral/directional and longitudinal dynamics causing enhanced system nonlinearities, therefore, next a standard nonlinear control algorithm namely the backstepping control was tried. Like the LQR, even though the backstepping control could execute the intended maneuvers for the nominal system, it also failed to execute them when the same controller was used under lateral c.g. variations. To overcome the shortcoming of the nominal backstepping control scheme, it was then proposed that the backstepping control be designed based on an ad-hoc representation of the coupled asymmetric aircraft equations of motion. The idea of this ad-hoc model was to represent the asymmetric dynamics by simply adding a moment due to gravity term (the c.g. moving away from the nominal reference point gave rise to this additional moment) to the standard nominal equations of motion. It was shown that this ad-hoc model was in strict feedback form and therefore amenable to backstepping design. Further, it was shown that the model was also affine in c.g. position and, therefore, an adaptive backstepping design was proposed where the actual c.g. position was estimated through an adaptation law. It was further mathematically proved that the c.g. estimation was accurate as the estimation error asymptotically converged to zero. Numerical simulations demonstrated that the nominal maneuver performance could be nearly completely recovered under c.g. variations on either side of the fuselage centerline.

A further improvement on the findings of these investigations of Chapter 2 was attempted in Chapter 4. Instead of the ad-hoc model, a more accurate model was derived, in a novel way, from the

asymmetric equations of motion under the reasonable simplifying assumption that the second order terms involving the shifts in c.g. position were negligible. It was shown that the derived model could also be cast in strict feedback form with affine c.g. position. Also, some favorable nonlinearities (from the perspectives of stability) were identified in the derived model. Thereafter, an adaptive backstepping control was proposed adapting to the c.g. position using this model and retaining the favorable nonlinearities. Again, asymptotic convergence of the c.g. estimate obtained from an adaptation law was theoretically established using LaSalle's invariance principle. Due to the less conservative nature of this control scheme as compared to the ad-hoc model based adaptive backstepping scheme proposed in Chapter 2, significant improvement in maneuver performance and robustness to the c.g. uncertainty was observed through numerical simulations.

To comprehensively address the effects of lateral c.g. uncertainty on aircraft flight dynamics and control, the more demanding high angle of attack maneuvers were investigated next and the findings were presented in Chapters 3 and 5 of the thesis. Two benchmark high alpha maneuvers cobra and Herbst were considered and the dataset of the F18-HARV aircraft (available in the open domain) was used for validation purposes. Since, the objective was to ensure a quick return of the aircraft under such unfavorable flight conditions, performing the Herbst maneuver which is basically a turn in the vertical plane (as opposed to the horizontal turn maneuver, which is a turn in the horizontal plane as the name suggests) was particularly emphasized on. In the high alpha regime, nonlinearities in the dynamics are much more pronounced due to aerodynamics and trigonometric nonlinearities, kinematic coupling etc. Asymmetric c.g. variations lead to even higher degrees of coupling and nonlinearities. Therefore, nonlinear control implementations become indispensable in this regime. Apart from gross nonlinearities, the dynamics also suffers significant uncertainties in the aerodynamic model because of flow separation. This called for considerable robustness enhancements of the closed loop nonlinear controls.

In Chapter 3, again the two-step adaptive backstepping control based on the ad-hoc model of the asymmetric dynamics was considered. However, a fast sliding mode control was combined in the second step for the necessary robustness enhancement. The main challenge and novelty of this work arose in the mathematical proof of stability, using Lypunov's direct method, as the input matrix associated with the virtual control input in the first step of the backstepping design turned out to be state dependent. The proof was established using interval analysis and simulation results demonstrated that the proposed controller maintained nearly the same level of maneuver performance despite the c.g. and aerodynamic uncertainties. Furthermore, when compared with a standard adaptive sliding mode control scheme, the proposed hybrid control demonstrated significantly superior robustness.

In line with the works on low alpha maneuvers, further performance improvement was attempted in high alpha maneuvers also and the details were presented in Chapter 5. The asymmetric dynamics were analyzed by ignoring second order terms of the c.g. shift from the nominal position and successfully converted to the required strict feedback form affine in c.g. position. This formulation led to the final model having one lumped disturbance term in each of the two individual steps of the adaptive backstepping setting. Therefore, as in Chapter 3, when sliding mode control was combined, it had to be combined in each of the two steps. This was a novel setting which, to the best of our knowledge, was not reported in the literature. Moreover, these two sliding mode controls were made adaptive estimating the unknown upper bounds of the two lumped disturbances. As in Chapter 4, again the favorable system nonlinearities were identified and retained in the proposed adaptive backstepping adaptive fast sliding mode hybrid control law and stability was proved from Lyapunov's direct method. Simulation results validated the usefulness of the proposed hybrid control scheme as the maneuver performance and robustness improved considerablyfrom that obtained in Chapter 3.

Hardware in loop simulations were also performed in both the low and high alpha cases to establish the real time viability of all the proposed controls. These results were given in an appendix.

6.2 Scope for Further Research

The present thesis highlights several areas ripe for further exploration and enhancement. Some of them are suggested below.

- Other sources of c.g shift introduce an additional layer of asymmetry to the aircraft. This heightened level of imbalance significantly amplifies the complexity of controlling and maneuvering the aircraft, adding an extra dimension of challenge.
- Modifications to the sliding mode control algorithm to furthrr strengthen the system's robustness against lateral center of gravity variations may also be tried.
- Hybridization of other nonlinear control techniques with the baseline adaptive backstepping control may be tried for further improvement in maneuver performance level.
- The large numbers of control parameters may be optimally tuned using some recent evolutionary optimization algorithms.
- Some Model Reference Adaptive Control (MRAC) schemes and their hybrids with Neuro-control may also be explored.
- The proposed controls may be extended to several other useful maneuvers.

Appendix-A: Real Time Simulation Results

The proposed control scheme is validated on a real time simulator "OP4512" by Opal-RT. This simulator facilitates rapid control prototyping and real-time testing through a controller hardware-in-the-loop (CHIL) platform. For the sake of brevity one each case (c.g. shift in either port side or star board side) of intended maneuvers as considered in chapters 4 and 5 is also validated on this CHIL platform. Figure A1 illustrates the CHIL experimental setup, while Figures A2-A5 presents the plots of relevant states, parameter and control efforts. It is needless to emphasize that the plots in Figures A2-A5 are identical to those in chapters 4 and 5.

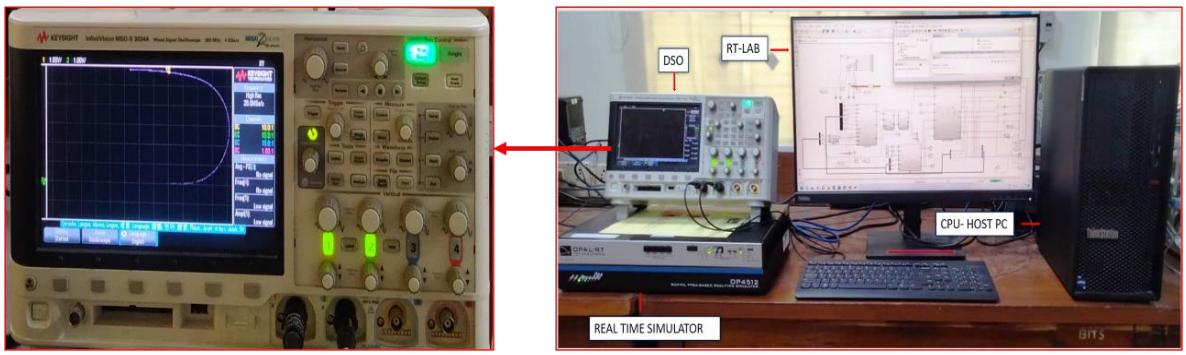

Figure A1. Complete work bench for real time CHIL Test

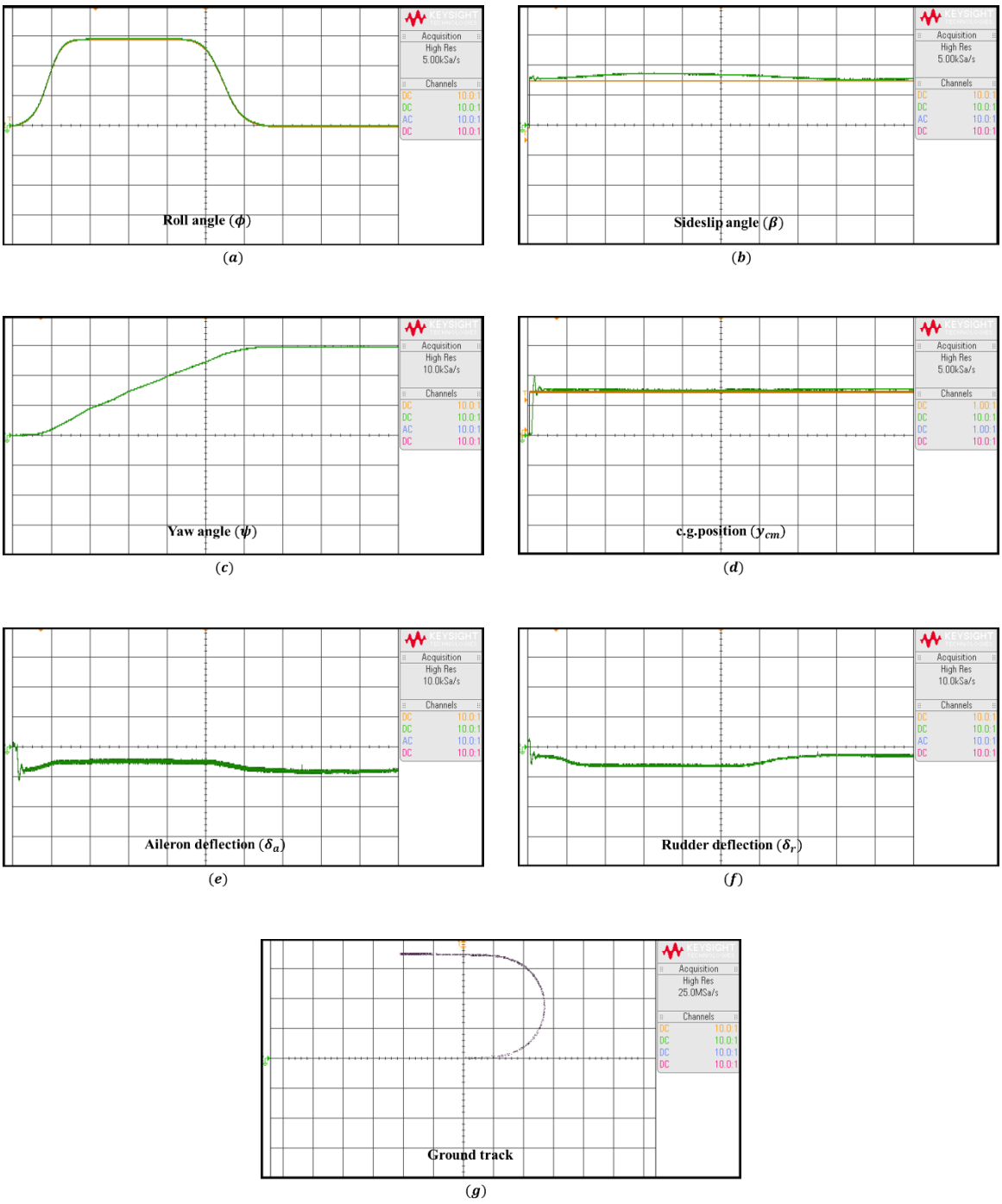

Figure A2. CHIL results for ground track, time profile of states, c.g. position and control deflections under positive c.g. shift: horizontal turn maneuver
(yellow line shows desired profile and green actual in plots (a), (b) and (d))

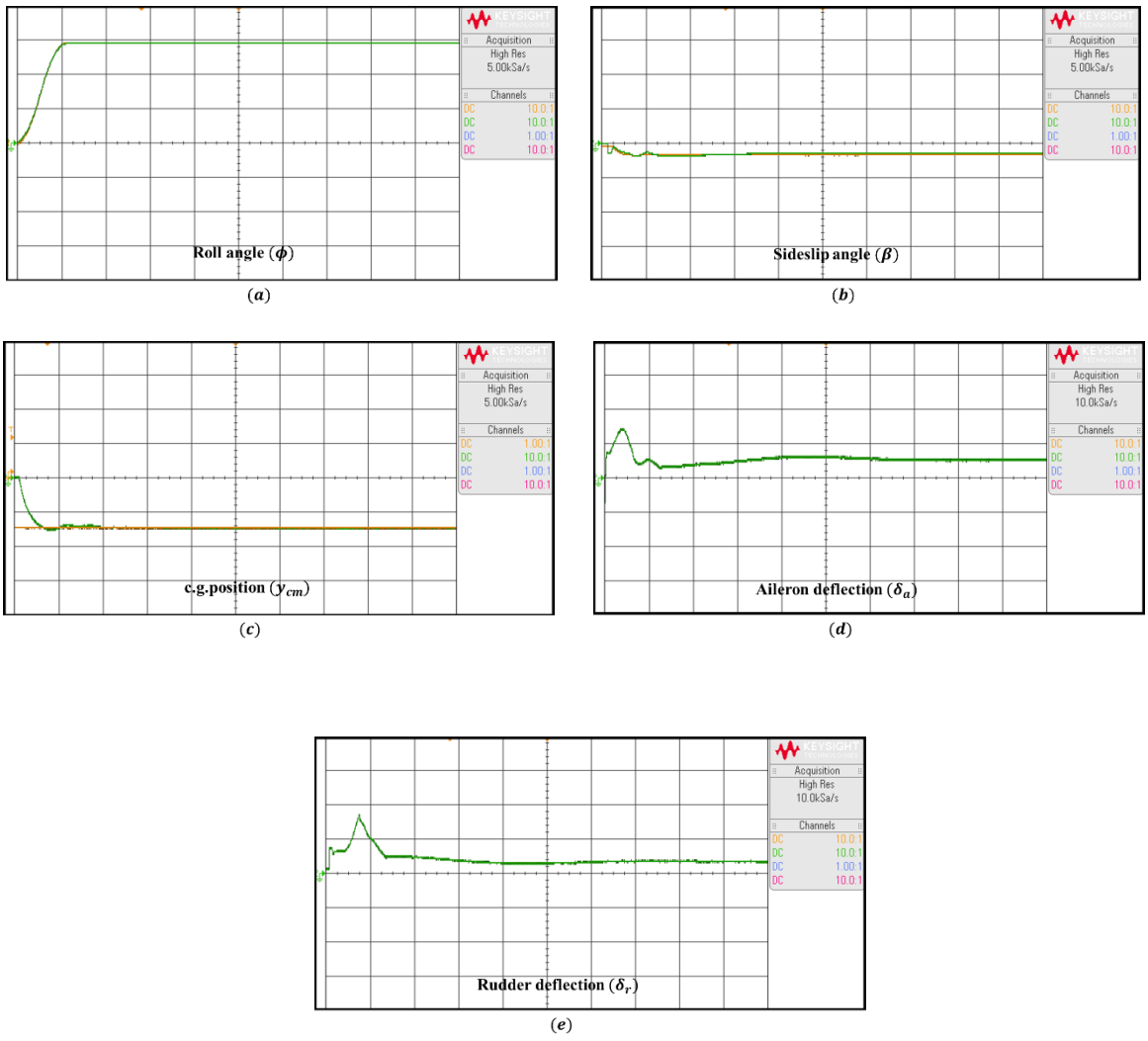

Figure A3. CHIL results for time profile of states, c.g. position and control deflections under negative c.g. shift: aileron roll maneuver
(yellow line shows desired profile and green actual in plots (a), (b) and (c))

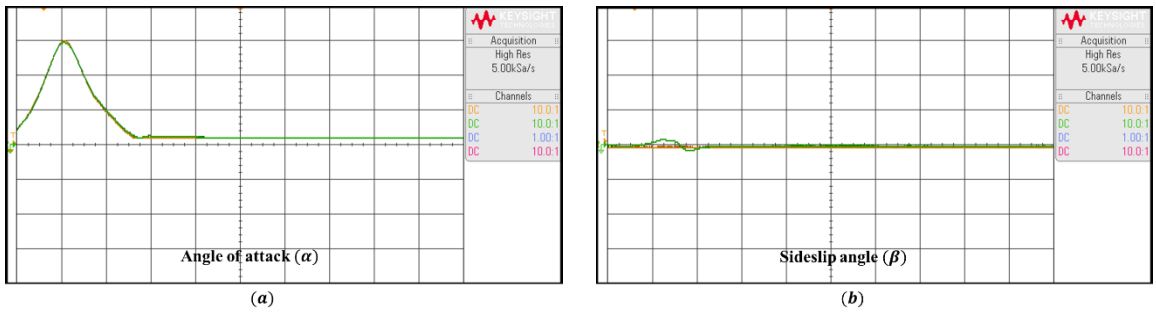

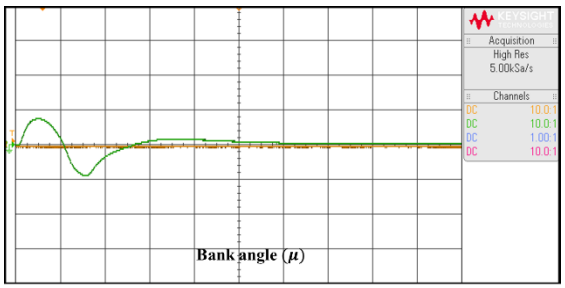
Bank angle (μ)

(c)

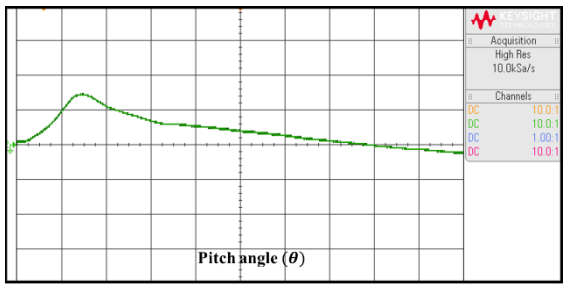
Pitch angle (θ)

(d)

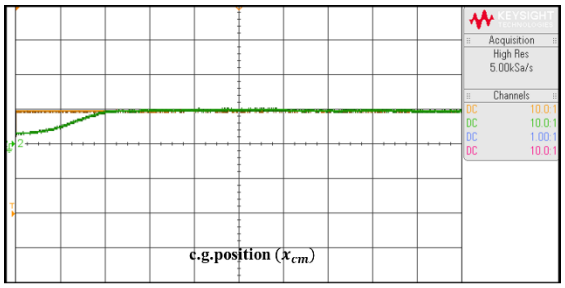
c.g.position (x_{cm})

(e)

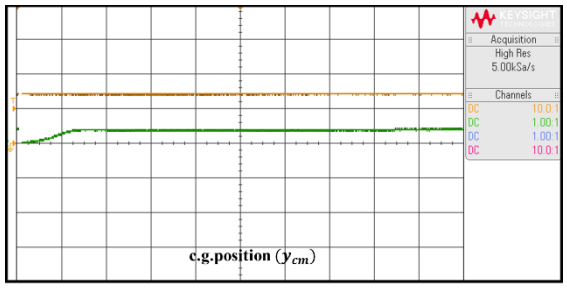
c.g.position (y_{cm})

(f)

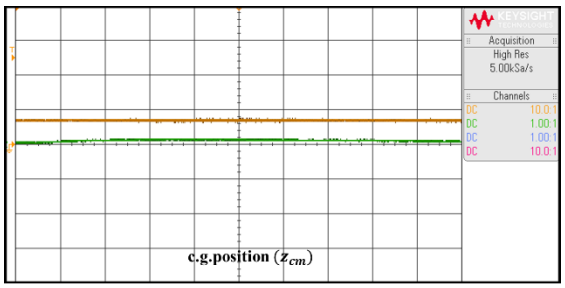
c.g.position (z_{cm})

(g)

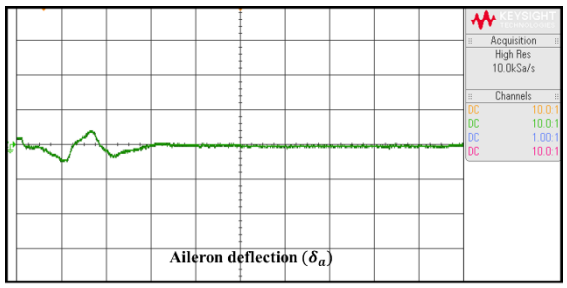
Aileron deflection (δ_a)

(h)

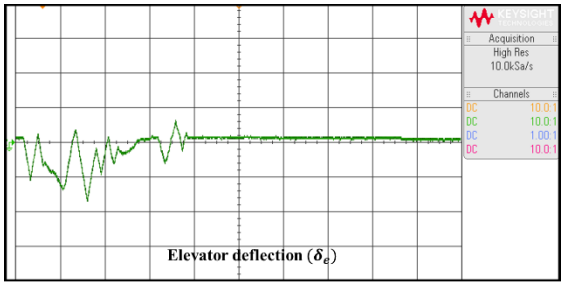
Elevator deflection (δ_e)

(i)

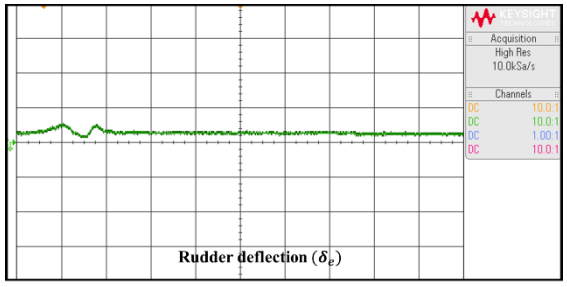
Rudder deflection (δ_e)

(j)

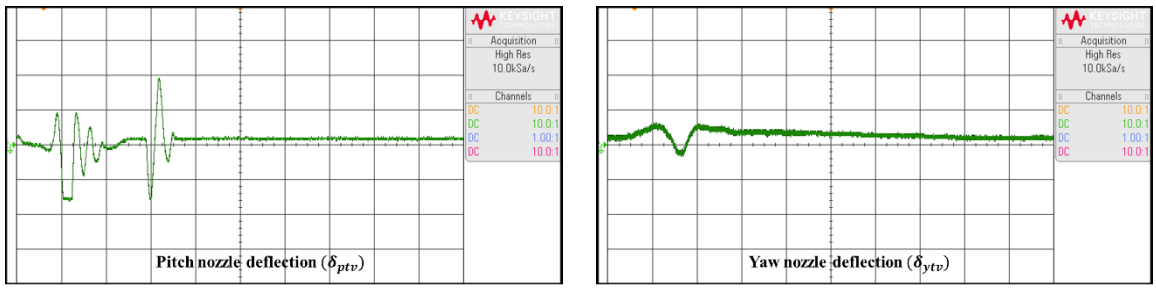

(k) (l)

Figure A4. CHIL results for time profile of states, c.g. position and control deflections under positive c.g. shift: cobra maneuver
(yellow line shows desired profile and green actual in plots (a), (b), (c), (e), (f), (g))

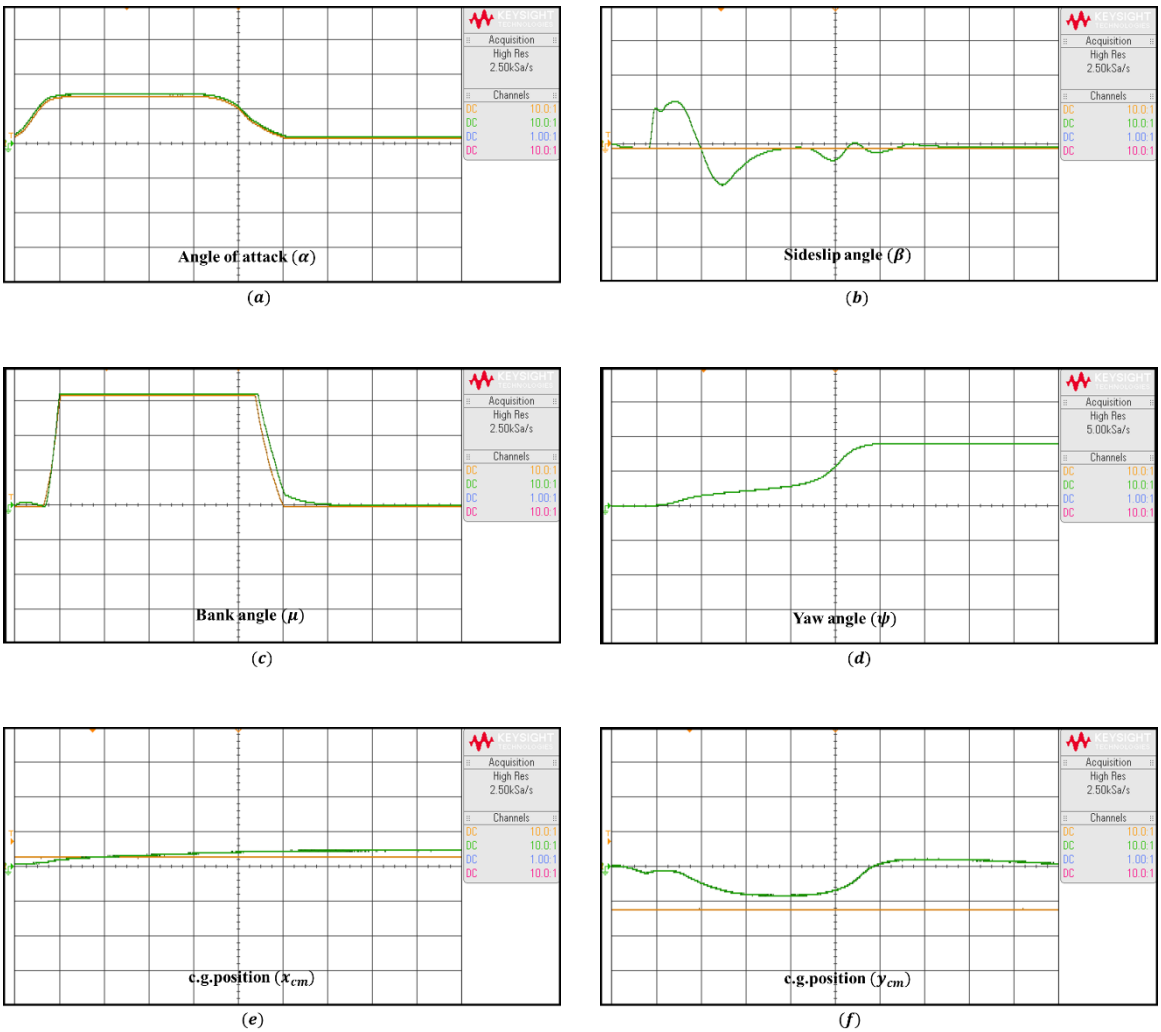

(a) (b) (c) (d) (e) (f)

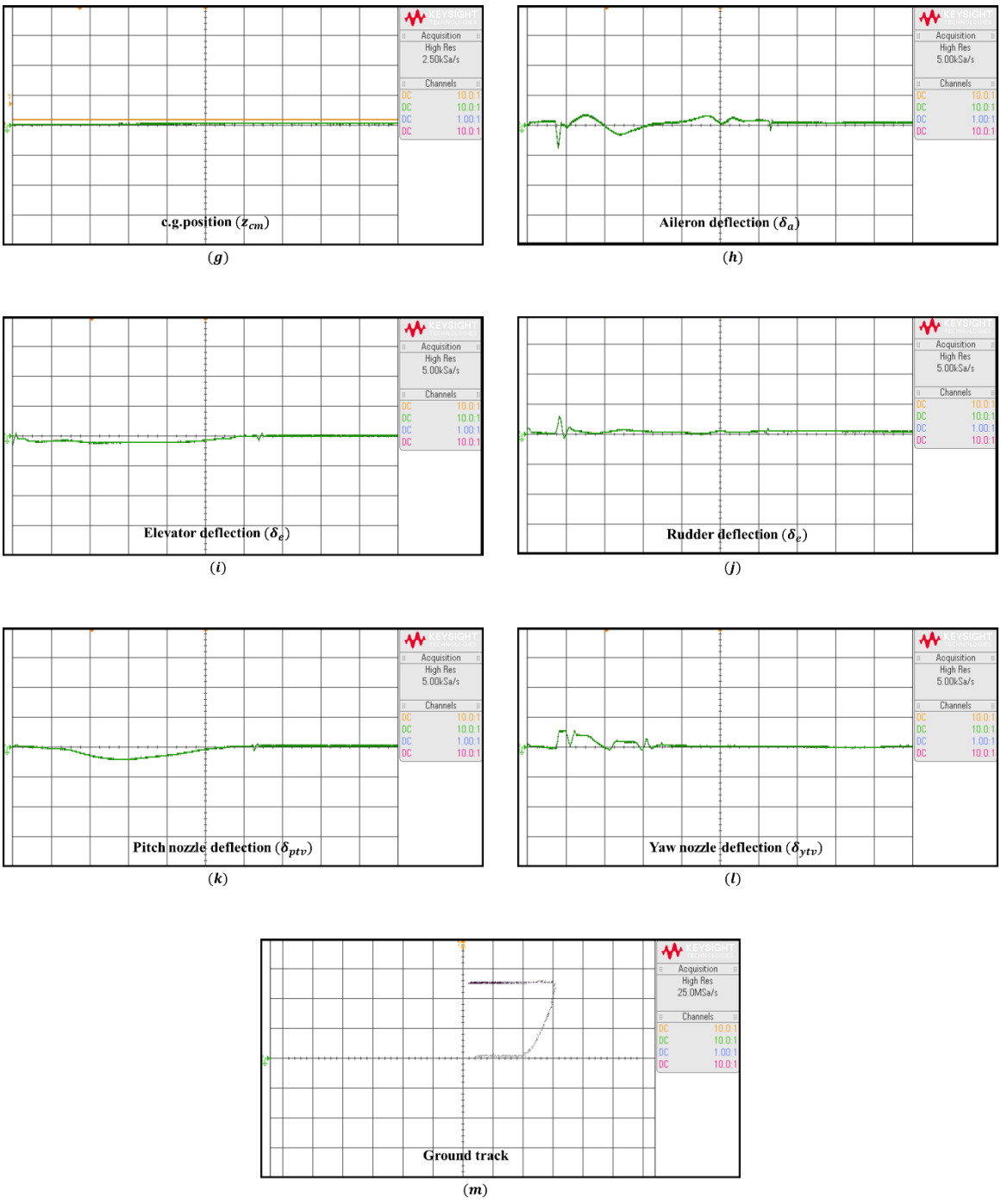

Figure A5. CHIL results for ground track, time profile of states, c.g. position and control deflections under negative c.g. shift: Herbst maneuver
(yellow line shows desired profile and green actual in plots (a), (b), (c), (e), (f), (g))

Appendix-B: A Review of Aircraft Dynamics

Aircraft Equations of Motion [83, 92]

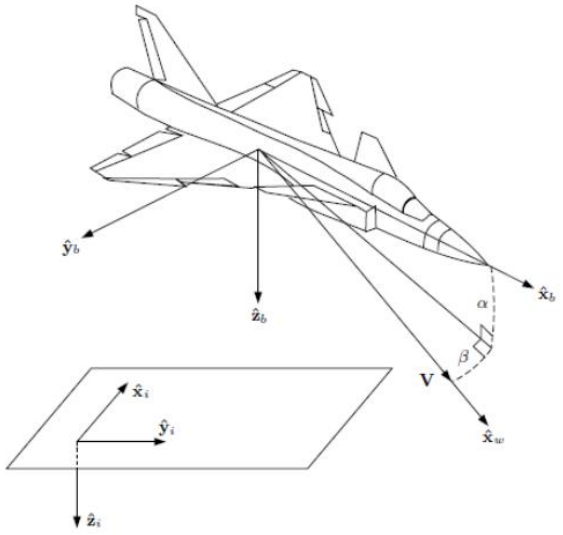

Figure B1. Illustration of the inertial, body, and wind axis systems

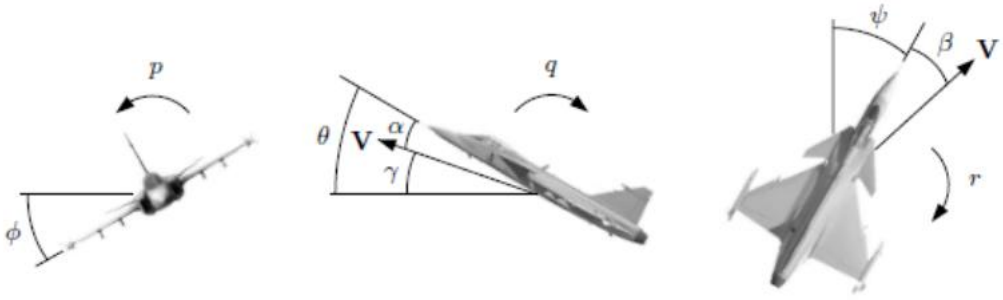

Figure B2. Illustration of the Euler angles and the aerodynamic angles

The standard six degree-of-freedom equations of motion of a rigid aircraft in body axes are as follows,

$$Translational\ Dynamics: \begin{bmatrix}\dot{u}\\ \dot{v}\\ \dot{w}\end{bmatrix} = \begin{bmatrix}-qw+rv\\ -ru+pw\\ -pv+qu\end{bmatrix} + \frac{1}{m}\begin{bmatrix}-mgsin\theta+\bar{q}SC_X+T_X\\ mgcos\theta sin\phi+\bar{q}SC_Y+T_Y\\ mgcos\theta cos\phi+\bar{q}SC_Z+T_Z\end{bmatrix}$$

$$Rotational\ Dynamics: \begin{bmatrix}I_{xx} & 0 & -I_{xz}\\ 0 & I_{yy} & 0\\ -I_{xz} & 0 & I_{zz}\end{bmatrix}\begin{bmatrix}\dot{p}\\ \dot{q}\\ \dot{r}\end{bmatrix} = \begin{bmatrix}(I_{yy}-I_{zz})qr+I_{xz}pq\\ (I_{zz}-I_{xx})rp+I_{xz}(r^2-p^2)\\ (I_{xx}-I_{yy})pq-Ixz_{qr}\end{bmatrix} + \begin{bmatrix}\bar{q}SbC_l+M_{TX}\\ \bar{q}S\bar{c}C_m+M_{TY}\\ \bar{q}SbC_n+M_{TZ}\end{bmatrix}$$

$$Translational\ Kinematics: \begin{bmatrix}\dot{X}\\ \dot{Y}\\ \dot{h}\end{bmatrix} = \begin{bmatrix}cos\psi cos\theta & -sin\psi cos\phi+cos\psi sin\theta sin\phi & sin\psi sin\phi+cos\psi sin\theta cos\phi\\ sin\psi cos\theta & cos\psi cos\phi+sin\psi sin\theta sin\phi & -cos\psi sin\phi+sin\psi sin\theta cos\phi\\ sin\theta & -cos\theta sin\phi & -cos\theta cos\phi\end{bmatrix}\begin{bmatrix}u\\ v\\ w\end{bmatrix}$$

$$Rotational\ Kinematics: \begin{bmatrix}\dot{\phi}\\ \dot{\theta}\\ \dot{\psi}\end{bmatrix} = \begin{bmatrix}1 & sin\phi tan\theta & cos\phi tan\theta\\ 0 & cos\phi & -sin\phi\\ 0 & sin\phi sec\theta & cos\phi sec\theta\end{bmatrix}\begin{bmatrix}p\\ q\\ r\end{bmatrix}$$

In the wind frame, the 6-DOF dynamics is described by the following equations,

$$Translational\ Dynamics: \begin{bmatrix}\dot{V}\\ \dot{\alpha}\\ \dot{\beta}\end{bmatrix} = \begin{bmatrix}-gsin\gamma+\frac{1}{m}F_X^w\\ q-pcos\alpha tan\beta-rsin\alpha tan\beta+\frac{g}{V}sec\beta cos\mu cos\gamma+\frac{1}{mV}sec\beta F_Z^w\\ psin\alpha-rcos\alpha+\frac{g}{V}sin\mu cos\gamma+\frac{1}{mV}F_Y^w\end{bmatrix}$$

$$Rotational\ Dynamics: \begin{bmatrix}I_{xx} & 0 & -I_{xz}\\ 0 & I_{yy} & 0\\ -I_{xz} & 0 & I_{zz}\end{bmatrix}\begin{bmatrix}\dot{p}\\ \dot{q}\\ \dot{r}\end{bmatrix} = \begin{bmatrix}(I_{yy}-I_{zz})qr+I_{xz}pq\\ (I_{zz}-I_{xx})rp+I_{xz}(r^2-p^2)\\ (I_{xx}-I_{yy})pq-Ixz_{qr}\end{bmatrix} + \begin{bmatrix}\bar{q}SbC_l+M_{TX}\\ \bar{q}S\bar{c}C_m+M_{TY}\\ \bar{q}SbC_n+M_{TZ}\end{bmatrix}$$

$$Translational\ Kinematics: \begin{bmatrix}\dot{X}\\ \dot{Y}\\ \dot{h}\end{bmatrix} = \begin{bmatrix}Vcos\gamma cos\chi\\ Vcos\gamma sin\chi\\ Vsin\gamma\end{bmatrix}$$

$$Rotational\ Kinematics:\ \begin{bmatrix}\dot{\mu}\\ \dot{\gamma}\\ \dot{\chi}\end{bmatrix}=\begin{bmatrix}pcos\alpha sec\beta+rsin\alpha sec\beta-\frac{g}{V}tan\beta cos\mu cos\gamma\\ -\frac{g}{V}cos\gamma\\ 0\end{bmatrix}$$

$$+\begin{bmatrix}\frac{1}{mV}tan\gamma cos\mu F_Y^w-\frac{1}{mV}(tan\beta+sin\mu tan\gamma)F_Z^w\\ -\frac{1}{mV}sin\mu F_Y^w-\frac{1}{mV}cos\mu F_Z^w\\ \frac{1}{mV}cos\mu sec\gamma F_Y^w-\frac{1}{mV}sin\mu sec\gamma F_Z^w\end{bmatrix}$$

The relation between wind and body axis force components are as follows,

$$\begin{bmatrix}F_X^w\\ F_Y^w\\ F_Z^w\end{bmatrix}=\begin{bmatrix}-\bar{q}SC_D\\ \bar{q}SC_Y\\ -\bar{q}SC_L\end{bmatrix}+\begin{bmatrix}cos\alpha cos\beta & sin\beta & sin\alpha cos\beta\\ -cos\alpha sin\beta & cos\beta & -sin\alpha sin\beta\\ -sin\alpha & 0 & cos\alpha\end{bmatrix}\begin{bmatrix}T_X\\ T_Y\\ T_Z\end{bmatrix}$$

The linear velocity components in body and wind frames are inter-related as

$$\begin{bmatrix}u\\ v\\ w\end{bmatrix}=\begin{bmatrix}Vcos\alpha cos\beta\\ Vsin\beta\\ Vsin\alpha cos\beta\end{bmatrix}$$

$$\begin{bmatrix}V\\ \alpha\\ \beta\end{bmatrix}=\begin{bmatrix}\sqrt{u^2+v^2+w^2}\\ \tan^{-1}\left(\frac{w}{u}\right)\\ \sin^{-1}\left(\frac{v}{\sqrt{u^2+v^2+w^2}}\right)\end{bmatrix}$$

Modern fighter aircraft are equipped with thrust vectoring capabilities in both pitch and yaw planes. If T is the total engine thrust then its components along the three body axes due to thrust vectoring are given by

$$\begin{bmatrix}T_X\\ T_Y\\ T_Z\end{bmatrix}=\begin{bmatrix}Tcos\delta_{ptv}cos\delta_{ytv}\\ Tsin\delta_{ytv}\\ -Tsin\delta_{ptv}cos\delta_{ytv}\end{bmatrix}$$

If the engine nozzle to the c.g. of the aircraft distance are l_x and l_z along x_b and z_b body axes respectively then the moment due to thrust along the body axes are given by

$$\begin{bmatrix}M_{TX}\\ M_{TY}\\ M_{TZ}\end{bmatrix}=\begin{bmatrix}l_zTsin\delta_{ytv}\\ -l_zTcos\delta_{ptv}cos\delta_{ytv}-l_xTsin\delta_{ptv}cos\delta_{ytv}\\ -l_xTsin\delta_{ytv}\end{bmatrix}$$

The aerodynamic force and moment coefficients are usually given as follows,

$$C_L = C_{L0} + C_{L\alpha}\alpha + C_{Lq}\frac{q\bar{c}}{2V} + C_{L\delta_e}\delta_e$$

$$C_D = C_{D0} + C_{D\alpha}\alpha + C_{Dq}\frac{q\bar{c}}{2V} + C_{D\delta_e}\delta_e$$

$$C_Y = C_{Y0} + C_{Y\beta}\beta + C_{Yp}\frac{bp}{2V} + C_{Yr}\frac{br}{2V} + C_{Y\delta_a}\delta_a + C_{Y\delta_r}\delta_r$$

$$C_l = C_{l0} + C_{l\beta}\beta + C_{lp}\frac{pb}{2V} + C_{lr}\frac{rb}{2V} + C_{l\delta_a}\delta_a + C_{l\delta_e}\delta_e + C_{lr}\delta_r$$

$$C_m = C_{m0} + C_{m\alpha}\alpha + C_{mq}\frac{q\bar{c}}{2V} + C_{m\delta_e}\delta_e$$

$$C_n = C_{n0} + C_{n\beta}\beta + C_{np}\frac{pb}{2V} + C_{nr}\frac{rb}{2V} + C_{n\delta_a}\delta_a + C_{n\delta_e}\delta_e + C_{nr}\delta_r$$

Appendix-C: Aircraft Dataset

C1. Aerosonde UAV Dataset

Figure C1. Aerosonde UAV

Parameter	*Value*	*Parameter*	*Value*
m	$13.5\ kg$	C_{Y_0}	0
I_{xx}	$0.8244\ kg-m^2$	C_{l_0}	0
I_{yy}	$1.135\ kg-m^2$	C_{n_0}	0
I_{zz}	$1.759\ kg-m^2$	C_{Y_β}	-0.98
I_{xz}	$0.1204\ kg-m^2$	C_{l_β}	-0.12
S	$0.55\ m^2$	C_{n_β}	0.25

Parameter	*Value*	*Parameter*	*Value*
b	$2.8956\ m$	C_{Y_p}	0
$\overline{c}$	$0.18994\ m$	C_{l_p}	-0.26
C_{L_0}	0.28	C_{n_p}	0.022
C_{D_0}	0.03	C_{Y_r}	0
C_{m_0}	-0.02338	C_{l_r}	0.14
C_{L_α}	3.45	C_{n_r}	-0.35
C_{D_α}	0.30	$C_{Y_{\delta_a}}$	0
C_{m_α}	-0.38	$C_{l_{\delta_a}}$	0.08
C_{L_q}	0	$C_{n_{\delta_a}}$	0.06
C_{D_q}	0	$C_{Y_{\delta_r}}$	-0.17
C_{m_q}	-3.6	$C_{l_{\delta_r}}$	0.105
$C_{L_{\delta_e}}$	-0.36	$C_{n_{\delta_r}}$	-0.032
$C_{D_{\delta_e}}$	0	δ_e limit	$\pm 30^0$
$C_{m_{\delta_e}}$	-0.5	δ_a limit	$\pm 20^0$
C_{D_p}	0.0437	δ_r limit	$\pm 30^0$

C2. F-18 HARV Dataset

Figure C2. F18 HARV Aircraft

Geometric Data:

Parameter	*Value*
m	$16375\ kg$
I_{xx}	$3.089\ \times 10^4\ kgm^2$
I_{yy}	$2.396\ \times 10^5\ kgm^2$
I_{zz}	$2.599\ \times 10^5\ kgm^2$
I_{xz}	$-3.124\ \times 10^3\ kgm^2$
S	$37.16\ m^2$
b	$11.40\ m$
$\bar{c}$	$3.51\ m$

Control Surface	*Position limit (deg)*	*Rate limit (deg/s)*	*Dynamics*	*Bandwidth*
δ_a	$(-35,35)$	± 100	1st order	10 Hz
δ_e	$(-25,10)$	± 40	1st order	10 Hz
δ_r	$(-30,30)$	± 82	1st order	10 Hz
δ_{ptv}	$(-20,20)$	± 80	1st order	10 Hz
δ_{ytv}	$(-20,20)$	± 80	1st order	10 Hz

Aerodynamic Data:

$C_{Y\delta_e} = 0, \qquad C_{l\delta_e} = 0$

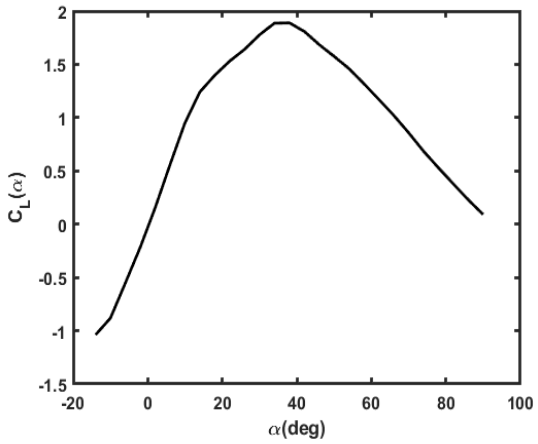

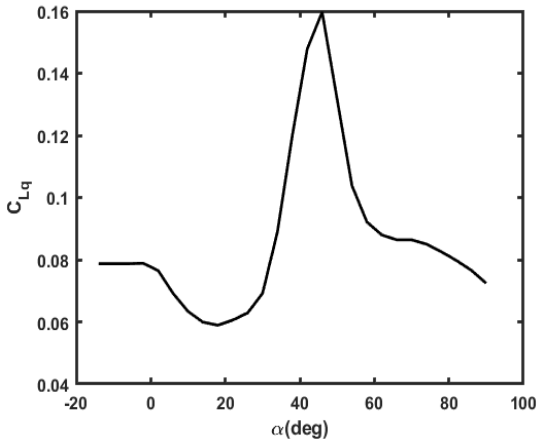

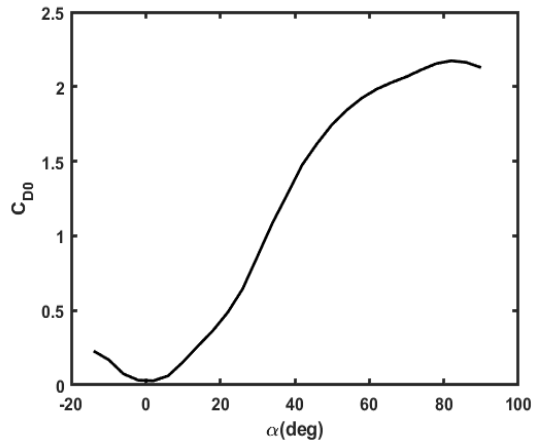
C_{D0}
α(deg)

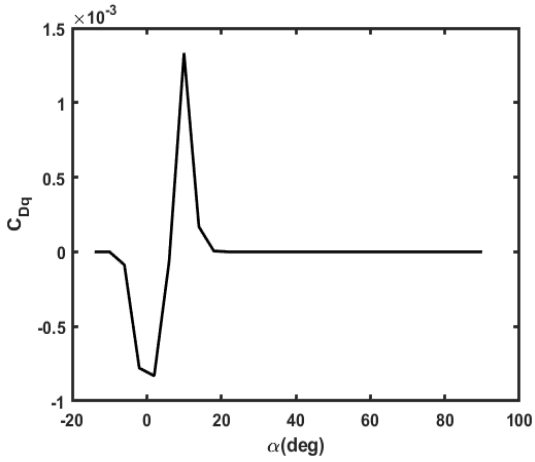
$\times 10^{-3}$
C_{Dq}
α(deg)

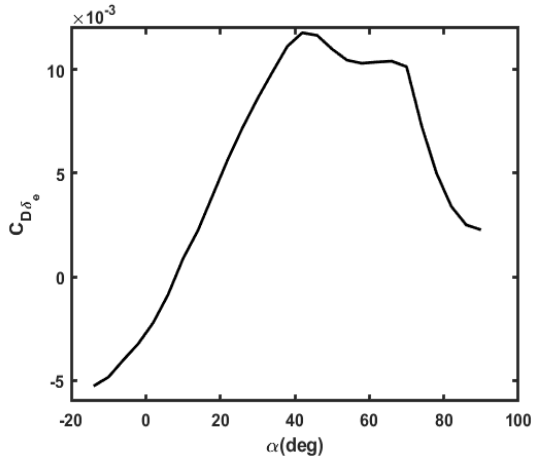
$\times 10^{-3}$
$C_{D\delta_e}$
α(deg)

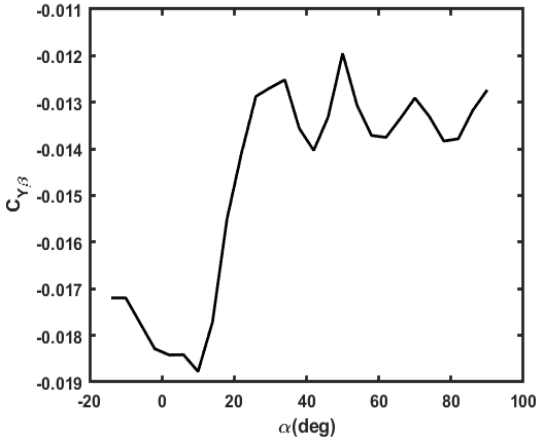
$C_{Y,\beta}$
α(deg)

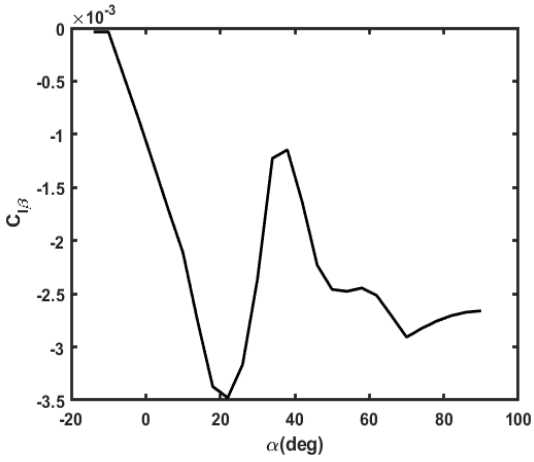
$\times 10^{-3}$
$C_{l,\beta}$
α(deg)

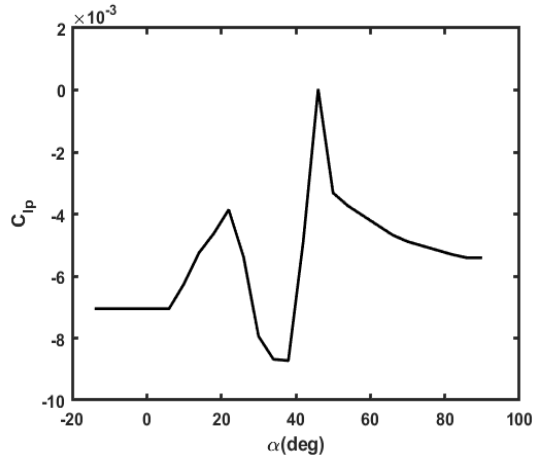
$\times 10^{-3}$
C_{lp}
α(deg)

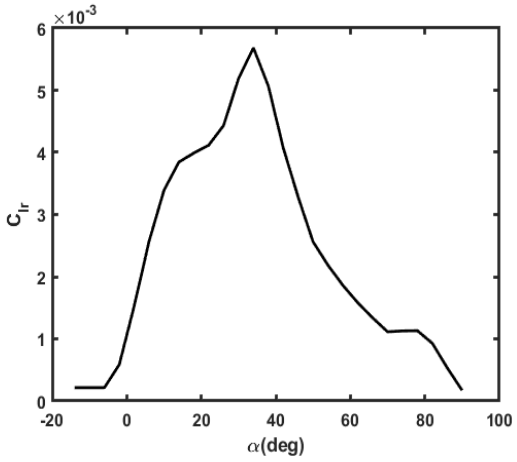
×10^-3
C_lr
α(deg)

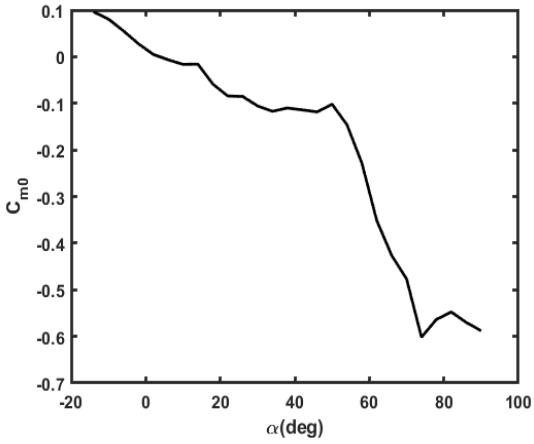
C_m0
α(deg)

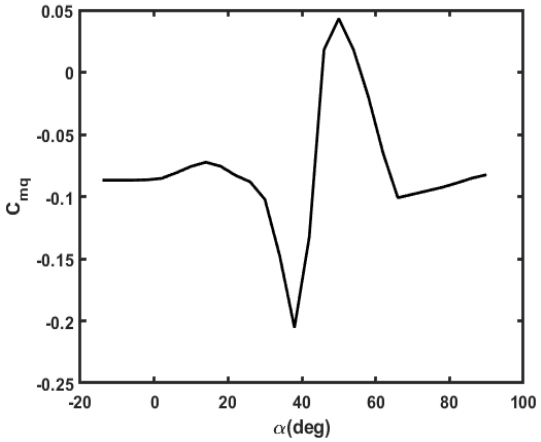
C_mq
α(deg)

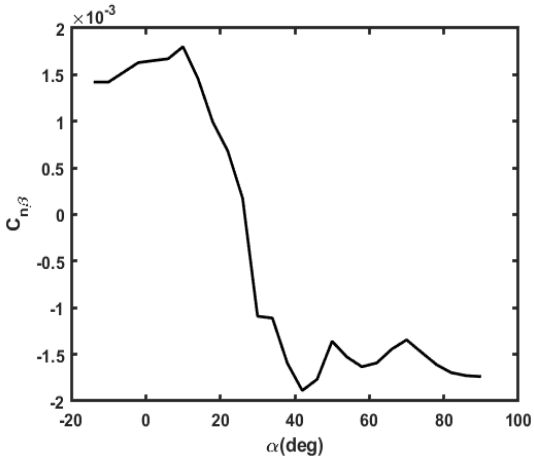
×10^-3
C_nβ
α(deg)

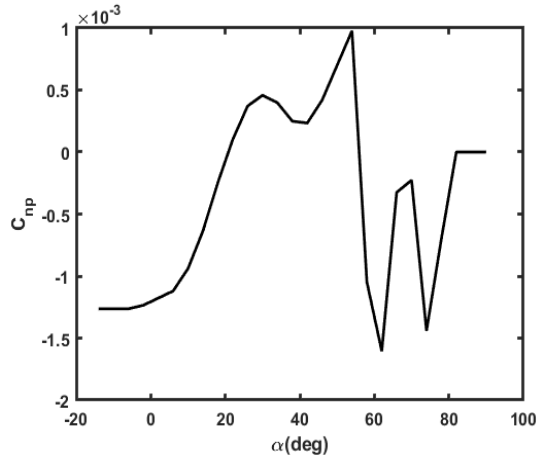
×10^-3
C_np
α(deg)

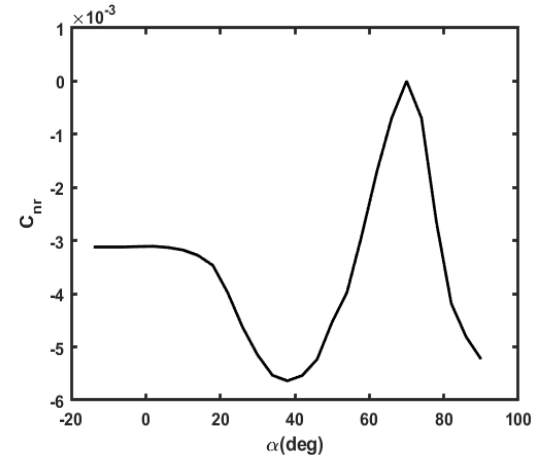
×10^-3
C_nr
α(deg)

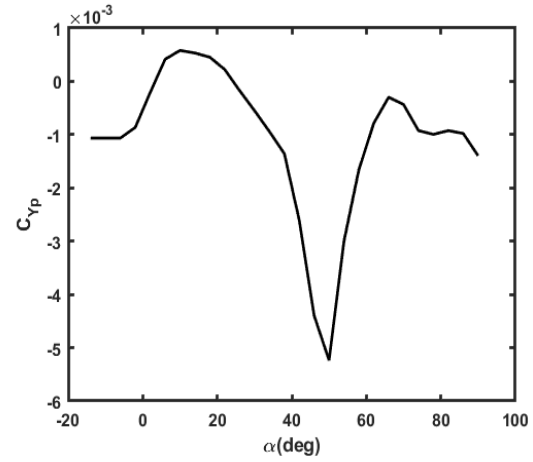
×10^-3
C_Yp
α(deg)

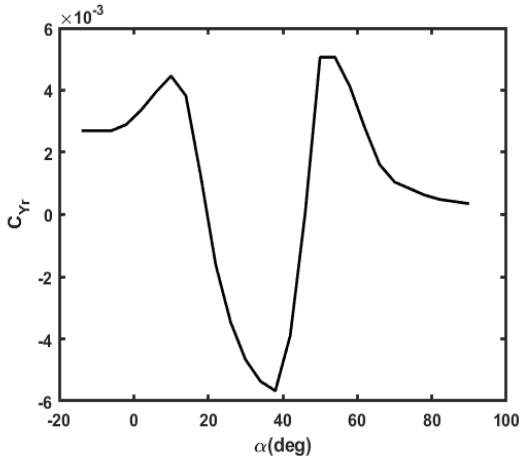
×10^-3
C_Yr
α(deg)

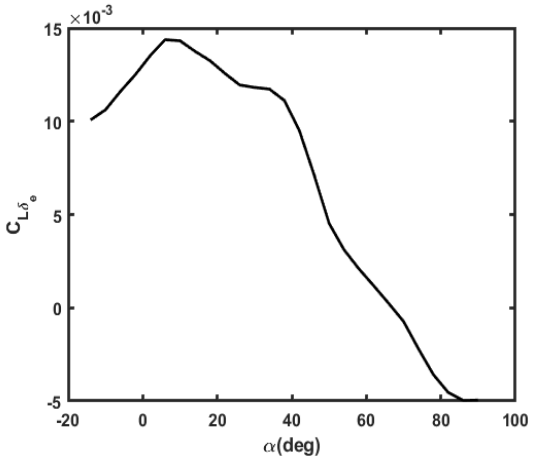
×10^-3
C_Lδe
α(deg)

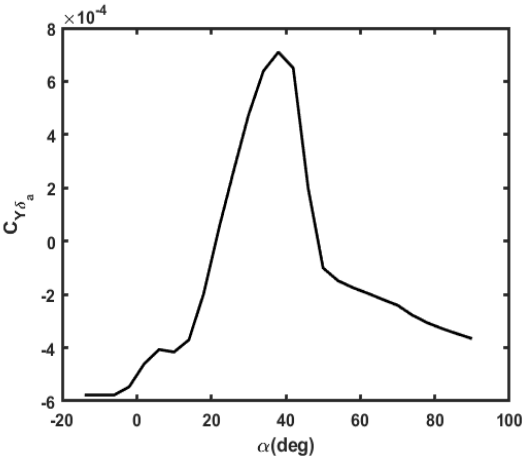
×10^-4
C_Yδa
α(deg)

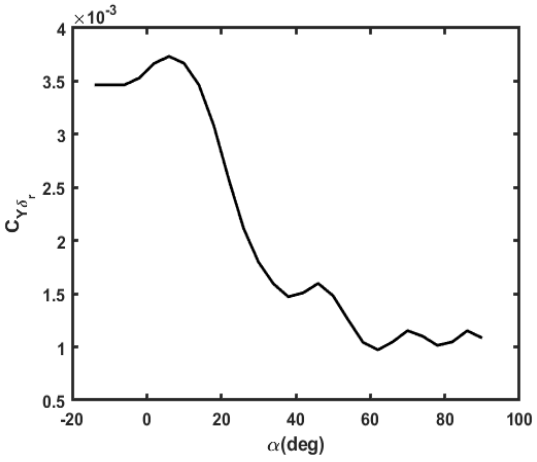
×10^-3
C_Yδr
α(deg)

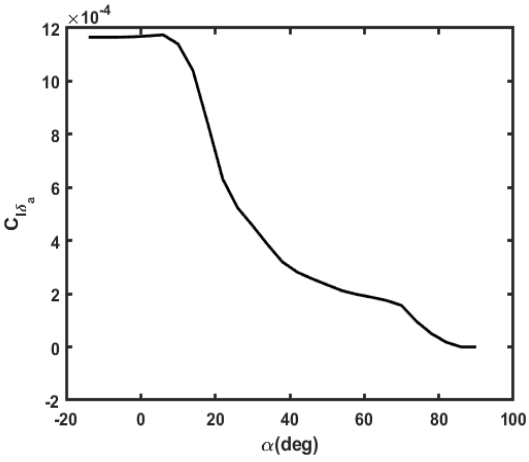
×10^-4
C_lδa
α(deg)

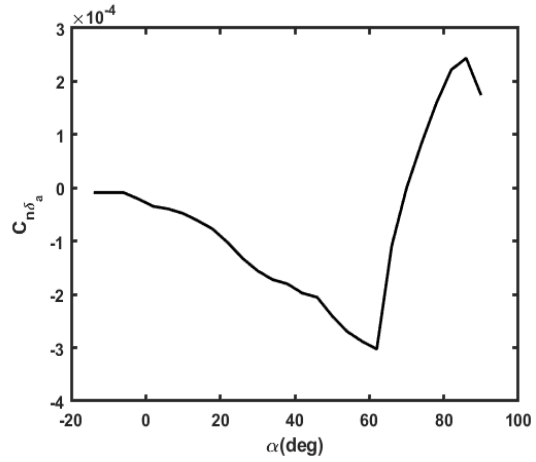
×10^-4
3
2
1
0
-1
-2
-3
-4
-20
0
20
40
60
80
100
α(deg)
C_nδa

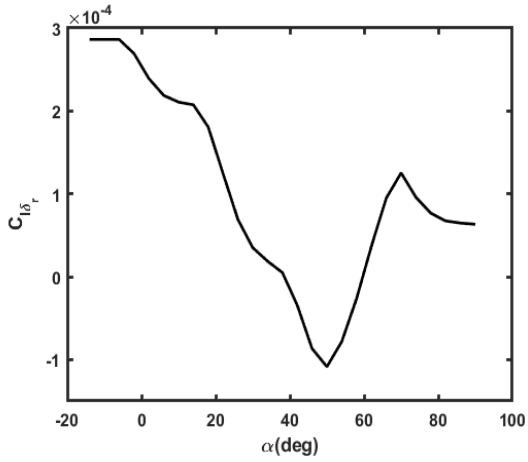
×10^-4
3
2
1
0
-1
-20
0
20
40
60
80
100
α(deg)
C_lδr

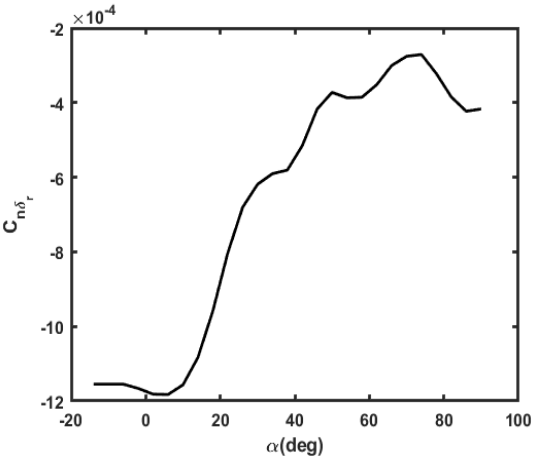
×10^-4
-2
-4
-6
-8
-10
-12
-20
0
20
40
60
80
100
α(deg)
C_nδr

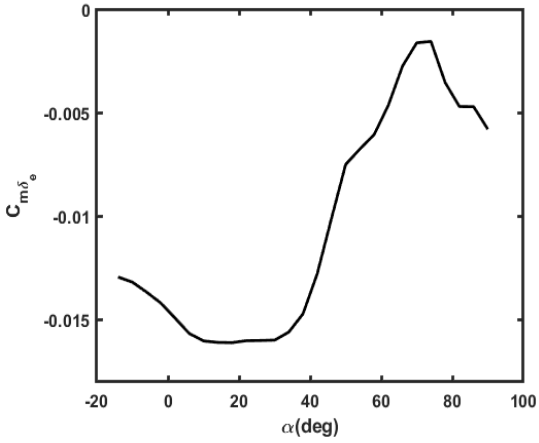
0
-0.005
-0.01
-0.015
-20
0
20
40
60
80
100
α(deg)
C_mδe

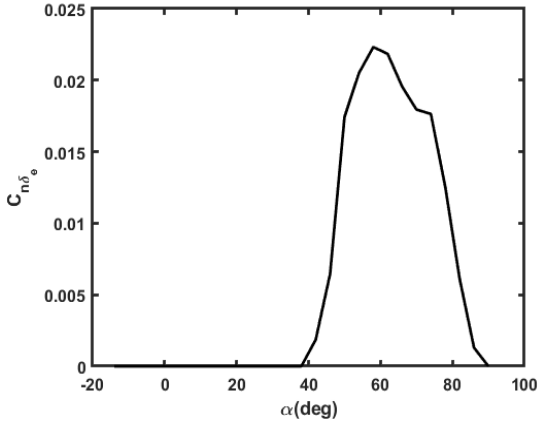
0.025
0.02
0.015
0.01
0.005
0
-20
0
20
40
60
80
100
α(deg)
C_nδe

Bibliography

[1] McRuer, D., Ashkenas, I, and Graham, D., Aircraft Dynamics and Automatic Control, Princeton University Press, New Jersey, 1973.

[2] Ananthasayanam, M. R., Ibrahim, K., and Muralidharan, M,R., Historical Evolution of the Military Fighter Airplanes Around the Twentieth Century, 43rd AIAA Aerospace Sciences Meeting and Exhibit, Reno, Nevada, 2005.

[3] Tsach, S., Tatievsky, A., Kleiman, D., and London, L., Military Airplanes, Encyclopedia of Aerospace Engineering, John Wiley & Sons, 2010.

[4] Green, W., and Swanborough, G., The Complete Book of Fighters: An Illustrated Encyclopedia of Every Fighter Aircraft Built and Flown, Salamander Books Ltd, 2001.

[5] Kopuletý, M., Palasiewicz, T., Advanced Military Robots Supporting Engineer Reconnaissance in Military Operations, Modelling and Simulation for Autonomous Systems, MESAS 2017. Lecture Notes in Computer Science, vol 10756. Springer, Cham., 2018

[6] Alcorn, C. W., Croom, M. A., Francis, M. S., and Ross, H., The X-31 Aircraft: Advances in Aircraft Agility and Performance, Progress in Aerospace Sciences, Vol. 32, 1996, pp. 377 413.

[7] Choudhary, S.K., Optimal feedback control of twin rotor mimo system with a prescribed degree of stability. International Journal of Intelligent Unmanned Systems, Vol.4, No.4, 2016, pp. 226–238.

[8] Choudhary, S.K., Optimal feedback control of a twin rotor mimo system. International Journal of Modelling and Simulation, Vol.37, No.1, 2017, pp. 46–53.

[9] Ashraf, A., Mei, W., Gaoyuan, L., Kamal, M.M., and Mutahir, A., Linear Feedback and LQR Controller Design for Aircraft Pitch Control, 2018 IEEE 4th International Conference on Control Science and Systems Engineering (ICCSSE), Wuhan, China, 2018, pp. 276-278

[10] Chrif, L., and Kadda, Z.M., Aircraft Control System Using LQG and LQR Controller with Optimal Estimation-Kalman Filter Design, Procedia Engineering, Vol. 80, 2014, pp 245-257.

[11] Gadewadikar J, and Lewis F.L., Aircraft flight controller tracking design using H-Infinity static output-feedback, Transactions of the Institute of Measurement and Control, Vol.28, No.5, 2006, pp. 429-440.

[12] Stengel, R.F., Flight dynamics. Princeton University Press, 2015.

[13] Wang, J., and Sundararajan, N., Extended nonlinear flight controller design for aircraft, Automatica, Vol.32, No.8, 1996, pp.1187–1193.

[14] Wigdorowitz, B., Application of linearization analysis to aircraft dynamics, Journal of Guidance, Control, and dynamics, Vol.15, No.3, 1992, pp. 746–750.

[15] Rugh, W.J., Analytical framework for gain scheduling, Control Systems, Vol.11, No.1, 1991, pp. 79-84.

[16] Rugh, W.J., and Je, S.S., Research on gain scheduling, Automatica, Vol.36, No.10, 2000, pp. 1401-1425.

[17] Halyo, N., Moerder, D.D., Broussard, J.R., and Taylor, D.B., A variable gain output feedback control design methodology, Technical Report NAS1-17493, NASA, 1989.

[18] Ostro, A.J., High-alpha application of variable gain output feedback control, Journal of Guidance, Control, and Dynamics, Vol.15, No.2, 1992, pp. 491-511.

[19] Enns, D., Bugajski, D., and Hendrick, R., Dynamic inversion: An evolving methodology for flight control design, International Journal of Control, Vol.59 No.1, 1994, pp.71-91.

[20] Lane, S.H., and Stengel, R.F., Flight control design using nonlinear inverse dynamics, Automatica, Vol.24, No.4, 1988, pp.471-483.

[21] Reiner, J., Balas, G.J., and Garrard, W.L., Robust dynamic inversion for control of highly maneuverable aircraft, Journal of Guidance, Control, and Dynamics, Vol.18, No.1, 1995, pp.18-24.

[22] Reiner, J., Balas, G.J., and Garrard, W.L., Flight control design using robust dynamic inversion and time-scale separation. Automatica, Vol.32, No.11, 1996, pp.1493-1504.

[23] Snell, S.A., Enns, D.F., and Garrard, W.L., Nonlinear inversion flight control for a supermaneuverable aircraft. Journal of Guidance, Control, and Dynamics, Vol.15, No.4, 1992, pp.976-984.

[24] Snell, S.A., and Stout, P.W., Flight control law using nonlinear dynamic inversion combined with quantitative feedback theory. Journal of Dynamic Systems, Measurement, and Control, Vol.120, No.2, 1998, pp. 208-215.

[25] Shin, Y., and Calise, A. J., Adaptive Control of Advanced Fighter Aircraft in Nonlinear Flight Regimes, Journal of Guidance, Control, and Dynamics, Vol. 31, No.5, 2008, pp. 1464–1477.

[26] Markerink, J. A., Design of a Robust Scheduled Controller Using m Synthesis Robust Flight Control: A Design Challenge, Lecture Notes in Control and Information Sciences, Vol. 224, Springer-Verlag, Berlin, 1997, pp. 503-522.

[27] Papageorgiou, G., Glover, K., and Hyde, R. A., The H∞ Loop Shaping Approach, Robust Flight Control: A Design Challenge, Lecture Notes in Control and Information Sciences, Vol. 224, Springer-Verlag, Berlin, 1997, pp. 464-483

[28] Adams, R. J., and Banda, S. S., Robust Flight Control Design Using Dynamic Inversion and Structured Singular Value Synthesis, IEEE Transactions on Control Systems Technology, Vol. 1, No.2, 1993, pp. 80-92.

[29] Wang, Q., and Stengel, R. F., Robust Nonlinear Flight Control of a High-Performance Aircraft, IEEE Transactions on Control Systems Technology, Vol. 13, No.1, 2005, pp. 15-26.

[30] Yee, J. S., Wang, J. L., and Sundararajan, N., Robust Sampled Data Hα Flight Controller Design for High a Stability-axis Roll Maneuver, Control Engineering Practice, Vol. 8, No.7, 2000, pp. 735-747.

[31] Kokotovic, P.V., The joy of feedback: Nonlinear and adaptive. IEEE Control Systems Magazine, Vol.12, No.3, 1992, pp.7-17.

[32] Freeman, R.A., and Kokotovic, P.V., Robust Nonlinear Control Design: State-Space and Lyapunov Techniques, Springer Science & Business Media, 2008.

[33] Tran, T.T., Choi, K.H., Chang, D.E., and Kim, D.S., Web tension and velocity control of two span roll-to-roll system for printed electronics, Journal of Advanced Mechanical Design, Systems, and Manufacturing, Vol.5, No.4, 2011, pp.329-346.

[34] Tran, T.T., Choi, K.H., Chang, D.E., and Kim, D.S., Backstepping controller-based web tension control for roll-to-roll web printed electronics system. Journal of Advanced Mechanical Design, Systems, and Manufacturing, Vol.5, No.1, 2011, pp.7-21.

[35] Tran, T.T., and Choi, K.H., A backstepping based control algorithm for multi span roll-to-roll web system. The International Journal of Advanced Manufacturing Technology, Vol.70, No.1-4, 2014, pp.45-61.

[36] Krstic, M., Kanellakopoulos, I., and Kokotovic, P.V., Nonlinear and Adaptive Control Design. Wiley, 1995.

[37] Farrell, J., Sharma, M., and Polycarpou, M., Backstepping-based flight control with adaptive

function approximation. Journal of Guidance, Control, and Dynamics, Vol.28, No.6, 2005, pp.1089-1102.

[38] Harkegard, O., Backstepping and Control Allocation with Applications to Flight Control. Linkping studies in science and technology. thesis no 820, Department of Electrical Engineering, Linkping University, Linkping, Sweden, 2003.

[39] Harkegard, O., and Glad, S.T., A backstepping design for flight path angle control. In Proceedings of the 39th IEEE Conference on Decision and Control, Sydney, NSW, 2000.

[40] Ju, H.S., and Tsai, C.C., Longitudinal axis flight control law design by adaptive backstepping, IEEE Transactions on Aerospace and Electronic Systems, Vol.43, No.1, 2007, pp.311-329.

[41] Lee, T., and Kim, Y., Nonlinear adaptive flight control using backstepping and neural networks controller, Journal of Guidance, Control, and Dynamics, Vol.24, No.4, 2001, pp.675-682.

[42] Sharma, M., and Ward, D.G., Flight-path angle control via neuro-adaptive back-stepping. In Proceedings of the AIAA Guidance, Navigation, and Control Conference, AIAA-2002-4451, Monterey, California, 2002.

[43] Narendra, K.S., and Annaswamy, A.M., Stable Adaptive Systems. Prentice Hall, Englewoods Cliffs, NJ, 1st edition, 1989.

[44] Sastry, S.S., and Bodson, M., Adaptive Control: Stability, Convergence, and Robustness. Prentice Hall, Englewood Cliffs, NJ, 1st edition, 1989.

[45] Astrom, K.J., and Wittenmark, B., Adaptive Control. Addison-Wesley, Reading, MA, 2nd edition, 1994.

[46] Ioannou, P.A., and Sun, J., Robust Adaptive Control. Prentice Hall, Upper Saddle River, NJ, 1st edition, 1996.

[47] Dydek, Z.T., Annaswamy, A.M., and Lavretsky, E., Adaptive control and the NASA X-15-3 flight revisited, IEEE Transactions on Control Systems, Vol.30, No.3, 2010, pp.32 –48.

[48] Lavertsky, E., and Wise, K, Adaptive flight control of manned/unmanned military aircraft. In Proc. American Control Conference, 2005.

[49] Patel, V.V., Cao, C., Hovakimyan, N., Wise, K.A., and Lavretsky, E., L1 adaptive controller for tailless unstable aircraft in the presence of unknown actuator failures, International Journal of

Control, Vol.82, No.4, 2009, pp.705–720.

[50] Gavilan, F., Acosta, J.A., Vazquez, R., and de Ingenieros, E.T.S., Control of the longitudinal flight dynamics of an uav using adaptive backstepping, Proceedings of the 18th IFAC World Congress, 2011, pp. 1892–1897.

[51] Gavilan, F., Vazquez, R., and Acosta, J.´A., Adaptive control for aircraft longitudinal dynamics with thrust saturation", Journal of Guidance, Control, and Dynamics, Vol.38, No.4, 2014, pp. 651-661.

[52] Swarnkar, S., and Kothari, M., A Simplified Adaptive Backstepping Control of Aircraft Lateral/Directional Dynamics", IFAC-Papers Online, 2016, Vol. 49, No. 1, pp. 579-584.

[53] Zhao, Y., A Sliding Mode Controller for Under-actuated VTOL Aircraft, International Journal of Control and Automation, Vol. 10, No. 7, 2017, pp. 149-162.

[54] Huang, Y.J., "Sliding Mode Control Design for Aircraft Control Systems", Proceedings, The First IEEE Regional Conference on Aerospace Control Systems, 1993, pp. 309-313.

[55] Xu, H., Mirmirani, M.D., and Ioannou, P.A., Adaptive sliding mode control design for a hypersonic flight vehicle, Journal of Guidance, Control, and Dynamics, Vol. 27, No. 5, 2004, pp. 829–838.

[56] Slotine, J. J. E., and Li, W., Applied Nonlinear Control, Prentice-Hall Inc., Engle-wood Cliffs, New Jersey, 1991.

[57] Singh, S. N., Steinberg, M. L., and Page, A. B., Nonlinear Adaptive and Sliding Mode Flight Path Control of F/A-18 Model, IEEE Transactions on Aerospace and Electronic Systems, Vol. 39, No.4, 2003, pp. 1250-1262.

[58] Xu, H., Mirmirani, M. D., and Ioannou, P. A., Adaptive Sliding Mode Control Design for a Hypersonic Flight Vehicle, Journal of Guidance, Control and Dynamics, Vol. 27, No.5, 2004, pp. 829-838.

[59] Seshagiri, S., and Promtun, E., Sliding Mode Control of F-16 Longitudinal Dynamics, American Control Conference, Washington, 2008.

[60] Khatri, A. K., Singh, J., and Sinha, N. K., Aircraft Maneuver Design Using Bifur-cation Analysis and Sliding Mode Control Techniques, Journal of Guidance, Control and Dynamics, Vol. 35, No.5, 2012, pp. 1435-1449.

[61] Bacon, B. J., and Gregory, I. M., General Equations of Motion for a Damaged Asymmetric Aircraft, AIAA Atmospheric Flight Mechanics Conference and Exhibit, South Carolina, Paper No.

AIAA 2007-6306, 2007.

[62] Guo, J., Tao, G., and Liu, Y., Multivariable Adaptive Control of NASA Generic Transport Aircraft Model with Damage, Journal of Guidance, Control, and Dynamics, Vol. 34, No.5, 2011, pp. 1495-1506.

[63] Liu, Y., Tao, G., and Joshi, S. M., Modeling and Model Reference Adaptive Control of Aircraft with Asymmetric Damage, Journal of Guidance, Control, and Dynamics, Vol. 33, No.5, 2010, pp. 1500-1517.

[64] Nguyen, N., Krishnakumar, K., Kaneshige, J., and Nespeca, P., Flight Dynamics and Hybrid Adaptive Control of Damaged Aircraft, Journal of Guidance, Control, and Dynamics, Vol.31, No.3, 2008, pp. 751-764.

[65] Arruda, M., and Steck, J., Dynamic Inverse Resilient Control of a Damaged Asym-metric General Aviation Aircraft, 48th AIAA Aerospace Sciences Meeting Including the New Horizons Forum and Aerospace Exposition, Orlando, Florida, Paper No. AIAA 2010-946, 2010.

[66] Ouellette, J. A., Raghavan, B., Patil, M. J., and Kapania, R. K., Flight Dynamics and Structural Load Distribution for a Damaged Aircraft, AIAA Atmospheric Flight Mechanics Conference, Chicago, Paper No. AIAA 2009-6153, 2009.

[67] Shah, G., Aerodynamic Effects and Modeling of Damage to Transport Aircraft, AIAA Atmospheric Flight Mechanics Conference and Exhibit, Hawaii, Paper No. AIAA 2008-6203, 2008.

[68] Mukherjee, B. K., and Sinha, M., Extreme Aircraft Maneuver Under Sudden Lateral CG Movement: Modeling and Control", Aerospace Science and Technology, Vol. 68, 2017, pp. 11-25.

[69] Mukherjee, B.K., and Sinha, M., “Nonlinear dynamics and control of a laterally mass varying fighter aircraft”, Proc. of IMechE Part G: Journal of Aerospace Engineering, Vol. 232, No.16, 2018, pp. 3118-3134.

[70] Truong, T.N., Vo, A.T., and Kang, H.J., A Backstepping Global Fast Terminal Sliding Mode Control for Trajectory Tracking Control of Industrial Robotic Manipulators, IEEE Access, Vol.9, 2021, pp.31921-31931.

[71] Hu, W., Ding, F., Zhang, J., Zhang, B., Zhang, N., and Qin, A., Robust adaptive backstepping sliding mode control for motion mode decoupling of two-axle vehicles with active kinetic dynamic suspension systems, International Journal of Robust and Nonlinear Control, Vol.30, No.8, 2020, pp. 3110-3133.

[72] Fu, C., Hong, W., Lu, H., Zhang, L., Guo, X., and Tian, Y., Adaptive robust backstepping attitude control for a multi-rotor unmanned aerial vehicle with time-varying output constraints, Aerospace Science and Technology, Vol.78, 2018, pp. 593-603.

[73] Asl, S.B.F., and Moosapour, S.S., Adaptive backstepping fast terminal sliding mode controller design for ducted fan engine of thrust-vectored aircraft, Aerospace Science and Technology, Vol.71, 2017, pp.521-529.

[74] Jia, Z., Yu, J., Mei, Y, Chen, Y, Shen, Y., and Ai, X., Integral backstepping sliding mode control for quadrotor helicopter under external uncertain disturbances, Aerospace Science and Technology, Vol.68, 2017, pp. 299–307.

[75] Cong, B., Liu, X., and Chen, Z., Backstepping based adaptive sliding mode control for spacecraft attitude maneuvers, Aerospace Science and Technology, Vol.30, No.1, 2013, pp. 1-7.

[76] Ran, M., Wang, Q., Hou, D., and Dong, C., Backstepping design of missile guidance and control based on adaptive fuzzy sliding mode control, Chinese Journal of Aeronautics, Vol.27, No.3, 2014, pp. 634-642.

[77] Adhikary, N., and Mahanta, C., Integral backstepping sliding mode control for underactuated systems: Swing-up and stabilization of the Cart–Pendulum System, ISA Transactions, Vol.52, No.6, 2013, pp. 870-880.

[78] Utkin, V., Sliding modes in control and optimization. Berlin: Springer-Verlag ,1992.

[79] Dai, P., Feng, D., Zhao, J., Cui, J., and Wang, C., Asymmetric integral barrier Lyapunov function-based dynamic surface control of a state-constrained morphing waverider with anti-saturation compensator, Aerospace Science and Technology, Vol. 31, Part A, 2022.

[80] Wu, D., Zhou, J., Ye, H., Disturbance observer–based neural flight control for aircraft with switched time-varying distributed delays, Proceedings of the Institution of Mechanical Engineers,

Part G: Journal of Aerospace Engineering, Vol. 235, No.16, 2021, pp. 2451-2465.

[81] Huang, Z., and Chen, M., Coordinated Disturbance Observer-Based Flight Control of Fixed-Wing UAV, IEEE Transactions on Circuits and Systems II: Express Briefs, Vol. 69, No. 8, 2022, pp. 3545-3549.

[82] McRuer, D., Ashkenas, I, and Graham, D., Aircraft Dynamics and Automatic Control, Princeton University Press, New Jersey, 1973.

[83] Nelson, R. C., Flight Stability and Automatic Control, 2nd Edition, McGraw-Hill Inc., New York, 1998.

[84] Anderson, B. D. O, and Moore, J. B., Optimal Control: Linear Quadratic Methods, Dover Publications, 2007.

[85] Hoffmann, G.M., Huang, H. and Waslander, S.L. Precision flight control for a multi-vehicle quadrotor helicopter testbed, Control Engineering Practice, Vol.19, No.9, 2011, pp. 1023–1036.

[86] Liu, M., Egan, G.K. and Santoso, F. Modeling, autopilot design, and field tuning of a UAV with minimum control surfaces, IEEE Transactions on Control Systems Technology, Vol.23, No.6, 2015, pp. 2353–2360.

[87] Meyer, G., Su, R. and Hunt, L. Application of nonlinear transformations to automatic flight control, Automatica, Vol.20, No.1, 1984, pp. 103–107.

[88] Ochi, Y. and Kanai, K. Design of restructurable flight control systems using feedback linearization, Journal of Guidance, Control, and Dynamics, Vol.14, No.5, 1991, pp. 903- 911.

[89] Menon, P. K. A., Badgett, M. E., Walker, R. A. and Duke, E. L. Nonlinear Flight Test Trajectory Controls for Aircraft, Journal of Guidance, Control, and Dynamics, Vol.10, No.1, 1987, pp. 67-72.

[90] Singh, S. N., Control of Nearly Singular Decoupling Systems and Nonlinear Aircraft Maneuver, IEEE Transactions on Aerospace and Electronic Systems, Vol.24, No.6, 1988, pp. 775-784.

[91] Ismail, S., Pashilkar, A. A., Ayyagari, R., and Sundararajan, N. Diagonally dominant backstepping autopilot for aircraft with unknown actuator failures and severe winds, The Aeronautical Journal, Vol.1207, 2014, pp. 1009-1038.

[92] Stevens, B. L., and Lewis, F. L., Aircraft Control and Simulation, 2nd Edition, John Wiley and Sons Inc., Hoboken, New Jersey, 2003

[93] Beard, R.W. and McLain, T.W. Small unmanned aircraft: Theory and practice, Princeton University Press, 2012.

[94] Rudra, S., Barai, R.K. and Maitra, M. Block backstepping design of nonlinear state feedback control law for underactuated mechanical systems , Springer, 2017.

[95] Barkana, I. Defending the beauty of the invariance principle, International Journal of Control, Vol.87, No.1, 2014, pp. 186-206.

[96] Barkana, I. Can stability analysis be really simplified? (revisiting Lyapunov, Barbalat, LaSalle and all that), AIP Conference proceedings of 11th International Conference on Mathematical Problems in Engineering, Aerospace and Sciences, La Rochelle, France 2016.

[97] Basin, M.V., Rodriguez-Ramirez, P., Sliding-mode filter design for linear systems with unmeasured states, IEEE Transactions on Industrial Electronics, Vol. 58, No.8, 2011, pp. 3616–3622.

[98] Basin, M.V., Rodriguez-Ramirez, P., Sliding mode controller design for linear stochastic systems with unknown parameters, Journal of Franklin Institute, Vol.351, No.4, 2014, pp. 2243–2260.

[99] Wei, Y, Deng, H., Pan, Z., Li. K., and Chen, H., Research on a combinatorial control method for coaxial rotor aircraft based on sliding mode, Defence Technology, Vol.18, 2022, pp. 280–292.

[100] Rouyan, N.M., Model simulation suitable for an aircraft at high angles of attack, MPhil Thesis, School of Engineering, Cranfield University, United Kingdom , 2016.

[101] Carter, B.R., Time-Optimization of High-Performance Combat Maneuvers, Naval Postgraduate School, California, USA , 2005.

[102] Durham, W., Bordignon, K.A., and Beck, R., Aircraft Control Allocation, John Wiley and Sons 2006.

[103] Liu, J., Chen, Z., Sun, M., and Sun, Q., Practical coupling rejection control for Herbst maneuver with thrust vector, Journal of Aircraft, Vol.56, No.4, 2019, pp. 1726-1734.

[104] Horn, R.A., and Johnson, C.R., Topics in Matrix Analysis, Cambridge University Press ,1994.

[105] Boyd, S., and Vandenberghe, L., Convex Optimization, Cambridge university press, 2004.

[106] Hickey, T., Ju, Q., and Emden, M.H.V, Interval arithmetic: From principles to implementation, Journal of the ACM, Vol.48, No.5, 2001, pp.1038-1068.

[107] Vukic, Z., Kulzaca, L., Donlagic, D., and Tesnjak, S., "Nonlinear control systems", Marcel Dekker, 2003.

[108] Nadda, S., and Swarup, A., On adaptive sliding mode control for improved quadrotor tracking, Journal of Vibration and Control, Vol.24, No.14, 2018, pp. 3219-3230.

[109] Karabacak, M., and Eskikurt, H.I., Design, modelling and simulation of a new nonlinear and full adaptive backstepping speed tracking controller for uncertain PMSM', Applied. Mathematical Modelling, Vol.36, No.11, 2012, pp. 5199–5213.

[110] Merei, M., and Tar, J.K. Adaptive Backstepping Control Design for Nonlinear System, IEEE 17th International Symposium on Applied Computational Intelligence and Informatics (SACI), Timisoara, Romania, 2023, pp. 147-152.

[111] Sadati, S.H, Parvar, M.S., Menhaj, M.B., and Bahrami, M. Backstepping Controller Design Using Neural Networks for a Fighter Aircraft, European Journal of Control, Vol.13, No.5, 2007, pp. 516-526.

[112] Yu, X., and Man, Z., Fast terminal sliding-mode control design for nonlinear dynamical systems, IEEE Transactions on Circuit and Systems, Vol. 49, No. 2, 2002, pp. 261–264.

[113] Wu, Y., and Yu, X., Terminal sliding mode control design for uncertain dynamic systems, System & Control Letters, Vol. 34, No. 5, 1998, pp. 281–287

[114] Venkataraman, S.T., and Gulati, S., Control of nonlinear systems using terminal sliding modes, Journal of Dynamic Systems Measurement and Control, Vol. 115, No. 3, 1993, pp. 554-560.

[115] Adhikary, N., and Mahanta, C., Sliding mode control of position commanded robot manipulators, Control Engineering Practice, Vol. 81, 2018, pp. 183-198.

[116] Yu S., Yu, X., Shirinzadeh, B., and Man, Z., Continuous finite time control for robotic manipulators with terminal sliding mode, Automatica, Vol. 41, 2005, pp. 1957-1964.

List of Publications

Journal Publications:

[1] A. Khanna, N. Singh, and B.K. Mukherjee, "Adaptive Block Backstepping Control for a UAV Performing Lateral Maneuvers under Lateral CG Uncertainty", *Aircraft Engineering and Aerospace Technology*, Vol. 94, Issue 7, 2022, pp. 1100-1108.

[2] A. Khanna, B.K. Mukherjee, and M. Sinha, "High-α Maneuver under Lateral CG Uncertainty: A Robust Adaptive Backstepping Control Scheme", *Proceedings of the Institution of Mechanical Engineers, Part G: Journal of Aerospace Engineering*, Vol. 238, Issue 13, 2024, pp. 1357-1373.

[3] A. Khanna, and B.K. Mukherjee, "Lateral Maneuvering with a UAV Mitigating Lateral CG Variations: Modelling and an Efficient Adaptive Backstepping Control", *Unmanned Systems*, 2024, pp. 1-17 (Accepted, In Press)

[4] A. Khanna, B.K. Mukherjee, and M. Sinha, "Autonomous Aircraft Maneuvering under Unknown CG Variations through a Robust Adaptive Backstepping Control", *Journal of Vibration and Control*, 2024, pp. 1-18 (Accepted, In Press)

Conference Publications:

[1] A. Khanna, and B.K. Mukherjee, "High Alpha Maneuvering with a Laterally Asymmetric Fighter Aircraft: A Backstepping Control Approach" in proceedings of *IEEE International Conference on Power Instrumentation Control and Computing*, Thrissur, Kerala, India, 17-19 December, 2020.

[2] A. Khanna, and B.K. Mukherjee, "Backstepping Control for Asymmetric Fighter Aircraft Executing High Alpha Herbst Maneuver" in proceedings of *International Conference on Mechanical and Aerospace Engineering (ICMAE)*, Athens, Greece, 16-19 July, 2021.

[3] A. Khanna, and B.K. Mukherjee, "UAV Performing Lateral Turn Maneuver under CG Offset: A Backstepping Control Scheme" in proceedings of *10th IEEE Uttar Pradesh Section International Conference on Electrical, Electronics and Computer Engineering (UPCON)*, Greater Noida, India, 01-03 December, 2023.

[4] A. Khanna, and B.K. Mukherjee, "Asymmetric UAV Performing Pointing Maneuver under Lateral CG Offset: An Adaptive Backstepping Control Approach" in proceedings of *20th IEEE India Council International Conference (INDICON)*, Hyderabad, India, 14-17 December 2023.

Brief Biography of the Candidate

Anukaran Khanna, son of Sri Deepak Kumar Khanna and Smt. Neelima Khanna, passed his 10th and 12th standard Board Examinations from Tagore Public School, Allahabad, India in 2000 and 2002 respectively. He completed his Bachelor of Technology in Applied Electronics and Instrumentation Engineering from Uttar Pradesh Technical University, India in 2007. After B.Tech. he worked with Golden Cross Pharma Pvt. Ltd. (a unit of Cipla Ltd.) as an instrumentation engineer in Rorathang, Sikkim. Thereafter, he earned his Master's Degree specializing in Control and Instrumentation Engineering from the Electrical Engineering Department of Motilal Nehru National Institute of Technology, Allahabad, India in the year 2013. Prior to joining the Ph.D. program at the Department of Electrical and Electronics Engineering, BITS Pilani, India. He was a faculty member at the Department of Electronics Engineering, United College of Engineering and Research, Allahabad, India, affiliated to Uttar Pradesh Technical University, India. His research interests lie in nonlinear, robust, and adaptive control techniques as applied to aircraft flight control.

E-mail Id.: anukaran.bits@gmail.com

Brief Biography of the Supervisor

Dr. Bijoy Krishna Mukherjee received B.E. degree in Electrical Engineering from North Bengal University, India in 2002; M.E. degree specializing in Control Systems from the Department of Electrical Engineering, Indian Institute of Engineering Science and Technology (IIEST) Shibpur, West Bengal, India in 2004; and the Ph.D. degree from the Department of Aerospace Engineering, Indian Institute of Technology (IIT) Kharagpur, India in 2017. Prior to joining the Ph.D. program at IIT Kharagpur, he was a faculty member at the Department of Electrical Engineering, Asansol Engineering College, Asansol affiliated to West Bengal University of Technology, India for nearly seven years.

He is serving as an Assistant Professor in the Department of Electrical and Electronics Engineering, Birla Institute of Technology and Science (BITS), Pilani, India since 2018. His primary research interests lie in nonlinear, robust and adaptive control techniques as applied to aircraft flight control and spacecraft attitude control problems. He is also interested in electrical power systems and electric drives applications of control theories. He has authored and co-authored over thirty research papers which are published in reputed international and national journals and conference proceedings. He is also involved in several research projects funded by various government agencies in the capacities of principal investigator and co-investigator.